Targeted microbubbles: A new strategy for biofilm imaging and destruction.

Jack Andrew Caudwell

Submitted in accordance with the requirements for the degree of
Doctor of Philosophy

The University of Leeds
School of Health and Medicine

September 2019

The candidate confirms that the work submitted is his/her own, except where work which has formed part of jointly-authored publications has been included. The contribution of the candidate and the other authors to this work has been explicitly indicated below. The candidate confirms that appropriate credit has been given within the thesis where reference has been made to the work of others. *Further details of the jointly-authored publications and the contributions of the candidate and the other authors to the work should be included below this statement.*

This copy has been supplied on the understanding that it is copyright material and that no quotation from the thesis may be published without proper acknowledgement.

The right of Jack Caudwell to be identified as Author of this work has been asserted by him in accordance with the Copyright, Designs and Patents Act 1988.

© 2019 The University of Leeds and Jack Andrew Caudwell

Acknowledgements

As Isaac Newton once said, ‘If I have seen a little further it is by standing on the shoulders of giants.’ A PhD project is no mean feat and this one would not have been possible without a myriad of these metaphorical, and in some cases literal, giants holding me aloft. The biggest being Bruce Turnbull, of course, for his plentiful wisdom. Further thanks go to Jon Sandoe for both fanning the scientific and creative parts of my brain, and finally to Steve Evans.

First and foremost I would like to thank the respective members of Lab 1.49, who took in a lost soul with no department to call his own. They say a good work environment is one in which one can feel safe asking a silly question, and not get a stupid response. Well they’ve fielded plenty of those from this PhD candidate. Thank you to my desk buddy Devon, who would never deny me the pleasure of a shared sing-a-long; to Ryan for a consistent source of high-grade banter; to Spud for putting up with my attempts at a scouse accent; to K-Dog for keeping the lab chilled and to Zoe for being the great post-doc she would never concede to actually being. To lab members of yester-year; thanks to Matt for taking a fresh faced graduate under your wing. Last but not least, thank you to Sarah for being my nerdy partner in crime, bearing the brunt of pretty much any emotion evocated by this project. Thank you for the laughs, the invaluable advice and the opportunity to work in an environment where one can perform science whilst also having fun.

A very special thank you to my Physics paramour, Jordan Tinkler. They say diamonds form under pressure, and our friendship blossomed from the charcoal grey that littered the overcast sky from our first meeting, to the shining gem it is now. The pressure of this work doing nothing more than forging an alliance built from the molten ferocity of shared experience, scientific teamwork and jovial comradery. I would like to highlight Dr Ben Johnson’s contribution to the development of this project. It is impossible to know how slowly this work would have moved without his expertise, priceless ingenuity and assumption that every time I asked him how he was that an inconvenient request would proceed. Finally a special thank you to the Leeds

Anniversary Scholarship for funding this project. Providing the not only the food on my table but inevitably the liquid refreshment that will be used to salute the terminus of this body of work.

Abstract

Staphylococci are the most common cause of infection in indwelling medical devices. [1, 2] Their ability to form ‘biofilms’ makes treatment difficult and can lead to reoccurring infection. This work presents a potential novel method for imaging biofilm in flow systems utilizing Microbubbles (MBs) as ultrasound contrast agents. The surface of these MBs were functionalized with an Affimer protein engineered to bind to Clumping Factor A, a virulence factor present on the surface of *S. aureus* cells. These functionalized MBs were found to bind to the *S. aureus* biofilm 10 times better than their controls, demonstrating the ability of these proteins to localize large macromolecular structures to the biofilm surface under flow conditions. The results show the potential of targeted microbubbles to be used as a novel method of biofilm imaging and destruction for biofilm related infections in the body.

Abbreviations

A647/488	Alexafluor647/488
AAC	Affimer ala-cys scaffold
ABBA	Affimer-biofilm binding assay
ABS	Acrylonitrile-butadiene-styrene
BHI	Brain Heart Infusion
ClfA	Clumping factor A
ClfA1	Clumping Factor A affimer 1
CLSM	Confocal laser Scanning microscopy
CV	Crystal violet
DIPEA	N,N-Diisopropylethylamine
DMF	N,N-Dimethylformamide
DTT	Dithiothreitol
EDTA	Ethylenediaminetetraacetic acid
ESMS	Electrospray Mass Spectrometry
EthD-III	Ethidium homodimer - III
FnBP	Fibrinogen binding protein
HCTU	O-(6-Chlorobenzotriazol-1-yl)-N,N,N′,N′-tetramethyluronium hexafluorophosphate
HEPES	4-(2-hydroxyethyl)-1-piperazineethanesulfonic acid
ITC	Isothermal titration calorimetry
LED	Light emitting diode
MB	Microbubble
MBL	Mannose binding lectin
MBP	Maltose binding protein

MSCRAMM	Microbial Surface Components Recognizing Adhesive Matrix Molecules
Ni-NTA	Nickel-nitrilotriacetic acid
PDMS	Polydimethylsiloxane
PNAG	poly-β-(1,6)-N-acetylglucosamine.
SDS-PAGE	Sodium dodecyl sulphate – polyacrylamide gel electrophoresis
SEC	Size exclusion chromatography
SPPS	Solid phase peptide synthesis
SPR	Surface Plasmon Resonance
TEMED	Tetramethylethylenediamine
TEV	Tobacco Etch Virus
TFA	Trifluoro acetic acid
TIS	Triisopropylsilane
Tris	Tris(hydroxymethyl)aminomethane
UV	Ultraviolet

Table of Contents

1 Introduction

1.1 Bacterial biofilms

Bacterial biofilms are ubiquitous in nature and represent the predominant mode of bacterial growth in the natural world and human infections.[3] Biofilms are surface bound agglomerations of microbes, together with a matrix of secreted microbial polymers and "scavenged" host molecules.[4] They have complex structures and contain bacteria in a variety of growth and metabolic states.[5] Most bacterial infections will at some point involve a biofilm, which is associated with a 10-100 fold decrease in susceptibility of bacteria to antibiotics when compared with a planktonic population.[6] Formation of biofilms on indwelling medical devices such as intravascular catheters, pacemakers and prosthetic joints makes infection hard to eradicate with antimicrobial therapy alone. Frequently, formation of a biofilm requires removal of the device.[7]

A wide range of bacteria and some yeasts can form biofilm infections in humans.[8] In particular, Staphylococci, including *S. aureus* and the large group of coagulase negative staphylococcal species, are the most common cause of infection in indwelling medical devices.[1] In particular, *S. aureus* is one of the most lethal causes of bloodstream infection, with a mortality rate of 46% in patients with severe sepsis.[9-11] The ability to form biofilms offers a unique bacterial defence against antimicrobials, making treatment of these infections a considerable challenge.[12]

1.1.1 Biofilm life cycle

The life cycle of a biofilm is thought to consist of three stages:

(i) Initial attachment of cells to a surface; (ii) maturation; and (iii) detachment.[13] Initial attachment has been shown to be facilitated by interactions between cell surface adhesins and the polymer or host surface components.[14] Once established, the production of an extracellular matrix allows the cells to proliferate into three-dimensional (3D) structures. The polysaccharide matrix offers many mechanisms for decreasing antibiotic activity through the biofilm. The matrix, acting as a pseudo-polysaccharide and glycoprotein gel can decrease antibiotic motility by a factor of two to three.[15] The antibiotic can be deactivated by an enzymatic reaction (examples

include beta-lactamases, chloramphenicol acetyltransferases and aminoglycoside-modifying enzymes), or sequestered by binding proteins that form part of the biofilm's matrix. Furthermore, differences in growth states of bacteria within the biofilm will affect their susceptibility to certain antimicrobial agents.[16] Microbes buried deep in the biofilm tend to exist in a slow growing state due to poor penetration of nutrients through the biofilm.[17] This can affect the bacteria's susceptibility to antibiotics such as beta-lactams, that target cell wall synthesis, which occurs predominantly during cell growth.[18]

Disassembly of the biofilm in *S. aureus* is mediated by the *agr* quorum-sensing system (1.1.4),[19] subsequent detachment of cells can then facilitate a colonisation at a secondary site.[5] The detachment of these cells from the biofilm then helps to alleviate nutrient depletion and helps sustain the life of the parent biofilm.[20]

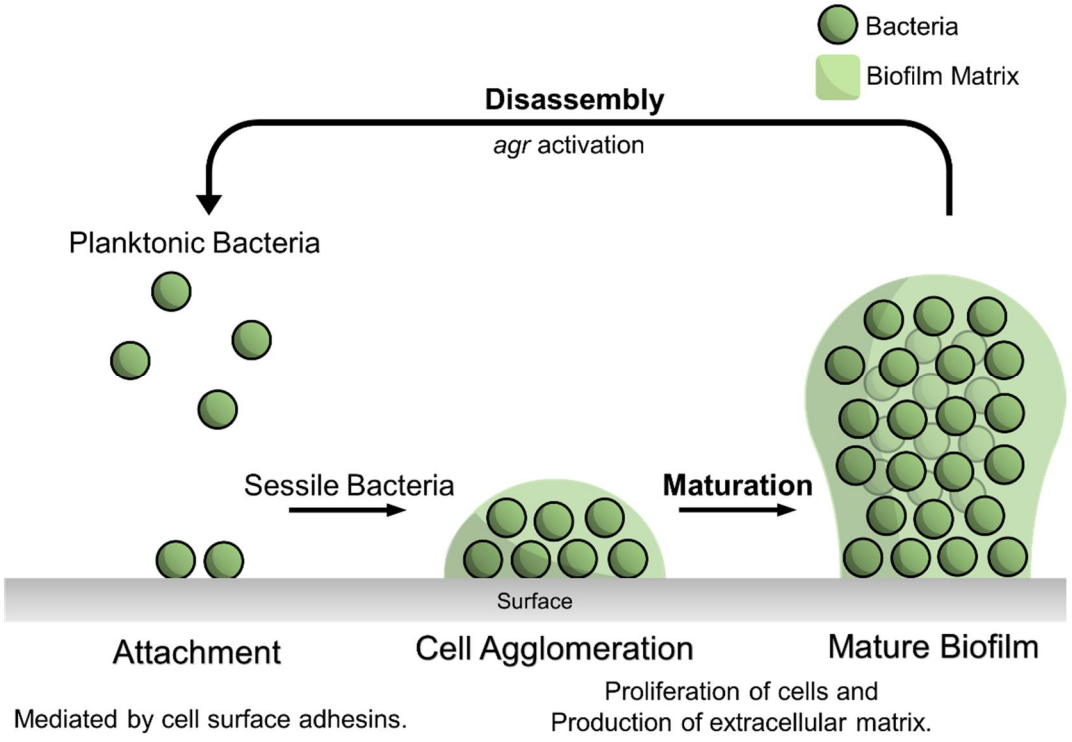

Figure 1.1. Illustration of the steps in the life cycle of a bacterial biofilm. Initial attachment is facilitated by the hydrophobicity of a polymer surface or host matrix proteins. Development of the extracellular matrix is followed by maturation of the biofilm, then disassembly and detachment of bacteria from the fully developed biofilm.[13]

1.1.2 *S. aureus* cell surface

The *S. aureus* cell surface contains a myriad of virulence factors, some of which facilitate the colonisation of surfaces leading to biofilm formation (Figure 1.2). These include a range of Microbial Surface Components Recognizing Adhesive Matrix Molecules (MSCRAMMs), all of which contribute towards the virulence of the species.[21] For instance, clumping factor A (ClfA),[22] clumping factor B (ClfB)[23] and fibronectin binding protein (FnBP)[24] are cell wall-associated proteins that contribute towards host-cell interactions. Protein A (SpA) is a multifunctional protein that binds Immunoglobulin G (IgG), von Willebrand factor (VWF) and other ligands.[25] SpA coats the bacteria in these ligands which results in decreased recognition of the pathogen by neutrophils, ultimately negating phagocytosis.[26] These proteins are anchored to the peptidoglycan of the cell wall via transpeptidases known as sortases.[27, 28] An example of one of these transpeptidases is Sortase class A, which recognises an LPXTG sequence present on the surface of protein precursors, and ligates them to oligoglycine species on the cell surface.[29-31] Other cell surface components such as wall teichoic acids (WTAs) are complicit in biofilm formation and are associated with the host-cell interaction.[32] These teichoic acids consists of repeat units of phosphodiester-linked polyol,[33] whose negatively charges backbone is implicated in a number of cell surface interactions.[34]

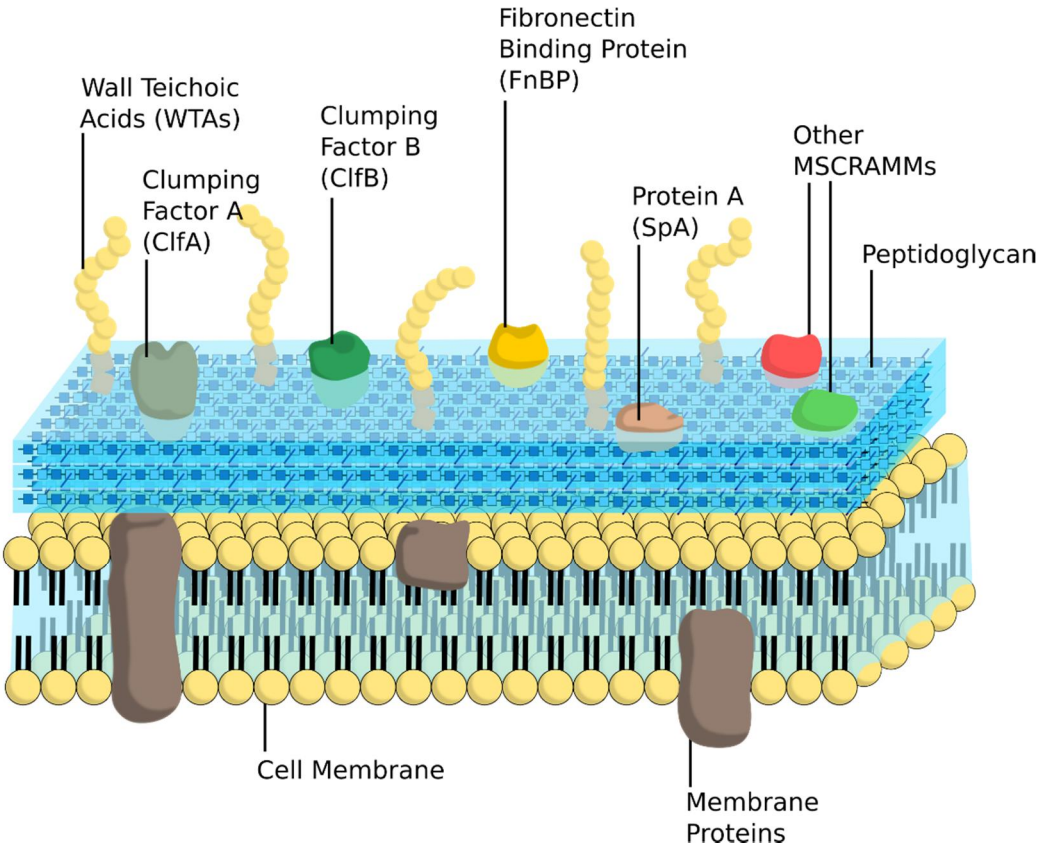

Figure 1.2. Illustration of the S. aureus cell surface.

The surface of the S. aureus bacteria consists of the cytoplasmic outer membrane, a layer of peptidoglycan and a network of cell surface associated proteins and glycoproteins.

1.1.3 The biofilm matrix

An important component of the biofilm structure is the network of proteins and polysaccharides that surrounds the bacterial cells and promotes intercellular and surface adhesion.[35] The main component of this extracellular matrix in staphylococci is the exopolysaccharide poly β(1,6)-*N*-acetylglucosamine (PNAG, structure shown in Figure 1.3), a positively charged molecule that helps aggregate cells utilising the negatively charged cell membrane, whilst also isolating the bacteria from antimicrobials.[36]

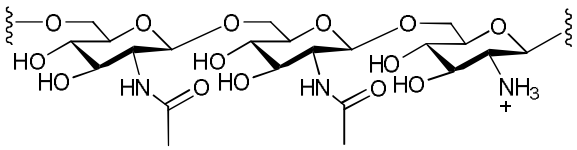

Figure 1.3. Structure of partially deacetylated poly-β-(1,6)-N-acetylglucosamine.
The main component in most biofilm matrices.

Though PNAG is considered the main component in the extracellular matrix, other molecules have been found to contribute toward the contents of the biofilm matrix such as proteinaceous adhesins bound to the cell surface and extracellular deoxyribose nucleic acid (eDNA) from lysed cells.[37] Many of these extracellular adhesive molecules are categorised as Secreted Expanded Repertoire Adhesive Molecules (SERAMs).[38] Table 1.1 shows the composite make-up of the *S. aureus* biofilm matrix. Many of these SERAMs are able to bind fibrinogen which helps aggregate cells by cross-linking receptors present on the cell surface.[38, 39] Fibronectin-binding proteins (FnBPs) are a common family of *S. aureus* cell surface adhesins that facilitate the colonisation of a biofilm via interactions with mammalian cell-surface fibronectin.[40]

Table 1.1. Components of the Staphylococcus aureus biofilm matrix and their functions. Taken from [12, 19].

Component	Function
Poly β(1,6)-*N*-acetylglucosamine	Aggregate cells
***S. aureus* Alpha-toxin (Hla)**	Potent cytolysin and virulence factor.
***S. aureus* Beta-toxin (Hlb)**	Sphingomyelinase, haemolytic, lymphocytic and binds eDNA.
Secreted Expanded Repertoire Adhesive Molecules (SERAMs):	
Extracellular Binding Protein	Adhesin, helps adhere cells to biofilm matrix.
Fibrinogen Binding Protein A (FbpA)	Homologous to coagulase, targets prothrombin, polymerises fibrin and forms staphthrombin.
Van Willebrand factor binding protein	Binds Van Willebrand Factor, has antiphagocytic activity.
Extracellular Fibrinogen Binding Protein (Emp)	Binds fibrinogen, fibronectin, vitronectin, collagen, adhesions of *S. aureus* to immobilised fibrinogen and fibronectin.
Extracellular Adhesive Protein (Eap)	Binds fibronectin, fibrinogen, eukaryotic cell walls, staphylococcal cells, mediates *S. aureus* adhesion to matrix protein, decreases phagocytic activity.
Phenol Soluble Modulins (PSMs)	Stability of biofilm, Amyloid formation.
eDNA	Intercellular adhesion.

1.1.4 *agr* quorum sensing system

The *agr* (*accessory gene regulator*) quorum-sensing system plays an integral role in the sustainability of a staphylococcal biofilm. The system operates by sensing the concentration of autoinducing peptide (AIP).[12] The general structure of an AIP is shown in Figure 1.4A, with the four API variants identified in *S. aureus* strains, shown Figure 1.4B.[41] All AIP variants contain a conserved thiolactone linkage that bridges the five C-terminal amino acids via a cysteine side-chain. AIP is derived from AgrD protein, which is first

processed by a membrane-bound peptidase to AgrB, that is exported across the membrane and subject to a second cleavage.[42] The mature AIP is then extracellularly transported. Once the AIP reaches a certain concentration (usually ~nM), it binds to the surface exposed histidine kinase AgrC, which triggers a two-component response, which leads to the activation of machinery that digests surface proteins associated with biofilm maintenance (Figure 1.5). Generally, induction of the *agr* system causes down-regulation of adhesins and up-regulation of secreted toxins and enzymes that cause disassembly of the biofilm.[12] This machinery plays a pivotal role in maintaining optimal conditions for biofilm longevity and offers a mechanism for potential secondary infection, by allowing release of bacterial cells from the biofilm.

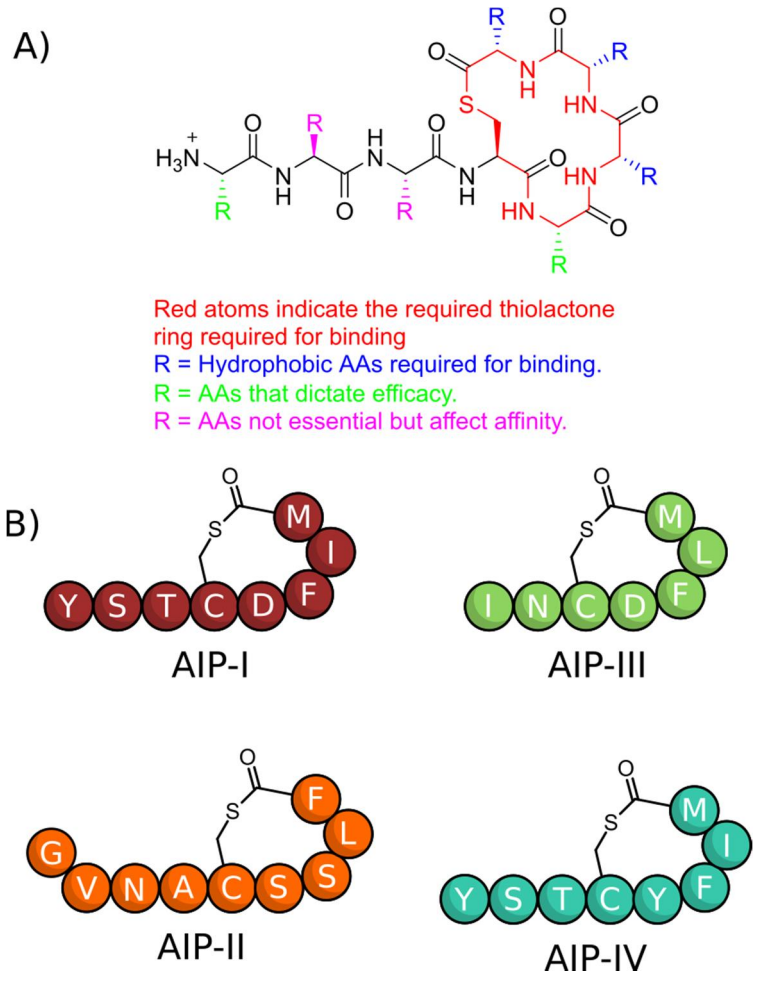

Figure 1.4. Structure of Auto-inducing Peptides in S. aureus.
A) Consensus chemical structure of the four AIP S. aureus subgroups. Red atoms show conserved thiolactone macrocycle common between all variants, with the R group variations essential for binding. B) Amino acid sequences of AIP-I, AIP-II, AIP-III and AIP-IV. Adapted from [42] .

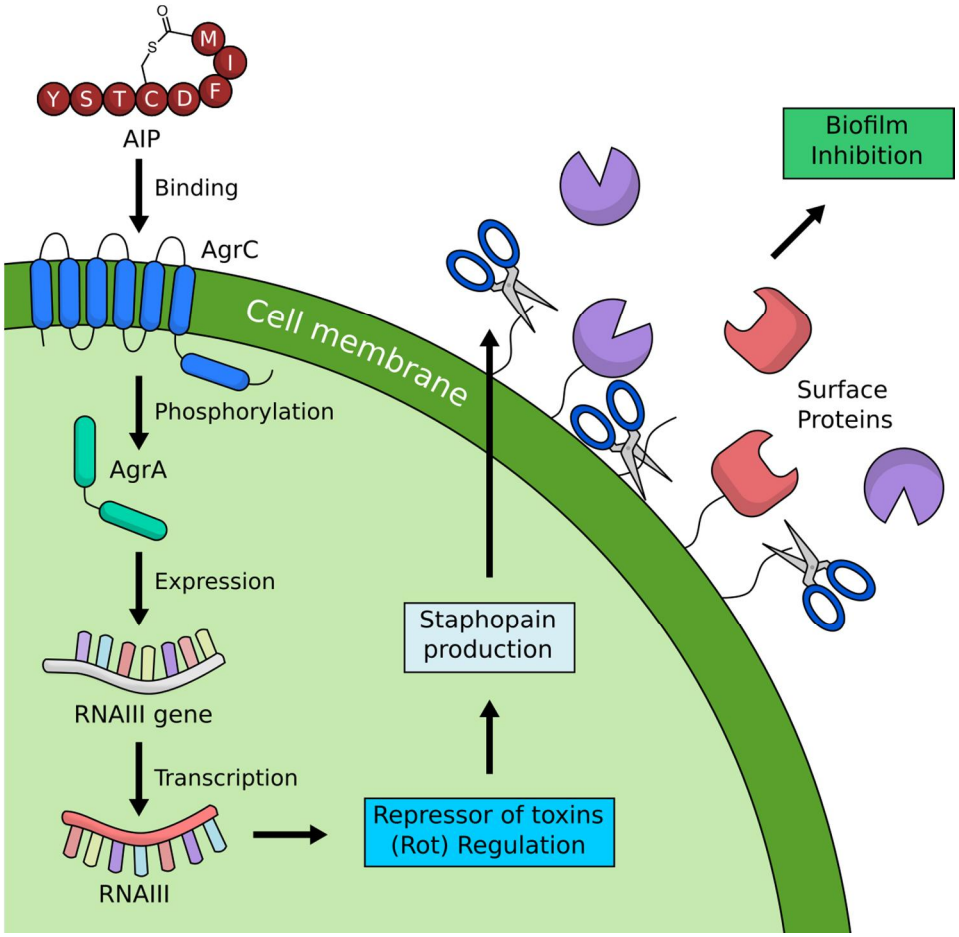

Figure 1.5. Cartoon representation of part of the agr quorum sensing pathway in S. aureus.

Cascade mechanism by which the agr quorum sensing machinery of S. aureus up-regulates the production of proteolytic enzymes than digest cell-surface proteins associates with cellular adhesion. Adapted from [12].

1.2 Imaging biofilms

Microscopy is a powerful tool for imaging biofilms *in vitro*, allowing imaging of both living and dead cells and observation of changes in topography.

Confocal laser scanning microscopy (CLSM) is an imaging technique that uses fluorescence to generate a real time visualisation of hydrated living

cells; conventionally it uses an upright or inverted epi-fluorescence microscope.[43, 44] Fluorescence can be achieved either by the inherent fluorescence of a microbe or more commonly, a specialised dye. In most cases, the two components of a live/dead stain contain a membrane permeable dye to stain living cells, and a non-membrane permeable dye to stain cells with compromised cell membranes.[45] Staining kits are available commercially that selectively dye living and dead cells with different coloured fluorophores in order to differentiate between the two, an example of which is calcein-AM and propidium iodide (PI).[46] Calcein-AM is a cell-membrane permeable molecule that once digested by esterase in living cells fluoresces green.[47] In contrast, PI cannot permeate living cells but can pass through disrupted membranes of dead cells and complex to double helical DNA to fluoresce red.[48]

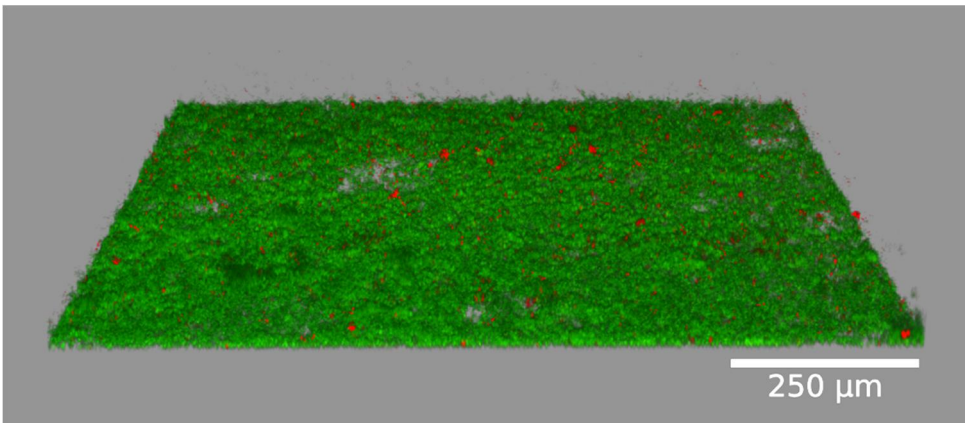

Figure 1.6. Lateral view of a two-day-old S. aureus biofilm imaged by confocal laser scanning microscopy.
The biofilm was stained with a live/dead stain. Living cells shown as green and dead cell components shown as red.

Although the use of this stain in tandem with CLSM can be used to visualise cells, it does not allow for imaging of all biofilm components. Imaging of the biofilm matrix can be achieved by targeting single components, using such things as fluorescently labelled polysaccharide binding proteins (lectins)[49] or protein binding dyes.[50] The multi-composite make-up of the biofilm matrix means that there is no dye for comprehensive staining of the

whole biofilm matrix. Use of multiple dyes in one system can prove problematic due to spectral overlap of their different characteristic excitation and emission wavelengths.[51]

While confocal microscopy is regarded as a powerful tool for imaging biofilms, new techniques have been developed that allow for greater resolution almost to a macromolecular scale. Development of cutting edge microscopic techniques has enabled imaging with greater resolution, thus expanding our understanding of biofilm structure. The resolution of light microscopy is usually limited to half the wavelength of the light used for imaging (diffraction limit). Structured Illumination Microscopy (SIM) illuminates the sample with a pattern of light at three different angles, which doubles the conventional resolution of 120 nm.[52] Stimulated Emission Depletion (STED) utilises two lasers; whilst one excites the sample creating a confocal spot, the second is used for shaping and focussing, however quenching locally requires high power and limits the imaging time.[44] Some commercial STED microscopes can reach resolutions of between 90-70 nm. However, it should be noted that though these techniques allow for the highest resolution they are limited with the regards to the choice of mounting the sample and thickness of their samples, making them unsuitable for imaging biofilms as whole entities [53].

1.3 Microfluidics for biofilm study

Microfluidics is the science and technology of micrometre scale systems that manipulate small amounts of fluids.[54] Biofilm studies have more commonly been performed on a macroscale. The emergence of microfluidics as the setting for studying bacterial biofilms has brought many of its advantages to light: Microfluidic systems allow for tighter control over the microenvironment, are relatively inexpensive to fabricate and their small sizes allow them to be easily integrated into a variety of sensing devices.[55]

The parameters of a microfluidic device design can be manipulated to allow for complex laminar flow systems: Greener and co-workers developed a microfluidic system for biofilm growth that restricted bacterial growth to one surface of the flow chamber.[56] By controlling the fluidic dynamics of the system

they were able to set up a stream of carbon rich media within a larger flow of carbon deficient media, isolated to one surface of the device. This isolated carbon rich 'stream' which mediated biofilm growth. Benoit and co-workers used microfluidic approaches to generate systems that mimic a 96-well plate and therefore could be easily integrated in to plate readers.[57] The microfluidic devices spatially mimicked a 96-well plate, with 96 flow cells in which biofilms were cultivated. These devices were able to quantify the amount of GFP-expressing bacteria present using a conventional plate reader and also using fluorescence microscopy. Yin and co-workers demonstrated the use of microfluidics to observe horizontal gene transfer between *Pseudomonas putida* and *Escherichia coli.*[58] Using microfluidics integrated into fluorescence microscopy and CLSM, they were able to observe the transfer of plasmid DNA that encoded for green fluorescent protein (GFP) fluorescence from a *P. putida* donor to a non-expressing *E. coli* strain. The versatility of microfluidic devices also allows for the easy integration of other materials into the flow cell. Cao and co-workers developed a microfluidic device that included a forward osmosis membrane, so that the biofouling ability of *Shewanella oneidensis* could be observed in real time using CLSM.[59] The use of the microfluidic device allowed them quantify the degree of biofouling without having to disassemble the equipment.

Use of microfluidic devices in this project allowed for easy integration of the fluidic system into a confocal microscope for cell imaging without it needing to be dismantled. This allowed for imaging of the biofilm when subjected to reagents, without sacrificing cell viability. These low volume flow systems allowed for the study of biofilms under flow conditions in an experimental design that can better mimic the *in vivo* environment – closer to that of the vascular system.

1.4 Microbubbles as biofilm therapy in medicine

Microbubbles (MBs) are micron-sized gas filled bubbles encapsulated in a thin shell of lipid or other surfactant based material.[60] MBs were first discovered in the late 1960's by Dr Charles Joiner, who observed their presence during an echocardiogram.[61] He observed a transient increase in

ultrasound (US) signal from the ventricle after each injection of indocyanine, made through a left ventricular catheter. Later research found this signal had arisen from small bubbles forming at the catheter tip. Decades later, MBs are engineered to be used as ultrasound contrast agents (UCAs) and are commercially available.[62-64] Fundamentally, MBs consist of a heavy molecular weight gas stabilised by an outer lipid monolayer (Figure 1.7. Cartoon representation of a 1 – 10 µM microbubble.). Typically, the gas core consists of highly insoluble fluorinated carbon or sulfur gases such as sulfur hexafluoride and decafluorobutane, which greatly improve microbubble stability.[65] Their ability to increase US signal intensity stems from an acoustic impedance mismatch between the gas core and its surrounding media.[62]

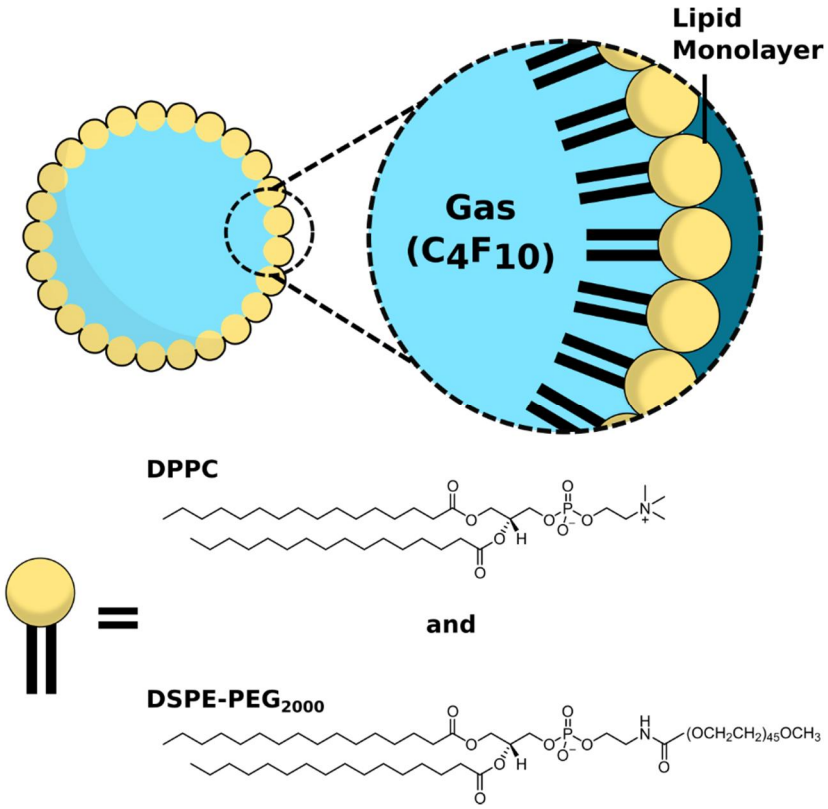

Figure 1.7. Cartoon representation of a 1 – 10 µM microbubble.
Outer shell consists of Dipalmitoylphosphatidylcholine (DPPC) and 1,2-Distearoyl-sn-glycero-3-phosphoethanolamine-PEG2000 (DSPE-PEG2000) lipids. Structure of the lipid are shown in the lower image.

Ultrasound can also be used to rupture microbubbles leading to a sudden energy release.[66] Although this characteristic may seem a detriment to viable human cells, it offers a unique pathway to destruction of pathogenic

bacteria.[67] Sonoporation (increase in cell permeability due to US) in conjunction with MBs can be caused by transient oscillation or complete MB rupture, both of which are mediated by US properties.[68] This method of membrane disruption using MBs has been used not only to destroy bacteria, but also to increase intracellular uptake of molecules in human cells.[69]

It has been demonstrated that microbubbles can be used as a method for imaging and disrupting biofilms, Kooiman and co-workers investigated a combination treatment of commercially available microbubbles (Definity UCA) and ultrasound alongside oxacillin against a blood clot-associated *S. aureus* biofilm.[70] The use of these components as a combined treatment achieved greater efficacy for biofilm loss than oxacillin, microbubble and US controls alone. This work demonstrated the ability of microbubbles to treat biofilm infections through sonobacteriocide - destruction of bacteria using antibiotics in conjunction with ultrasound and ultrasound contrast agents.[71] Yu and co-workers demonstrated an increase in *S. epidermidis* biofilm vancomycin susceptibility when exposed to vancomycin, MBs and ultrasound via sonoporation.[72, 73] The findings showed the presence of MBs coupled with ultrasound ameliorated the effects of sonoporation, and thus susceptibility of the bacteria to vancomycin. Similarly, Qu and co-workers tested the efficacy of a US-MB treatment on *S. epidermidis* biofilm-infected polyethylene dishes, implanted in rabbits.[74] These *in vivo* studies displayed a significant decrease in colony forming units of bacteria in rabbits treated with MBs in conjunction with ultrasound and vancomycin, compared to that of the single treatment controls.

Although previous work has demonstrated the therapeutic benefit of microbubbles to aid sonobacteriocide and sonoporation, the efficacy of these treatments could be optimised if the microbubbles could be localised to the site of infection. Matter and co-workers demonstrated the synergy of microbubble and targeted monoclonal antibodies (mAbs) as a novel method of non-invasive molecular imaging of biofilms (Figure 1.8).[75]

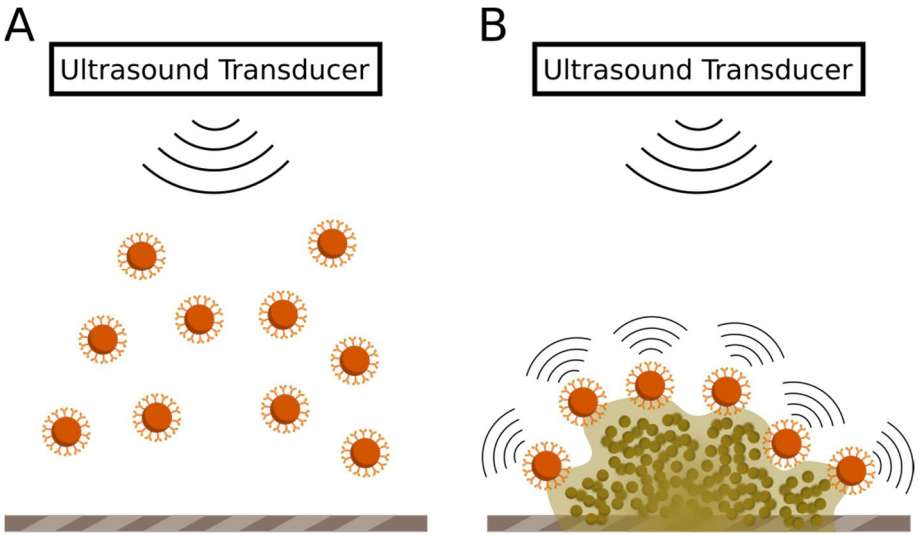

Figure 1.8. Cartoon representation of Ultrasound contrast agents (UCAs) used to treat biofilms.
A) Ultrasound sonification of free floating UCAs, gives a different acoustic signature to that of biofilm-bound UCAs. B) UCAs specifically bound to biofilm matrix being detected by ultrasound. Reproduced from [75].

Using biofilm targeted microbubbles as ultrasound contrast agents (UCAs), they were able to use high-frequency acoustic microscopy to ascertain the spatial resolution and quantify the biofilm's mechanoelastic properties. These results allude to the potency of targeted microbubbles for not only the imaging of the bacterial biofilm, but also treatment and destruction. For such a method to be developed one must first identify potential binding partners for the microbubble and determine their specificity.

A potential issue that may arise from microbubble therapies for biofilm related infections is potentially putting pressure on the immune system. Some of the bacteria residing within the biofilm may not invoke an immunogenic response, but a microbubble mediating therapy may dislodge those bacteria causing an immune response. A sudden increase in planktonic bacteria within the blood exposes a number of toll-like receptors (TLRs) on the surface of immune cells to their bacterial cell wall-associated targets, which in turn provoke an immune response leading to cytokine production.[76] The potential over-production of these cytokines can cause inflammatory diseases and pose considerable risk to a patient, such as sepsis.[77] Indeed, Shaddox and

co-workers observed an increase in cytokine production when biofilms were mechanically disrupted and brought into contact with a patient's mononuclear cells.[78] The evidence suggests that an augmented immune response may arise from biofilm dispersal, but an assessment may need to be made as to whether the need to treat a persistent biofilm infection outweighs the potential side-effects of its treatment.

1.5 Monoclonal antibodies for biofilm targeting

Monoclonal antibodies are often used to target biologically relevant species on bacteria including bacterial toxins,[79-81] capsular polysaccharides [82-84] and surface proteins.[85-88] In particular work has been performed to identify mAbs that bind to *S. aureus* specific targets such as cell surface adhesins,[89-95] the biofilm matrix [96-100] and bacterial toxins.[101-103]

Matter and co-workers (mentioned in section 1.4) utilised an anti-protein A antibody to target Protein A found on the surface of *S. aureus* bacteria.[104] This allowed specific binding of the ultrasound contrasts agents to the bacteria, and thus greatly improved their method's specificity for the *S. aureus* biofilm.

Though varied in their potential applications, mAbs often have their limitations for therapeutic use. Murine derived mAbs stimulate an immunogenic response; their uptake into tissue is influenced by molecular size, shape and valency.[105] When the molecular weight exceeds the renal threshold of around 70 kDa, removal by the kidney glomerulus is prevented.[106] Moreover, production costs arising from the need for complex eukaryotic machinery to manufacture multimeric proteins with multiple disulphide bonds, and specialised purification columns, often comes at great financial cost.[107] These factors have galvanised a move away from conventional antibody use, towards that of antibody mimetics.

1.5.1 Antibody mimetics as antibody alternatives

As their title indicates, antibody mimetics are proteins that mimic the properties of antibodies but with fewer structural drawbacks.[108] These non immunoglobulin-based scaffolds are small in size, lack disulfide bonds and require no post-translational modification. Molecules that fall under the

umbrella of antibody mimetics include Adhirons/ Affimers,[109, 110] Affibodies [111] and DARPins.[112] These proteins are selected using a process called phage display.[113]

Phage display is an efficient method of identifying polypeptide chains that specifically bind to a desired target.[114] The concept of phage display was first proposed in 1985, but has now been adapted into a universally used method in the biopharmaceutical industry.[115] More recently, Sir George P. Winter was jointly awarded the Nobel Prize in Chemistry for 2018 for his work with the phage display of peptides and antibodies.[116]

The method of phage display, described below is, used for Affimer selection as described by Tiede *et al.*[109] Generally the procedure for phage display is as follows: filamentous phage are a family of non-lytic ssDNA viruses that infect Gram-negative bacteria.[117, 118] Genes encoding for the protein scaffold (Ig for example) are inserted into the phagemid vector, a DNA-based cloning vector carried by bacteriophages,[119] to generate a fusion protein between the scaffold protein and a bacteriophage coat protein. This fusion protein then allows the desired protein to be presented on the surface of the phage. Within the structure of the expressed protein are a number of hyper-variable loops, which are designated as the protein's 'binding site'. The peptide sequence of these loops can be randomised by manipulating the codons that encode for their amino acid sequence using site-directed mutagenesis. This library is then "screened" against an immobilised target; a process which allows those phage that express a protein on their surface which binds to the target (via this 'binding site') to bind; this process is called 'bio-panning'. Phage 'hits' caused by non-specific interactions are reduced during rigorous wash steps which can contain denaturants, organic solvents, different temperatures, or increasing concentrations of competing ligands. The phage 'positives' can then be recovered and further amplified in *E. coli* before undergoing another round of 'bio-panning' to identify an ideal candidate. This reiterative process identifies the sequence of amino acids at the binding regions of the protein that facilitate binding to the target. The gene for expression of this binding protein is then transfected into *E.coli* for overexpression and purification.

Affibody molecules are also small proteins (size) that can be selected for binding to a certain target through this process of phage display.[120] Lindborg *et al* used phage display to identify affibody molecules that effectively bound staphylococcal protein A with a pM K_D, which represents binding with a high affinity and specificity and would make them attractive bacterial targeting candidates.[121] These antibody mimics have been shown to have low toxicity and immunogenicity, so have potential for diagnostic and imaging applications.[122]

1.6 Mannose Binding Lectin for biofilms targeting

Mannose-binding lectin (MBL, also known as mannose-binding protein) is an important component of the human innate immune system.[123] It acts by binding to the surface of invading pathogens expressing suitable target molecules.[124] MBL is a member of a Ca^{2+} dependent family of proteins characterised by a collagenous region and a lectin (sugar binding) domain.[125] It comprises three identical polypeptide chains; α-helices from each monomer form a coiled coil bundle that holds together the globular carbohydrate recognition domains (Figure 1.9).[126] The structure is often referred to as a ‘bouquet’ due to its arrangement.

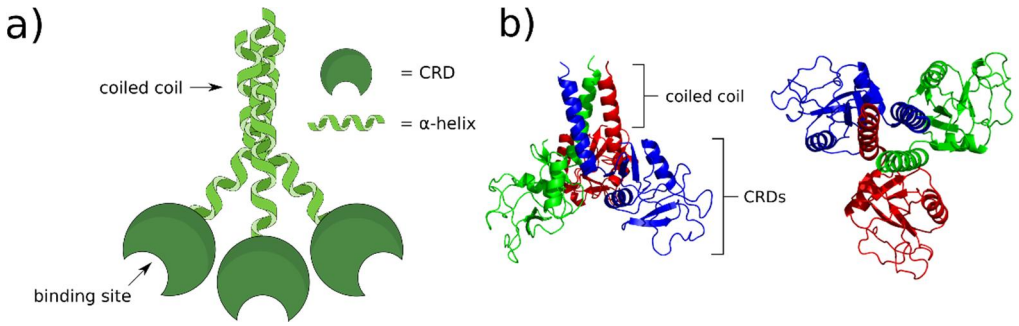

Figure 1.9. Cartoon representation of Mannose-binding lectin and protein crystal structure.

a) Diagram showing position of Carbohydrate Recognition Domains (CRDs) and alpha helices involved in the coil coiled interaction. b) crystal structure of human MBL, lateral view on the left and top view on the right, each single protomer shown in a different colour. The crystal structure image was created using PyMol visualisation programme for structure 1HUV taken from the protein data base (pdb).

MBL binds a variety of different cell surface carbohydrates with the following selectivity N-acetylglucosamine > mannose, N-acetylmannosamine and fucose > maltose > glucose>> galactose and N-acetylgalactosamine.[127] Although binding to these sugars is weak for a single protomer (K_d ~ 10^{-3} M), binding for the overall macromolecule with the three CRDs clustered in the oligomer allows the protein to achieve a stronger association with the cell wall.[128] *In vivo*, single iterations of the MBL trimer can conglomerate to form larger order macromolecules such as dimers, trimers and tetramers.[129] These associations are facilitated by disulfide bonds forming between cysteines in adjacent coiled coil peptide chains (Figure 1.10).[124]

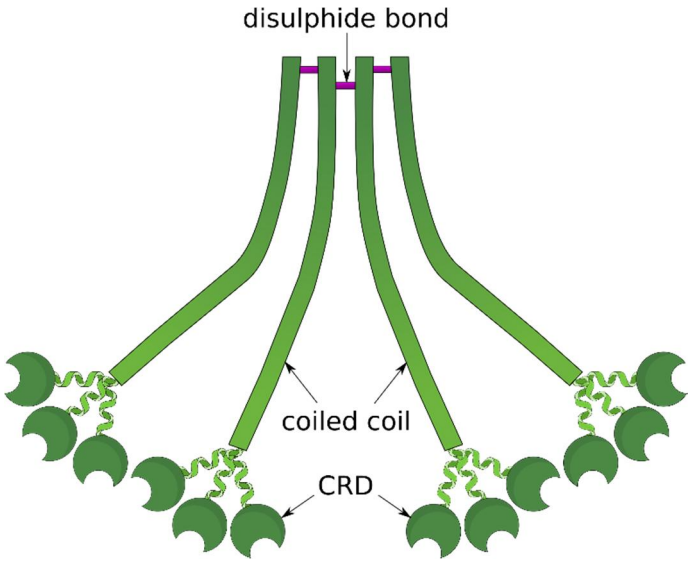

Figure 1.10. Cartoon representation of the tetrameric MBL oligomer. The coiled coils of adjacent MBL molecules form intermolecular disulfide bonds.

Once bound to the surface of a bacterial cell, MBL stimulates a number of responses by the innate immune system (Figure 1.11).[124] Surface bound MBL associates with MBL-associated serine proteases (MASPs). The MBL-MASP complex can bind directly to phagocytes acting as a cross link between cell and phagocyte, or the conformational change in MASP once it is bound to MBL allows it to covert complement proteins 4 and 2 (C4 and C2 respectively), into a C3 convertase enzyme (C4b2a).[130] This enzyme anchors fragments of complement protein 3 (C3) on to the cell wall. These C3b fragments act as ligands for receptors on the surface of phagocytes, allowing another pathway for the phagocyte to bind (Figure 1.11).

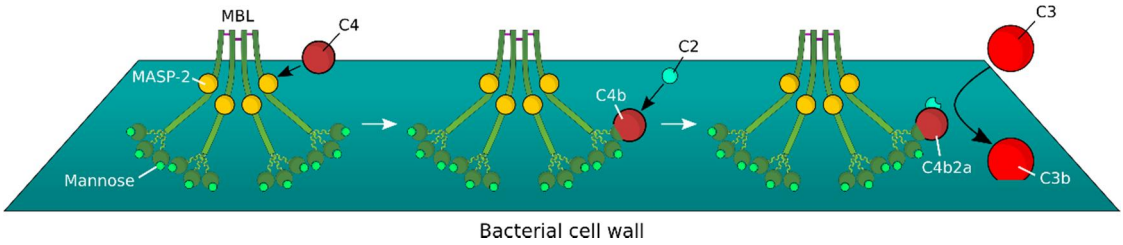

Figure 1.11. Cartoon representation of the process by which the MBL-associated serine proteases (MASP) complex anchors C3b to cell walls. The binding of MASP-2 to MBL causes a conformational change in the protein which allows it to covalently link C4 to either the cell wall or the MBL-MASP complex. C4b then exposes a focus point for the attachment of C2 to C4b by MASP-2. The resultant C4b2a complex acts as a C3 convertase and converts C3 into cell surface bound C3b.

Work by Neth *et al,* demonstrated how MBLs integration in the innate immune response affords it the ability to bind to the surface of a myriad of clinically relevant bacterial strains.[131] 80 clinically relevant microorganisms were screened for MBL binding and it was found that half, including *S. aureus,* bound MBL in some way. It has also been demonstrated that magnetic beads coated with MBL protein can be used to isolate bacteria using microfluidic devices.[132] The use of a human mannose binding lectin as a potential biofilm binding partner helps overcome the potential barrier presented by immunogenicity, as the protein itself is part of the human innate immune system. Therefore, in theory, the treatment would translate more easily to an *in vivo* experimental set up.

1.7 Project Aims

The overall aim of this project was to develop a novel method for biofilm imaging and treatment utilising microbubbles with surfaces that had been functionalised with ligands that bind staphylococcal biofilm components, as shown in Figure 1.12. This premise can then be brought forward as a novel method for imaging biofilms within the body on indwelling medical devices. A secondary aim was to develop a microfluidic system for biofilm growth that allowed non-invasive imaging of biofilms using confocal microscopy.

Chapter two of this body of work will describe the processes by which the biofilm targeting proteins were identified and developed, including their purification and 'screening' against biofilm targets. Chapter three will describe the development of the microfluidic system that was used for biofilm cultivation and imaging. Finally, chapter four will describe the experimental work performed to study the interaction between protein-conjugated microbubbles and *S. aureus* biofilms cultivated in the microfluidic flow system.

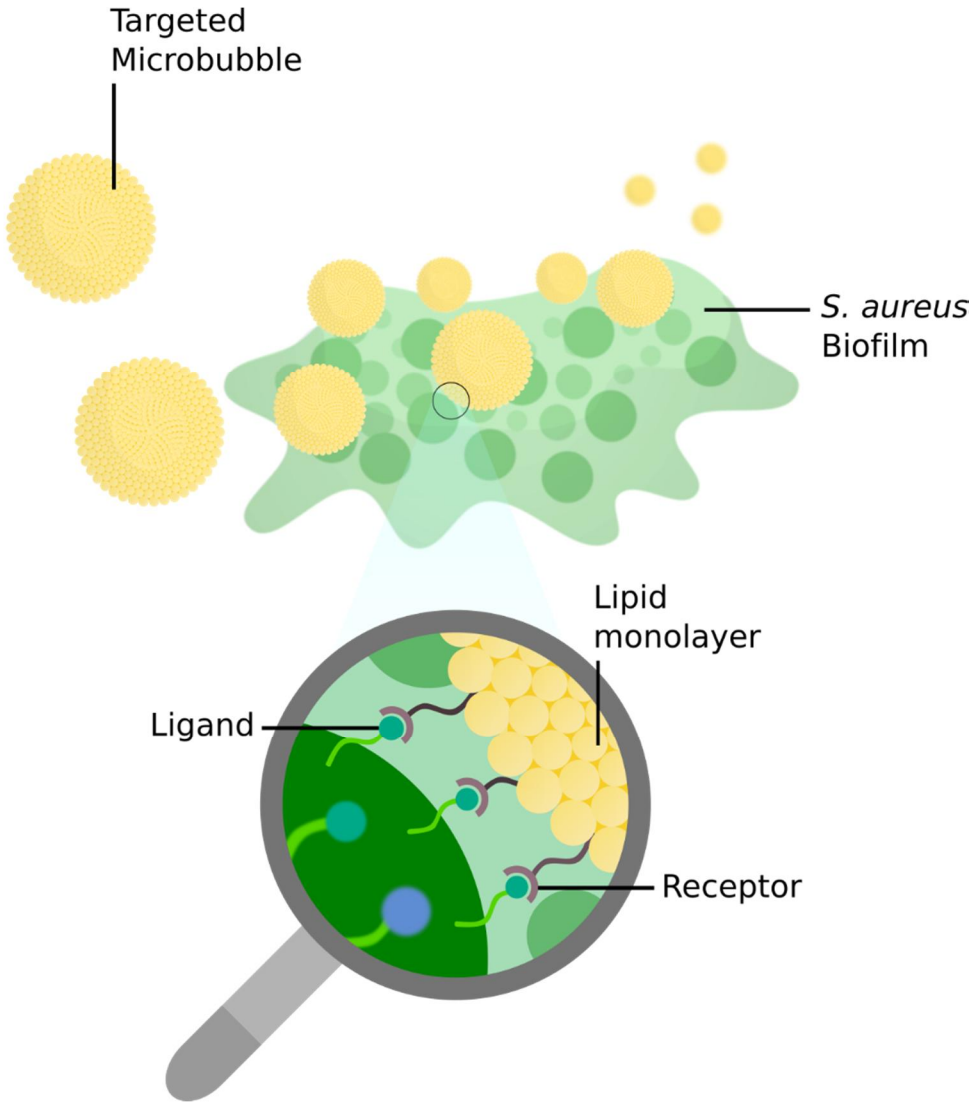

Figure 1.12. Cartoon representation of project aims.
Microbubbles are bound to staphylococcal biofilm. Microbubbles are coated in ligands that bind selectively to the surface of the biofilm, localising them to the site of infection.

2 Preparation and screening of biofilm targeting proteins

Results and Discussion

Part 1

This chapter of work explores the identification of suitable proteins that target the *S. aureus* biofilm. As introduced in Chapter 1, the two protein systems that were investigated were mannose binding lectin (MBL) and antibody mimetics known as 'Affimer' proteins. The practicality of expressing these proteins in an *E. coli* expression system was assessed along with the propensity of these proteins to bind a static biofilm prior to use in a microfluidic flow system.

2.1 Investigation of mannose binding lectin as a potential microbubble surface targeting molecule.

Figure 2.1. Work flow for work performed for the investigation into mannose binding lectin as a protein candidate.

2.1.1 Overexpression and purification of mannose binding lectin

Human mannose binding lectin (MBL) was chosen as a viable candidate for the protein-conjugated microbubbles. Its role in the innate immune system theoretically reduces risk of immunogenicity if taken through

to *in vivo* human experimentation. The procedure used for overexpression and purification of the protein in *E. coli* is detailed in the Biological Methods Section 6.2.4. *E. coli* cells harbouring the plasmid encoding the expression of the MBL protein (provided by Kurt Drickamer, Imperial College London) were cultured, lysed and the protein purified from the cell lysate adapted from work by Drickamer and co-workers that had already established that the human MBL protein could be expressed in a prokaryotic expression system, such as that of *E. coli*.[133] MBL's ability to bind surface mannose sugars was exploited during purification using an affinity resin consisting of mannose covalently linked to insoluble beads (Figure 2.2) to "capture" MBL from the cell lysate. MBL was then eluted from the resin using ethylenediaminetetraacetic acid (EDTA), which complexes and sequesters the Ca^{2+} ions, which the protein requires for binding. The method used in this project had previously been employed to isolate MBL by Butler and co-workers, and is a common method of purifying MBL from various media.[134]

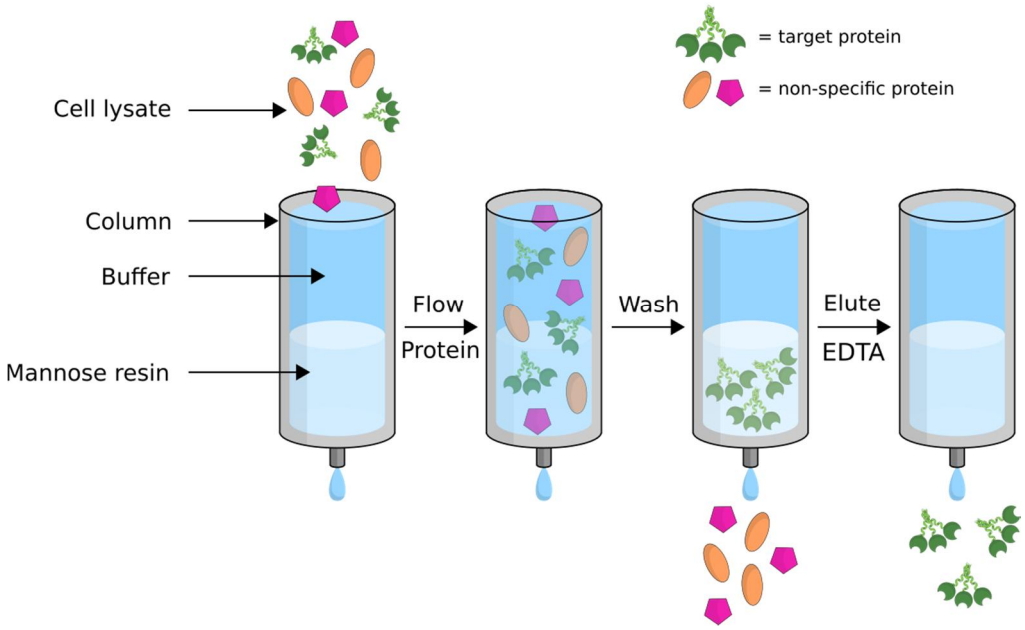

Figure 2.2. Cartoon representation of mannose affinity chromatography. The cell lysate contains a number of soluble proteins including mannose binding lectin (MBL). When flowed over the mannose affinity resin, only MBL is retained and the protein impurities elute from the column. The addition of EDTA removes Ca^{2+} ions required for binding of MBL to mannose, which causes the protein to elute from the column.

Fractions from the mannose affinity column were analysed by sodium dodecyl sulphate polyacrylamide gel electrophoresis (SDS-PAGE), a technique that separates proteins by their molecular weight (Figure 2.3).[135] This technique helps to determine the protein content of a sample, and using a set of protein markers as a standard, gives an approximate weight.

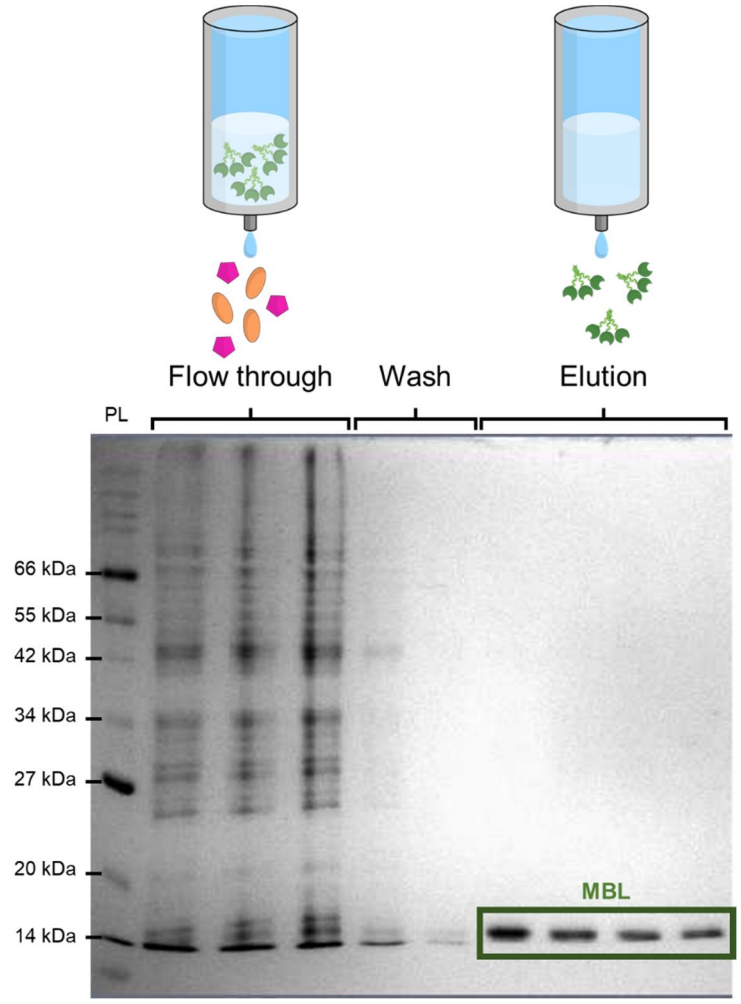

Figure 2.3. SDS-PAGE gel of mannose affinity chromatography purification of MBL from the cell lysate.

The protein marker ladder (PL) gave an approximate position of molecular weights on the gel. Flow through was the cell lysate after it was flowed over the resin, lanes show the presence of proteins in the cell lysate that do not bind the mannose resin. Washes were performed by flowing buffer over the resin. Protein still bound to the column was removed by buffer containing EDTA. Presence of bands at around ~ 16 kDa were attributed to MBL.

Although SDS-PAGE can give an initial indication as to whether the target protein had been isolated from the cell lysate, this cannot be confirmed until a precise weight is measured. The elution fractions were therefore analysed by liquid chromatography mass spectroscopy (LCMS) (Figure 2.4).

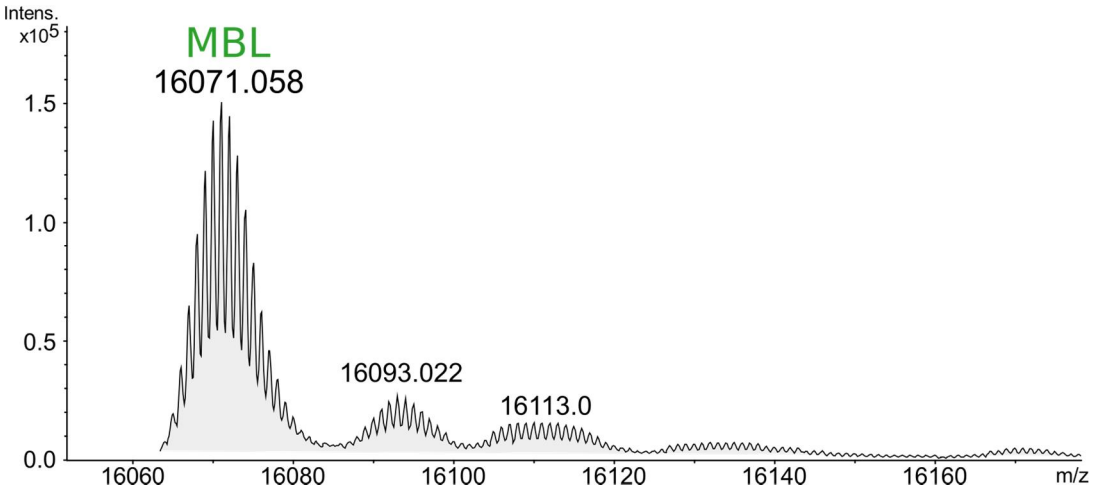

Figure 2.4. The deconvoluted mass spectrum of EDTA elutions from mannose affinity chromatography purification of MBL.
This mass spectrum shows a peak at 16,071 Da. Presence of this peak indicated that the sample contained MBL. Peaks at 16093 and 16113 Da associated with sodium and potassium adducts.

2.1.2 Chemical Ligation methods

After successful purification of the MBL protein, work-flow focussed on employing chemical ligation methods to conjugate the protein to the surface of the microbubbles. There are a variety of chemical ligation pathways that can be utilised to functionalise proteins with chemical tags. The first system investigated was the use of a biotin-streptavidin-biotin interaction.

2.1.2.1 Sortase A Ligation

Sortase A is a transpeptidase enzyme that catalyses the anchoring of proteins to bacterial cell walls such as that of *S. aureus*.[136] Sortase A recognises peptides with an LPXTG sequence, where L is leucine, P is proline, X is any amino acid, T is threonine and G is glycine (Figure 2.5). A catalytic cysteine residue at the enzyme's active site forms a thioacyl intermediate when the threonine-glycine peptide bond is cleaved. This thioacyl

intermediate can then accept an N-terminal oligoglycine nucleophile to create a new peptide bond.[137] Sortase A can be applied practically for use as a protein labelling device, with the essential components for the labelling reaction being the LPXTG binding motif on the substrate protein attached to a desired label and a second molecule having an N-terminus with a suitable number of glycine residues, to act as a nucleophile [138].

The process itself is reversible therefore a large amount of nucleophilic labelling regent is needed to shift the equilibrium towards product formation. In contrast, the use of a depsipeptide substrate releases an alcohol upon ligation, which is a poor nucleophile and does not react with the tagged protein product to re-establish the depsipeptide reagent (Figure 2.5, b).[138]

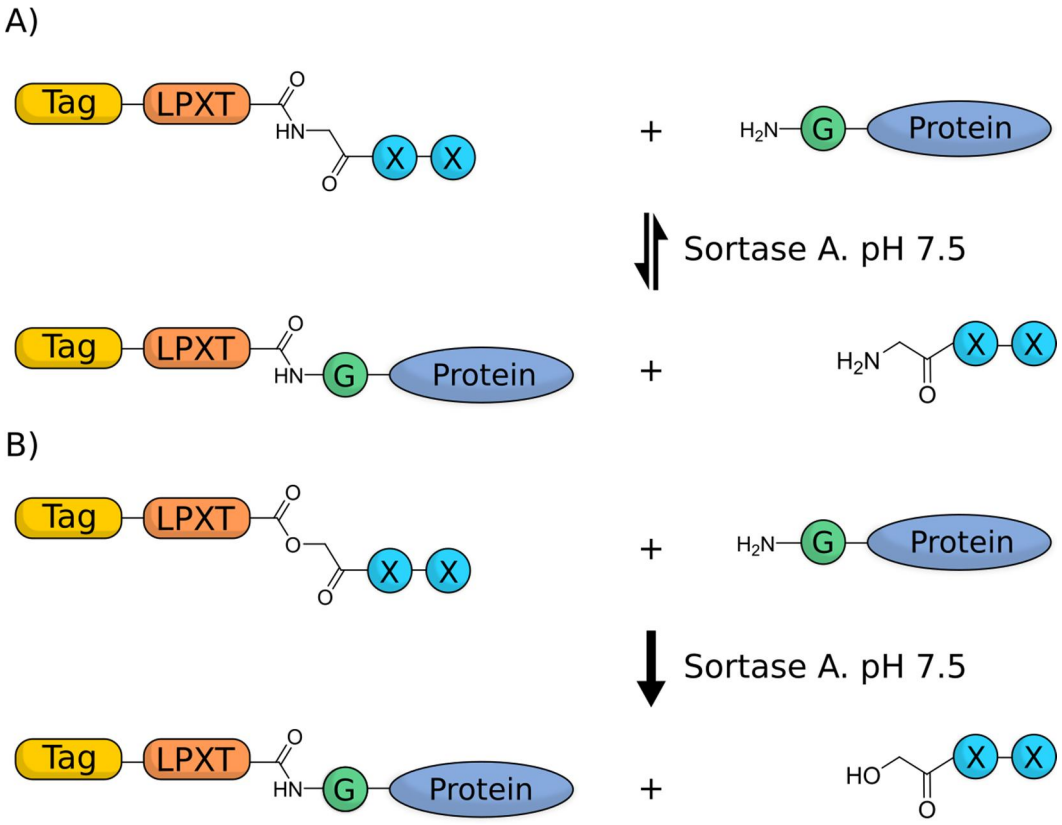

Figure 2.5. The reaction scheme for Sortase A ligation of a tag onto a protein. Scheme (a) shows when the peptide has an amide bond between the threonine and glycine residues the reaction is reversible. Scheme (b) shows that incorporating an ester linkage here instead stops the reverse reaction.

The aim was to conjugate MBL to the surface of the bubble using the association of biotin to streptavidin, a commonly used conjugation system due

to the high affinity (K_d = 4 x 10^{-14} M [139]) of the biotin-streptavidin interaction (Figure 2.6).

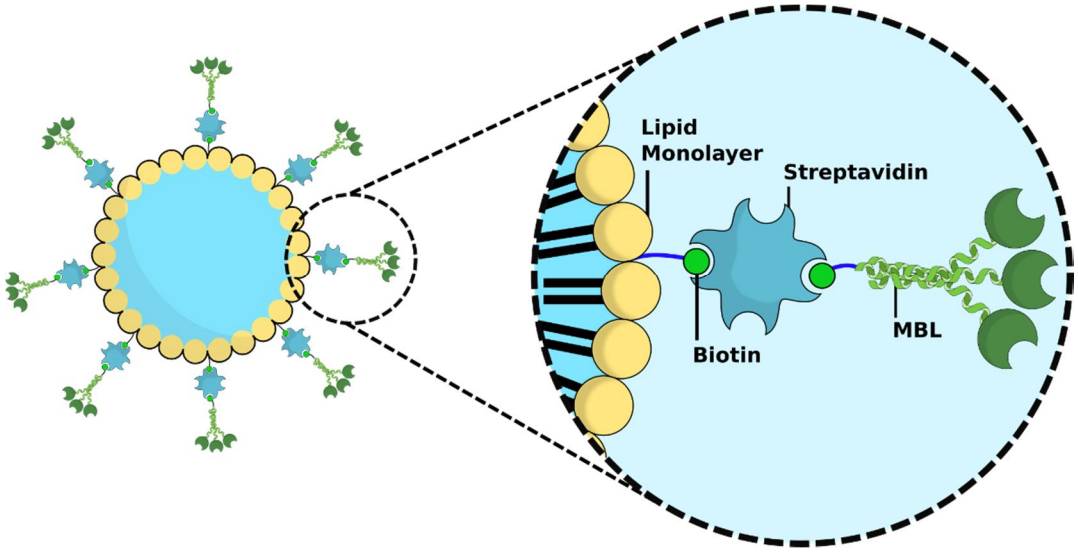

Figure 2.6. The proposed system for conjugation of MBL to the microbubble surface.
The lipid monolayer and MBL will be functionalised with biotin, streptavidin is then used to bridge the two components together.

The use of the biotin-streptavidin reaction is one common in current methods for manufacturing targeting microbubbles. Although these targeted-MBs are more commonly used to target mammalian cells, such as those concerned with cancers, a common thread is the use of the biotin-streptavidin association as a strong anchor for targeting molecules.[140, 141]

In order to label MBL with biotin, a depsipeptide substrate for the sortase ligation reaction, see Figure 2.5b, incorporating the LPXTG motif and biotin moiety had to be synthesised.

2.1.2.2 Solid Phase Peptide Synthesis

Although biological systems can generate polypeptide chains hundreds of amino acids long, synthetic routes for polypeptides chain production are limited in the length they can achieve. Furthermore, incorporation of a depsipeptide is impractical through bacterial expression due to the need for an ester-linked peptide. A common technique used to synthesise peptides of

relatively short lengths is solid phase peptide synthesis (SPPS). In SPPS, polypeptides are synthesised from C- to N-terminus, in a step-wise manner on a solid support (Figure 2.7). The method outlined in Figure 2.8 was used to synthesise the Biotin-GYLPEToGG ('o' denoting the location of the ester linkage) depsipeptide. Detailed experimental procedures for synthesis can be found in Section 6.1.1.

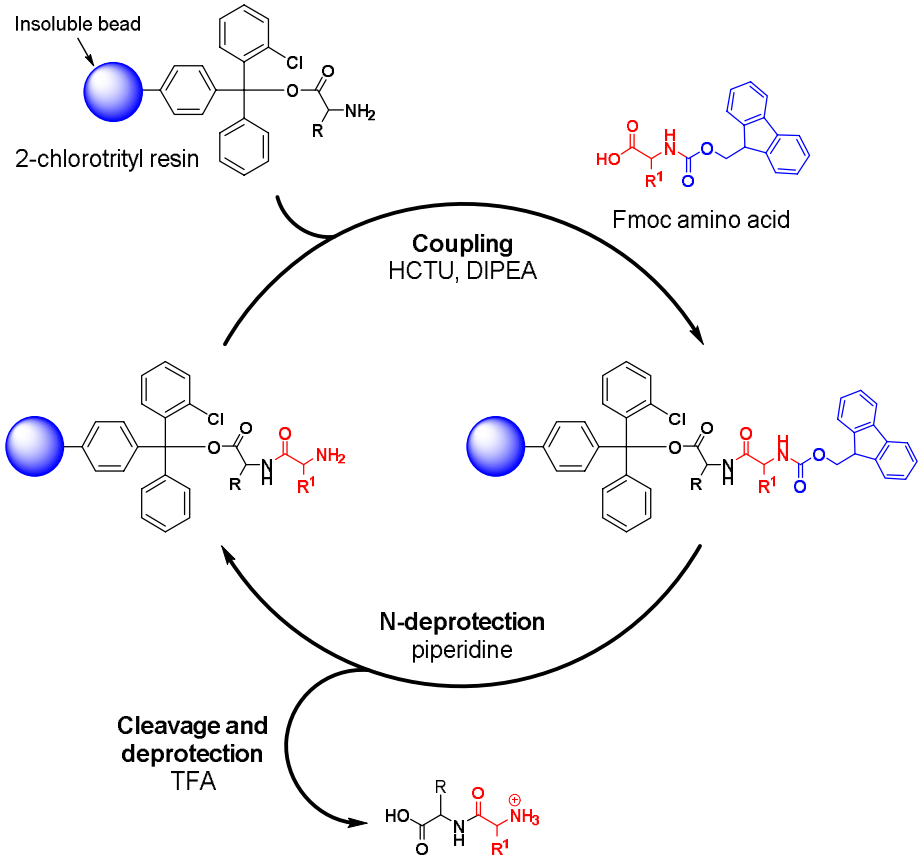

Figure 2.7. Solid Phase Peptide Synthesis cycle reaction scheme using 2-chlorotrityl resin.

The resin is functionalised with the C-terminal amino acid in the intended sequence. The resin is then coupled with an amino acid building block that has an Fluorenylmethyloxycarbonyl chloride (Fmoc) chemical group (shown in blue), preventing the N-terminal amino group from reacting. HCTU and DIPEA are used as coupling agents. Once coupled, the polypeptide has the Fmoc protecting group removed with piperidine. From this point the polypeptide can either be cleaved from the resin and purified, or it can be coupled again with another amino acid building block. The cycle can be repeated until the required polypeptide sequence is achieved, with the final step being cleavage of polypeptide from the resin.

The polypeptide chain was synthesised by SPPS up to the N-terminal glycine. It was then functionalised with biotin by reacting the N-terminal amino group with a biotin N-hydroxysuccinimide (NHS) ester.

The Biotin-NHS could either be coupled with the polypeptide on the resin, or the polypeptide can be cleaved off the resin and reacted with the Biotin-NHS in solution. The resin provides an insoluble support for the peptide reaction and therefore unwanted reactants and products can be removed by washing through a filter that retains the insoluble resin whilst removing soluble waste. However this method requires a higher relative amount of the NHS ester. Performing the reaction with the peptide in solution allows for the use of fewer molar equivalents of the NHS ester, but purification from all the other reagents could be more problematic without the insoluble resin support.

In order to preserve Biotin-NHS stocks the reaction was performed in solution. The purified biotin depsipeptide was aliquoted and freeze dried.

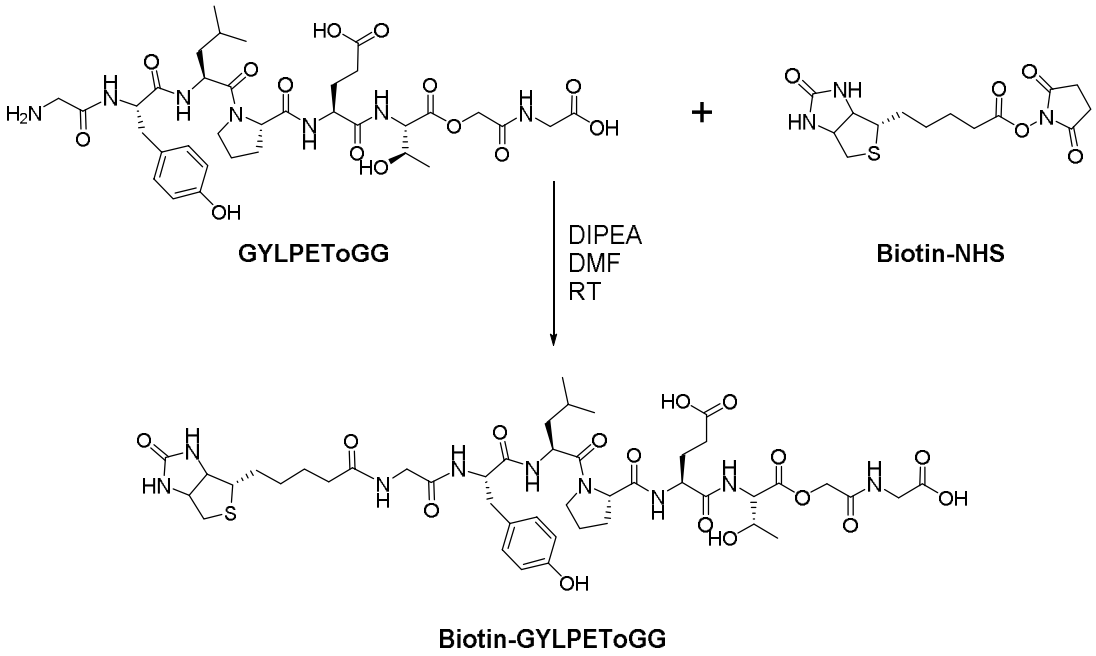

Figure 2.8. Reaction scheme for the coupling of the depsipeptide to Biotin-NHS ester.

2.1.2.3 Sortase labelling reaction

Sortase ligation was performed with MBL and the synthesised Biotin-depsipeptide. The N-terminal glycine required for sortase ligation to the protein was present in the MBL construct.

Variants of the sortase A enzyme that have improved catalytic activity exist; these are named sortase 5M and sortase 7M, which are named accordingly to the number of point mutations that differ in the amino acid sequence from wild-type sortase A. Of these three sortase enzymes, only the sortase 7M enzyme was successful for labelling MBL with the biotin-depsipeptide (Figure 2.9). The experiment yielded only a small amount of biotinylated MBL protein, which may be attributed to the sortase 7M enzyme hydrolysing the biotin group from the tagged protein. Although only a small amount of MBL was biotinylated by the enzyme, subsequent attempts to repeat the experiment with increasing quantities of biotin depsipeptide and MBL concentration proved fruitless.

The experimental results from Figure 2.9 could not be replicated. Moving forward it was decided that a different route to labelling MBL with biotin should be investigated.

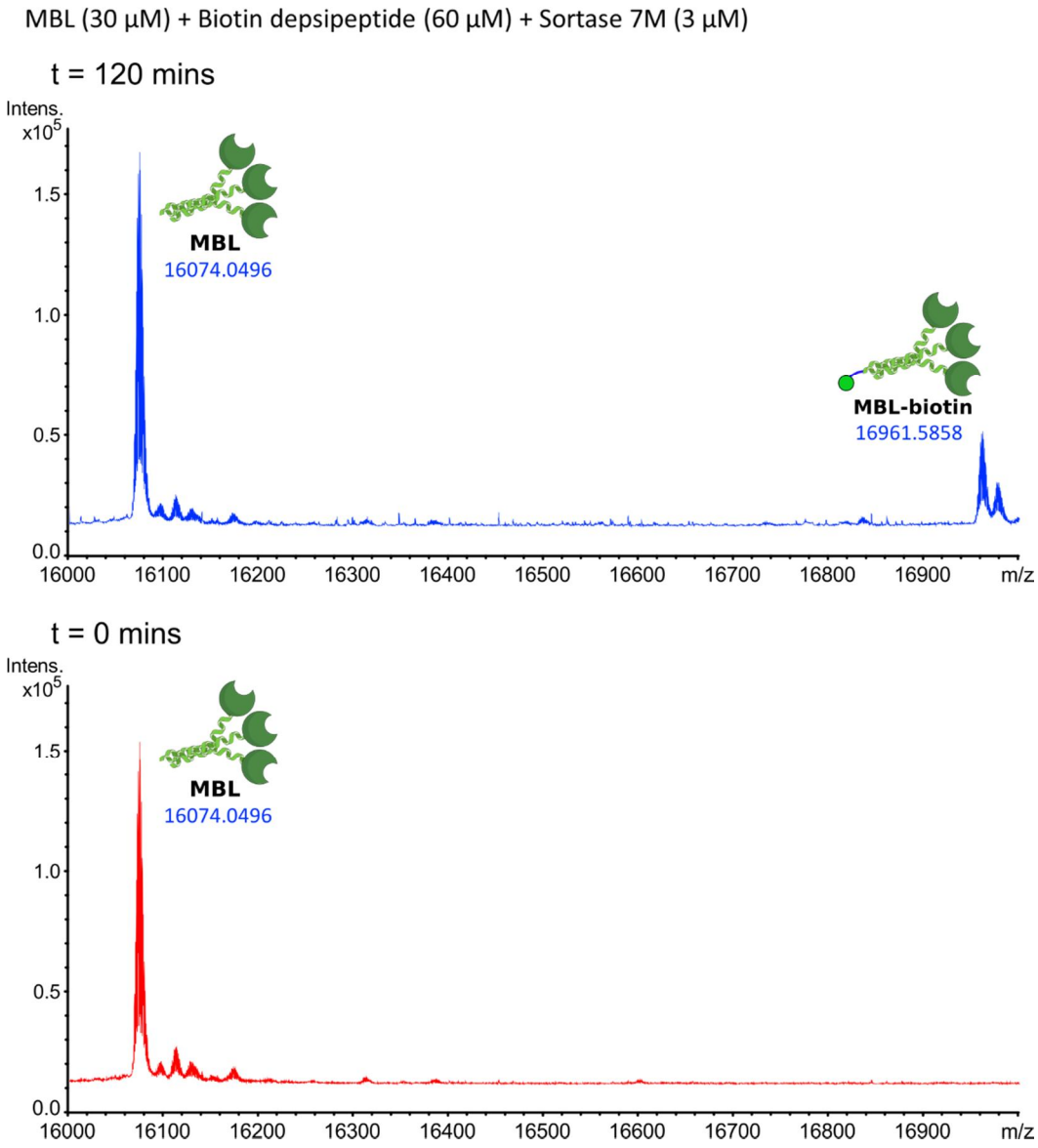

Figure 2.9. LCMS spectra of sortase 7M ligation of MBL.

Time course reaction of Sortase 7M enzyme attaching biotin to the proteins N-terminus via the biotin-depsipeptide substrate. Spectra show reaction contents at t = 0 mins and 120 mins. Peak at 16,074 Da shows presence of MBL and peak at 16,961 Da shows presence of biotin-tagged MBL protein.

2.1.2.4 Mutation of MBL to enable oxime ligation

Oxime ligation involves covalent attachment of a molecule of interest bearing an oxyamine group to a macromolecule that has an aldehyde or ketone function to form an oxime bond, which is stable under physiological conditions (Figure 2.10).[142] Site-directed mutagenesis was performed to change the codon for the N-terminal glycine of MBL to a codon for a serine at

that position; oxidation of the resulting serine would allow oxime ligation to covalently label the MBL with biotin.

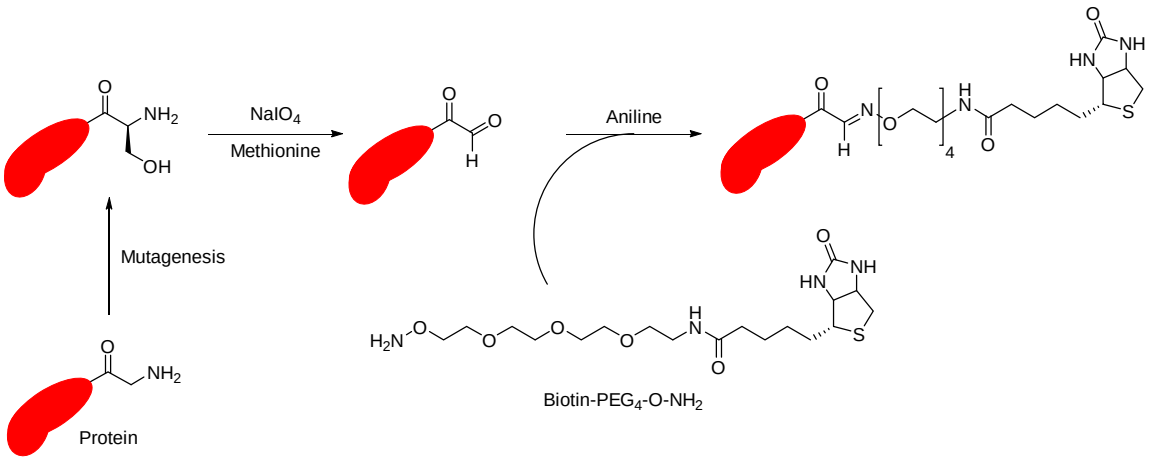

Figure 2.10. Reaction scheme of an oxime ligation.
A plasmid coding for a protein with an N-terminal glycine was modified by site-directed mutagenesis to yield a protein with an N-terminal serine. The protein was then oxidised with sodium periodate to yield an aldehyde group. This aldehyde group was then reacted with biotin-PEG$_4$-O-NH$_2$, covalently linking biotin to the protein.

2.1.2.5 Site-Directed Mutagenesis of MBL plasmid

Plasmid pINIIIompA2 is a plasmid donated by Kurt Drickamer (Imperial College London) that encodes for the expression of human MBL. DNA primers were designed that were complementary to the section of the MBL expressing plasmid coding for the N-terminus of the MBL protein, with one base pair change that would change the codon to one that would encode for a serine residue (see method section 6.2.12). When the primer annealed to the plasmid during PCR, the amplified DNA would carry the codon for serine at this position instead of glycine. The mutated nucleotide sequence encoded a new MBL mutant, named G1S. The first letter of the mutant label corresponds to the amino acid from the wild-type protein you are mutating, the number is the position in the amino acid sequence that residue is, and the final letter is the amino acid you are substituting in. For this mutant, the glycine (G) at

position 1 in the amino acid sequence was substituted for a serine (S), hence G-1-S. The nucleotide sequence of the new plasmid confirmed that it had the correct DNA sequence, for the expression of the G1S mutant.

The new plasmid DNA was extracted and then transfected into *E. coli* BL21 Gold cells, which overexpressed the MBL G1S mutated protein. The protein was purified on a mannose affinity resin as in section 6.2.6.1 and concentrated. However, during concentration of the protein, a precipitate began to form. The concentration of the protein was measured by recording its absorbance at 280 nm using a UV-vis spectrometer.[143] A decrease in A_{280} indicated that the precipitate contained proteins.

Sample analysis using Ultraviolet – visible light (UV-Vis) spectroscopy was expected to show maximum absorbance at 280 nm, as is the case with protein in solution, however the spectrum (Figure 2.11) showed the maximum absorbance of the G1S mutant was at 260 nm, which indicated the presence of DNA in the sample. As DNA should not have any affinity for the mannose resin, this observation suggested that the protein itself was somehow associating with DNA in the cell lysate. If this was the case, DNA fragments may have been causing aggregation of protein molecules in solution which could cause the MBL to precipitate.

During lysis of the cells, DNAse enzymes were used to digest any DNA that was present in the cell lysate, so this process was clearly failing. If the DNA generating the A_{260} absorbance maxima in the UV/Vis spectrum was not being digested by the DNAse, it was hypothesised that DNA was being protected through an association to the MBL protein.

The pINIIIompA2 MBL plasmid encodes for an N-terminus that has a periplasmic targeting peptide sequence that shuttles it into the periplasm of the *E. coli* cell, known as a signal peptide.[144] The targeting peptide is cleaved to yield the MBL construct.[145] To remove the possibility of MBL coming into proximity to DNA during the purification procedure, a periplasmic extraction was performed (Section 2.1.3.1) to isolate the protein from the cells but without the need for cell lysis in an attempt to reduce the risk of exposing MBL to DNA. By ejecting the MBL from the periplasm, the likelihood of MBL encountering any DNA was mitigated by omitting the cell lysis step.

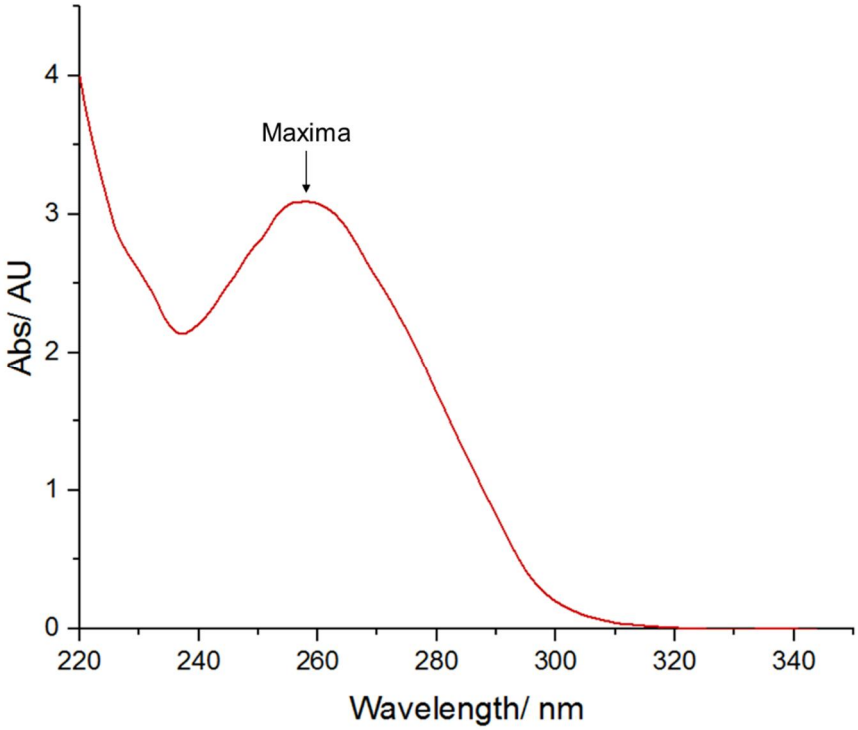

Figure 2.11. UV-vis spectrum of mannose binding lectin mutant G1S, post mannose affinity purification.
Maxima at A260 indicates presence of DNA in sample.

2.1.3 Solubility issues of MBL

2.1.3.1 Periplasmic Extraction of MBL

Periplasmic extractions were performed by suspending cells in a high sucrose solution, then re-suspending the cells in cold water. The osmotic shock causes the outer membrane of the cells to rupture, thus releasing any proteins within the periplasm without lysing the cells.[146] Once the proteins had been extracted, they were concentrated using ultrafiltration. Again, a precipitate began to form during ultrafiltration, which was assumed to be MBL and the experiment was abandoned.

2.1.3.2 Comparison of *E. coli* Rosetta and BL21 Gold DE3 cells for expression of MBL.

Subsequent overexpression of the MBL protein was fruitless and it appeared MBL was being produced in cells at relatively low amounts. Analysis of the protein's DNA sequence revealed the presence of a number of 'rare

codons'. Rare codons are defined as codons that don't regularly appear in *E. coli* DNA, and are sometimes less frequently translated by the bacteria.[147] The presence of these rare codons may have been contributing to the inability of the cells to produce MBL in large amounts. A possible solution was to express the protein in *E. coli* Rosetta cells, which carry a plasmid encoding the rare tRNAs and synthetases needed to attach their cognate amino acids when expressing these rare codons. An expression study was therefore performed where the ability of these Rosetta cells to express MBL was analysed against that of the BL21 Gold cells.

The plasmid containing the MBL expressing gene was transfected into Rosetta *E. coli* cells which were cultured alongside the traditionally used BL21 Gold *E. coli* cells. The ability of these cells to express MBL protein was analysed by monitoring the protein content of different parts of the cell lysate. The different components of the cell lysate were analysed by SDS-PAGE (Figure 2.12)

The expression study showed that although the MBL expressing plasmid did contain 'rare codons', Rosetta cells did not synthesise MBL more efficiently than the previously used *E. coli* BL21 Gold DE3 cells. Therefore the issue surrounding the poor expression of the MBL protein did not pertain to its rare codons. At this stage, issues had arisen for both the solubility of the MBL protein, and poor expression of the protein in *E. coli* cells. To ameliorate the latter, all plasmids designed for protein expression in future experiments had their nucleotide sequences 'codon optimised' to omit rare codons.

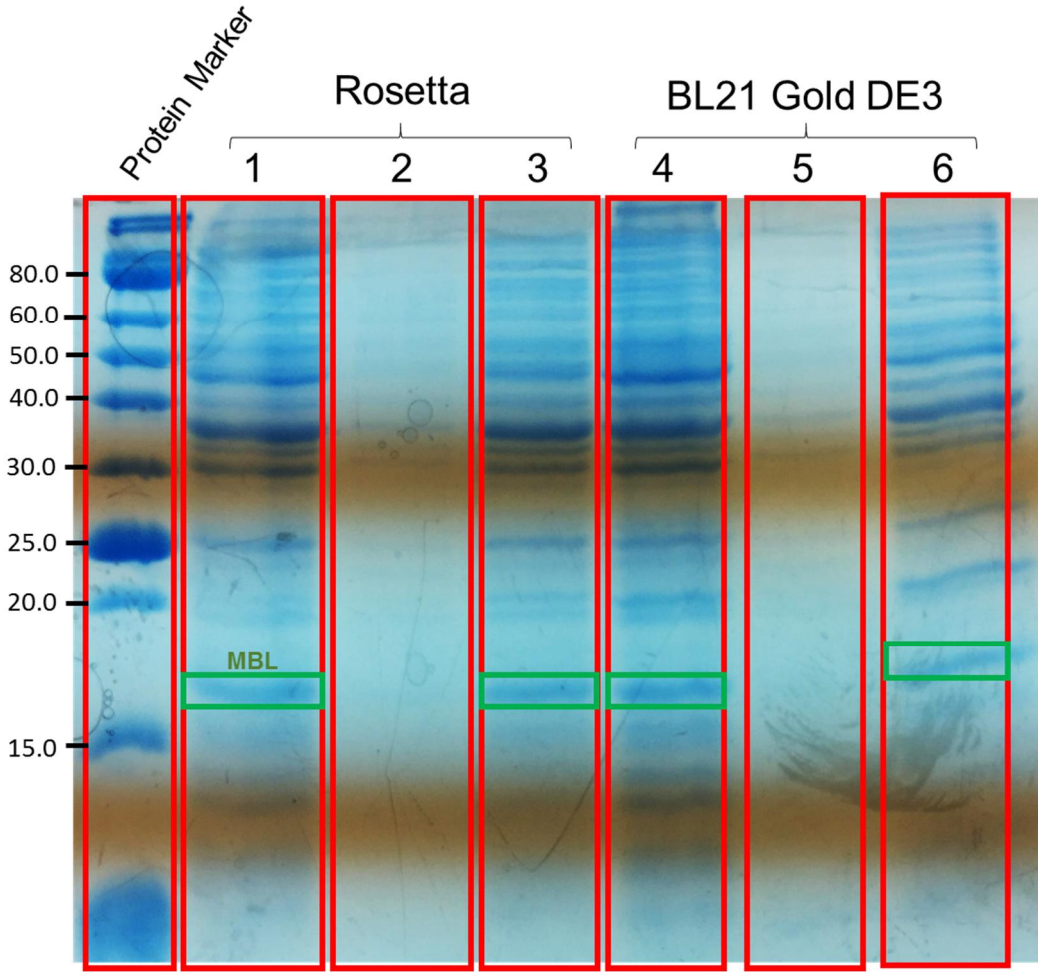

Figure 2.12. SDS-PAGE gel of E. coli expression study.
Numbers 1-3 are samples from Rosetta cell expression and 4-6 for BL21 Gold cells. 1,4) Proteins precipitated from the surrounding cell media by addition of ethanol, 2,5) sample of cells post lysis, containing soluble and insoluble components, 3,6) Soluble components of cell lysis, with insoluble components removed by ultracentrifugation. Bands at around 16 kDa correspond to MBL. Relative intensities of MBL bands indicate Rosetta do not overexpress MBL protein any more efficiently than BL21 Gold cells.

2.1.3.3 MBP-MBL Fusion Protein

It became apparent that in order to successfully express and isolate MBL protein the issue of solubility needed to be addressed. By incorporating a protein of choice into a fusion protein, which contains a different protein whose solubility is significantly higher, the latter protein can be used as a

solubility tag to help improve the solubility of the whole fusion protein complex.[148] Maltose binding protein (MBP) is a commonly used solubility tag.[149] When incorporated into a fusion protein, its affinity to amylose can also be utilised as a purification method using amylose affinity chromatography. In practice, this method aligns exactly with the affinity chromatographies outlined previously (Figure 2.2), with the protein being eluted from the resin either using a glucose, amylose or maltose solution [150].

A new protein construct was designed which incorporated MBP into a fusion protein with MBL (Figure 2.2). MBP was used to purify the fusion protein by amylose affinity chromatography. The lysate was flowed over amylose immobilised to an insoluble resin, to capture the fusion protein. A solution of maltose was then used to elute the protein from the amylose resin, as MBP preferentially binds maltose over the amylose resin. MBP has a high affinity for maltose (K_D = 2 µM [151]) so it is difficult to remove maltose post purification in order to reuse the protein as a purification tag. To circumvent this issue, a polyhistidine purification tag (His-tag) was placed between the MBP and MBL sites. A His-tag is a sequence of usually six histidine residues in a peptide sequence that can be utilised for purification.[152] Histidine's imidazole ring can complex to immobilised metal ions such as Nickel. In addition to this, a tobacco etch virus (TEV) protease cleavage site was added between the two protein domains, so once the fusion protein had been purified, the two proteins could be separated by an enzymatic digestion (Figure 2.13, a, b). A TEV protease enzyme was used that also had a His-tag in its peptide sequence, so that the MBP and the protease could be sequestered from the MBL solution in the same purification step (Figure 2.13, c).

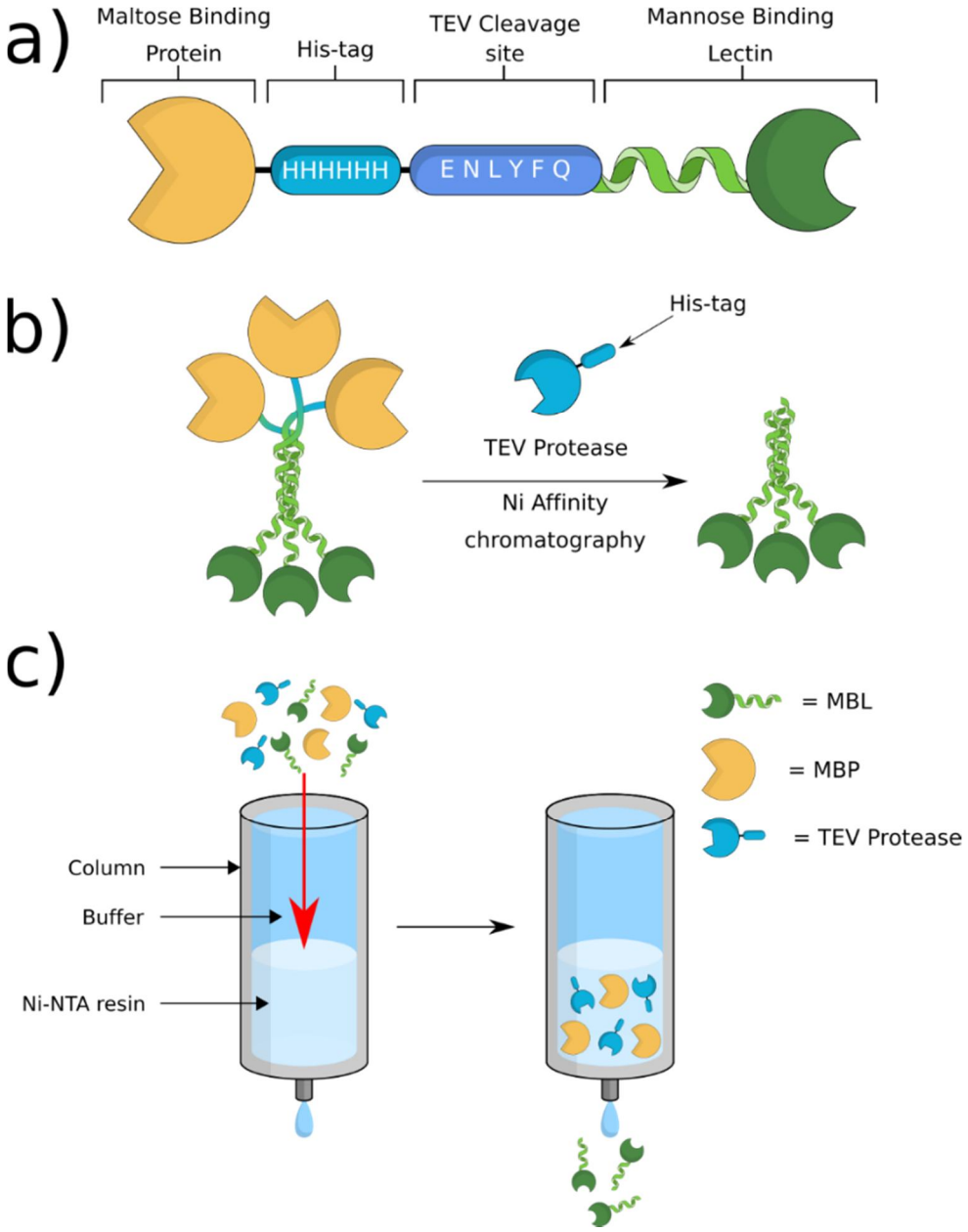

Figure 2.13. Cartoon representation of new MBP-MBL construct, method of cleavage and its purification.

a) protein construct of MBP-MBL fusion protein and cartoon representation beneath. b) Proposed method of purification after cleavage of two proteins with TEV protease. On the left the expected bouquet-like structure of the MBP-MBL trimer and on the right the cleaved MBL trimer. Both the cleaved MBP and TEV protease contain a his-tag required for Nickel affinity chromatography. c) proposed method of purification of MBL from crude cleaved protein solution. The his-tagged TEV protease and MBP should be retained on a Ni affinity resin and only MBL should be eluted.

2.1.3.4 MBP-MBL overexpression and purification

A pMalp5x vector containing genetic code for the expression of the MBP-MBL fusion protein was designed and ordered from Genscript, then transformed into *E. coli* BL21 Gold cells as described in section 6.2.3. The cells were then used to overexpress the fusion protein. The cells were lysed and the fusion protein isolated from the cell lysate by amylose affinity chromatography.

Analysis of the elution fractions by SDS-PAGE showed the presence of two protein species, one band at ~56 kDa and another at around ~38 kDa (Figure 2.14, a). Analysis of elution fraction 3 by LCMS showed the presence of a number of protein species (Figure 2.14, b). The signal at 58924 Da corresponds to the MBP-MBL fusion protein, while the signals between 42 and 44 kDa are thought to correspond to MBP. These species may have been wildtype MBP expressed naturally by the cell or variants of recombinant MBP caused by incomplete expression of the gene i.e. a truncate fusion protein. As an amylose resin had been used for purification, any proteins with the ability to bind amylose i.e. MBP and the MBP-MBL fusion protein, were retained on the column from the cell lysate.

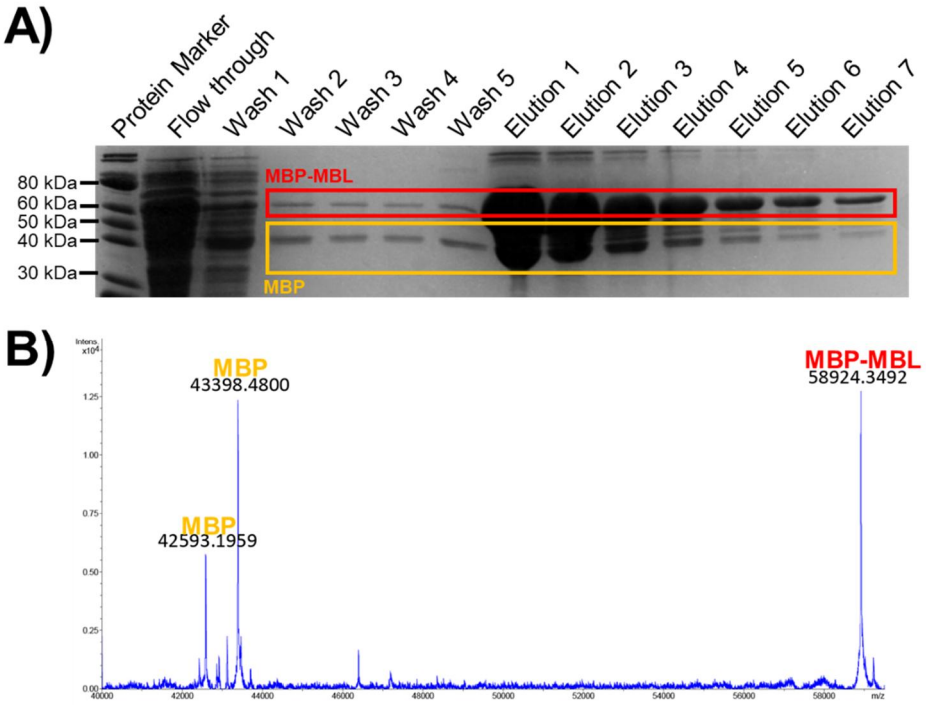

Figure 2.14. SDS-PAGE gel analysis of MBP-MBL purification and LCMS of eluted protein.

a) SDS-PAGE gel of amylose affinity chromatography purification. Bands highlighted in red attributed to MBP-MBL and bands highlighted in yellow to MBP. b) LCMS of elution 3 from amylose column. Peaks between 42-44 kDa attributed to MBP species, peak at 58924 Da attributed to MBP-MBL.

2.1.3.5 Purifying the Fusion Protein from MBP.

Two methods of removing the MBP impurity were investigated. If the MBP protein impurity was a result of natural MBP expression of the *E. coli* cells, the fusion protein could be separated from the crude solution by Nickel affinity chromatography utilising its his-tag. Alternatively, the fusion protein's MBL component could be used to purify the protein by mannose affinity chromatography. If the impurity was due to incomplete expression or premature cleavage of the fusion protein, then the MBP may still have its own his-tag as a legacy from the fusion protein. Fractionation of the crude fusion protein solution was assessed by both of these methods in order to identify the most effective means of purification (Figure 2.15).

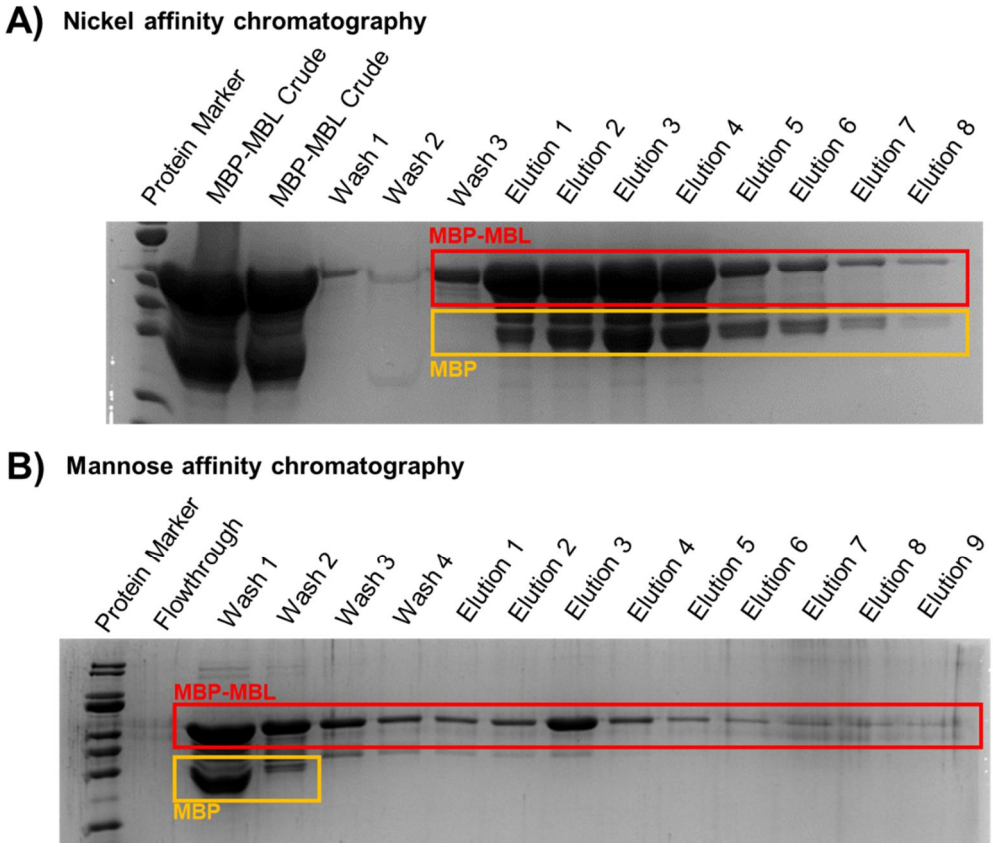

Figure 2.15. Nickel and mannose affinity chromatography SDS-PAGE gel analysis of MBL-MBP purification.
A) SDS-PAGE gel of nickel affinity chromatography purification of crude MBP-MBL stock. Elutions show that the MBP impurity does in fact contain a his-tag. B) SDS-PAGE gel of mannose affinity chromatography purification of crude MBP-MBL stock. Absence of MBP band in elutions show that MBP-MBL can be purified from crude stock with mannose affinity resin.

Though the most effective route to purifying the MBP-MBL fusion protein was in fact mannose affinity chromatography, the nickel affinity chromatography SDS-PAGE gel highlighted an important point, that the MBP impurity had affinity for the nickel resin. Therefore if the crude MBP-MBL mixture containing the MBP impurity was combined with the TEV protease cleavage step, then upon passing the whole cleavage cocktail over a nickel affinity column, the only component that would not adhere to the resin would be cleaved MBL. This would mean that the crude MBP-MBL stock would not need to be purified pre-cleavage reaction.

The crude MBP-MBL stock (100 µM) was combined with TEV protease (25 mol%) and incubated overnight at 4 ºC. The resultant cleavage solution was flowed over a nickel affinity column containing 3 mL of resin (Figure 2.16).

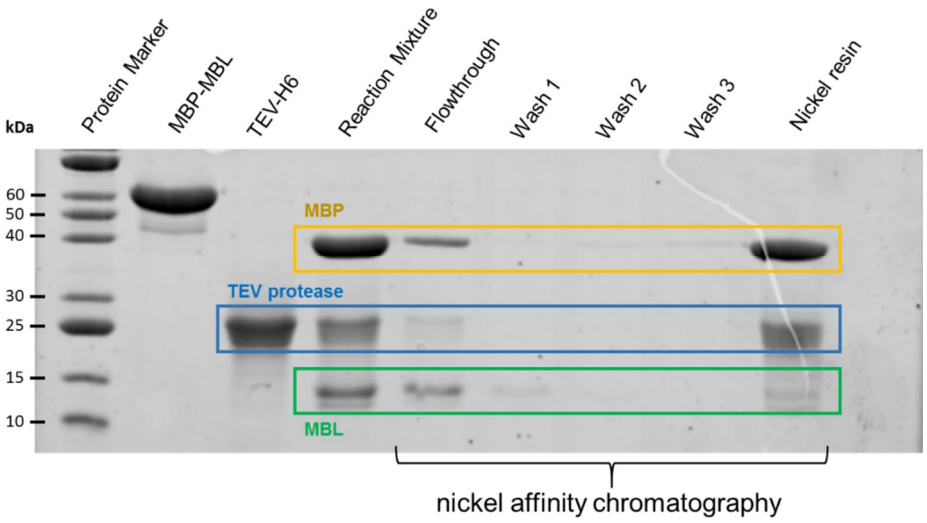

Figure 2.16. SDS-PAGE gel of cleavage reaction and accompanying nickel affinity column of MBP-MBL protein.
The reaction mixture shows no band for MBP-MBL indicating full cleavage of fusion protein. Bands for MBP, TEV-protease and MBL are present in the reaction mixture. The reaction mixture is then flowed over nickel affinity resin, then washed. Nickel resin was also loaded onto the gel to ascertain what species had bound. Flow through indicates that the resin may have been overloaded due to the presence of the MBP band. Presence of MBL band in nickel resin indicates that some MBL is adhering to the nickel resin.

The resultant SDS-PAGE gel indicated that both the cleaved MBP and the cleaved MBL were adhering to the nickel resin. In order to eliminate the presence of MBP in the flow through, the experiment was repeated with a higher volume (9 mL) of nickel resin (Figure 2.17, a). SDS-PAGE was performed on the resultant fractions, and buffer containing 300 mM imidazole was flowed over the resin to remove any bound protein species. The elution was then analysed by LCMS (Figure 2.17, b), which showed the presence of MBL in the elution, indicating MBL was in fact adhering to the nickel resin.

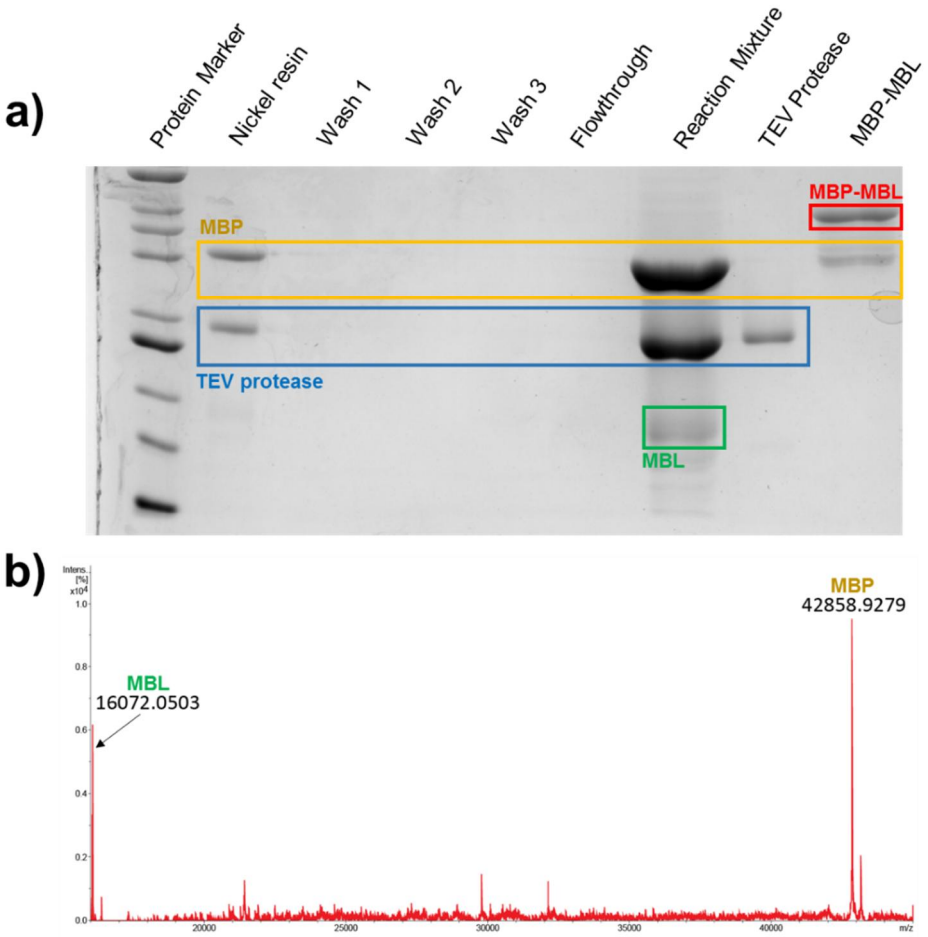

Figure 2.17. SDS-PAGE gel analysis of MBP-MBL cleavage reaction and LCMS of reaction mixture.

a) SDS-PAGE gel of cleavage reaction and Nickel affinity chromatography column. No protein appears to be present in flowthrough, however MBL does not seem to be present in the resin lane. b) LCMS spectra of elution from nickel resin, shows nthe presence of cleaved MBL at 16072 Da and cleaved MBP at 42858 Da, indicating MBL had adhered to the nickel resin.

The binding of MBL to the nickel resin indicated that the MBL complex had an unexpected affinity for nickel. A possible reason may be that the trimeric MBL oligomer is forming a complex consisting of two copies of the MBL monomer and one copy of uncleaved MBP-MBL fusion protein. However, if there was MBP-MBL within the complex the protein would appear as a band on the SDS-PAGE gel and have a signal in the LCMS spectrum. This method of purifying the MBP-MBL cleavage product was deemed ineffective and a

new method utilising size exclusion chromatography (SEC) was chosen for further investigation.

2.1.3.6 Size Exclusion Purification of MBP-MBL

Size exclusion chromatography (SEC), also known as gel filtration chromatography, is a method of purifying proteins according to their relative sizes.[153] This technique employs a column packed with insoluble, but highly hydrated polymer beads which have pores that act as channels. Small proteins can enter these pores and therefore have access to a larger volume of liquid, whereas larger molecules do not and move faster through the column. This means larger molecules elute more quickly than smaller molecules (Figure 2.18).

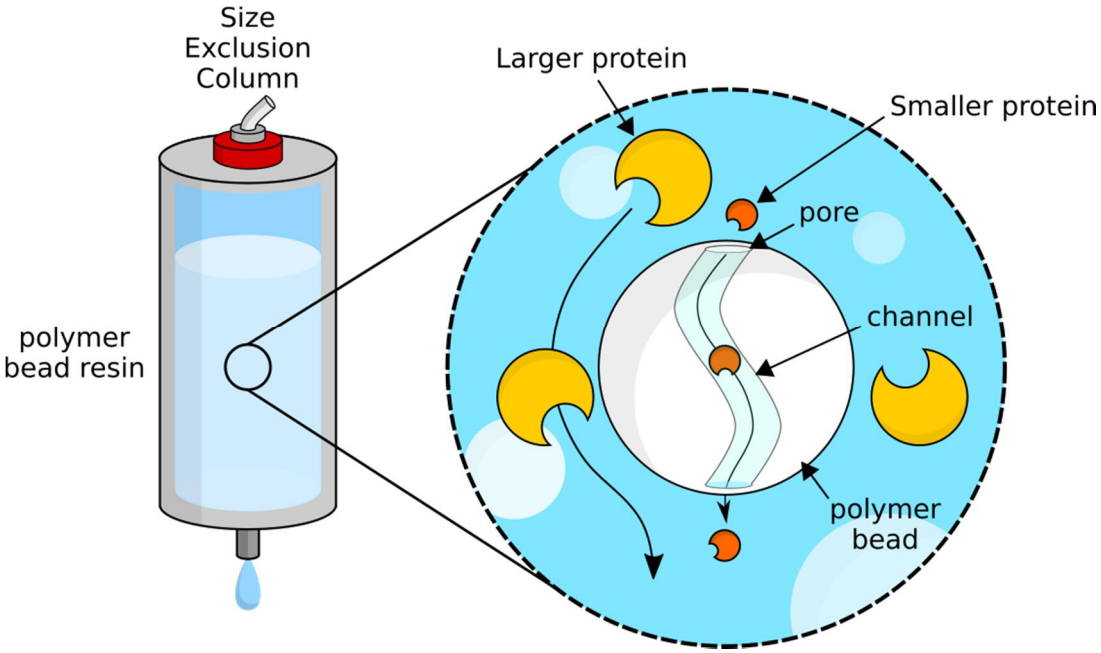

Figure 2.18. Cartoon representation of size exclusion chromatography. Crude protein mixture is flowed through a column containing polymer bead resin. The beads contain small pores and channels. Smaller molecules can move through these channels and thus move through the resin slower than their larger counterparts.

As before, a cleavage reaction was set up in which MBP-MBL (100 µM) was combined with TEV protease (25 mol%) and incubated at 4 ºC overnight. The resultant cleavage mixture was loaded onto a Superdex 75 16/60

(agarose and dextran polymer beads) size exclusion column, equipped with a UV-vis spectrometer that monitors the A_{280} of the eluting solution. The resulting chromatogram trace shows at what volume a protein species begins to elute from the column (Figure 2.19a). The chromatogram indicated the presence of three protein species. The fractions from the SEC column were analysed by SDS-PAGE (Figure 2.19b). The gel showed that the cleaved MBP and TEV protease were co-eluting together, and the cleaved MBL had been isolated from the two components and eluted earlier. MBL unexpectedly eluted from the column first (it has a lower mass than the other proteins); this suggested it was eluting as a trimer. However, the trimeric protein would not be expected to elute as early as it did in the chromatogram, which could be attributed to aggregation of the protein into higher order oligomers. Also, the reaction volume of 500 µL was too small to allow effective isolation of the MBL on the Superdex 75 16/60 column, which had a column volume of 120 mL. Such a large difference in volume caused a dilution in the products eluted generating a large volume of eluent that was impractical to concentrate.

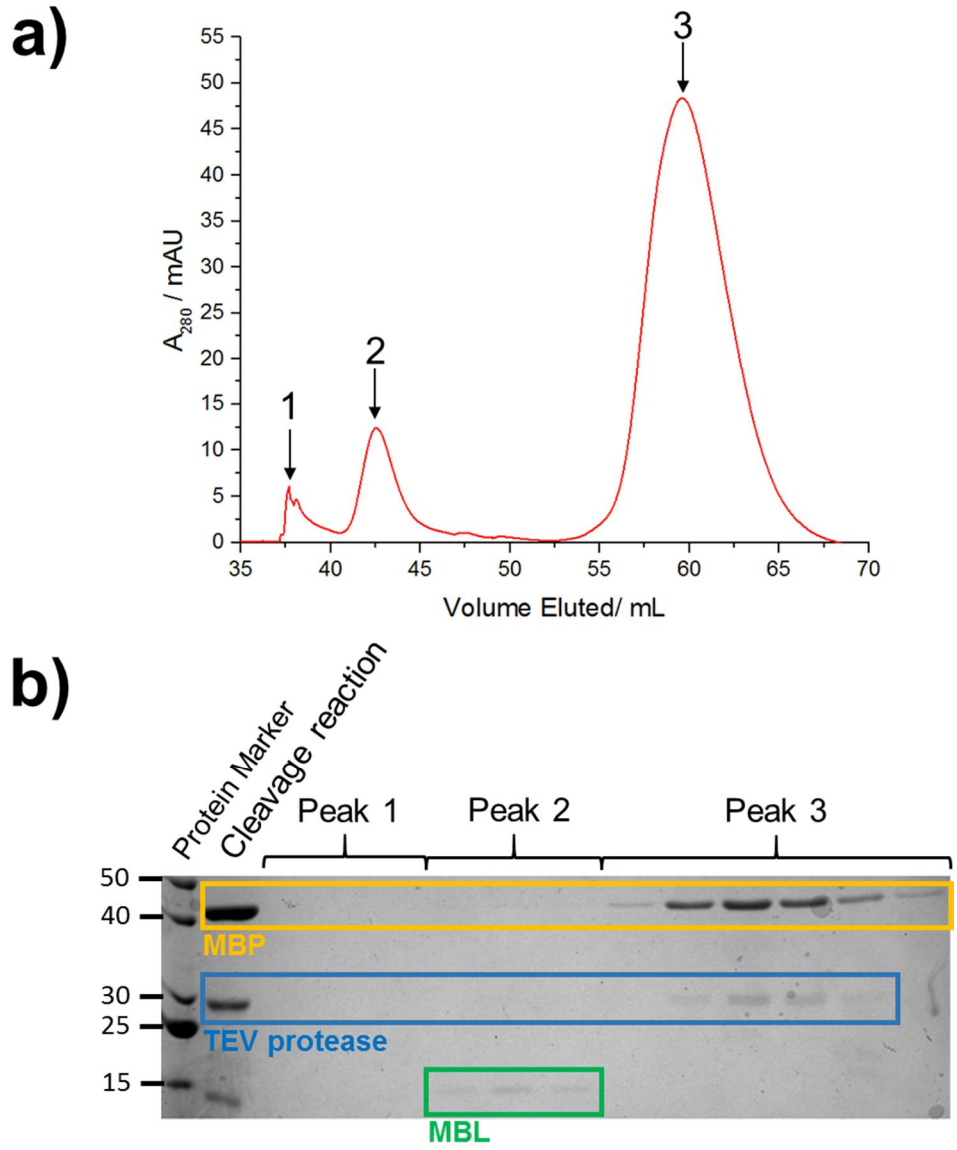

Figure 2.19. SEC purification of MBP-MBL A280 chromatogram and SDS-PAGE analysis of eluent.

a) chromatogram of the absorbance of eluent at 280 nm. Increase in A280 indicates presence of protein species. Peaks 1, 2 and 3 shows the presence of 3 protein species at 3 distinct elution volumes. b) SDS-PAGE gel of fraction corresponding to peaks 1, 2 and 3. Peak 1 appeared to have no protein species. Bands in lanes corresponding to peak 2 fractions show the presence of cleaved MBL. Bands in fractions corresponding to peak 3 indicates cleaved MBP and TEV protease co-eluted from the column.

2.1.3.7 Consecutive Nickel and mannose affinity purification of MBP-MBL

Section 2.1.3.5 showed that the MBP-MBL could be purified using two different kinds of affinity chromatography with the mannose affinity purification yielding a cleaner sample of MBP-MBL. The protein was expressed in BL21 Gold *E. coli* cells harbouring the gene for the MBP-MBL fusion protein. Figure 2.20A shows the SDS-PAGE analysis of the fractions taken from these affinity resins.

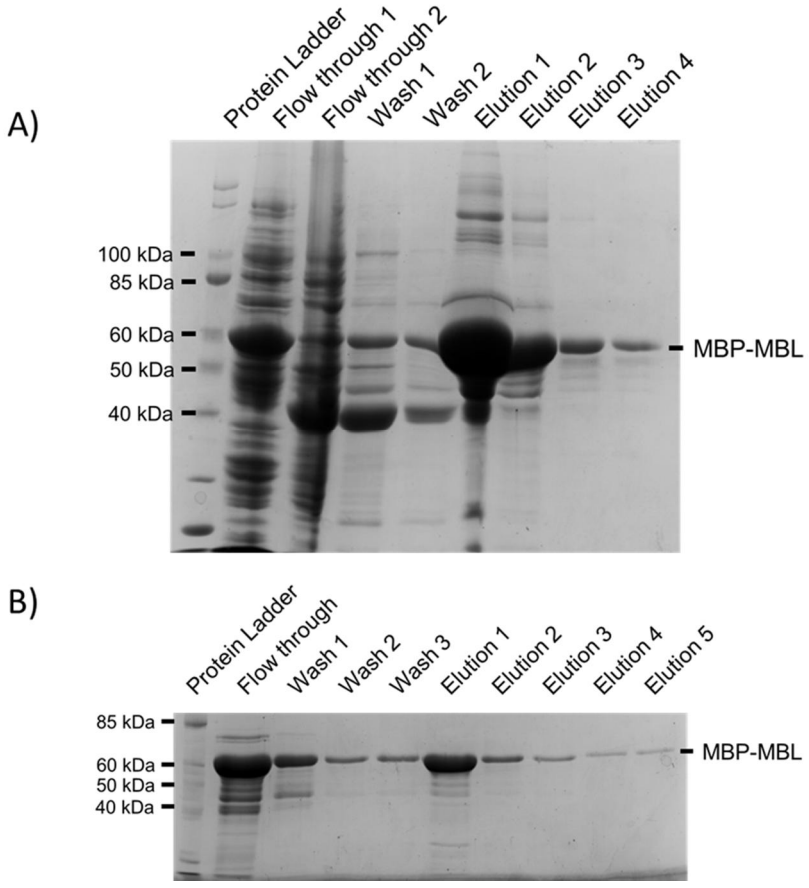

Figure 2.20. SDS-PAGE analysis of MBP-MBL purification by nickel and mannose affinity chromatography.

A) nickel affinity chromatography purification of MBP-MBL fusion protein from cell lysate and B) mannose affinity chromatography of MBP-MBL from elutions from nickel affinity chromatography. Bands at ~ 59 kDa associated with the presence of MBP-MBL protein.

The SDS-PAGE gels in Figure 2.20 A,B show that the elution from the mannose affinity column yielded a clean protein solution containing a band corresponding to MBP-MBL at ~59 kDa. Elution fractions taken from the mannose affinity column were analysed further by mass spectrometry (Figure 2.21).

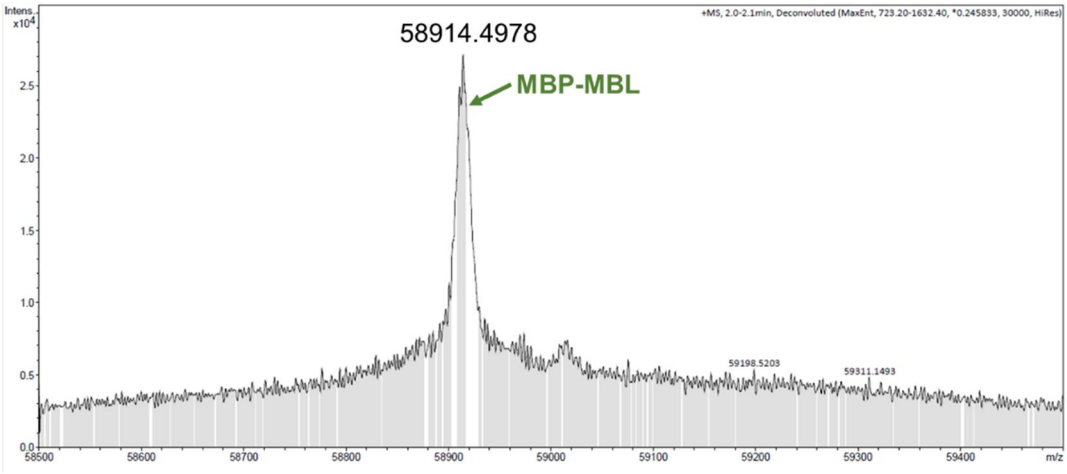

Figure 2.21. Mass spectrum of elution fractions taken from mannose affinity chromatography purification of MBP-MBL.
Peak at 58914 Da associated with MBP-MBL protein MW = 58915 Da.

Though this method of purification yielded a clean MBP-MBL protein, the amount of protein that could be loaded onto the mannose affinity resin was low, of the six litres of cell culture only 10 mg of protein could be isolated by the mannose affinity resin. This included the elution from the mannose column being reloaded onto the column once the first batch had been eluted.

The experiment showed that the best method for purification of the fusion protein was initial purification with nickel affinity chromatography then an additional mannose affinity chromatography step. Future purifications required larger amount of resin to load protein onto.

Due to time constraints is was decided that future work to study the interaction between MBL and the *S. aureus* biofilm would use the MBP-MBL fusion protein, in order to maintain protein solubility. Protein from this final overexpression of MBP-MBL was used in subsequent experiments (sections 2.3.1.3 and 4.2.4).

2.2 Affimer protein

Affimers are small (~12 kDa), heat stable binding proteins that are being developed as stable replacements for antibodies for a wide variety of techniques.[109] Affimer proteins have a conserved cystatin scaffold and two hyper-variable loops, the amino acid sequence of which dictates the affinity of an Affimer to its desired target (Figure 2.22). It is the loop sequence which gives each individual Affimer its own 'fingerprint' and unique binding affinity.[110] All Affimer protein sequences used in this project contained a polyhistidine tag for purification and a cysteine residue for chemical ligation utilising the free thiol group.

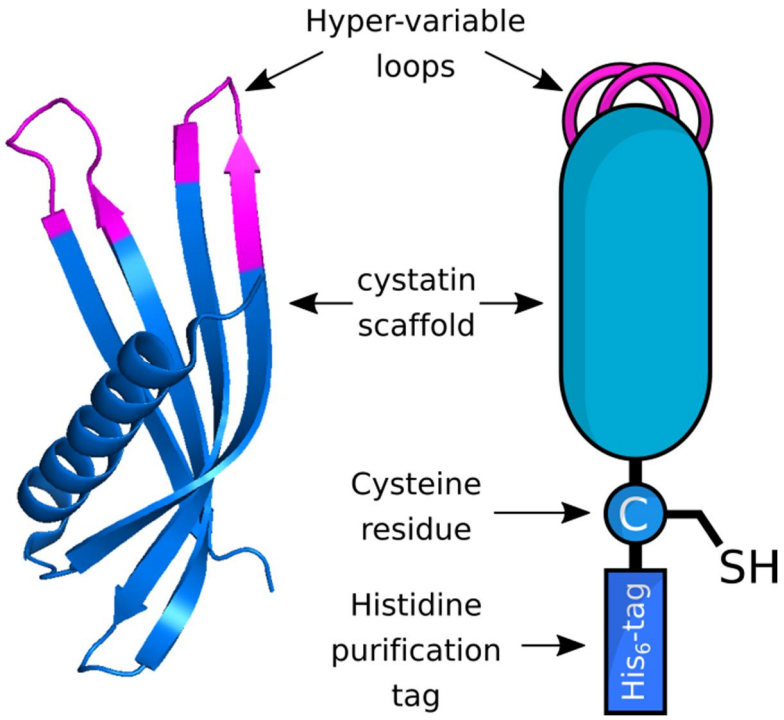

Figure 2.22. Crystal structure of the Affimer protein (left) and a cartoon depiction (right).

The conserved cystatin scaffold is shown in blue on the crystal structure and the hyper-variable loops shown in pink. Each Affimer protein has a polyhistidine tag for purification and a cysteine for chemical ligation.

Previous work by Lia de Faveri (Tomlinson lab, University of Leeds) and Fayez Alsulaimani (McDowall lab, University of Leeds) generated a group/selection of 'Affimer proteins' that had been found to bind to three different strains of *S. aureus* biofilm (SH1000, USA300 and UAMS1) and the clumping factor A protein found on the surface of *S. aureus*.[154] Affimer protein constructs were provided by Prof Kenneth McDowall (University of Leeds) and are identified using the letters in the name of their raised strain and numbers after to distinguish between them. e.g. an Affimer raised against the SH1000 strain was named 'SH31.' Affimers named 'ClfA' were raised against clumping factor A.

Affimer proteins were overexpressed in *E. coli* cells and purified using nickel affinity chromatography. Purity of elution fractions was assessed by SDS-PAGE and if impurities were found, the Affimers were further purified by size exclusion chromatography (section 6.2.5). Purified Affimers were then labelled using fluorescein-5-maleimide which modifies the free thiol group with a fluorescent dye molecule. For all 10 Affimer proteins, 100% protein labelling was ascertained using mass spectroscopy.

2.2.1 Affimer-Biofilm Binding Assays (ABBA)

The Affimer proteins were then screened against all three *S. aureus* biofilm strains in a 96-well plate, cultivated using the protocol outlined in material and methods 6.2.23. Figure 2.23 shows the relative binding profiles of 10 Affimers screened. Each point on the curves is an average of the fluorescent signal observed for the SH1000, USA300 and UAMS1 strains at a given concentration of Affimer (individual strain curves for each Affimer can be found in Appendix 7.7).

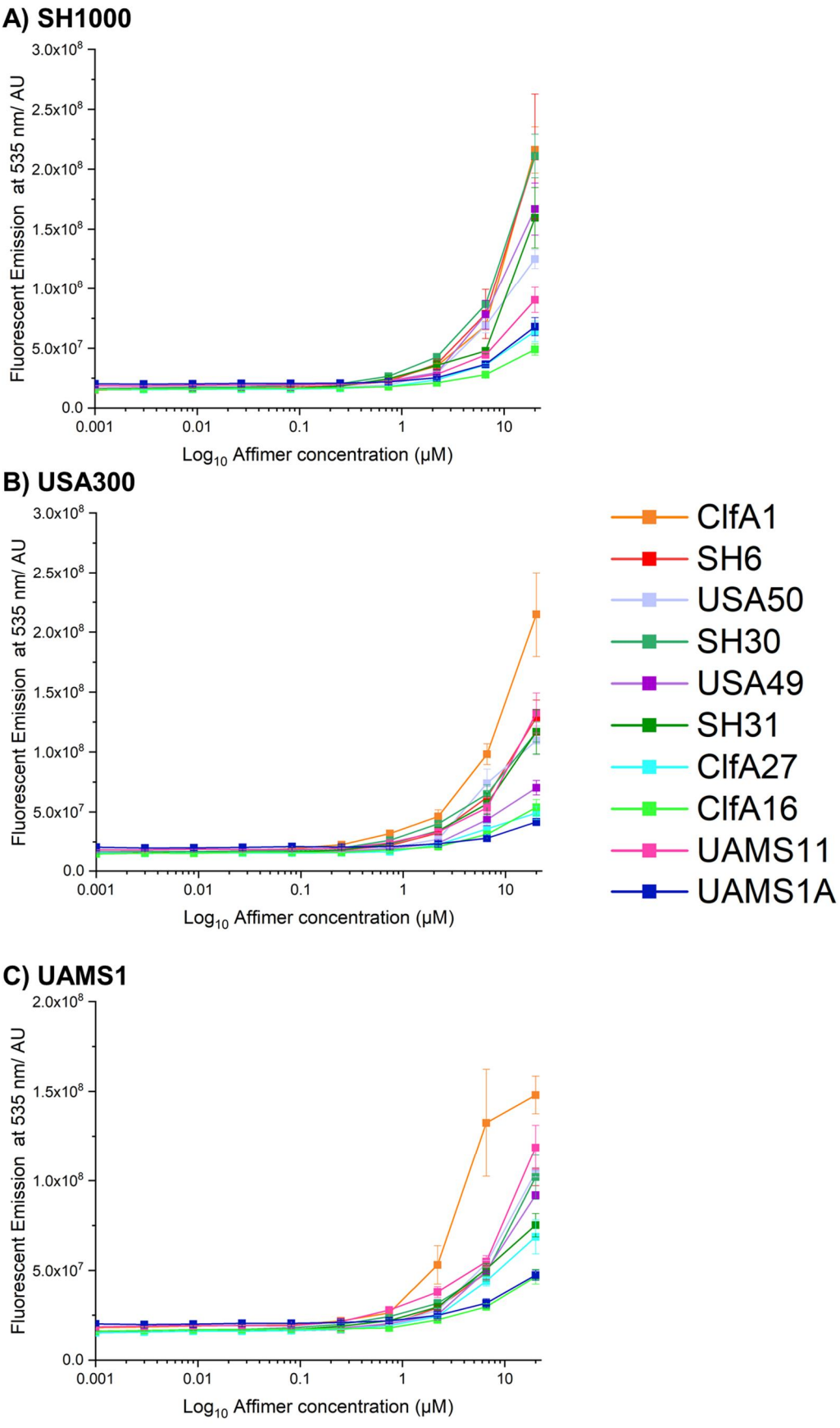

Figure 2.23. Plots of average difference in fluorescent emission of Affimer-fluorescein at a given concentration screened against three strains of biofilm.

Biofilms were cultivated then washed with phosphate buffer, 50 µL of Affimer-fluorescein was added at various concentrations and incubated at RT for 1 hour. After this the wells were washed again with phosphate buffer and the fluorescent emission of fluorescein at 535 nm measured using an Envision plate reader. Fluorescent emission at 535 nm is associated with the presence of Affimer-fluorescein and is attributed to the binding of the protein to each of the S. aureus biofilm and their associated SEM values (n = 3 for each technical repeat) shown as error bars. Affimers were screened against three strains of biofilm; A) SH1000, B) USA300 and C) UAMS1. Legend shown on the right.

All 10 Affimer proteins showed some degree of binding to the static *S. aureus* biofilm and although none of the curves displayed saturation at the maximum Affimer concentration, the data may give some indication as to the relative affinities of each protein. The maximum concentration of Affimer used was limited by the amount of labelled protein available. ClfA1 is an Affimer raised against anti-clumping factor A (ClfA); a protein present on the surface of *S. aureus* cells. This Affimer had the highest apparent affinity for all three *S. aureus* biofilm strains and could be rationalised by the assumption that ClfA is expressed by all three strains. However, little is known about the binding partners for the Affimers not raised against ClfA. Generally it is understood that these Affimers bind the biofilm that they were raised against, but further work would be needed to ascertain specifically what these Affimers bind and indeed if their targets are strain specific. The fluorescence data from the curves for ClfA1 binding to all three bacterial strains is shown in Figure 2.24. However, the fact that ClfA16 and ClfA27 Affimer proteins - which also bind ClfA - had much lower fluorescence, contradicted this hypothesis. ClfA(n) Affimers, where (n) is a numeric label, were raised against an isolate of ClfA protein and therefore the ClfA16 and ClfA27 Affimers may bind a different epitope of the protein that is not accessible when it is part of the biofilm. Regardless, the higher binding of ClfA1 for all three strains made it the ideal candidate for initial experiments binding in the microfluidic biofilm model.

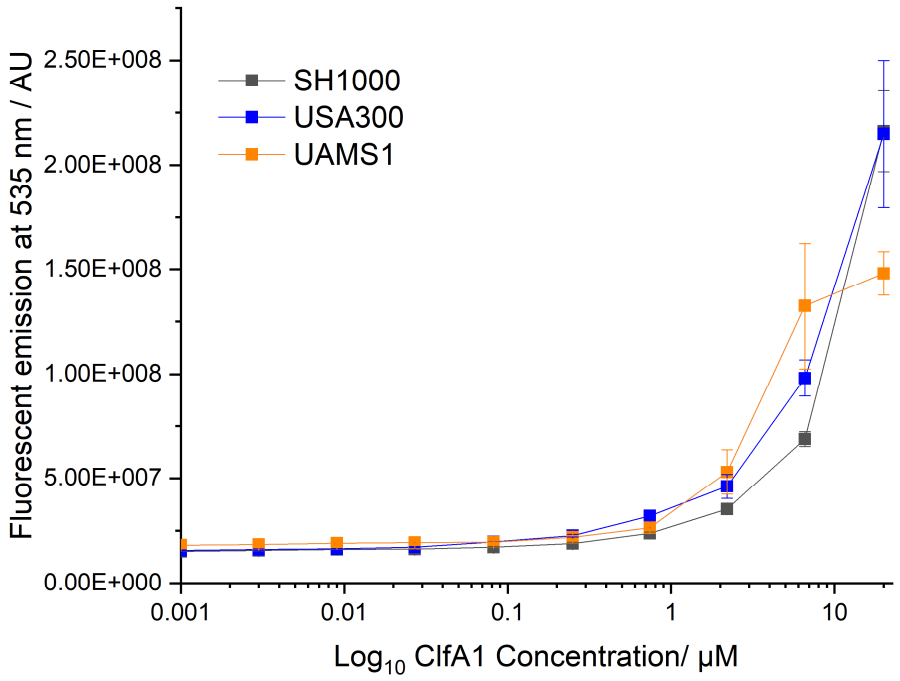

Figure 2.24. Plot of fluorescent emission of Affimer-fluorescein at a given concentration screened against SH1000, USA300 and UAMS1 strains of S. aureus biofilm individually.

Biofilms were cultivated then washed with phosphate buffer, 50 µL of Affimer-fluorescein was added at various concentrations and incubated at RT for 1 hour. After this the wells were washed again with phosphate buffer and the fluorescent emission of fluorescein at 535 nm measured using an Envision plate reader. Fluorescent emission at 535 nm is associated with the presence of Affimer-fluorescein and is attributed to the binding of the protein to the S. aureus biofilm and their associated SEM values shown as error bars. Affimer was screened against three strains of biofilm; SH1000, USA300 and UAMS1.

Assuming that the wells of the 96 well plate are covered with biofilm, if the number of ligands on the biofilm outnumbered the number of receptors it could be argued that the trend in fluorescent signal could be attributed to increasing concentration of Affimer protein, as opposed to affinity of Affimer for the ligand. This was further investigated by extending the ABBA binding curve beyond the top concentration of 20 µM. Should the current binding curve be a function of the Affimer protein's affinity for the biofilm and not a product of surplus binding sites on a comparatively large biofilm, then an extension of

the curve into higher concentrations should see the formation of a sigmoid that eventually reaches saturation. The data in appendix 7.8 indicated that the ABBA assay did not give a clear picture as to which Affimer proteins were better at binding the *S. aureus* biofilm than others. In order to characterise the interaction, ClfA1 was taken forward for further binding studies as the specific target for this Affimer was known and could be biosynthesised in order to probe the binding interaction.

2.2.2 Investigation into interaction between ClfA1 and clumping factor A

For Affimers raised directly against the *S. aureus* biofilm, further work outside the scope of this thesis would need to be done to ascertain exactly what those Affimers bind to at the molecular level; the only conclusion that can be made is that those Affimer proteins bound to a *S. aureus* biofilm component in those specific strains. Affimer proteins (named ClfA*n*) were raised against the MSCRAMM protein clumping factor A, present on the surface of *S. aureus* cells. Because their specific molecular target was known, provided ClfA could be produced and isolated effectively, the interaction between ClfA and ClfA-Affimers could be studied and better understood.

In order to probe the interaction between ClfA1 and ClfA, a plasmid was designed and ordered from Genscript to induce overexpression of the ClfA protein in a protein expression strain of *E. coli*. The clumping factor A protein was expressed as part of a MBP fusion protein to increase the protein's solubility. This was a pre-emptive measure in case the ClfA protein had any issues staying in solution. Figure 2.25 shows the fusion protein complex. This included a TEV protease site to allow separation of the two proteins with TEV protease enzyme. The His-tag would allow purification of the cleaved ClfA protein using Ni-NTA affinity chromatography.

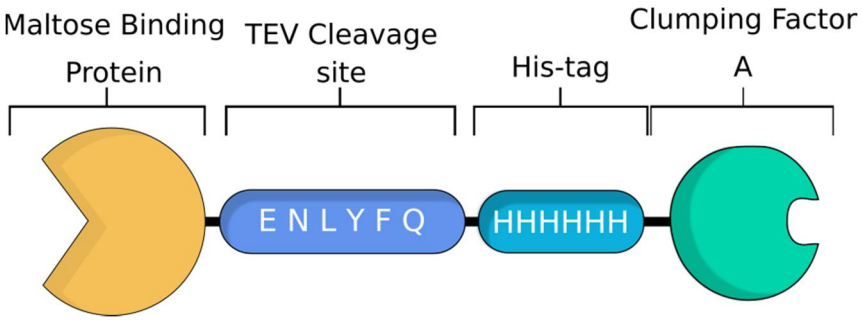

Figure 2.25. Cartoon representation of MBP-ClfA complex that was purified from E. coli cell lysate.

2.2.2.1 Overexpression and Purification of MBP-ClfA.

The clumping factor A protein was first overexpressed in *E. coli* (described in section 6.2.4) and purified from the cell lysate via nickel affinity chromatography, utilizing the polyhistidine tag incorporated into the design, adjacent to the clumping factor A protein. The elution fractions from the nickel column were analysed by SDS-PAGE, shown in Figure 2.26.

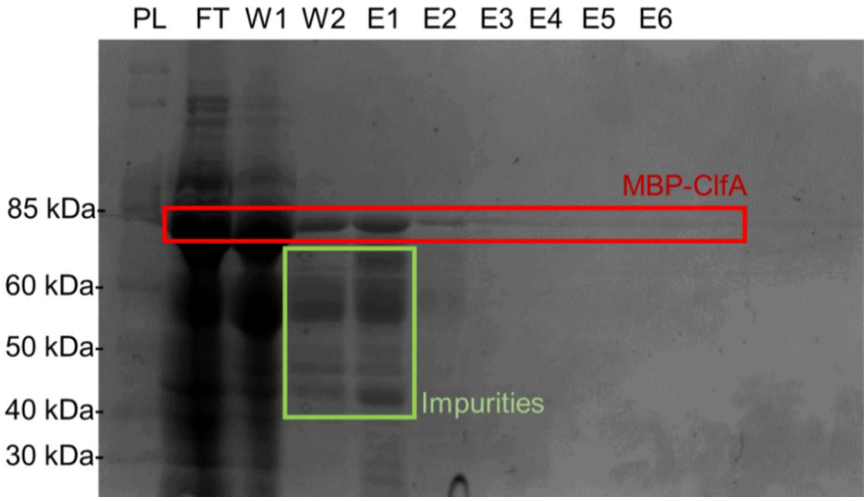

Figure 2.26. SDS-PAGE analysis of MBP-ClfA purification by nickel affinity chromatography.
Bands at ~ 79 kDa associated with the presence of MBP-ClfA protein. PL = Protein Ladder, FT = Flow through, E = Elution, W = Wash.

SDS-PAGE analysis of the nickel elution fractions showed the presence of impurities that had associated with the Ni-NTA resin, this method of purification initially seemed ineffective. The elution fraction from the nickel

column was then further purified by amylose affinity chromatography, which would isolate components that had MBP protein associated with them. Figure 2.27 shows the SDS-PAGE analysis of the amylose affinity purification.

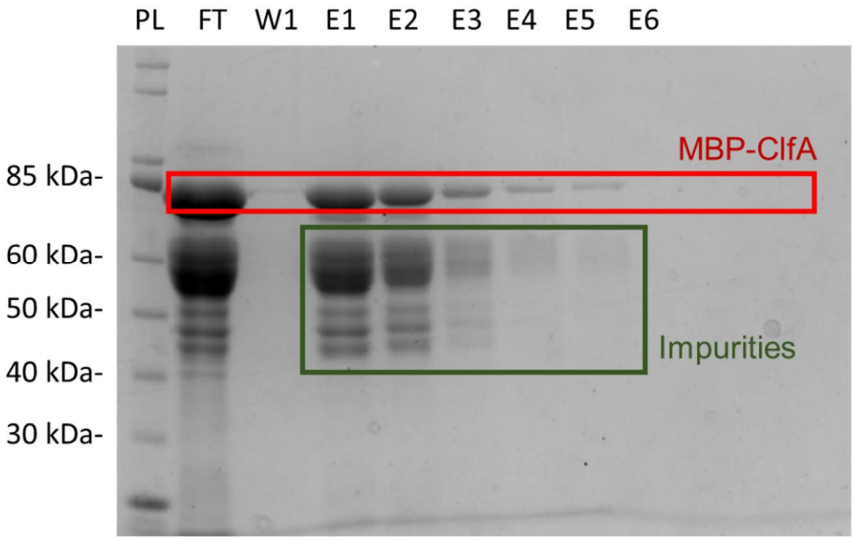

Figure 2.27. SDS-PAGE analysis of MBP-ClfA purification by amylose affinity chromatography.
Bands at ~ 79 kDa associated with the presence of MBP-ClfA protein. PL = protein Ladder, FT = flow through, E = elution, W = wash.

The amylose affinity chromatography method isolated both the MBP-ClfA fusion protein and also some of the impurities isolated in the nickel affinity purification step. Both the nickel and amylose affinity purification methods therefore proved ineffective in removing the lower molecular weight impurities. In order to remove these impurities, a further purification step was employed to try to separate out the constituent proteins by size using size exclusion chromatography. The combined elution fractions from the amylose purification were run through a Superdex™ 200 16/600 size exclusion column (Figure 2.28). In this chromatogram proteins eluting from the column are detected using their absorbance at 280 nm. Ten fractions corresponding to different points on the chromatogram trace were analysed by SDS-PAGE (Figure 2.28B).

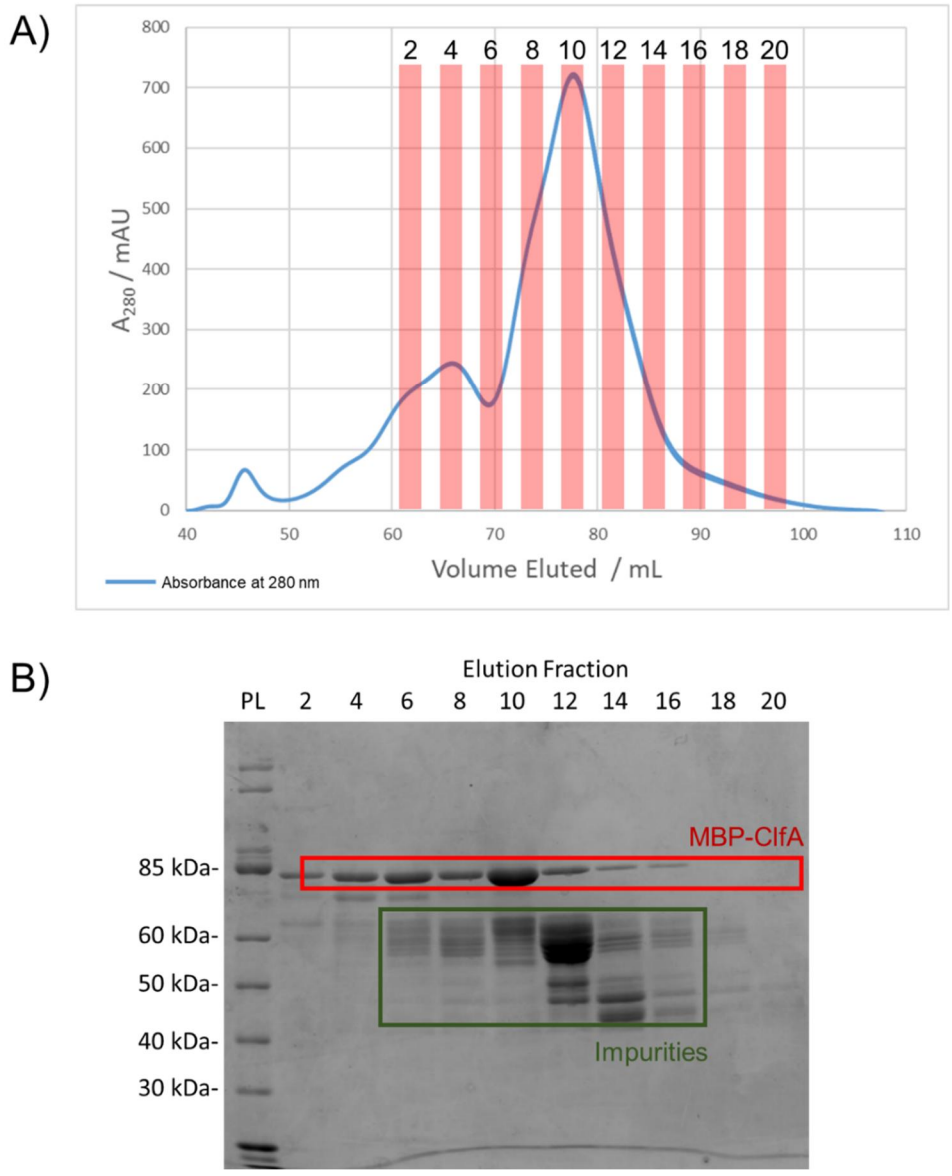

Figure 2.28. Chromatogram and SDS-PAGE analysis of MBP-ClfA purification by size exclusion chromatography.

Bands at ~ 79 kDa associated with the presence of MBP-ClfA protein. A) The chromatogram trace of the Size exclusion chromatography purification of the MBP-ClfA complex. B) SDS-PAGE analysis of fraction taken from the SEC purification, corresponding to the numbered red sections in A). PL = Protein Ladder.

Size exclusion chromatography was not completely effective in removing the impurities. The lower molecular weight impurities may have been associating with some of the MBP-ClfA protein in some way, so that they move through the column resin together. The three purification methods that

had been employed to remove the impurities were proven ineffective. A different method of purification was therefore used to further purify the elution fractions of this size exclusion purification.

Ion exchange chromatography separates proteins out by their overall net charge at a given pH.[155] The isoelectric point (pI) of a protein is the pH at which the proteins overall net charge is 0 and all the negatively and positively charged amino acid side chains have cancelled each other out. If the pH of a buffer is above or below the pI of a protein within it, it will give the protein a net negative or positive charge, respectively – depending on the relative values of the pH and the protein's pI. For instance, the theoretical pI of the MBP-ClfA fusion protein was calculated (ExPASY Protparam tool) as 4.88, so, in phosphate buffer of pH 7.4, which is more basic than pH 4.88, acidic amino acid side chains are deprotonated, giving the protein a net negative charge. Therefore, the MBP-ClfA protein should have associated with a positively charged resin via electrostatic interaction. The protein can subsequently be eluted from the resin by the addition of negatively charged ions that can take its place. This can be achieved by using the Cl^- ions in NaCl. So, if the protein is loaded onto a negatively charge ion exchange resin, at pH 7.4, with no NaCl in the buffer, it will associate to the positively charged resin. Any other protein impurities in the column will have a unique pI and thus have a different net charge. By flowing buffer over the resin and slowly increasing the NaCl concentration, the Cl^- ions remove and separate proteins by their relative pI values. This method was used for the elution fractions of the SEC purification of MBP-ClfA. Figure 2.29 shows the chromatogram trace from the ion exchange column and the SDS-PAGE analysis of the eluent.

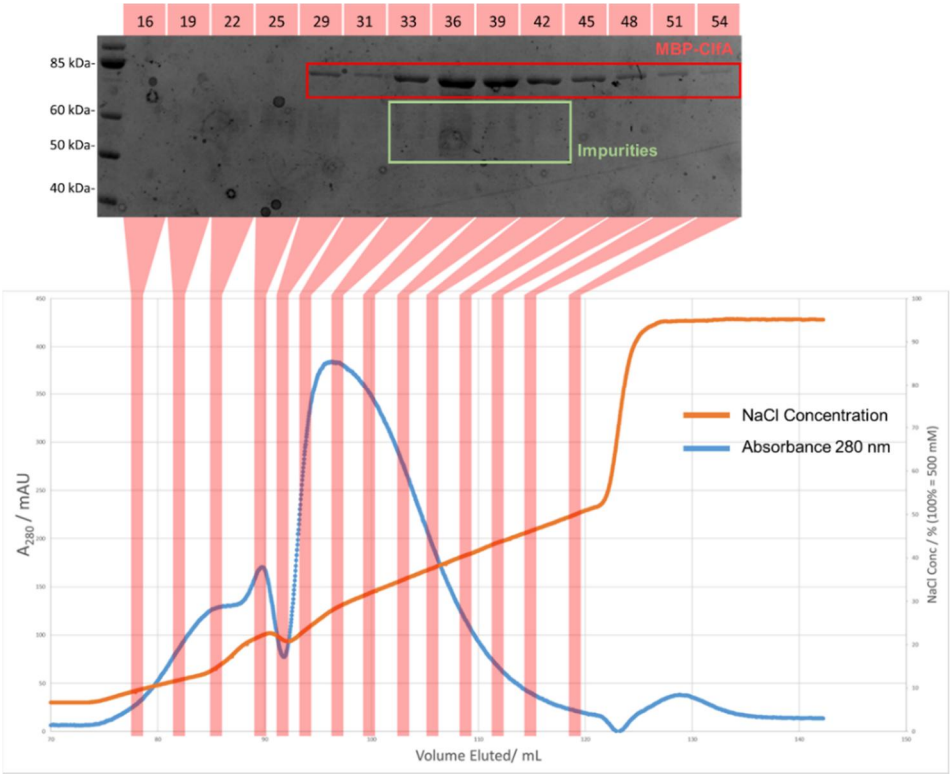

Figure 2.29. Chromatogram and SDS-PAGE analysis of MBP-ClfA purification by Ion Exchange chromatography.

A) SDS-PAGE analysis of fraction taken from the Ion Exchange purification, corresponding to the red sections in B). Bands at ~ 79 kDa associated with the presence of MBP-ClfA protein. B) The chromatogram trace of the Ion Exchange chromatography purification of the MBP-ClfA complex. Blue line shows the absorbance of the eluent at 280nm, and the orange line shows the change in NaCl concentration as more eluent is removed from the system. Far Left lane = Protein Ladder.

The ion exchange resin appeared to give the cleanest sample of MBP-ClfA of all four purification methods. There seemed to be a small amount of impurity present in the elution fractions, but these were negligible in comparison to the amount of MBP-ClfA present. The protein stock was concentrated by ultracentrifugation, aliquoted and flash frozen at -80 ºC.

2.2.2.2 TEV cleavage of MBP-ClfA

Once a protein stock had been attained through rigorous purification, TEV protease was used to ascertain if digestion of the complex in to its constituent proteins would affect solubility. Figure 2.30 shows the planned method of digestion and purification of the ClfA protein from its MBP-ClfA fusion protein.

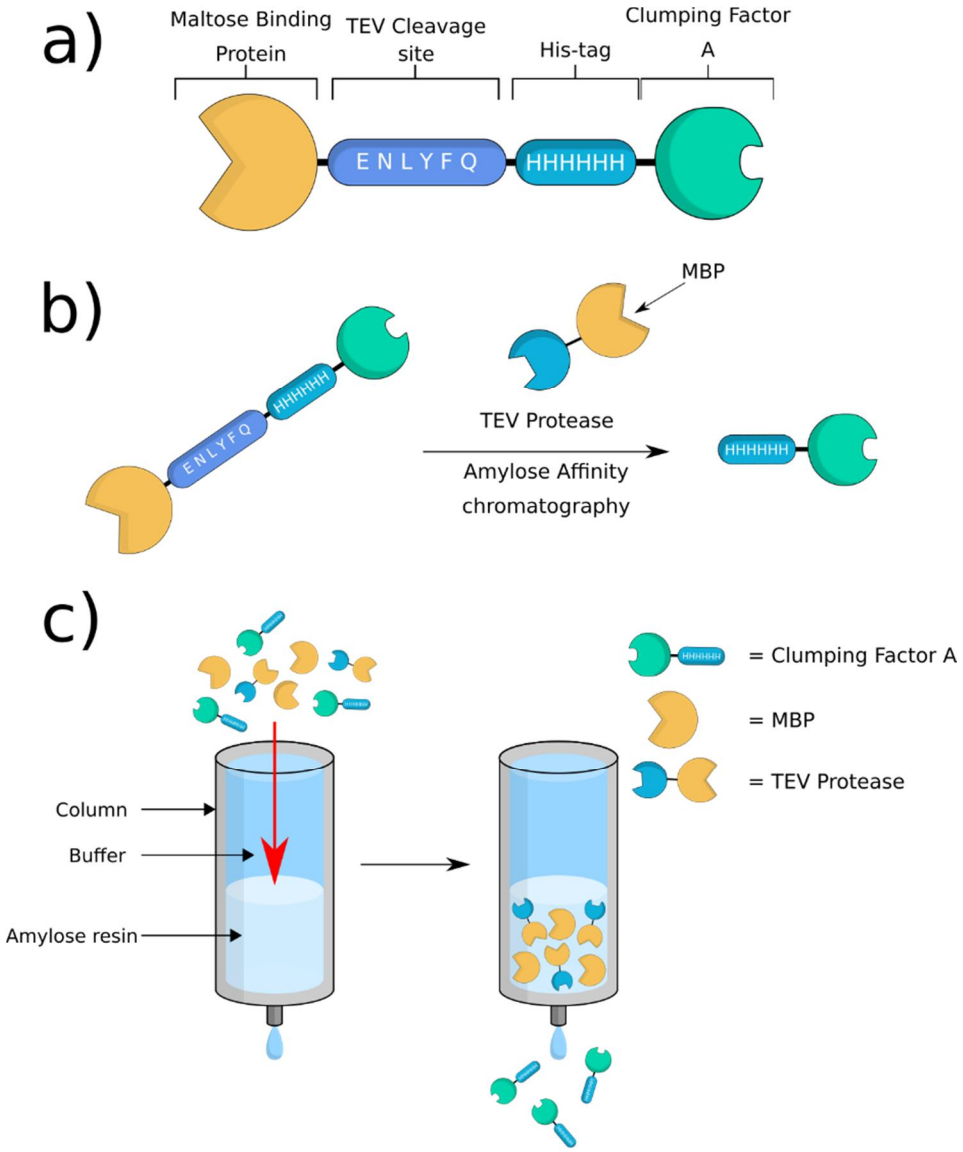

Figure 2.30. Cartoon representation of MBP-ClfA construct, method of cleavage and its purification.

a) cartoon representation of protein construct of MBP-ClfA fusion protein. b) Proposed method of purification after cleavage of two proteins with TEV protease. On the left the fusion protein complex, on the right the isolated ClfA cleavage product. Both the cleaved MBP and TEV protease can bind amylose

resin, due to the presence of the MBP fusion protein on the TEV protease. c) proposed method of purification of MBL from crude cleaved protein solution. The MBP-tagged TEV protease and MBP should be retained on a amylose affinity resin and only ClfA should be eluted.

After enzymatic cleavage and separation using an amylose affinity resin (Method Section 6.2.6.2), the fractions eluted from the amylose column were analysed by SDS-PAGE, shown in Figure 2.31.

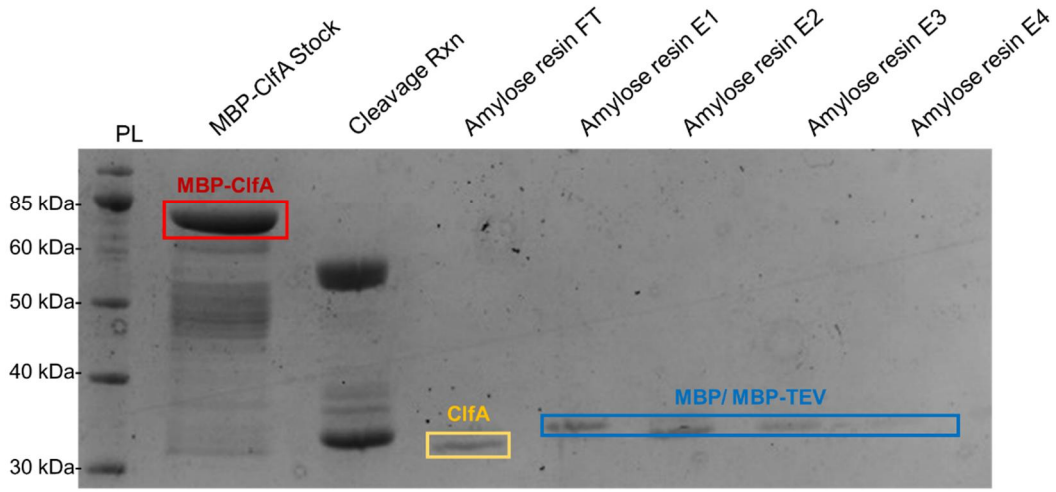

Figure 2.31. Chromatogram and SDS-PAGE analysis of MBP-ClfA TEV protease cleavage reaction purified by Amylose chromatography.
Bands at ~ 79 kDa associated with the presence of MBP-ClfA protein, band at ~ 37 kDa associated with ClfA, larger impurities associated with MBP containing constituents such as cleaved MBP and TEV-MBP. PL = Protein ladeer, FT = Flow through, E = Elution.

As ClfA should not have any associated MBP after the enzymatic cleavage, it should not adhere to an amylose affinity resin and should be present in the 'flow through' solution. A band at ~ 37 kDa was consistent with the ClfA protein and was analysed by mass spectroscopy, for confirmation, shown in Figure 2.32.

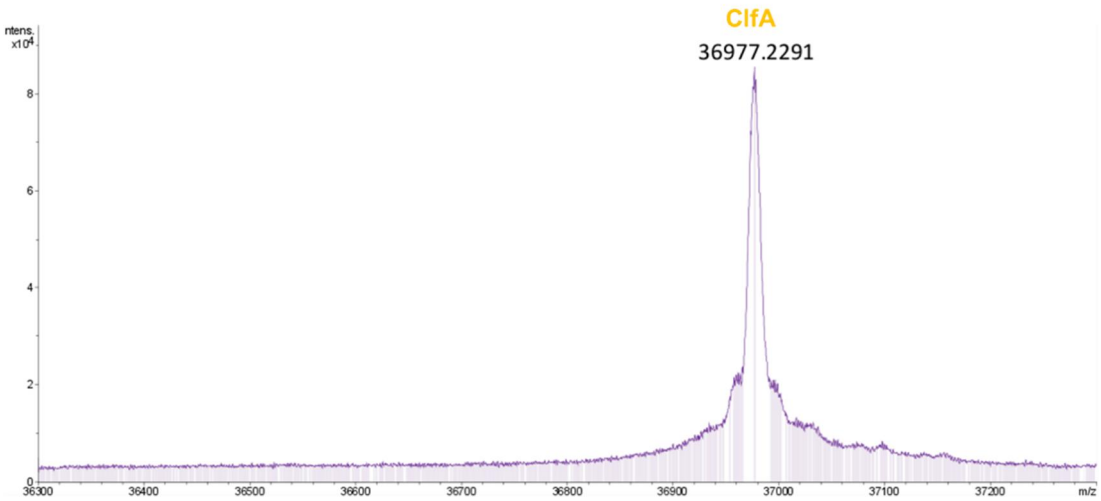

Figure 2.32. Mass spectrum of flow through fraction taken from the amylose affinity chromatography purification of the MBP-ClfA-TEV protease cleavage reaction.
Peak at 36977 Da associated with ClfA protein MW = 36978 Da.

The mass spectrum shows the presence of pure ClfA protein from the amylose affinity purification of the cleavage reaction. The results showed that the MBP-ClfA fusion protein could be cleaved using TEV-MBP protease to yield a mixture from which pure ClfA could be isolated using amylose affinity chromatography.

2.2.2.3 Isothermal Titration Calorimetry analysis of ClfA1 and ClfA

Non-specific interaction between ClfA1 and the ClfA may result from non-specific interaction between the Affimer scaffold and not the binding loops. The use of an Affimer scaffold control was used to probe the extent of interaction between the scaffold and ClfA.

The Affimer scaffold was overexpressed and purified from BL21 DE3 *E. coli* cells. Figure 2.33 shows the structure of the Aff-Ala-C (AAC) Affimer scaffold compared to that of the standard Affimer structure. The main difference is the absence of the hypervariable loops, that have been replaced with alanine repeats to preserve the tertiary structure of the protein. The

absence of the binding loops allows for observation of potential non-specific interaction between the cystatin scaffold and ClfA.

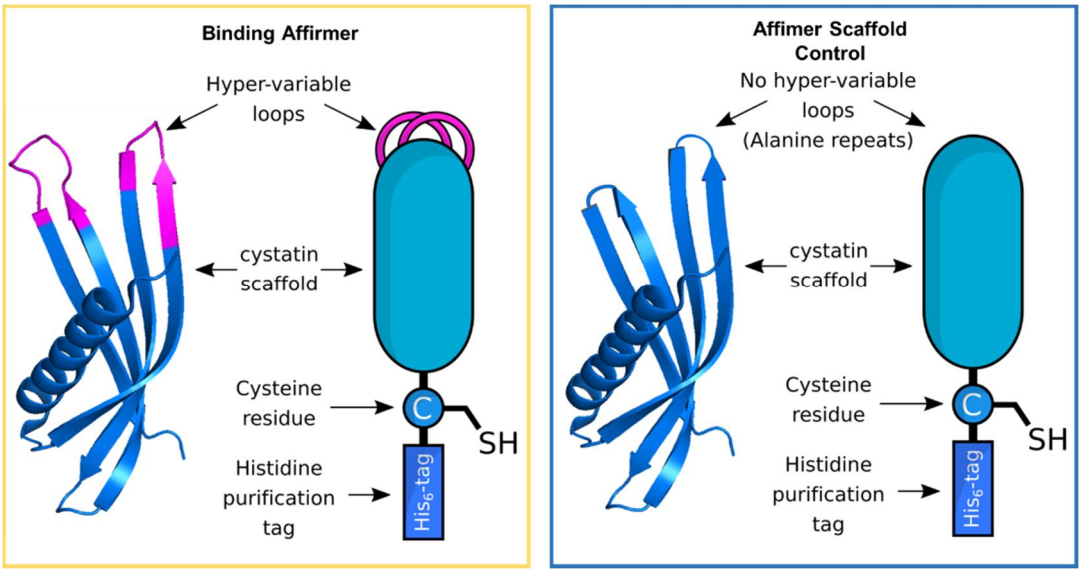

Figure 2.33. Structural difference between a standard Affimer and a cystatin scaffold Affimer control.
Left, crystal structure (PDB: 5A0O) and cartoon representation of standard Affimer protein. Right, crystal structure of the Affimer scaffold (AAC) and cartoon representation. Absence of hypervariable loops eliminates binding ability of Affimer to its particular target.

Isothermal titration calorimetry (ITC) is an analytical method in which bimolecular interactions can be studied to understand function and mechanism at a molecular level. ITC was used to measure the heat change when a ligand binds to its host. From these experiments one could ascertain such values as binding constants (K_D), enthalpy (ΔH), entropy (ΔS) and stoichiometry (n).[156]

ClfA1 Affimer (200 µM) was titrated into ClfA (16 µM) in phosphate buffer. The resultant ITC trace (Figure 2.34) showed a high binding affinity with a $K_D = 62 \pm 3$ nM. The stoichiometry was shown as n ~ 1, confirming that only one molecule of the ClfA1 Affimer was associating with a single ClfA protein.

The data shows that the ClfA1 Affimer interacts strongly with the ClfA protein, when compared with a non-binding Affimer Scaffold. The Affimer was to be taken forward for use in the flow system, and as part of the targeted MB conjugation system.

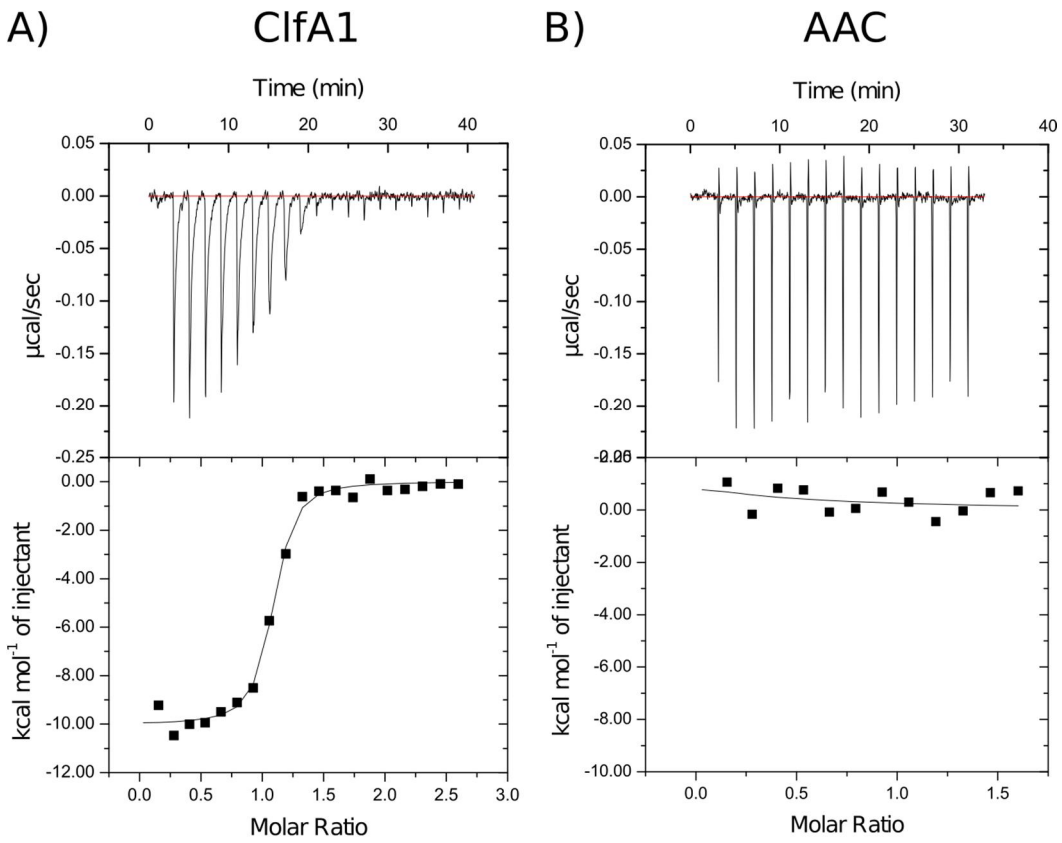

C)

K_D nM	125 ± 51
ΔH kcal / mol	-9830 ± 272
ΔS cal/ mol*K	-0.62

Figure 2.34. ITC trace for the interaction between ClfA1 Affimer and ClfA proteins and associated thermodynamic data.

ClfA1 Affimer (200 µM) was titrated into ClfA protein (20 µM). Top panel shows the raw data and the lower panel the integrated heat exchange on each subsequent addition of protein.

2.3 Polyvalent Protein Bead Conjugation

Now that a suitable biofilm-targeting protein candidate had been identified, their ability to function as microbubble conjugation systems was first probed in a static biofilm model; polystyrene beads were used as testing parameters for the microbubbles.

Mannose binding lectin is a protein that functions as part of a trimer of identical proteins. A single monomer has low affinity for mannose than it's trimeric counterpart. The polyvalent binding of the three binding sites, in close proximity, increases the affinity of the whole complex. In the innate immune response, the trimeric protomers form larger oligomers; dimers, trimer and tetramers that then further cooperate together to increase their affinity to cell surface-bound mannose (see Figure 1.10). This multivalency play an important role in many biological processes and is regarded as essential for some carbohydrate-protein interactions.[157, 158] Single iterations of proteins conjugated to a common surface, such as on the surface of a microbubble, may increase their avidity for the cell surface through cooperativity in a similar way to how the carbohydrate binding domains function in MBL.

As microbubbles are inherently buoyant, they cannot be used in conjunction with a plate based biofilm assay. In fact, work by Liou and co-workers demonstrated that MBs are so buoyant that targeted microbubbles can be used as a method of sorting cells, being able to lift specific breast cancer cells from a cell pellet.[159] Although useful in this context, the buoyancy raises issues with MB-biofilm contact in a system where the biofilm is grown on an upright surface, such as that of a 96 well plate. However commercial products exist that can mimic the physical dimensions of a microbubble without the inherent buoyancy. Micromod manufacture polystyrene polymer beads that are 2 µm in diameter, comparable to the size of a microbubble, with a Ni-NTA functionalised surface. These beads have a density of 1.03 g mL^{-1}, similar to that of water (1.0 g mL^{-1}) and therefore can act as diffuse molecules for short periods of time. Proteins can be conjugated to their surface using a polyhistidine tag, a feature present on all proteins manufactured thus far.

These polystyrene beads can offer a scaffold by which to observe potential cooperativity effects of proteins conjugated to a common surface that mimic the same paradigm as will be observed on the microbubble surface.

2.3.1.1 Protein loading efficiency of polystyrene beads

The loading efficiency of the proteins on to the polystyrene bead surface was determined using fluorescein-labelled ClfA1 Affimer. As mentioned previously the protein can conjugate to the bead surface via its polyhistidine purification tag. Lukáč and co-workers showed this method can also be used to conjugate molecules to the surface of MBs when a Ni-NTA lipid is incorporated into the lipid monolayer, and allows for a variety of biomolecules to be incorporated using a common recombinant purification tag.[160] However, issues may arise with nickel toxicity if this method was to be used with patients.

The polystyrene particles were washed with phosphate buffer by pelleting the beads via centrifugation, decanting away the liquid and re-suspending in phosphate buffer.

ClfA1 was diluted to give samples with concentrations varying from 15 µM – 0 µM, the beads were then washed. The concentration of the decanted protein solution, containing unbound protein was measured. The concentration difference between protein solutions before and after the beads were added was used to calculate a loading efficiency. Protein was also eluted from the protein-treated beads by adding phosphate buffer spiked with imidazole.

Figure 2.35 shows fluorescence images acquired for the different bead and protein solutions using a GelDoc camera. Figure 2.35 shows fluorescent beads after the protein had been added and the beads had been washed. The bead-bound protein was eluted using imidazole. The fluorescent intensity of the eluted solution is higher than that of its bead-bound counterpart. This observation may be due to self-quenching of the fluorescein molecules which is observed when the distance between molecules is < 42 Å [161], which may be the case on the surface of the beads. Alternatively, polystyrenes has been observed to quench fluorescence and therefore the polystyrene within the beads may be quenching the fluorescent emission of fluorescein.[162] Therefore

future use of polystyrene beads in conjunction with plate based biofilm assays required a step in which an elution buffer was added to remove the protein from the beads to allow more accurate determination of fluorescent emission.

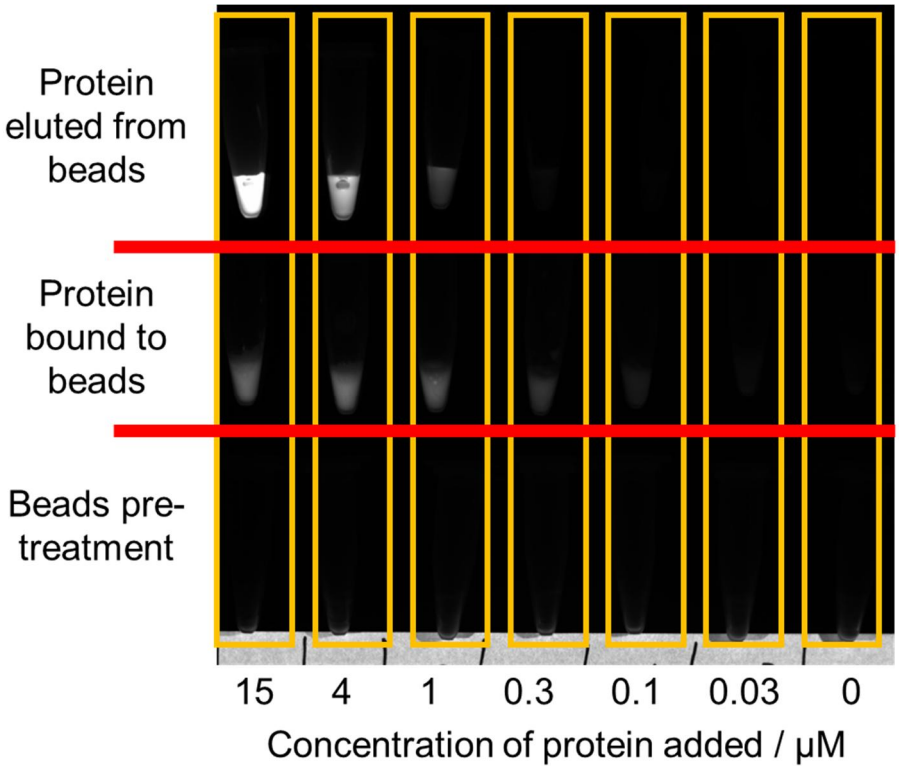

Figure 2.35. Composite fluorescent images acquired of different solution containing both beads both treated and untreated with protein, and the protein eluted off the treated beads.

Increase brightness of a sample corresponds to higher fluorescent light emission at 535 nm. Protein conjugated to bead surface appears to emit more fluorescent light once eluted from the bed surface using imidazole.

2.3.1.2 Fluorescent label optimisation for polystyrene beads

In this experiment beads were treated with ClfA1 Affimer with two different fluorescent dyes attached. ClfA1 was used as a model protein instead of MBP-MBL as more material was available. One ClfA1 stock was labelled with Alexafluor488 and the other with Alexafluor647. These fluorophores were attached using their succinimidyl ester derivatives, which label primary amines on protein molecules (lysine and N-terminal amines). These two dyes both emit light at different wavelengths (535 and 638 nm respectively). If the beads absorb light in the range of the alexafluor488 dye (similar spectral profile to that of fluorescein), then beads treated with the same concentration of Affimer labelled with Alexafluor647 will be considerably brighter. As before beads were treated with 15 µM ClfA1 Affimer, and fluorescent images were acquired at each step using a GelDoc camera (Figure 2.36).

Beads treated with the Alexafluor647 labelled ClfA1 saw little change in fluorescent intensity when the polystyrene beads were added. The beads did not seem to quench the emission from the Alexfluor647 dye compared to that of the Alexafluor488 dye. When the beads were added to the protein solution, even before they were washed, a significant dulling of the fluorescent light emitted was observed. These results indicate that the beads were in fact affecting the light emitted from the Alexafluor488 dye. Future experiments using the polystyrene beads required the use of Alexafluor647 as a fluorescent marker for binding proteins.

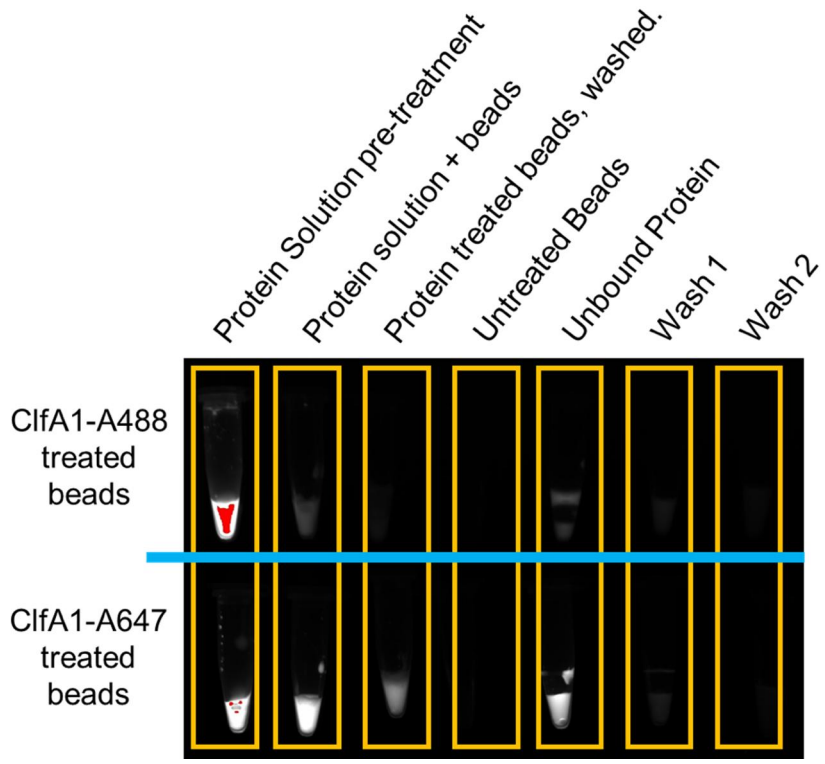

Figure 2.36. Composite fluorescent images at each step of addition of ClfA1-A488 and ClfA1-A647 to polystyrene beads.
Both alexafluor488 and 647 were imaged at their emission wavelengths (535 and 650 nm respectively). Red colour associated with saturated pixels.

2.3.1.3 MBP-MBL-Alexafluor647 polystyrene bead binding assays

MBP-MBL protein labelled with Alexafluor647 NHS-ester fluorescent dye which label primary amines (fluorescein was not used as MBP-MBL did not have the required free thiol for maleimide conjugation), was conjugated to the surface of the polystyrene beads and screened against three strains of *S. aureus* biofilm (SH1000, USA300, UAMS1). These biofilms were cultivated as described in section 6.2.23.

Polystyrene beads were functionalised with MBP-MBL (15 µM), which associated to the bead surface by nickel chelation of the polyhistidine purification tag. For measuring the concentration of the unbound protein in solution after incubation with beads, the concentration of on-bead protein can be calculated by subtracting the un-bound concentration from the initial concentration. In this case it was ascertained to be 2.35 µM at a bead concentration of 1 $\times 10^9$ beads mL^{-1}. This was used as the top concentration in a 1 in 3 dilution series. 50 µL of MBP-MBL beads were added to biofilms

of each strain of *S. aureus*, incubated at RT for 1 hour and then washed. Fluorescent emission at 535 nm was then measured. Protein was eluted from any beads bound to biofilm using phosphate buffer spiked with imidazole. The plate was then reloaded into the plate reader and the emission measured a second time, a fluorescence intensity increase should be observed as the protein transitions from bead-bound to in solution. A control was carried out alongside this experiment with unbound MBP-MBL in solution at the same concentrations.

Figure 2.37 shows a plot of concentration against fluorescent intensity for each reagent used. The conjugation of the MBP-MBL protein to the surface of the bead did not seem to have a higher affinity than that of the protein in solution. This may have been be due to single iterations of the protein complex being too far apart on the bead surface to have a multivalent binding effect. The protein bound to the beads are locked in positions across its surface. At any one time, only a small section of the bead's overall surface area is in contact with the biofilm surface, restricting the access for the rest of the surface-bound protein. Protein in solution has access to a larger area of the biofilm than that of protein fixed to the bead surface, which is why a higher signal is observed for the protein in solution.

Alternatively, the dye itself may have labelled a lysine close to the binding site of the protein and the fluorophore may reduce binding of mannose into the active site.

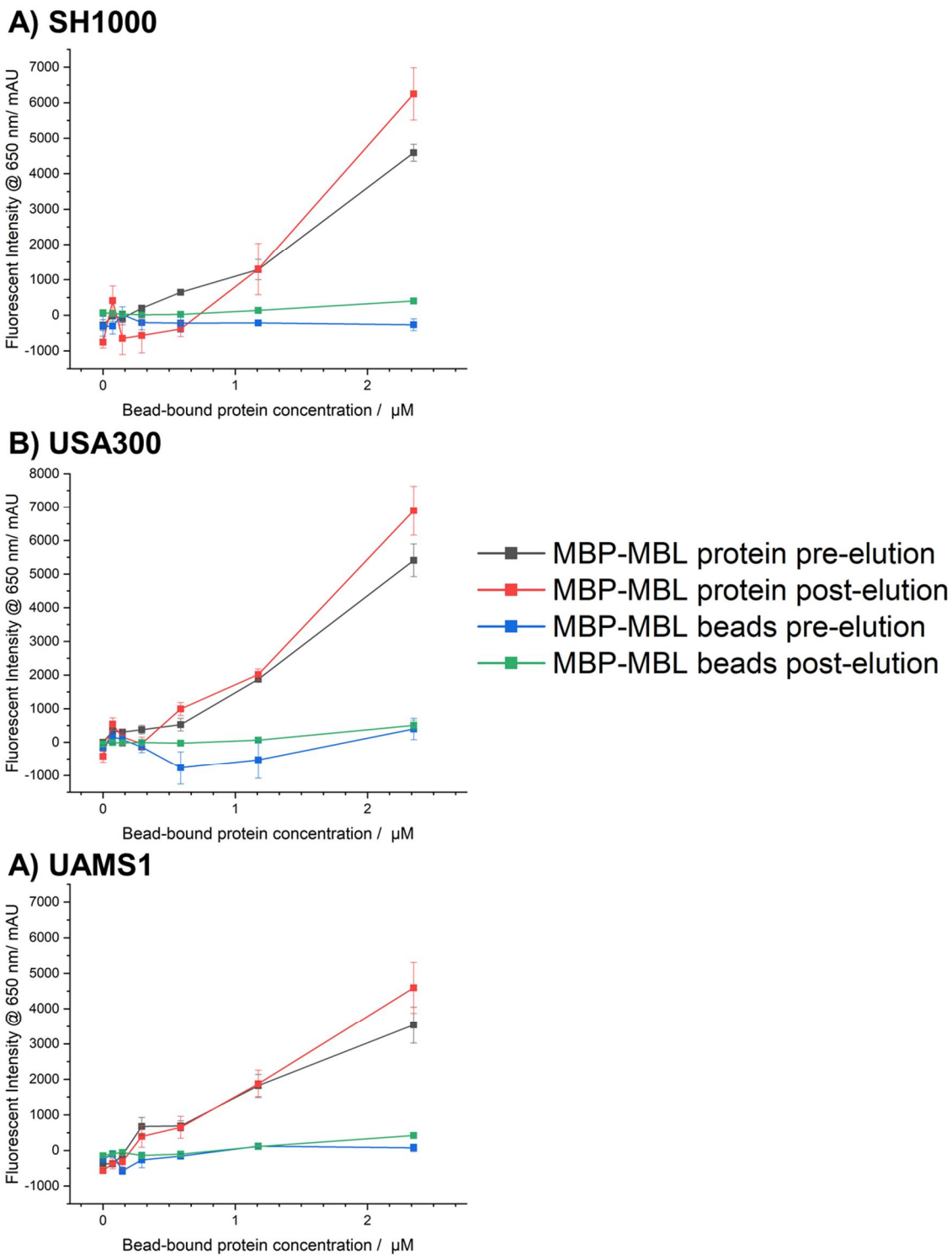

Figure 2.37. Plot of fluorescent emission of alexafluor647 labelled MBP-MBL protein and labelled MBP-MBL protein bound to polystyrene beads at a given concentration screened against SH1000, USA300 and UAMS1 strains of biofilm individually.

Biofilms were cultivated then washed with phosphate buffer, 50 µL of protein or beads was added at various concentrations and incubated at RT for 1 hour. After this the wells were washed again with phosphate buffer and the fluorescent emission of alexafluor647 at 650 nm measured using an Envision plate reader. Protein was then eluted with imidazole and emission at 650 nm was read again. Fluorescent emission at 650 nm is associated with the presence of MBP-MBL or MBP-MBL beads and is attributed to the binding of the protein to the S. aureus biofilm and their associated SEM values (n = 3 for each technical repeat) shown as error bars. Protein was screened against three strains of biofilm; A) SH1000, B) USA300 and C) UAMS1. Legend shown on the right

2.3.1.4 ClfA1-Alexafluor647 polystyrene bead binding assay

ClfA1 protein labelled with Alexafluor647 was conjugated to the surface of polystyrene Ni-NTA polystyrene beads via the polyhistidine tag, as before. The concentration of loaded protein was calculated and the bead concentration varied to yield a 1 in 2 dilution in protein concentration. Unbound protein of the same concentration was also screened as a control.

Figure 2.38 shows a plot of concentration vs fluorescence intensity for each reagent. ClfA1 protein conjugated to the surface of the polystyrene beads gave a stronger fluorescent signal compared to their unbound counterparts of the same concentration.

Although initially, it appeared that the beads were bound to the biofilm, the fluorescent signal from the protein beads could mostly be attributed to non-biofilm-associated Affimer molecules on the bead surface. If the proteins that bind the bead to the biofilm surface occupy the same number of sites as the solute proteins in the control, the well containing the protein beads will give a much higher fluorescent signal. This would be due to the un-utilised fluorescent protein present across the whole bead surface. The higher fluorescent signal may be due to the fact that the overall concentration of the ClfA1 bead wells is higher due to all the loaded protein. What could be concluded is the ClfA1-beads were interacting with the static biofilm.

It was not possible to conclude with the data from this experiment that the interaction between the beads and the biofilm was mediated by the ClfA1 Affimer protein. In order to make such a judgement, an extra bead control would need to be included to ascertain that the binding interaction was specifically caused by the Affimer protein.

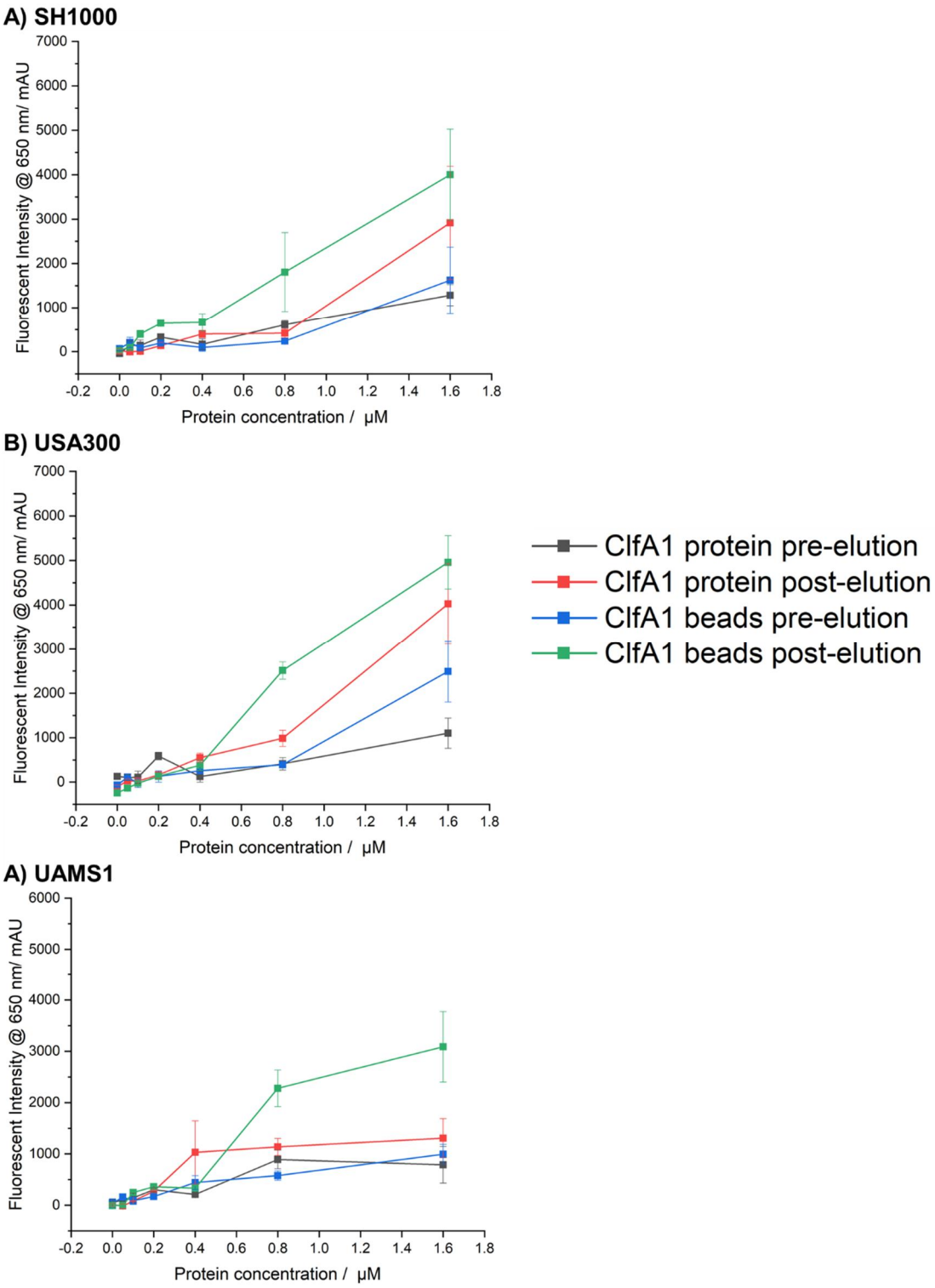

Figure 2.38. Plot of fluorescent emission of Alexfluor647 labelled ClfA1 protein and labelled ClfA1 protein bound to polystyrene beads at a given concentration screened against SH1000, USA300 and UAMS1 strains of biofilm individually.

Biofilms were cultivated then washed with phosphate buffer, 50 µL of protein or beads was added at various concentrations and incubated at RT for 1 hour.

After this the wells were washed again with phosphate buffer and the fluorescent emission of alexafluor647 at 650 nm measured using an Envision plate reader. Protein was then eluted with imidazole and emission at 650 nm was read again. Fluorescent emission at 650 nm is associated with the presence of ClfA1 or ClfA1 beads and is attributed to the binding of the protein to the S. aureus biofilm and their associated SEM values (n = 3 for each technical repeat) shown as error bars. Protein was screened against three strains of biofilm; A) SH1000, B) USA300 and C) UAMS1. Legend is shown on the right.

2.3.1.5 Non-specific bead-biofilm interaction

Affimer bound to beads was detected using an appropriate fluorescent label, covalently attached to the protein. In order to measure non-specific bead interactions between unconjugated beads and biofilm, a different technique needed to be employed due to the absence of a fluorescent species. By adding fluorescent species to the bead surface, the beads will not represent non-functionalised bead control. This experiment used light microscopy to quantify relative bead concentrations for comparison of bead-biofilm affinities. Biofilms were cultivated using methods outlined in Section 6.2.23. Beads with and without ClfA1-A647 were screened against the UAMS1 *S. aureus* biofilm. Unconjugated beads were suspended in phosphate buffer containing 300 mM imidazole to prevent interaction between Ni-NTA on bead surface and histidine residues on cell-surface bound proteins. All bead samples were ~ 1 x 10^{10} particles mL^{-1}. Wells were then washed, bacteria were killed using a paraformaldehyde solution and the contents were agitated mechanically with the end of a pipette tip. The well contents were aspirated and pipetted between a glass slide and a cover slip separated by 50 µm spacers.

The glass slides were then mounted onto an optical microscope and images were acquired of the samples at 40X magnification. Figure 2.39 shows images acquired for each experimental condition.

All images taken for each sample were then analysed using MATLAB. Script written by Damien Batchelor (University of Leeds) which counted the number of circular (spherical) entities present, and their sizes. For each

sample, the program provides a histogram of the size distribution and extrapolates to give their concentration in the sample. Figure 2.40 shows the size distribution histograms of samples taken from each experimental condition. Peaks for both the beads at 2 µm and for *S. aureus* cells at 1 µm were seen.

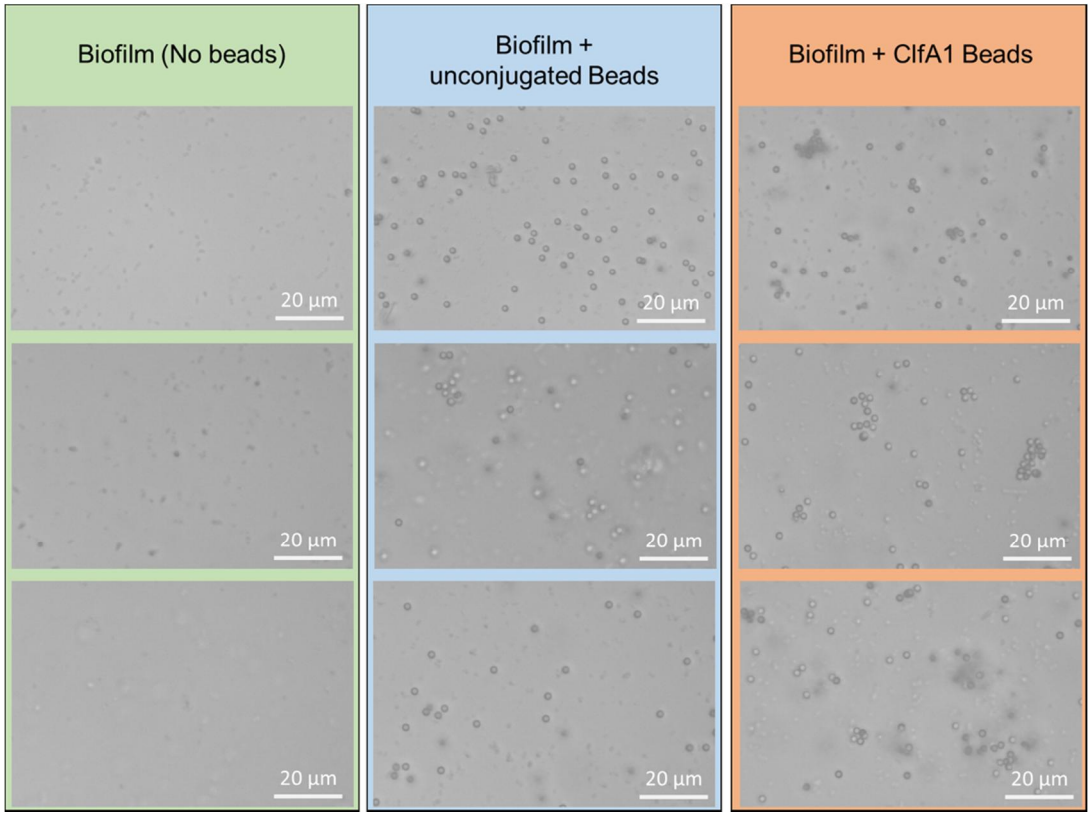

Figure 2.39. Images acquired at 40X magnification of UAMS1 S. aureus biofilm samples treated with polystyrene polystyrene bead species.
Left column shows images taken from samples of biofilm not treated with any beads. Middle column shows images of biofilm treated with unconjugated beads. Right column shows images of biofilm treated with ClfA1-A647 conjugated beads. Scale bar shows 20 µm. Species with dark halos and brighter centres are attributed to the presence of the polystyrene beads.

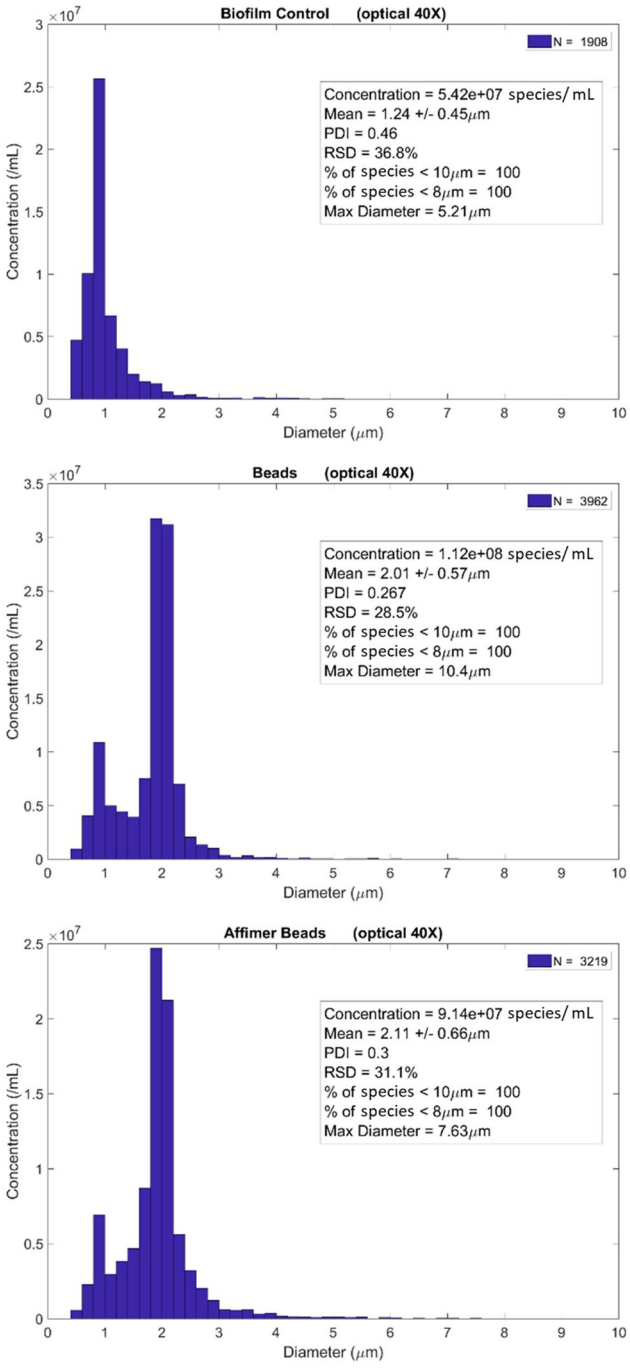

Figure 2.40. Size distribution histograms for biofilm samples treated with ClfA1-A647 beads and unconjugated beads.

Top, size distribution histogram of a biofilm control sample; middle, biofilms treated with unconjugated beads; bottom, biofilms treated with ClfA1-A647 beads. For each histogram the concentration of species is given along with the mean size, polydispersal index, relative standard deviation, % of species < 10 µm, % species < 8 µm and the max diameter of the counted species. Populations at ~2 µm associated with beads and populations at ~ 1 µm associated with S. aureus cells.

Beads were present in both samples with and without ClfA1 conjugated to the surface. The presence of beads in the unconjugated bead samples indicated that there were non-specific interactions between beads and biofilm components; indicated by objects between 1.9 – 2.1 µm in size. Figure 2.41 shows the average concentration of entities in this size range for the three experimental conditions. Biofilm samples treated with unconjugated beads have a higher concentration of beads present at 6.44 x 10^7 particles/ mL compared to that of ClfA1-A647 treated beads at 3.7 x 10^7 particles/ mL.

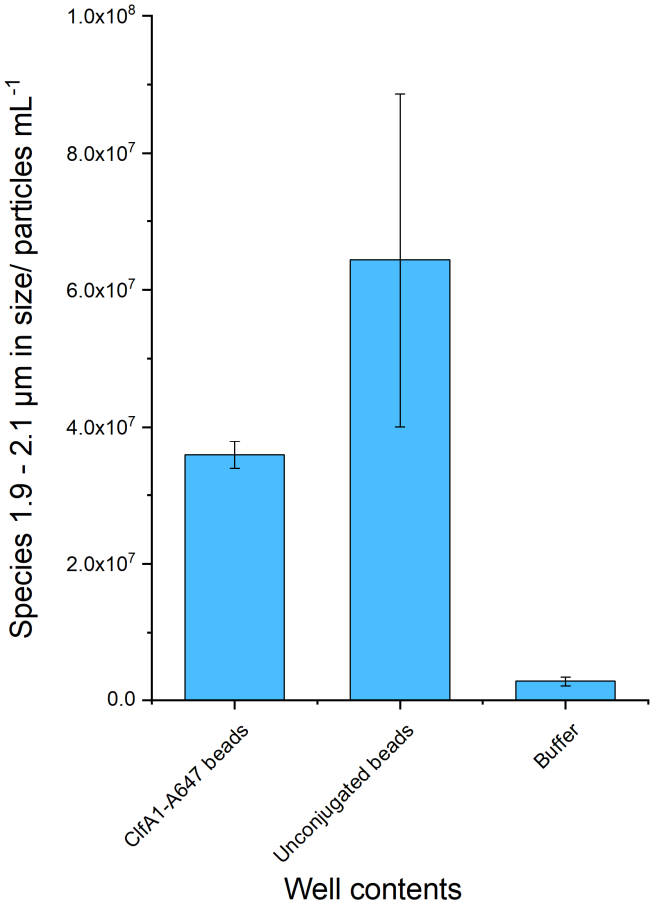

Figure 2.41. Bar chart showing concentrations of species between 1.9 – 2.1 µm in biofilm samples treated with 2 µm beads.
x-axis shows contents of wells and y-axis the concentrations of particles between 1.9 - 2.1 µm in particles mL^{-1}. Biofilm samples were treated with 50 µL of reagent. Standard error of the mean (n = 20, for 20 images taken across each set of experimental conditions) shown as error bars.

Calculations of particle concentration using the MATLAB script relies on species being perfect spheres. Images in Figure 2.39 shows the presence of large clumps of particles that appear more frequently in the sample with bead-bound ClfA1 than in that of the unconjugated beads. The formation could be attributed to the cross linking of beads on adjacent proteins via the *S. aureus* cells. These clumps were largely ignored by the MATLAB software which may have contributed to a lower experimental calculated concentration. Though the inability of the software to delineate the number of particles in these clumps can explain the difference in concentration, the presence of beads in the unconjugated control shows that the beads do interact with biofilm component and therefore non-specific interactions will play a factor in the association of Affimer-beads to *S. aureus* biofilms.

The presence of these clumps may infer a specific interaction between Affimer-beads and bacteria. The images form this experiment were reanalysed, species consisting of five or more beads clustered together were considered ‘cluster positive’ and any other species ‘cluster negative’, the number of clusters was then plotted in Figure 2.42.

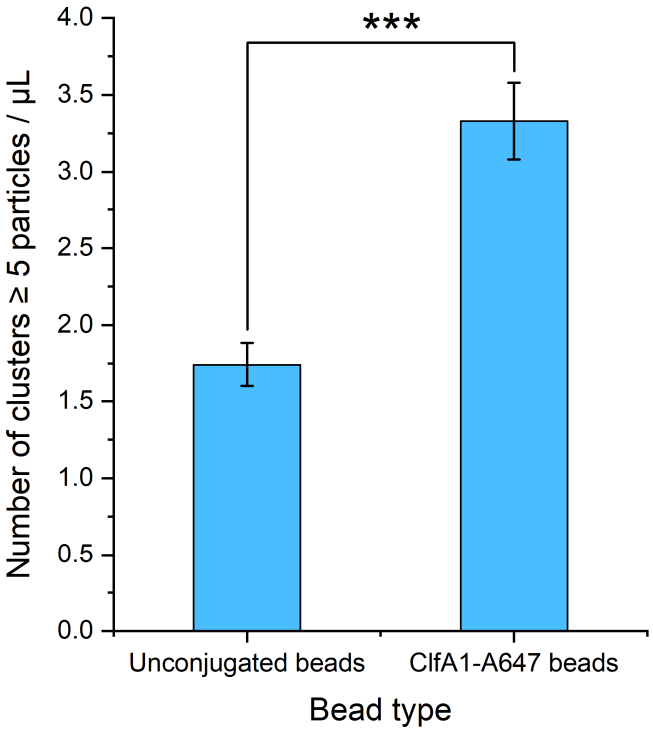

Figure 2.42. Bar graph showing the number of cluster species formed when UAMS1 S. aureus biofilm was treated with bead species.
Graph shows results for non-specific beads, which do not have protein on the surface and are supplemented with imidazole to prevent interaction between the Nickel-NTA on the surface and biofilm components. ClfA1-A647 beads have surfaces functionalised with ClfA1 Affimer which a covalently attached to a Alexafluor647 molecule. Wash buffer : Phosphate Buffer with 150 mM NaCl. Error bars show SEM values (n = 20, for 20 images taken across each set of experimental conditions) associated with means and their associated P value (paired student's t test, < 0.05).

To minimise non-specific interaction between non-conjugated beads and ClfA1-A647 beads, the salt concentration of the phosphate buffer was increased from 150 mM NaCl to 500 mM NaCl. Furthermore, the nickel present on the surface of the beads was stripped by the addition of 100 mM EDTA. The EDTA sequesters nickel atoms attached to the beads, which should have eliminated the ability of the beads to interact with any histidine residues present on proteins at the biofilm-bead interface. Figure 2.43 shows the concentration of beads in each sample calculated for each bead type,

Figure 2.44 shows the observed number of clusters in each experimental sample compared with that of the experiment.

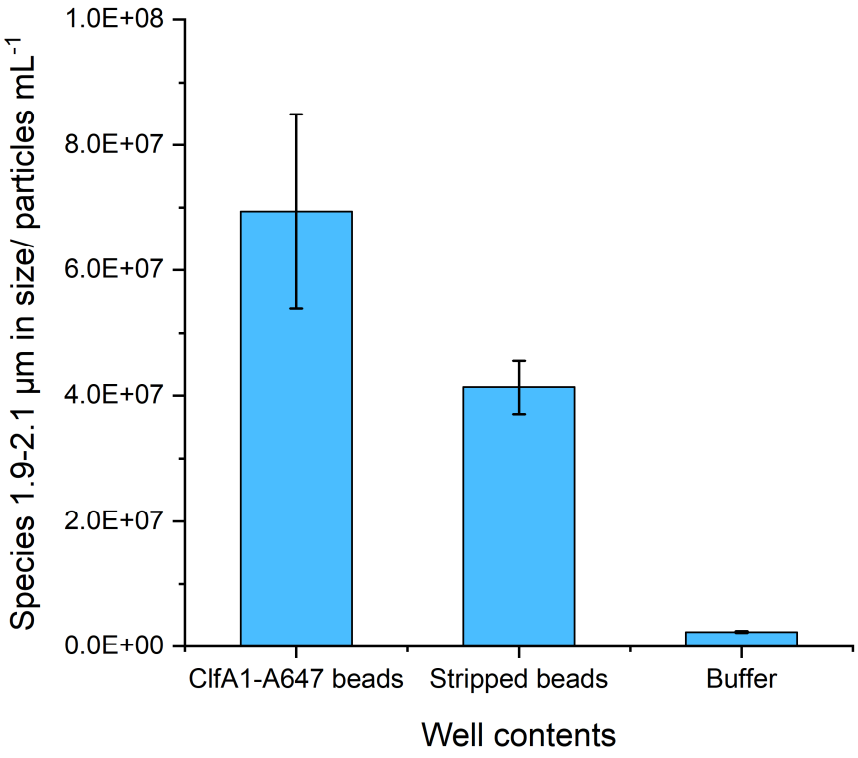

Figure 2.43. Bar chart showing concentrations of species between 1.9 – 2.1 µm in biofilm samples treated with 2 µm beads, both with ClfA1-A647 attached and ones stripped of Nickel with EDTA.

The x-axis shows contents of wells and y-axis the concentrations of particles between 1.9 - 2.1 µm in particles mL^{-1}. Biofilm samples were treated with 50 µL of reagent. Standard error of the mean (n = 20, 20 images acquired for each set off experimental conditions) shown as error bars.

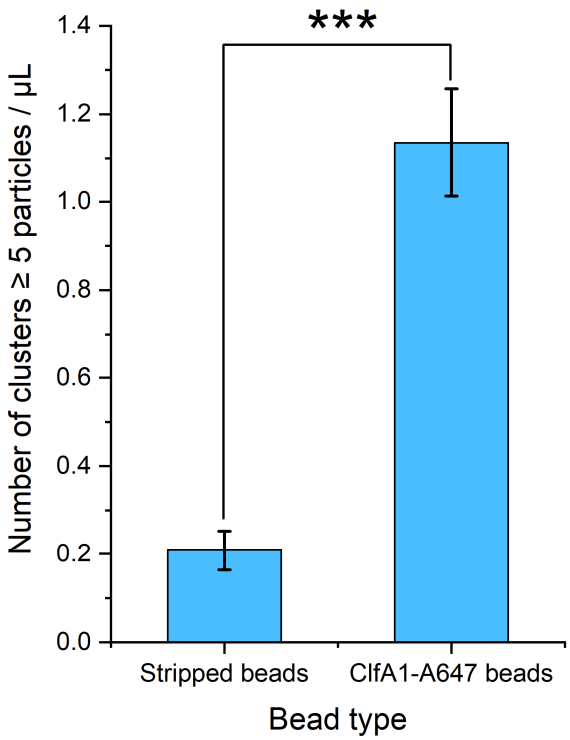

Figure 2.44. Bar graph showing the number of cluster species formed when UAMS1 S. aureus biofilm was treated with bead species.
Graph shows results for non-specific beads, which do not have protein on the surface and have had nickel removed to prevent interaction between the Nickel-NTA on the surface and biofilm components. ClfA1-A647 beads have surfaces functionalised with ClfA1 Affimer which a covalently attached A647 molecule. Wash buffer : Phosphate Buffer with 500 mM NaCl. Error bars show SEM values (n= 20, 20 images acquired for each set of experimental conditions) associated with means and their associated P value (paired student's t test, < 0.05).

The addition of a higher salt wash buffer and sequestering of the nickel from the polystyrene beads has caused a relative increase in ClfA1-A647 bead concentration to that of the stripped non-specific beads. The number of clusters observed generally decreases between experiments but a statistically significant increase is observed between ClfA1-A647 and stripped beads. The general decrease in cluster population can be explained by the elimination of non-specific cluster formation by the high salt buffer. The reproducibility in high cluster formation in ClfA1 conjugated bead samples indicates that the ClfA1 Affimer is responsible for increased cluster formation. This maybe be

being caused by crosslinking of beads by cells or by other biofilm components via the ClfA1 Affimer.

However, by only treating the control beads with EDTA, and not using EDTA to sequester Nickel ions from the beads with Affimer bound, the controls used in this experiment may not represent the most accurate data set. There is still a possibility that the un-conjugated Ni-NTA species on the beads loaded with the Affimer protein may be contributing towards their interactions with the *S. aureus* bacteria, as well as the Affimer itself. Given time, this experiment should be repeated using either some sort of blocking species to occupy the Ni-NTA sites on the control beads and also empty sites on the Affimer-beads, maybe using the control AAC Affimer as mentioned previously.

2.4 Chapter conclusions

The overall aim of the body of work covered in this chapter was to ascertain a protein target that could effectively bind the *S. aureus* biofilm and could be used in conjunction with microbubbles to localise them to the site of a biofilm infection.

Of the two candidates investigated, the ClfA1 Affimer was identified as a prime candidate for use in the microfluidic flow system. Throughout this body of work many issues arose working with the MBL protein, and even when expressed as part of a MBP fusion protein, purification of the complex proved problematic. Though the application of this protein for use in the context of this project may eventually prove successful, this claim falls outside the scope of this thesis due to time constraints.

The ClfA1 Affimer protein, through static biofilm screening and binding interaction experiments was shown to bind to the *S. aureus* biofilm. The ITC showed a tight binding interaction between ClfA1 and its binding partner ClfA, found on the *S. aureus* cell surface. This data coupled with the demonstrated ability of the ClfA1 Affimer to localise the polystyrene bead to a static biofilm indicated that it was the front running candidate for use in conjunction with microbubbles in a microfluidic system. From this point, work with ClfA1 was prioritised over the use of MBL protein due to the abundance of material and ease of use.

There may be some limitations using ClfA1 to target biofilms. The ClfA1 Affimer targets a cell surface protein (ClfA), whose expression on the cell surface can be dictated by different stages in cell growth.[163] This variation in cell surface expression of the target may affect the efficacy of the Affimer to localise the MBs to the biofilm. Furthermore, if the target is cell surface-associated, the Affimer protein's ability to bind the biofilm will be dictated to by the bacterial composition of the biofilm and the instances of cells existing at the edge of the extracellular matrix. The bacterial composition of a biofilm varies between 5-20 % of the total volume and are usually distributed randomly which may decrease the amount of possible interactions with bacteria cells.[164]

Mannose binding lectin is a protein that functions as part of a trimer of identical proteins. A single monomer has low affinity for mannose than its trimeric counterpart. The cooperativity of the three binding sites, in close proximity, increases the affinity of the whole complex. In the innate immune response, the trimeric proteomers form larger oligomers; dimers, trimer and tetramers that then further cooperate together to increase their affinity to cell surface-bound mannose. Single iterations of the Affimer proteins conjugated to a common surface, such as on the surface of a microbubble, may increase their avidity for the cell surface through cooperativity in a similar way.

3 Development of a microfluidic system for biofilm study

Results and discussion

Part 2

An aim of this thesis was to design a microfluidic system to allow the study of biofilms under conditions of flow. In pursuit of this aim, a microfluidic device was designed based on simple flow systems previously described in the literature. The benefits of using a microfluidic flow system is that their small size allows them to be integrated into a number of different imaging techniques; they are more efficient; and, they allow control experiments to be run in parallel, under the same conditions as the test. The use of microfluidics within this project allowed for the imaging of the biofilm by confocal laser scanning microscopy (CLSM) without having to dismantle the experimental system or disrupt the cultivated biofilms.

3.1 Initial microfluidic device design

For preliminary proof of concept, a microfluidic device was designed utilising the dimensions of a flow cell used by Greener *et al*.[56] Though research exists that uses more complex systems effectively (described in section 1.3) a more 'stripped-back' system was used that could cultivate biofilms easily, without the need for too strenuous optimisation. Figure 3.1 shows the proposed microfluidic device. The height was set to 180 µm to keep the volume of the device small, and width and depth of 4 mm and 20 mm, respectively, to provide a large surface area for potential bacterial colonisation.

The proposed biofilm chip was electronically designed using AutoCAD (AutoDesk, CA, USA) software by Dr Peng Boa (University of Leeds, School of Physics and Astronomy). The microfluidic 'chip' was then manufactured using method described in section 6.3.1. A glass slide (50 x 22 x 1 mm) was chosen as the base of the chip for use on a confocal microscope, as it allowed for both dry and oil immersion lens use. The polymer used for the device was polydimethylsiloxane (PDMS). PDMS is often chosen for cell culture use in microfluidic devices due to a number of favourable characteristics:[165] PDMS is optically transparent which allows for the use of many optical detection methods; The polymer is also gas permeable;[166] inert so can allow for coating of the chamber surfaces with protein;[167] and has low auto-fluorescence.[168] These factors make the device biocompatible and ideal for biofilm cultivation.

Once the device was manufactured, a bespoke 3D printed bracket was designed and manufactured by Dr Ben Johnson (University of Leeds, Department of Physics and Astronomy) to integrate the microfluidic chip onto a CLSM. The chip consisted of three parts; a base plate into which the chip was inserted, and two mounting brackets that were magnetically held in place by the base plate to secure the chip in the bracket (Figure 3.2). This bracket kept the chip rigid during image acquisition, minimising movement caused by mechanical stress from oil immersions lenses and movement of the automated stage.

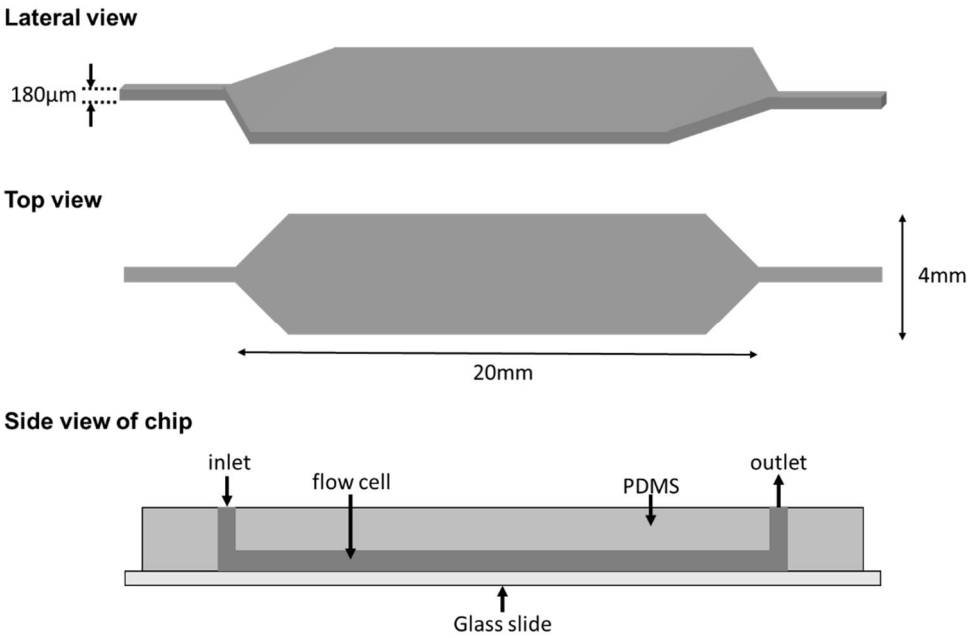

Figure 3.1. Diagram depicting the dimensions and design of the biofilm growth flow cell on the microfluidic device V1.0.
Lateral (top) and top view (middle) shown. Flow cell was designed to eliminate 90 º corners, which cause areas of dead volume. Bottom image shows side view of the chip.

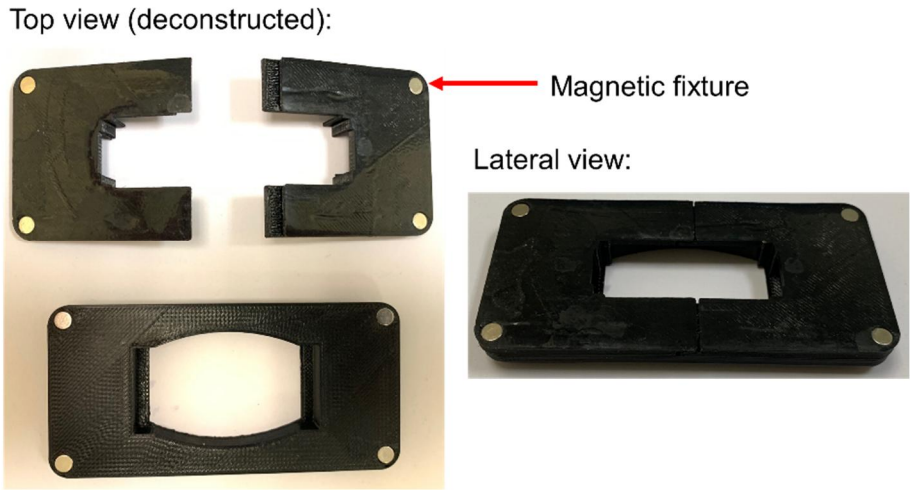

Figure 3.2. Photograph of 3-D printed microfluidic chip-holding bracket. Top view shows bracket deconstructed, with interlocking top plates and base plate. Magnetic fixtures indicated by the red arrow secure chip in place in the holder. Lateral view shows bracket fully constructed.

3.1.1 Initial biofilm flow system V1.0.

To supply media and bacteria to the microfluidic chamber, a flow system was developed in collaboration with Dr Ben Johnson (University of Leeds, School of Physics and Astronomy), that would allow for a constant flow of media through the microfluidic chip in a controlled temperature incubator. Figure 3.3 shows a schematic of the initial biofilm growth chamber, consisting primarily of Tygon tubing, Luer lock fittings, sterile sample tubes and a mp6 piezoelectric diaphragm micro-pump (Bartels mikrotechnik) pump. A piezoelectric diaphragm micro-pump moves liquid by the vibration of a diaphragm;[169] their small size allowed easy integration of the flow chamber into a bench-top incubator. All fixtures and fittings were connected using male and female Luer lock adapters.

To secure the flow system in place, 3-D printed brackets were designed and manufactured to house all necessary components of the flow system. The thermoplastic Acrylonitrile-Butadiene-Styrene (ABS) was used as the 3-D filament material for the housing due to its excellent heat retention properties.[170] This meant that any media reservoirs housed in 3-D printed

brackets would retain their heat for short periods of time, if removed from the incubator. The chamber was magnetically held in place in the incubator using magnets integrated into the brackets and the base of the incubator. Liquid was pumped through the system by the piezo pump connected to a control box. The system was designed to minimise risk of contamination of, and from, the surrounding environment, with the air being drawn in and passed out passed a 0.22 µm male Luer lock filter. Tygon tubing inserted directly into the microfluidic chip was sealed with UV-curable adhesive to prevent leakage. The system operated as a closed flow system without instances of leaking; movement of the system from one location to another could be performed easily using a secondary closed container without disruption to the system. Figure 3.4 shows the final manufactured biofilm growth chamber placed within a bench-top 37 ºC incubator. Mobility and constant flow integrity were not the only facets of the design that needed to be demonstrated, the sterility of the system needed to be tested to ensure experimental reproducibility and validity.

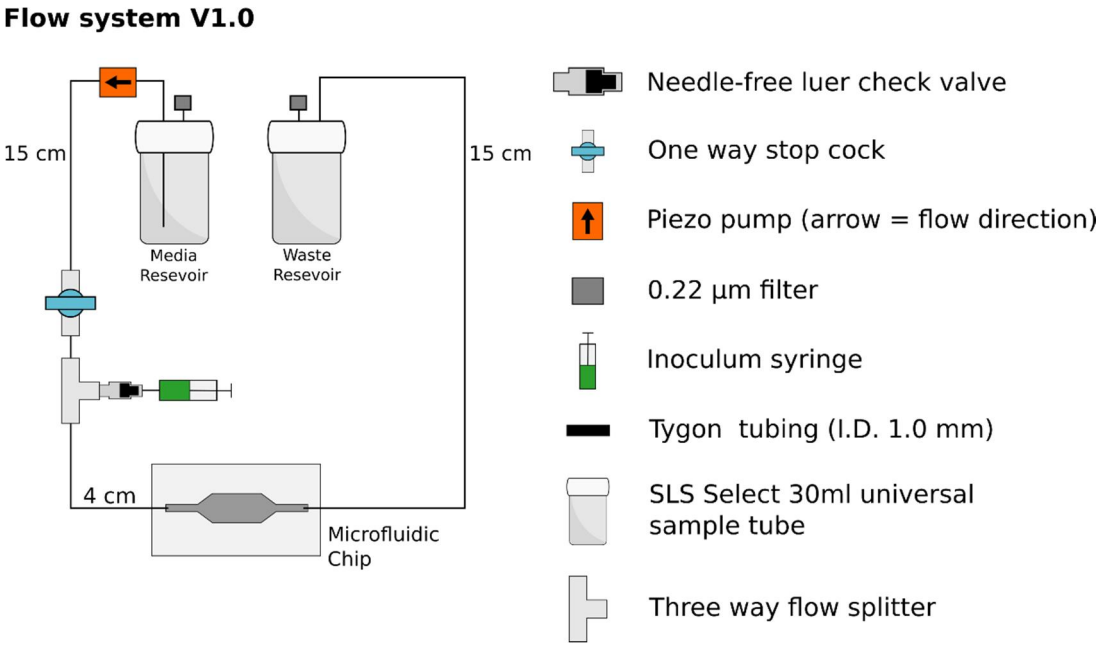

Figure 3.3. Schematic representation of Flow system V1.0.

30 mL sample tubes were used as media and waste reservoirs. Both were fitted with a metal needle via a male Luer lock connector. Luer lock connectors were fitted to sample tubes by drilling a hole in the tube lids, and sealed with UV curable adhesive. Tygon tubing (I.D. 1.0 mm) was used to supply media to the microfluidic chip and back to waste. A one-way stopcock was used to isolate the media inlet from the inoculum syringe. Needle-free Luer check valve fitted to incorporate the inoculum syringe into the system. This allowed for introduction of the inoculum to the chip without contaminating the media reservoir. Tygon tubing was inserted into holes in the PDMS of the microfluidic chip to allow for flow of media through microfluidic chamber. 0.22 µm filters were fitted on the media and waste lids in order to prevent air contamination of system.

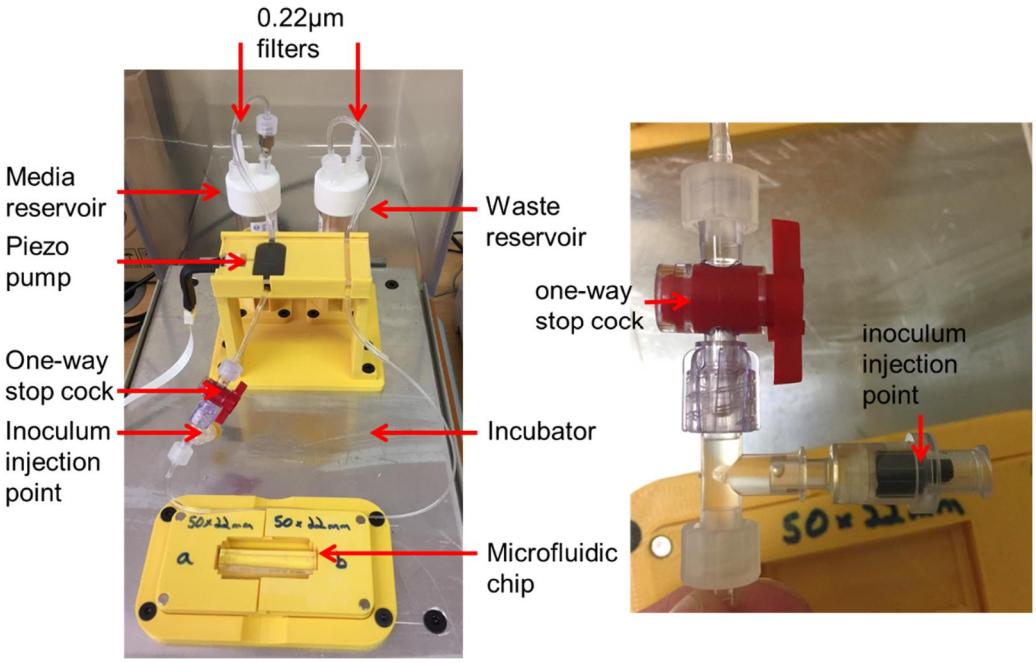

Figure 3.4. Photograph of biofilm growth chamber in an incubator.
Top image shows whole flow system in incubator and the bottom image a close up of the inoculation injection point and tap. Tap is designed to prevent flow of inoculum in to pump. More detailed description of biofilm chamber can be found in 'Microfluidic Methods'.

3.1.2 Sterilisation protocol

To establish a robust sterilisation protocol, different sterilisation techniques were investigated for use with the biofilm flow system. Samples of all components were autoclaved to determine reusability of each element should they be repeatedly steam sterilised. Any component that contained moving parts (stock-cocks and inoculation port) were found to become warped during the autoclave process and was more susceptible to cause leaks in the sterilised system. Components such the microfluidic chip, micro-pump and tygon tubing were able to survive the autoclave process. Those that did not survive the autoclave were washed with 70% aqueous ethanol and incubated under a UV lamp for 30 minutes. Table 3.1 shows the sterilisation techniques used to sterilise each component of the system.

Table 3.1. Sterilisation techniques used to sterilise flow cell components. Shows each components and the sterilisation technique used before inoculation. If a component was not autoclaved it was rinsed with ethanol, allowed to dry and placed under a UV light for 30 minutes.

	Sterilisation technique		
Component	Rinse with 70% EtOH (aq)	UV Light (30 mins)	Autoclave
Microfludic chip	✓	✗	✓
Piezo pump	✓	✗	✓
one-way stop cocks	✓	✓	✗
Three-way splitter	✓	✓	✗
Male/Female luer lock adapters	✓	✗	✓
Needle-free luer check valve	✓	✓	✗
Tygon tubing	✓	✗	✓

To check the success of sterilisation, autoclaved brain heart infusion (BHI) broth was flowed through the system, incubated at RT overnight and the effluent media was plated out onto a 2% horse blood agar and Sabouraud agar plates (the former is a general medium able to support growth of a wide range of bacteria and Sabourauds was used to culture fungi). These plates were incubated at 37 ºC for 72 hours, after which no colonies were observed on either agar dish. Once the flow chamber and all its components had been constructed and sterilised, its ability to cultivate biofilm was tested.

3.2 Microfluidic Biofilm study system (MBSS) development and optimisation

3.2.1 Initial biofilm cultivation

The system was sterilised and equilibrated with BHI broth as described in protocol in 6.3.4. The microfluidic chip was then inoculated with a culture of *S. aureus* SH1000 *lux* cells (provided by Dr Chris Randall, University of Leeds, Faculty of Biological Sciences), that had been cultured overnight. The *lux* strain is bioluminescent, which presented an opportunity for imaging the bacteria cells. Figure 3.5 shows images of species attributed to biofilms cultivated in the microfluidic device (V 1.0).

The bioluminescence of the cells proved an ineffective way of imaging the cells as bioluminescence requires long exposure times in order to accumulate enough photons to detect a signal.[171] Biofilm formation occurs when bacterial cells adhere to surfaces in the body (i.e. medical devices), followed by cell proliferation.[3] It was initially assumed that the cells would adhere to all surfaces in the microfluidic device and form biofilms over all surfaces within it. However, the biofilms observed in this experiment appeared to be patchy and polymorphic, with no real correlation between biofilm location and size. While this first biofilm cultivation experiment showed a promising start to being able to study biofilms in this novel flow cell, the bacteria could not be imaged using their innate bioluminescence and an alternative imaging method needed to be investigated.

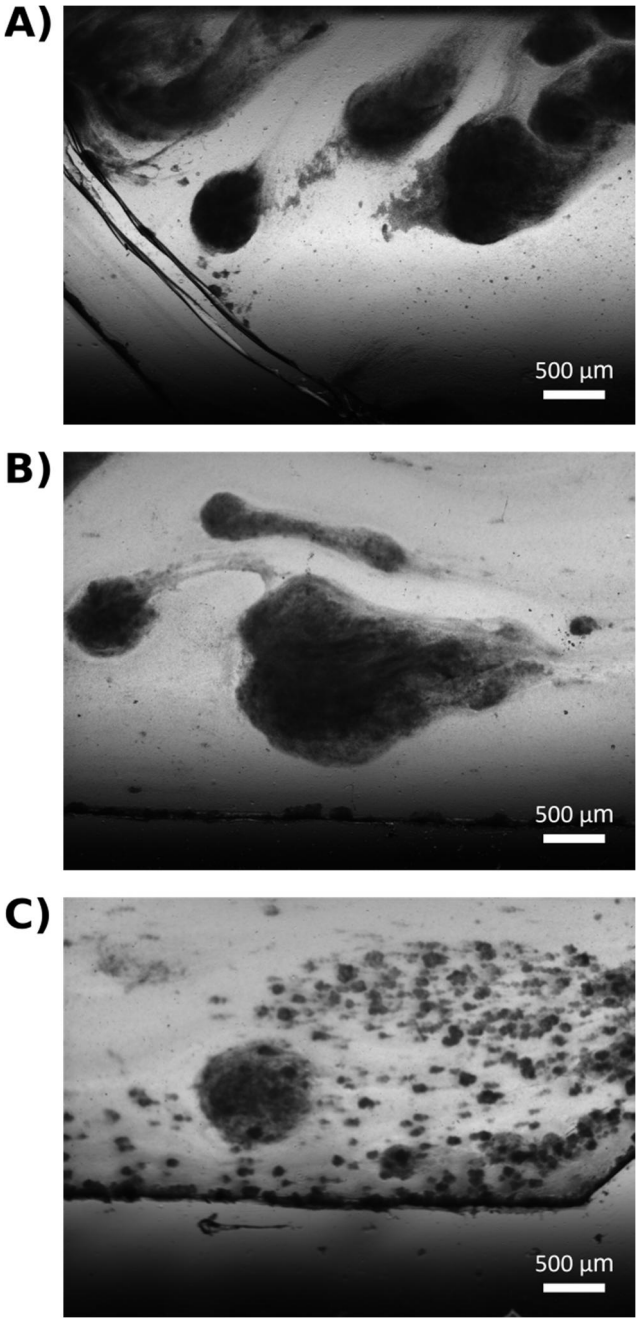

Figure 3.5. Bright Field light microscopy image of biofilm chamber at three points.

A) towards the end of the chamber, B) the middle of the chamber and C) the start of the chamber. In all images the direction of nutrient flow is from left to right. The dark shapes are assumed to be biofilms consisting of SH1000 lux S. aureus cells.

3.2.2 LIVE/ DEAD staining of biofilms

The use of LIVE/ DEAD stain when imaging cells for use in confocal microscopy is common practice.[172] Using such stains also allows use of a wider range of cells strains without the need of innate luminescence/ fluorescence. The dyes used were DMAO and EthD-III (Ethidium bromide homodimer – III) Live/ Dead stain (Biotium). DMAO is a membrane permeable dye that fluoresces when it binds double stranded DNA.[173] DMAO stains both living cells and dead cells and causes these cells to fluoresce green (λ_{em} maxima = 535 nm), as DNA from cells with disrupted membrane (dead cells) will still make contact with the dye. EthD-III is also a DNA binding molecule but is not membrane permeable and therefore can only bind DNA from cells with compromised cell membranes (dead cells).[174] Once bound, EthD-III fluoresces red (λ_{em} maxima = 590 nm). In this experiment the parent strain of the *S. aureus* SH1000 *lux* strain, SH1000, was used to inoculate the system and the biofilm was cultivated over the course of 48 hours at a flow rate of ~ 80 µL min^{-1}. The dye was introduced using a syringe into the tubing upstream of the media inlet, which caused some bubbles to enter the system. Figure 3.6 shows a composite image of the bright field images taken of the microfluidic chip. Each image has been arranged to show their relative position on the device. Figure 3.7 shows some of the images acquired utilising the fluorescence from the LIVE/ DEAD cell viability stain.

Figure 3.6. Bright field images of 3 distinct areas of the microfluidic device after 48 hour biofilm cultivation at 2X magnification.
Green arrow shows direction of nutrient flow and arrows to the left and right show inlet and outlet of media and waste. Dark 'meteorite' species show biofilms formed in the flow chamber, large bubbles visible attributed accidental introduction of air into system during addition of dye.

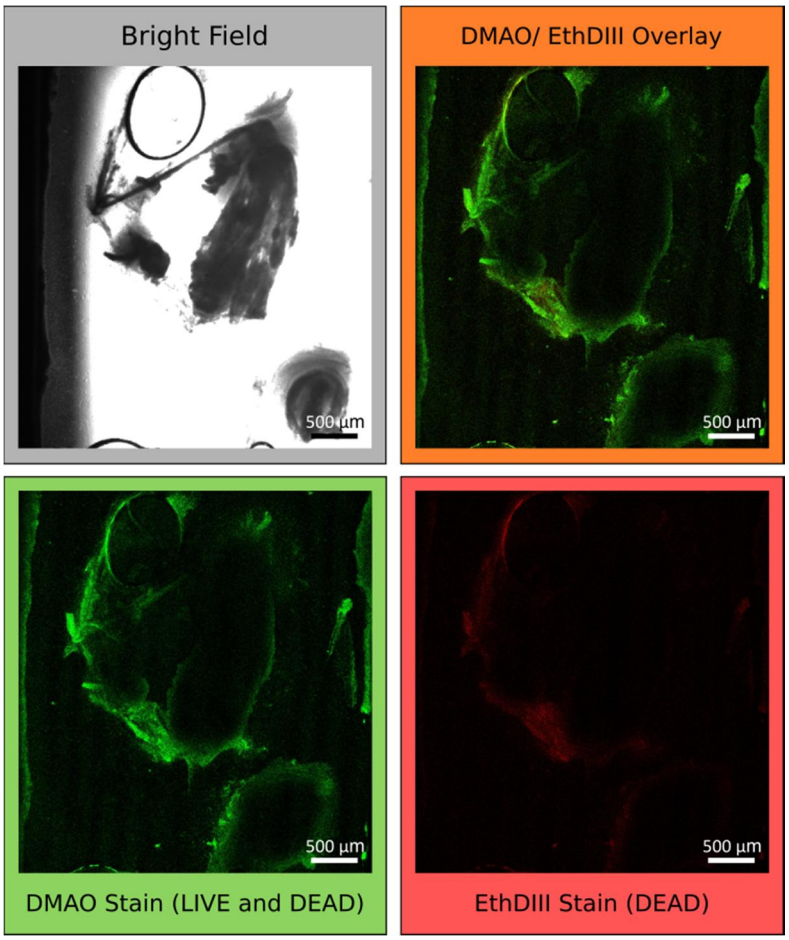

Figure 3.7. Biofilm species cultivated on a microfluidic chip stained using a cell viability LIVE/ DEAD stain.
Top left, bright-field image of the biofilm at 2X magnification. Top right, overlaid image of DMAO and EthD-III LIVE/DEAD stain imaging channels. Bottom left, DMAO stained species representing living and dead cells. Bottom right, EthD-III stained cells, representing dead cell components.

Initially, it seems that bacteria within the biofilms have been stained by the LIVE/ DEAD stain, with the overlay displaying that the biofilm comprised viable cells, indicated by the predominantly green colour in the overlays (as opposed to a more red colour associated with greater DEAD stain emission). Dead cell components within the biofilm should show orange/ red in overlaid images. It is assumed the intensity of the red colour may be attributed to the proportion of EthD-III fluorescence in that area of the image. Those cells with more damaged membranes will likely display a more intense red colour than those with little to no membrane integrity. The low signal associated with the dead stain was attributed to the cells with compromised membranes and

eDNA in the biofilm matrix. However, only the peripheral cells had been stained, indicating poor dye penetration to the centre of the biofilm. This is not uncommon among biofilm staining procedures for CLSM, and poor dye penetration can lead to an underestimation of biofilm thickness.[175]

A z-stack is a composite image of images taken in the xy plane arranged by their relative positions moving through the z plane, the result is a rendered 3-D image of the confocal sample. Analysis of these biofilms by compiling a z-stack showed that the dye had indeed not been able to penetrate the whole biofilm (figure 3.8). The issue of penetration was not a huge detriment to the develop of the flow system, as enough of the outer layer of bacteria cells were stained in order to give a representation of interactions at the surface. Having demonstrated that the flow system was suitable for cultivating biofilms, the next steps were to develop methods to introduce other reagents (MBs, proteins, etc.) into the chamber

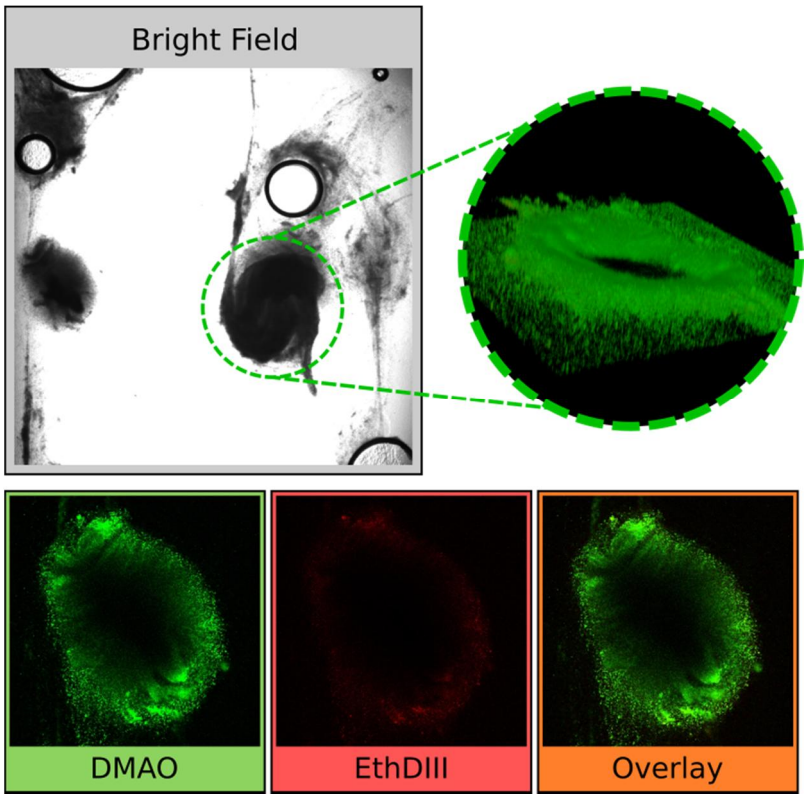

Figure 3.8. Z-stack analysis of a biofilm cultivated on chip.
Top left, a bright field image of the middle third of the chip including a highlighted biofilm. Top right, a 3D rendering of a z-stack performed on the biofilm in the green circle of the left image. Bottom, images taken through the centre of the biofilm through the xy plane. From left to right shows live and dead staining with DMAO, dead staining with EthD-III and an overlay of the two staining channels. The predominant green colour in the overlay shows presence of mostly live cells.

3.2.3 Introduction of reagents to microfluidic chip

The successful introduction of reagents to the flow cell was essential for further work. In order to introduce these reagents to the cultivated biofilms, a hole was punched in the PDMS downstream of the media inlet port, shown at the top of Figure 3.9. Tygon tubing was attached through this port, which allowed reagents to be flowed in from an Eppendorf through a secondary piezo pump, shown in the flow system diagram in . Figure 3.10 shows red dye being flowed through this inlet in a flow system test experiment and indicates minimal backflow to the media inlet.

A reoccurring issue with the system associated with Figure 3.9 is that bacteria were found to colonise surfaces upstream of the inoculum inlet, and in some cases, the back-flow contaminated the media reservoir. Biofilms growing in the tubing increased the likelihood of a leakage forming. If a blockage formed, the back pressure prevented the piezo pump from working. A modification was made to the biofilm incubation chamber to prevent biofilms growing up-stream of the media piezo pump and contamination of the media reservoir. Figure 3.11, shows the layout of a new flow system (V1.2). The inoculum was injected into the microfluidic device at a secondary introduction point on the chip. When the one-way stopcocks are closed, backflow of cell culture from the inoculation point was minimal and therefore little to no biofilms grew upstream of the chip.

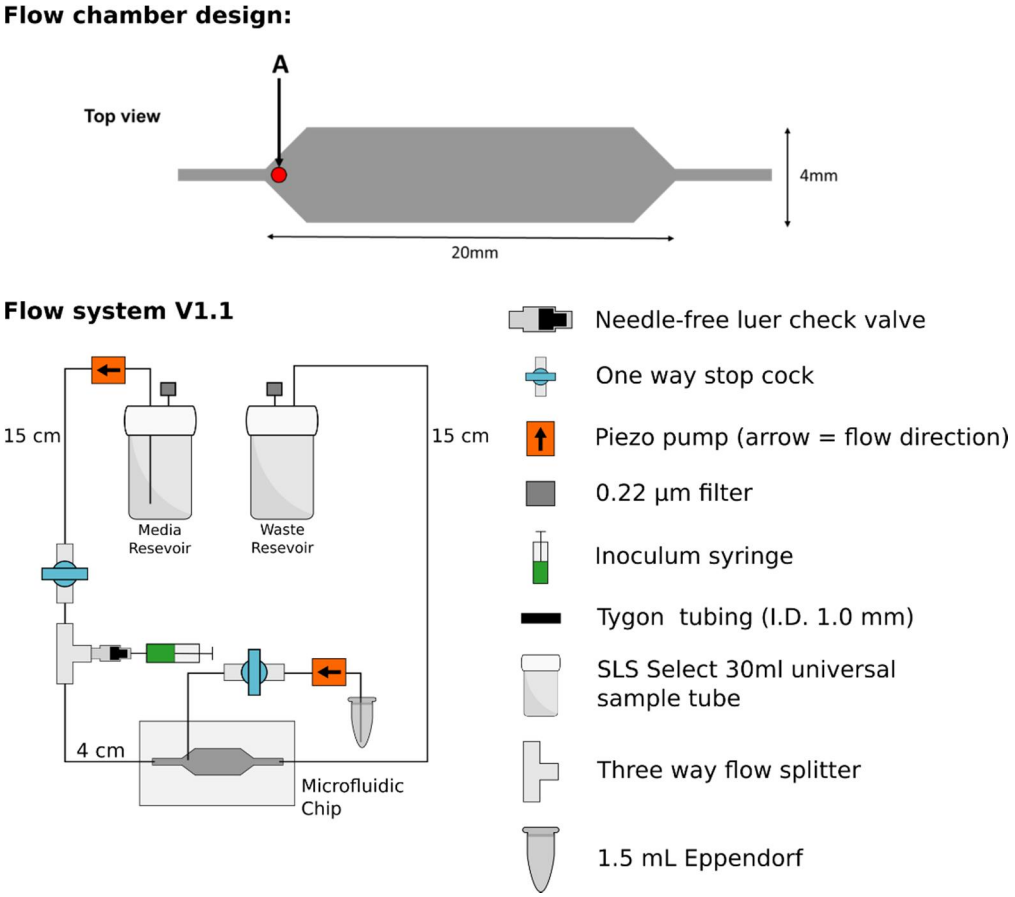

Figure 3.9. Flow cell design and 2D schematic of biofilm growth chamber with integrated port for treatment of biofilms in flow cell, flow system V1.1.
Above, Top view of microfluidic flow cell (V 1.1). *Point A indicates location of hole where reagents was be introduced. Below shows flow system schematic. Reagents were introduced into flow cell by a new hole punched in the PDMS. This is connected to tubing with a one-way stopcock on the end. The tap is then connected to a secondary piezo pump and Eppendorf that contained the desired reagents.*

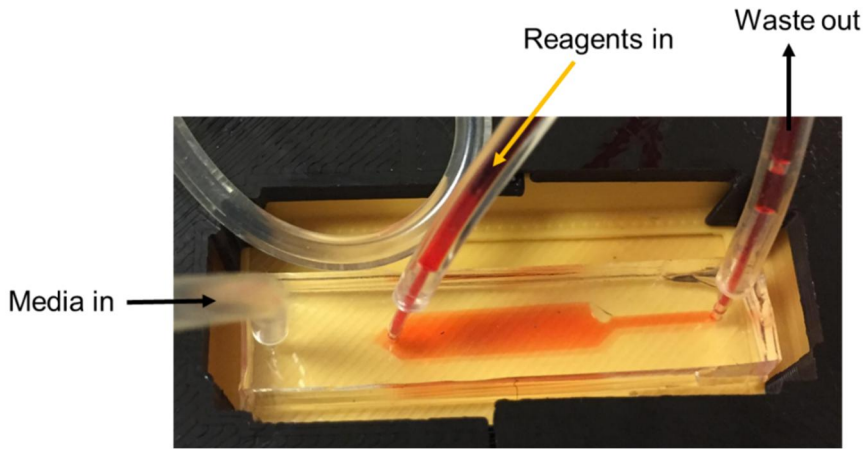

Figure 3.10. Photograph of microfluidic chip integrated in to the flow system. Media in and waste out tubes indicated with arrows whose directions signify direction of flow. Reagent flow is labelled with direction of flow. Red dye flowing into the flow cell seems to flow from reagent inlet to waste out with minimal back flow to media in. Pump supplying media through the media inlet is switched off.

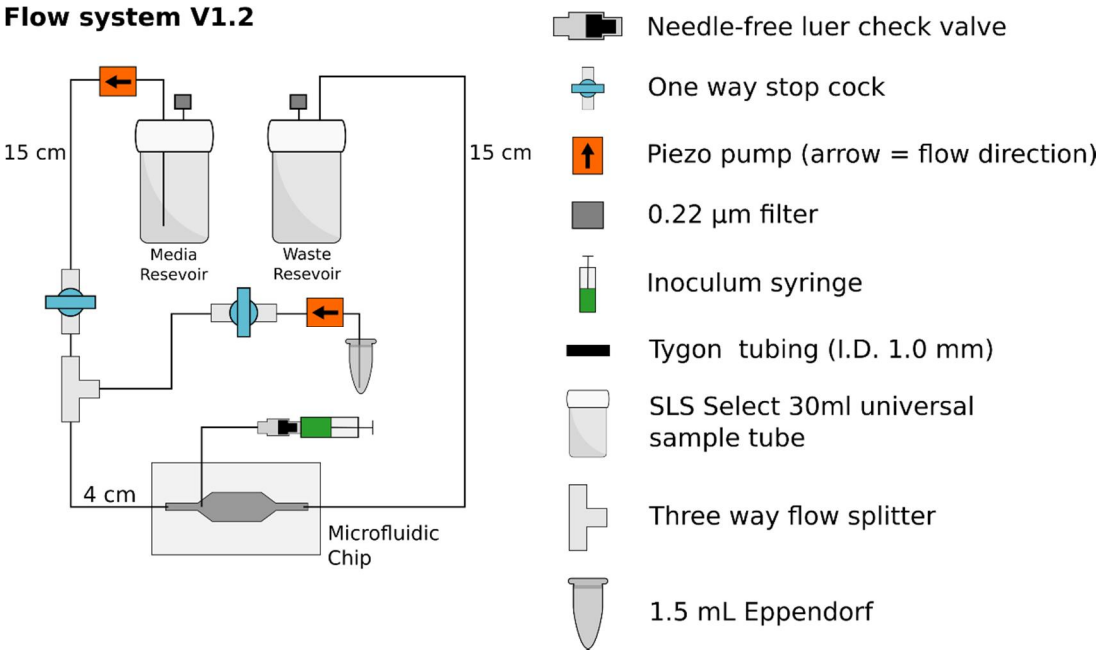

Figure 3.11. Schematic representation of biofilm flow model V1.2. Inoculation point was introduced further downstream of the T-junction via a hole punched in the PDMS. The reagent is introduced at the T junction between the microfluidic chip and media stop-cock.

The system was sterilised and constructed; *S. aureus* UAMS1 was used to inoculate the system using the new inoculation port. A bright field image was taken at three points along the whole microfluidic chip, shown in figure 3.13.

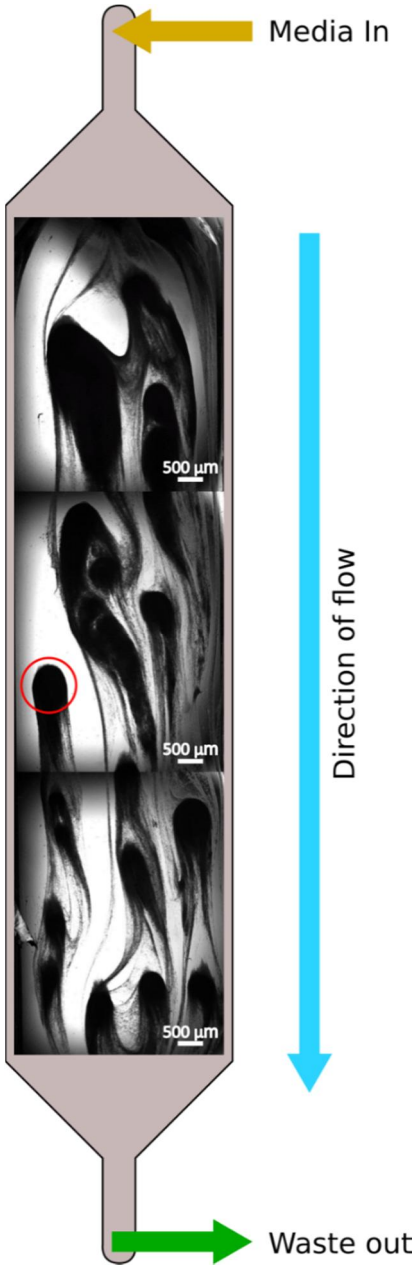

Figure 3.12. Composite images of bright field images taken from 3 areas on the microfluidic chip after SH1000 S. aureus biofilm growth.
The grey outline in the background approximates the relative location of the images on the chip. The arrow indicates direction of flow. The biofilm shown in the red circle was selected as the biofilm to be studied in the experiment. This biofilm appeared to have fewer biofilms growing in its proximity to inhibit flow of media around it.

Figure 3.13, shows a bright field image of the studied biofilm (a magnified section shown in the red circle of Figure 3.12) before the flow experiment. Fluorescein-labelled UAMS11 Affimer (10 µM, 1 mL) was flowed through the microfluidic device. Figure 3.13 shows fluorescence images of the biofilm over the progression of the experiment. The biofilm was first rinsed with buffer and a ‘pulse’ of protein was introduced at t ~ 14 minutes. The loss of fluorescent signal between 16 – 44 minutes resulted from the protein solution no longer flowing through the system. At this point a blockage formed in the tubing downstream of the chip and the flow rate had to be increased to clear it. The image at t = 50 minutes shows a second pulse of fluorescent protein flowing through the system. This could be explained by fluorescent protein pooling up in an area of dead volume upstream of the biofilm, and increasing the flow rate eventually ruptured a nearby biofilm and releasing the pool of fluorescent protein (illustrated in Figure 3.13). The final image at t = 56 minutes indicated the biofilm had also changed morphology over the course of the experiment, likely caused by the increasing flow rate. The fluorescein isothiocyanate (FITC) channel image at t = 56 minutes, modified to increase the brightness (right), revealed a region of low fluorescence intensity at the biofilm periphery, indicating that there is an area where UAMS11-Fluorescein was still bound.

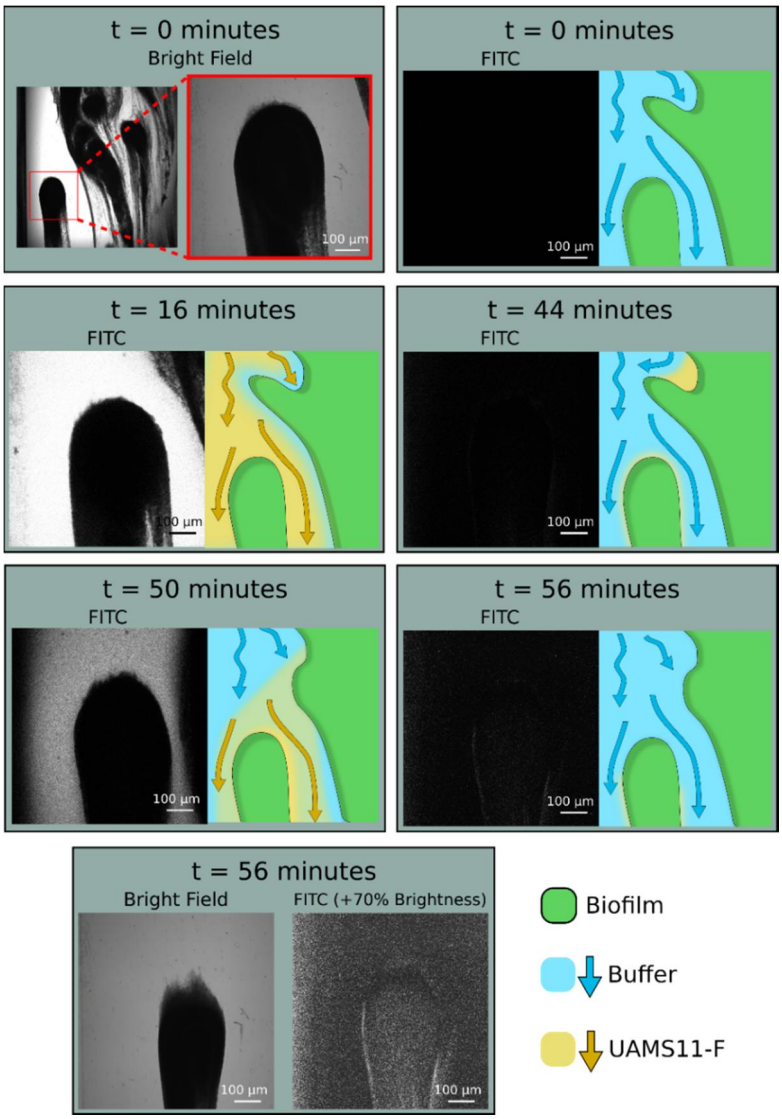

Figure 3.13. CLSM images of UAMS1-F Affimer biofilm binding experiment in microfluidic device.

Each box shows fluorescein isothiocyanate (FITC) emission channel CLSM images with a cartoon representation of the experimental environment surrounding the biofilm. At t = 16 minutes, Affimer UMAS1A-F has filled the flow cell. At t = 44 minutes buffer is washing the biofilm, but a "reservoir" of retained Affimer is hypothesised to exist upstream of the biofilm. The spike in fluorescence around t = 50 minutes was attributed to the "spillover" of protein solution from the hypothesised "reservoir". This reservoir may have been caused by an area of static volume within the flow cell, likely caused by the shape of an upstream biofilm. At t = 56 minutes the biofilm is being washed again with buffer. The final box shows the bright field image of the observed biofilm and the FITC images adjusted for brightness to show areas on the biofilm with low fluorescent signal associated.

Images acquired every two minutes of the observed biofilm were analysed using ImageJ software version 1.8.0 (FIJI). The software used the brightness values of the pixels in the image to assign a numerical value to the fluorescent signal in regions of interest set by the user. In a standard 8-bit JPEG image, pixels can have a value between 0 – 255, a zero value corresponding to black (no fluorescence), 255 corresponding to a white (maximum fluorescence or ‘saturation’). These fluorescent emission values for regions of interest shown in Figure 3.14 labelled ‘control area’ and ‘biofilm area’ were taken for each time point image. Figure 3.14 shows these values plotted against time, for both the control area and the biofilm area.

The analysis area for each of the fluorescence curves are set by the user in the ImageJ software. Therefore, areas set for the control were chosen by eye, in parts of the image considered to not contain biofilm. Without a LIVE/DEAD stain (not used here as DMAO and fluorescein have overlapping emission spectra), it could not be presumed that the area was devoid of bacteria species, and may not have represented an accurate control for the experiment. Since the image was acquired in the *xy* plane and was not acquired at the glass-liquid interface (in the *z* plane), the area where buffer was being flowed through ‘dead’ space was used to give control values. The control could therefore give an idea if any difference in fluorescence was due to biofilm or background fluorescence from the buffer.

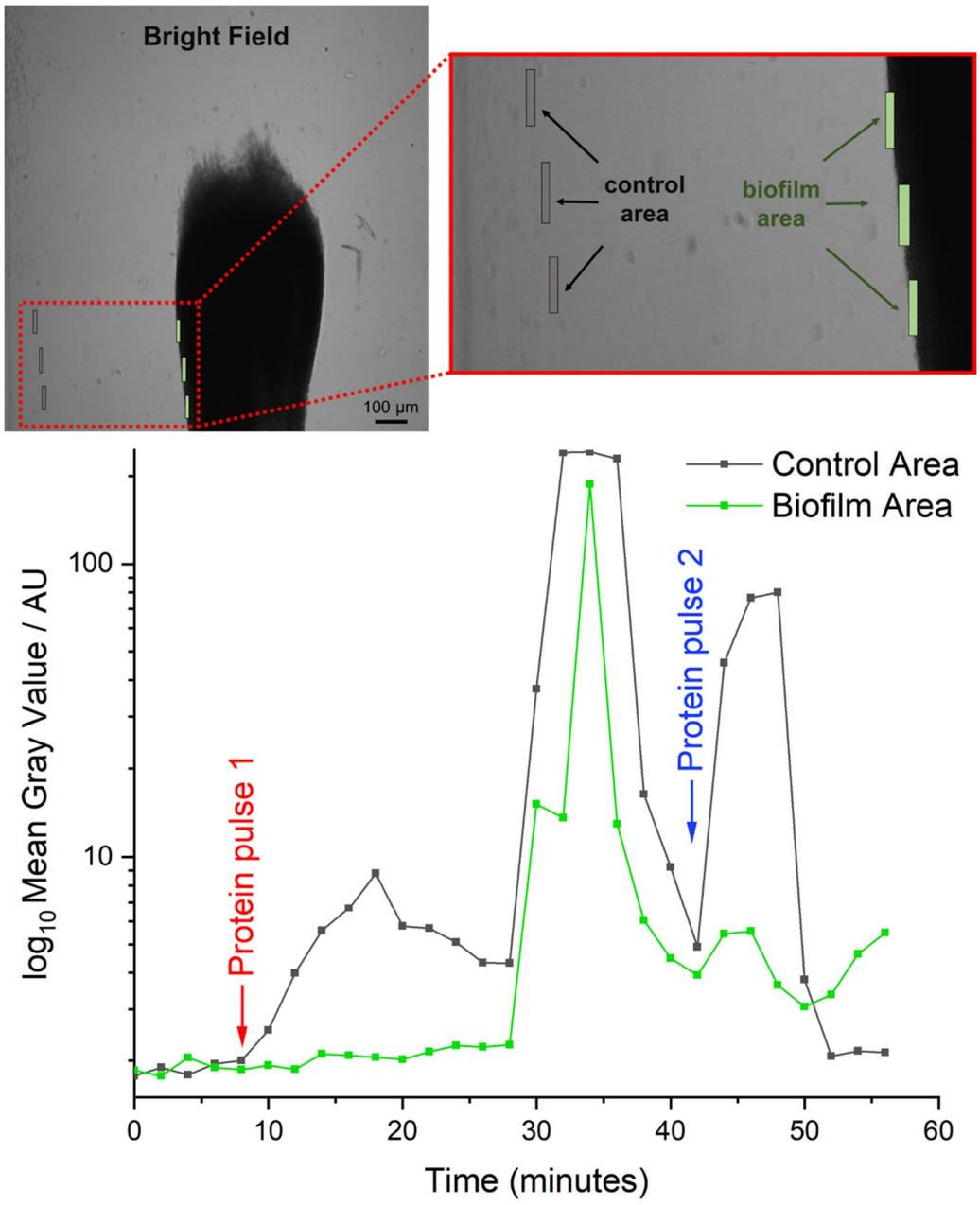

Figure 3.14. Mean Grey Value analysis of fluorescent CLSM images.
Top shows the regions of interest (ROIs) where mean grey valued was measured for FITC emission images acquired using confocal microscopy. The average pixel brightness for each area is plotted against time (values ranging from 0 – 255). Red arrow indicates introduction of UAMS11-F protein pulse, blue arrows shows reintroduction of protein pulse from a disrupted biofilm upstream. By 56 minutes, there is a higher fluorescent signal associated with the biofilm ROI compared to that of the non-biofilm associated ROI.

By the final time point, the fluorescent signal associated with the biofilm area was higher than that of the control area and its initial fluorescent signal value: indicating that protein was bound to the biofilm. The biofilm moved over the course of the experiment, which caused the biofilm to ‘drift’ in and out of the region of interest. This issue was attributed to the increase in fluorescence for the biofilm area between 50 – 56 minutes in Figure 3.14. During this time, the edge of the biofilm drifted into the ROI bringing protein bound to the biofilm’s edge into the analysis window; although this was the case, the final fluorescence values are higher for biofilm than that of the control area, indicating bound UAMS11-F protein.

The experiment showcased the functionality of flow cell V1.2 which allowed the introduction of reagents to biofilms cultivated on the microfluidic chip. However, the system was prone to regular blockages. Changes needed to be made to the microfluidic system that would allow for uninterrupted flow experiments.

3.2.4 Flow cell design V2.0 modification to prevent blockage

Although the system had produced some evidence that it could be used to cultivate and study biofilms, issues were consistently arising due to blockages in the system. When a biofilm forms in the body on a medical device, the initial attachment is mediated by interactions between the surface of the bacteria and the artificial surface.[13] Therefore, it can be assumed that interactions of this nature will occur at every point in the flow system where bacteria meet an artificial surface. This would include tubing from the inoculum port to the microfluidic chip, and tubing from the chip to the waste reservoir. In practice, this was an issue that caused blockages along the whole system during an overnight incubation period. Biofilms cultivated in the presence of a blockage, grew under flow for only part of the 18 hour incubation period; i.e. once a blockage had formed the system would become ‘static,’ with no flow of media. When being prepared for analysis the following day, the blockages needed to be cleared in order to stain the biofilms. The flow rate of the system therefore had to be increased in order to clear the blockage. In the process, the sheer stress of flow, once the blockage had cleared, would weaken the structural integrity of the remaining biofilms, or in some cases strip the

microfluidic chamber of all its biofilm. Blockages could occur from the point of the staining the biofilm right up to, and during, the flow experiment. Sheering off all or part of the biofilm could cause secondary blockages, repeating the cycle up to the point of experimental failure.

It was hypothesised that a build-up of biofilm was causing the blockages and that the narrowest parts of the system might be most susceptible . One way to mitigate against the risk of blockage was therefore to increase the diameter of the tubing supplying and draining the media to and from the microfluidic chip. The tubing was changed to have an internal diameter of 1.6 mm (previously 1.0 mm). However, due to the size of the pump inlet ports, the tubing was kept at 1.0 mm either side of the pump for a length of 2.0 cm. The smaller tubing that bridged the gap between the media tubing and the chip was replaced with metal rod adapters with an ID of 2.0 mm. This meant that the hole punched into the PDMS chip needed to be 2.0 mm wide, therefore the chip had to be redesigned to accommodate the change in tubing size.

When designing the new microfluidic chip layout, some other improvements were incorporated. Flow cell designs were undertaken in collaboration with Jordan Tinkler, and fabrication of flow cells was performed by Jordan Tinkler. In previous experiments, when biofilms did form they were distributed randomly at points that spanned the surface of the flow chamber, indicating that there was no preference for site of biofilm formation. This allowed for the design of a shorter flow chamber with the future aim of eventually fitting multiple chambers on the same chip. The bacterial inoculum was introduced via a channel on the microfluidic chip to prevent biofilms growing on tubing upstream of the media inlet. The channel taking the ‘waste’ off-chip to the waste reservoir was increased in width (1.2 mm from 1.0 mm) to prevent blockages forming downstream of the flow cell. Figure 3.15 shows the design of the proposed flow cell (V 2.0).

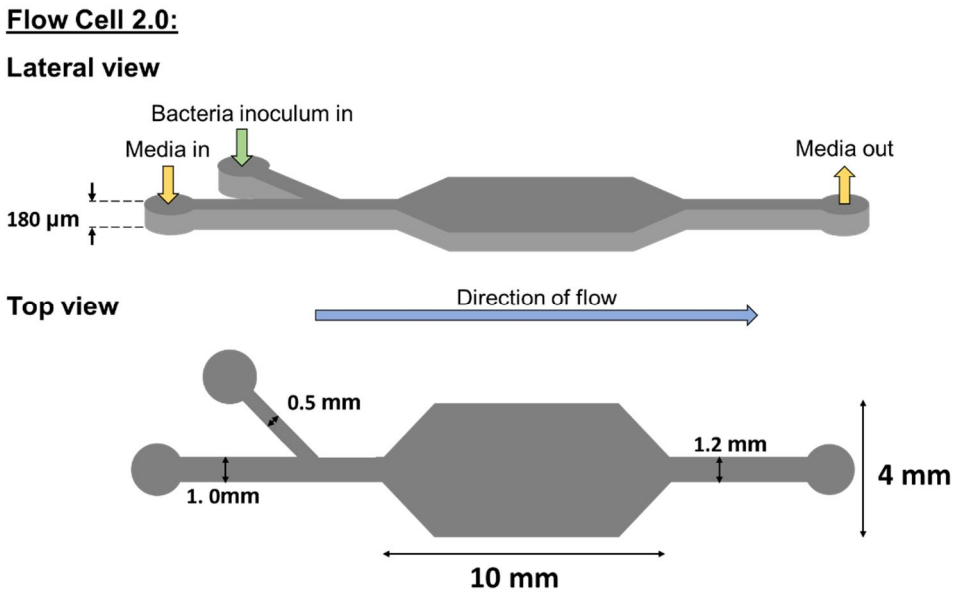

Figure 3.15. Schematic of new flow cell design (V 2.0).
Top image shows the lateral view and direction of flow from media in, inoculum in and waste out. Dimensions of all channels in the flow cell shown in top view. Blue arrow indicates direction of flow.

The new flow cell design (V 2.0) was tested using the same protocol as used in previous biofilm experiments (outlined in section 6.3.4). Figure 3.16 shows the layout of the new flow system. The presence of a 'reagent loop' was added to subvert problems arising from the introduction of bubbles to the chamber when flowing the LIVE/ DEAD stain through the system. Figure 3.17 shows the layout of the reagent loop. Using four three-way stopcocks in the given configuration, the loop could be primed with buffer without introducing bubbles. Introduction of a three-way stopcock at the T-junction between the chip and media reservoir allowed for the introduction of reagents into the loop whilst being isolated from the main flow system. Media reservoirs were changed from 30 mL SELECT tubes to 100 mL Duran bottles to allow for longer incubation periods before they needed refilling.

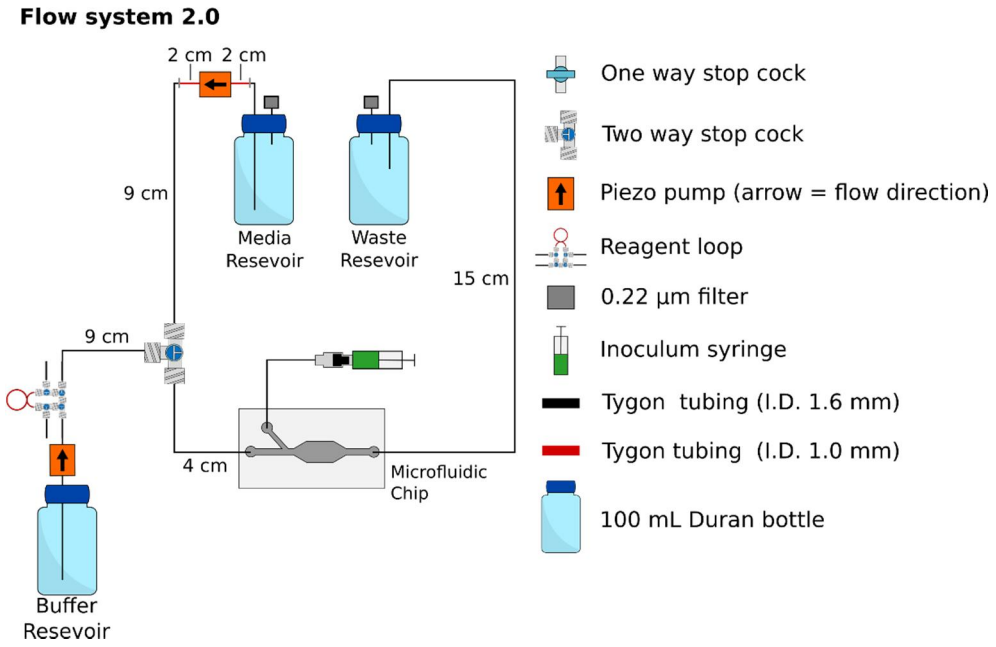

Figure 3.16. Schematic representation of microfluidic biofilm study system V2.0.

New system includes a reagent loop connected to a buffer reservoir. Reagents were pushed into cell using a secondary piezo pump located between the loop and the buffer reservoir.

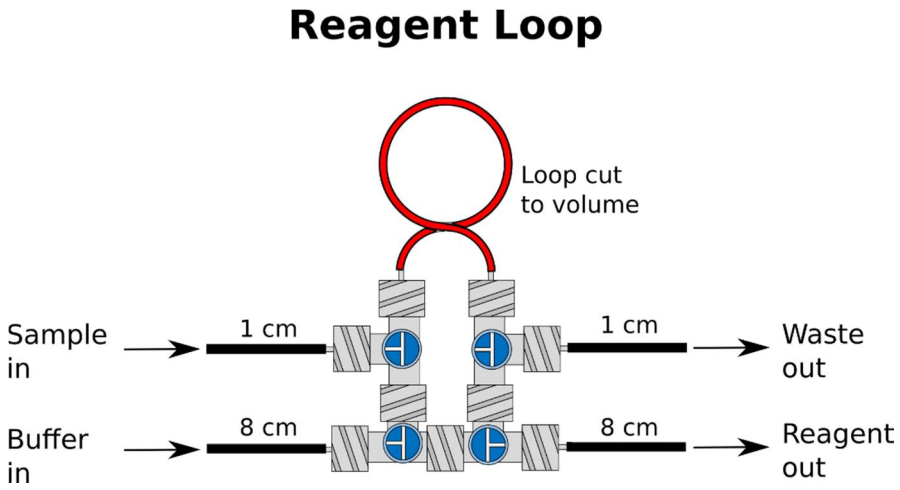

Figure 3.17. Schematic representation of reagent loop.

Loop designed to be primed with media or buffer using media in and other inlets with the blue two way stopcocks in various configurations to pull liquid through with a syringe via a female Luer lock adapter. Loop could be loaded by injecting sample into the sample in, through the loop, to waste out with stopcocks leading to media in and out to chamber isolated. The system could be purged to remove bubbles before adding reagent.

S. aureus UAMS1 biofilms were grown in the flow cell (V 2.0). Once the system had been washed, LIVE/ DEAD stain (1X DMAO/ EthD-III, 200 µL) was loaded into the reagent loop and pumped into the microfluidic device using the reagent pump. Figure 3.18 shows images attained from 10× and 40× magnifications of a selected biofilm that had been isolated to the flow chamber of the microfluidic chip.

Images taken at 10× magnification show the presence of a biofilm containing both living and dead cell components. In the overlays, orange/ red pixels are associated with dead cells and green with live. For both overlays at 10× and 40× magnification, the biofilm contains both living and dead cells components. Interestingly, most of the dead cells in the biofilm were located at the periphery. These cells may not be encapsulated effectively within the biofilm matrix, which means they may not experience the homeostatic benefits afforded to those within the matrix.[176] Regardless of this, 0.85% NaCl is not known to be cytotoxic to bacteria and is therefore unlikely to have caused the death of these peripheral cells. This buffer was recommended for use with this dye and the salt concentration provides osmotic protection for microbial cells. There seemed to be better penetration of the dye throughout the biofilms cultivated in this experiment compared to experimental results from section 3.2.2, which could be attributed to the comparatively lower thickness.

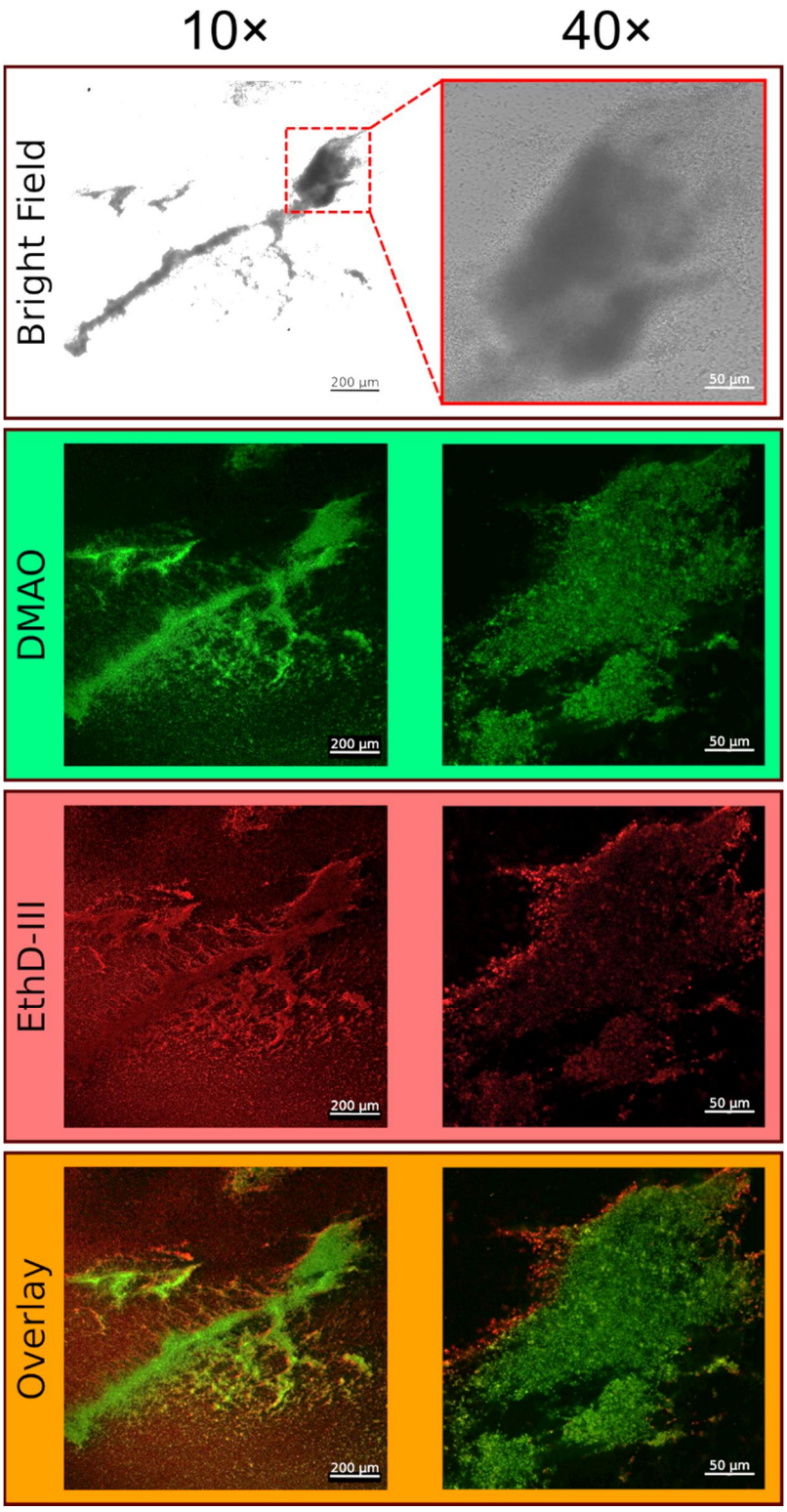

Figure 3.18. Confocal microscope images of biofilms grown on a microfluidic device V2.0 at 10× and 40× magnification.

For each magnification (column) the Bright Field, DMAO, EthD-III and DMAO/EthD-III overlay images are shown. Green is associated with living and dead cells, orange / red is associated with dead species.

3.2.4.1 Quantification of biofilm volume

For each magnification of the biofilm, a z-stack composite image showing DMAO (live and dead) and EthD-III (dead) stains was acquired (Figure 3.19). The *xy* 'slices' were analysed using ImageJ software to quantify the fluorescent signal. The brightness of a pixel was attributed to a fluorescent signal, as described in section 3.2.3. These pixels were counted and an approximate area of 'fluorescent' pixels was calculated. Using MetaData from the confocal image one can set the physical dimensions of a pixel for each magnification. In the case of 10×: 1 pixel was 1.29 μm^2. This can then be used to quantify the physical size of the pixelated area and thus the area of biofilm component, per 'slice.' It is then possible to convert this information to give a 3-dimensional volume by multiplying the 'slice' fluorescence coverage area by the z-distance between xy 'slices. This then transforms the pixel unit (2-D measurement of area) to a voxel unit (a pixel in 3 dimensions), which can be used to quantify the biofilm volume. Table 3.2 shows the translation of values attained from the image into physical dimensions. Using this method the volume of a biofilm can be ascertained from experimental images obtained from the confocal microscope.

The final volume for the biofilm shown in the 10× z-stack was shown to be 1.17 $\times 10^{-5}$ cm^3, which converts to 11.7 nL. The use of voxels limits the approximation of the biofilm to these defined cuboidal blocks (voxels), meaning that in some areas of the biofilm, a voxel will overestimate the volume of the biofilm contained within it, illustrated by Figure 3.20. However, the volume of each voxel (7.1 μm^3) in comparison to the calculated biofilm volume (1.17 $\times 10^7$ μm^3) makes this effect negligible.

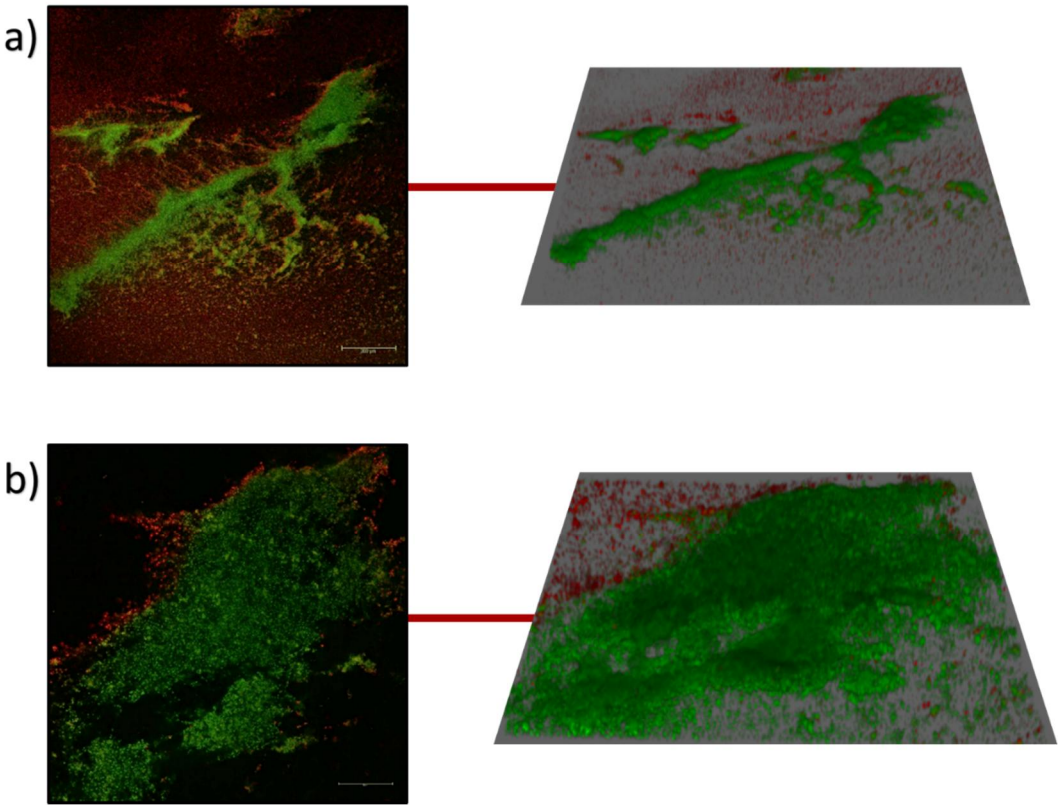

Figure 3.19. Overlaid images of DMAO and EthD-III stained biofilm.
a) 10X and b) 40X magnification, right is a composite image of slices taken in the xy plane to form a 'z-stack' at both magnifications. Green indicates living cells where red and orange indicate dead cell components.

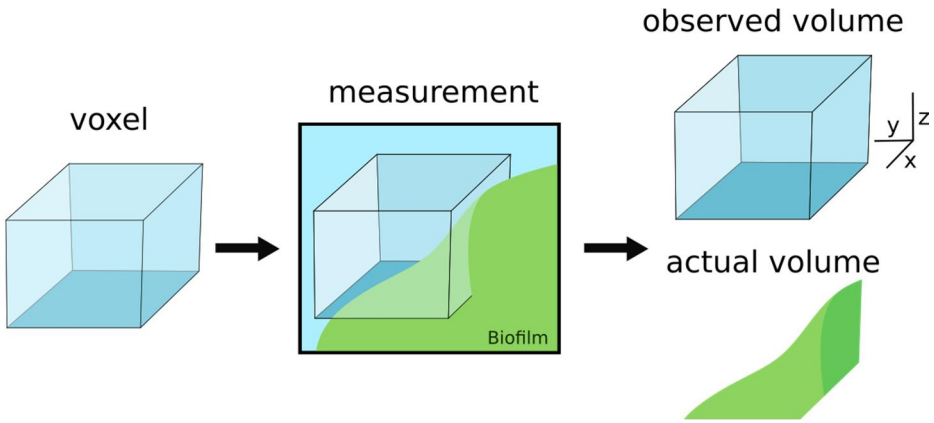

Figure 3.20. Illustration of how the above volume calculation overestimates biofilm volume.
The voxel is a defined 3-D cuboidal shape, during measurement, only part of the biofilm will occupy this space, leading to an overestimation of that area of the biofilm. The observed biofilm volume will be higher than the actual biofilm volume.

Table 3.2. Pixel counting values taken from analysis of confocal images using ImageJ software.

Live + Dead

	Pixel values							**Volume**		
Slice #	Count	Total area	Av. size	%Area	IntDen	Area/ µm^2	z/ µm	µm^3	mm^3	cm^3
1	2937	11996	4.084	1.144	1041.532	15474.84	4.272	66108.5165	6.61E-05	6.61085E-08
2	3044	16580	5.447	1.581	1388.929	21388.2	4.272	91370.3904	9.14E-05	9.13704E-08
3	2965	23345	7.874	2.226	2007.749	30115.05	4.272	128651.494	0.000129	1.28651E-07
4	2980	31209	10.473	2.976	2670.569	40259.61	4.272	171989.054	0.000172	1.71989E-07
5	2929	41256	14.085	3.934	3591.765	53220.24	4.272	227356.865	0.000227	2.27357E-07
6	3149	52607	16.706	5.017	4260.014	67863.03	4.272	289910.864	0.00029	2.89911E-07
7	3310	65037	19.649	6.202	5010.403	83897.73	4.272	358411.103	0.000358	3.58411E-07
8	1375	54667	39.758	5.213	10138.24	70520.43	4.272	301263.277	0.000301	3.01263E-07
9	1359	69394	51.063	6.618	13020.95	89518.26	4.272	382422.007	0.000382	3.82422E-07
10	1344	87068	64.783	8.303	16519.6	112317.72	4.272	479821.3	0.00048	4.79821E-07
11	1435	57125	39.808	5.448	10151.13	73691.25	4.272	314809.02	0.000315	3.14809E-07
12	1219	61208	50.212	5.837	12803.97	78958.32	4.272	337309.943	0.000337	3.3731E-07
13	1801	69202	38.424	6.6	9798.173	89270.58	4.272	381363.918	0.000381	3.81364E-07
14	2595	83983	32.363	8.009	8252.665	108338.07	4.272	462820.235	0.000463	4.6282E-07
15	4355	99633	22.878	9.502	5833.85	128526.57	4.272	549065.507	0.000549	5.49066E-07
16	7455	116972	15.69	11.155	4001.054	150893.88	4.272	644618.655	0.000645	6.44619E-07
17	10691	119948	11.22	11.439	2860.98	154732.92	4.272	661019.034	0.000661	6.61019E-07
18	13211	119075	9.013	11.356	2298.397	153606.75	4.272	656208.036	0.000656	6.56208E-07
19	11699	106838	9.132	10.189	2328.72	137821.02	4.272	588771.397	0.000589	5.88771E-07
20	8956	241415	26.956	23.023	6873.697	311425.35	4.272	1330409.1	0.00133	1.33041E-06
21	12583	217471	17.283	20.74	4407.145	280537.59	4.272	1198456.58	0.001198	1.19846E-06
22	9757	141428	14.495	13.488	3696.232	182442.12	4.272	779392.737	0.000779	7.79393E-07
23	7242	94811	13.092	9.042	3338.415	122306.19	4.272	522492.044	0.000522	5.22492E-07
24	5916	65639	11.095	6.26	2829.267	84674.31	4.272	361728.652	0.000362	3.61729E-07
25	5253	43304	8.244	4.13	2102.136	55862.16	4.272	238643.148	0.000239	2.38643E-07
26	4820	29263	6.071	2.791	1548.146	37749.27	4.272	161264.881	0.000161	1.61265E-07
							TOTALS	11685677.8	0.011686	1.16857E-05

Columns coloured in orange are values attained from ImageJ, columns coloured in blue are values calculated using the Excel. Area in µm^2 is calculated by multiplying values in Av. Area column by the pixel size (in this example 1 pixel = 1.29 µm^2) for each slice. This value is then multiplied by the distance between Z- stack slices to give a volume for the pixelated area. This value in then converted into a mm^3 and cm^3 value. The total volume is then calculated for the biofilm using the sum of all the individual slice volumes.

3.2.5 Fibrinogen coating of biofilm chamber

In previous experiments, there was a persistent issue with biofilm detaching under the mechanical stress of flow and moving through the device during experiments, which in some cases led to the complete stripping of the biofilm from the flow cell. It may have been that in previous experiments the biofilms were growing as species trapped or 'pinched' between the PDMS and the glass slide. These biofilms may only have had a small proportion of their surface area attached to the glass slide and therefore did not have a rigid

foundation, illustrated by Figure 3.21. This hypothesis is based on the morphology of biofilms from previous experiments. These biofilms often have a ‘tear-drop’-like structure and tend to move in response to flow, such as the one observed in Figure 3.13 of section 3.2.3. Some method of ensuring better biofilm adhesion to surfaces needed to be established for the flow cell.

A literature search found that fibrinogen is often used to promote bacterial adhesion to surfaces used for biofilm cultivation.[177, 178] Interaction between fibrinogen on an experimental surface and fibrinogen binding proteins (FnBPs) on the bacterial cell surface initiates bacterial adhesion and begins the process of biofilm formation.

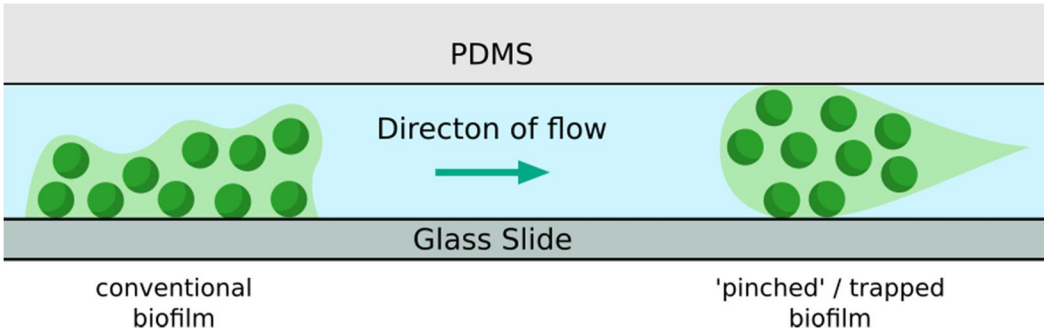

Figure 3.21. Illustration of proposed ‘pinched’/ trapped biofilm model. Instead of growing upwards from a solid foundation, the biofilms are growing and becoming trapped between the PDMS and the glass slide.

At this juncture, whilst the design of the flow cell was being optimised for experimental reproducibility, a new device was designed in which the chip had three tandem flow chambers. The presence of three flow chambers would allow for on-chip controls for a given experiment. Figure 3.22 shows the layout of the new triple flow cell chip V3.0. Using the new flow cell design, an experiment was performed to ascertain the efficacy of fibrinogen for promoting more ‘stable’ biofilms on the chip.

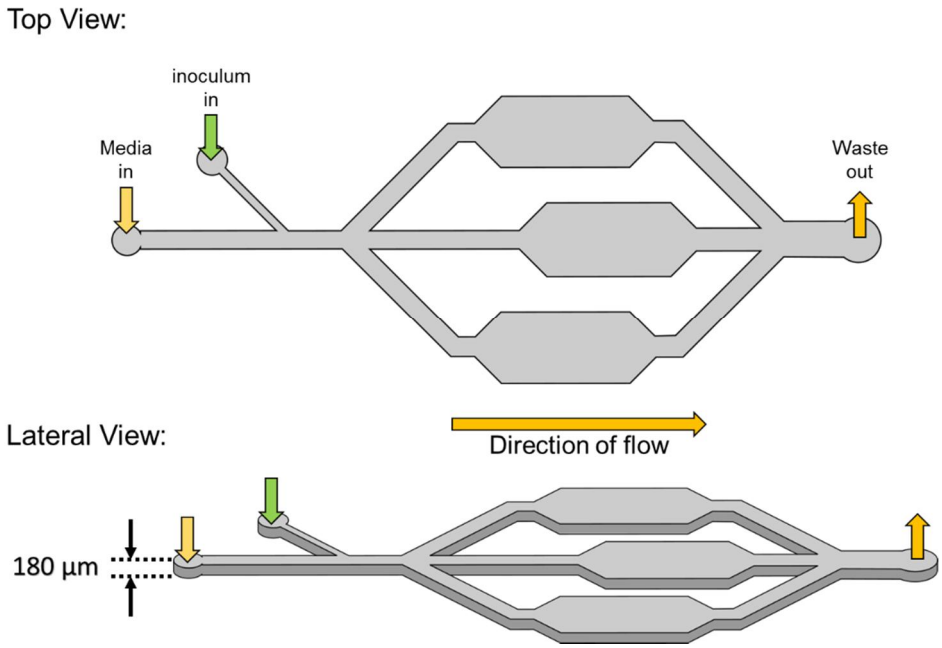

Figure 3.22. Schematic of flow cell with three parallel chambers (V 3.0). Media in, inoculum in and waste out specified by arrows indicating direction of flow. All three chambers are supplied by the same media channel and feed to the waste outlet.

The protocol was performed for on chip biofilm cultivation as outlined in section 6.3.4, *S. aureus* UAMS1 was used to inoculate the biofilm chambers. The morning before inoculation with bacteria, fibrinogen (5 mg/ mL) in PBS buffer was injected into the flow cell via the inoculum point using a 5 mL syringe. Once the solution was in the chamber it was incubated statically at RT for 6 hours to allow the protein to coat the microfluidic chip surfaces.

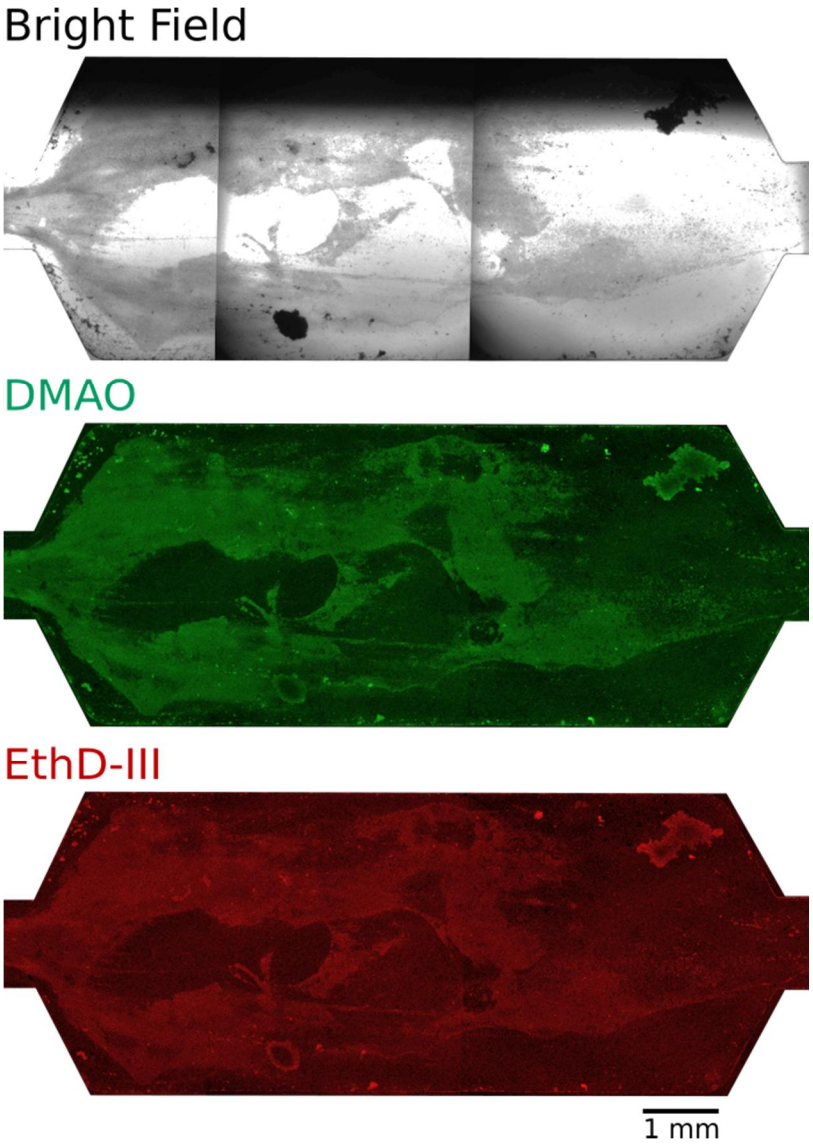

Figure 3.23. Composite confocal image of the middle biofilm chamber of the microfluidic chip at 2X magnification.
Top image is bright field, middle is DMAO stained biofilm and bottom EthD-III stained biofilm.

Figure 3.23 shows the presence of a well-established biofilm spanning across the flow cell. The morphology of this biofilm is different from that seen in previous experiments. The biofilm seems to be one continuous body instead of intermittent 'tear drop' like shapes. The bright field image shows the presence of larger structures appearing in the middle of what seems to be shallower regions of biofilm growth.

Further imaging by confocal microscopy analysis showed that biofilms in these shallower areas were comparatively thinner, with a layer of cells

growing over the glass slide surface. Figure 3.24 shows a 3-D rendered z-stack (Leica LasX software) of a biofilm taken at 100× magnification

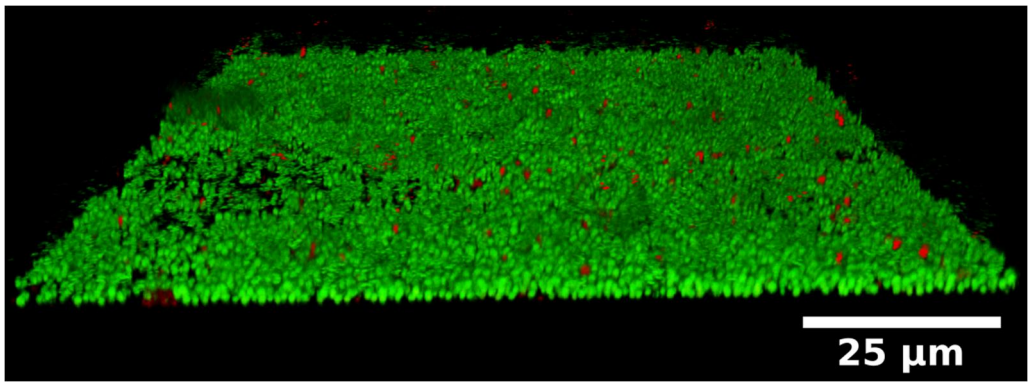

Figure 3.24. 3-D Z-stack image of biofilm grown on microfluidic device. Green species represents living cell components and orange/ red representing dead cell components. Darker areas of image indicate 3D structures growing upwards of the glass slide surface. Biofilm height (from highest point) = 24 µm, volume = 0.3 nL.

The addition of fibrinogen to the flow cell surface caused the growth of these ‘lawn-like’ biofilms. The darker areas on the image show additional 3D structures growing above the ‘lawn’. Though the biofilms are growing in a uniform manner, there is still propensity for more complex 3-D structures. These ‘lawn-like’ biofilms appear to have a large surface area, maximising the biofilm-buffer interface. This large surface area is ideal for observing interactions between reagents and biofilm components under flow. The composite xy images in this z-stack were analysed using ImageJ software. The height of the biofilm in Figure 3.24 is 24 µm at its highest. The volume of the biofilm area is 0.3 nL.

Figure 3.25 shows an overlaid image acquired in the xy plane at 100× magnification. In this image the resolution of single cells can be seen within the biofilm. Resolution to this degree would give a useful insight into the ratio of living to dead cells when using the LIVE/ DEAD stain, for experiments that assess the effect of different reagents on cell viability.

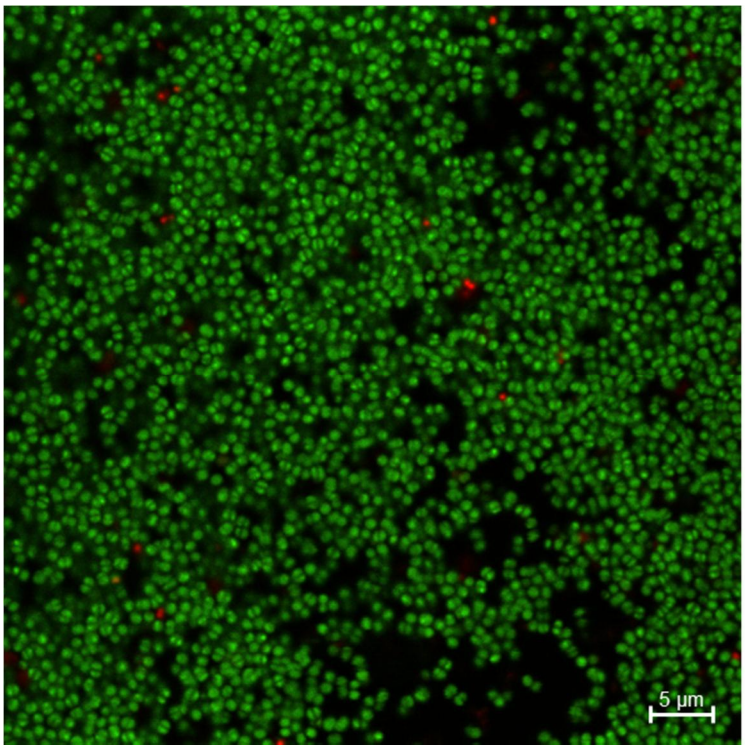

Figure 3.25. Overlaid image of Live/ Dead (DMAO) and dead (EthD-III) acquired by confocal microscopy of a S. aureus (UAMS1) biofilm.
Green represents living cells whereas orange/ red represents dead cells. Scale bar represents 5 µm.

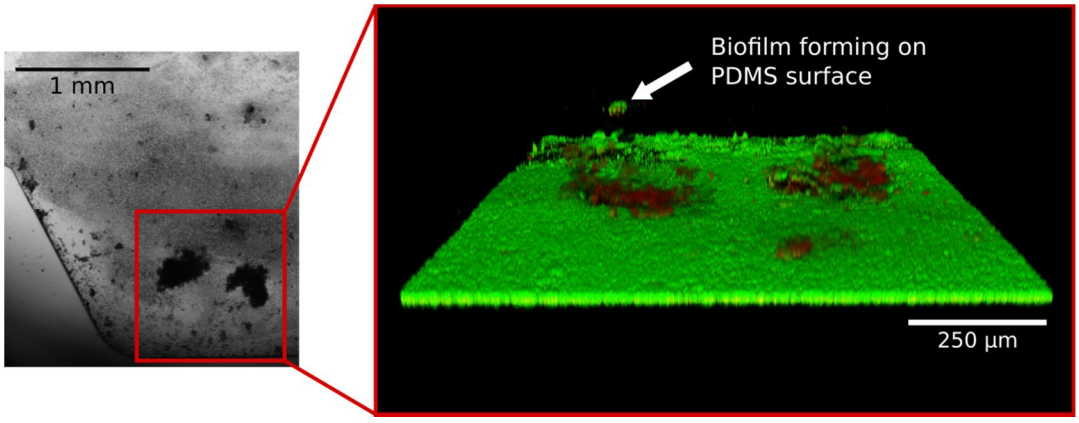

Figure 3.26. Bright field of microfluidic device taken at 10× magnification and confocal z-satck at 40×.
Area in red is shown as a Z-stack taken at 40× magnification on the right. Green is associated with living cells and orange/ red is associated with dead cell components. Species indicated with white arrow assumed to be biofilm growing on PDMS surfaces in the device.

Another 3-D z-stack showed the presence of a biofilm growing on the PDMS surfaces in the microfluidic flow cell. Figure 3.26 shows the z-stack of an area taken at 40× magnification. The presence of bacterial cells detached from the glass-bound biofilm bulk on the upper PDMS surface is indicated by the white arrow. The presence of two larger regions of biofilm indicated that biofilms grown using this method can vary from the 'lawn-like' biofilms observed above, to more traditional 'mushroom-cloud-like' structures regularly illustrated in the literature.[13]

For the most part, the majority of the biofilms grown have done so on the glass slide surface of the microfluidic chambers; fibrinogen coating facilitated the cultivation of biofilms with a larger surface area and a shallow volume, but did not facilitate biofilm growth that completely covered every chamber surface. However, Figure 3.26 shows evidence of growth on the upper PDMS surface in the microfluidic chamber alongside the glass-surface-bound biofilm.

The use of fibrinogen for promoting bacterial cell adhesion to microfluidic chamber surfaces had proven successful. From this point on, fibrinogen-coating was incorporated into the standard operating procedure for biofilm cultivation.

3.2.6 Living and dead cell quantification

As the relative fluorescence emission intensities for each of the dyes is not known for a given concentration of living/ dead cells, the percentage of living and dead cells in the sample cannot be calculated from their absolute fluorescence intensity values. This is further complicated by the fact that the dead DNA dye can diffuse away from the dead cells as they do not become cross-linked to DNA, meaning the intensity may decrease over time.[179] Nonetheless, the ratio of fluorescence intensities for live and dead to dead cells can be used to give a measure of changes in cell death over time. Photo-bleaching of the dyes, when exposed to UV light, may also affect the ratio of these relative intensity values. The aim of this experiment was to see how the ratio of DMAO and EthD-III emission changes over time after multiple exposures with the excitation lasers, to ascertain if this could lead to photo-bleaching of the dyes between excitations. The experimental protocol was the

same as the previous experiment and involved coating the chamber with fibrinogen. Figure 3.28 shows the composite z-stack of a biofilm grown in the flow cell (V 3.0, Figure 3.22) at five different time points.

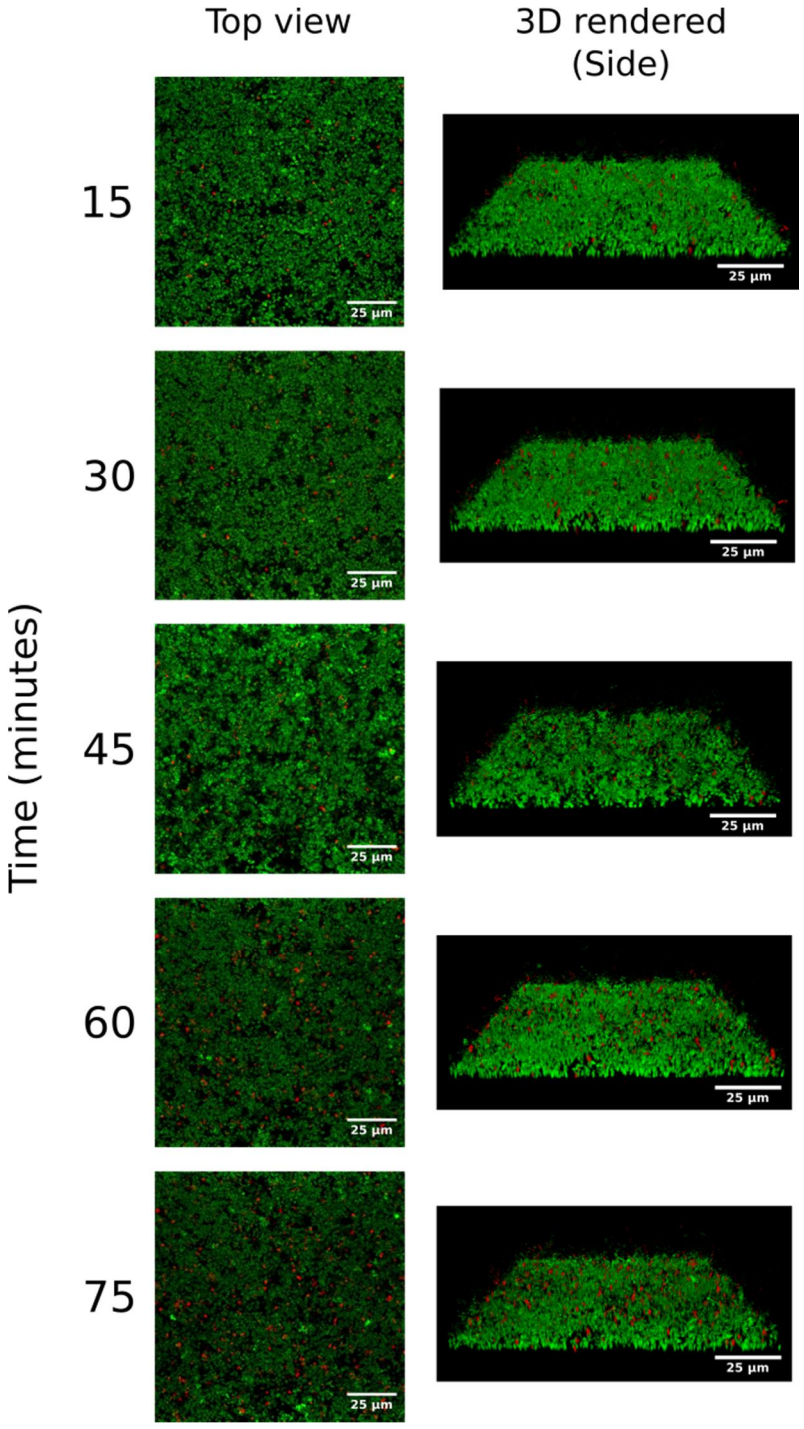

Figure 3.27. Composite Z-stack images of biofilm area imaged with a 5 minute acquisition time starting at 15 minute intervals.
Cells are stained with DMAO and EthD-III Live/ Dead cell dyes. Green pixels represent living and dead cell components whereas red represents dead cell components. Scale bar represents 30 µm.

For a z-stack at a given time point, each image in the xy plane of the stack was imported in to ImageJ, and the total pixel brightness (fluorescent signal) was measured across the whole stack. The fluorescence intensity will scale with concentration of activated dye. For each image, the total brightness of all the pixels was measured using the ImageJ software. For both the DMAO and EthD-III dyes, the z-position of each slice of the stack was plotted against total pixel brightness (fluorescent intensity). The graph plotted shows how the fluorescence intensity of the biofilm changes as you move through the z-axis. An example of one of these plots is shown in Figure 3.28 for time point t = 75 mins. The area under the curve was then calculated to give the total fluorescence emission of the whole z-stack, and therefore the studied biofilm. Figure 3.29 shows the ratio of the total DMAO emission to total EthD-III emission for each time point.

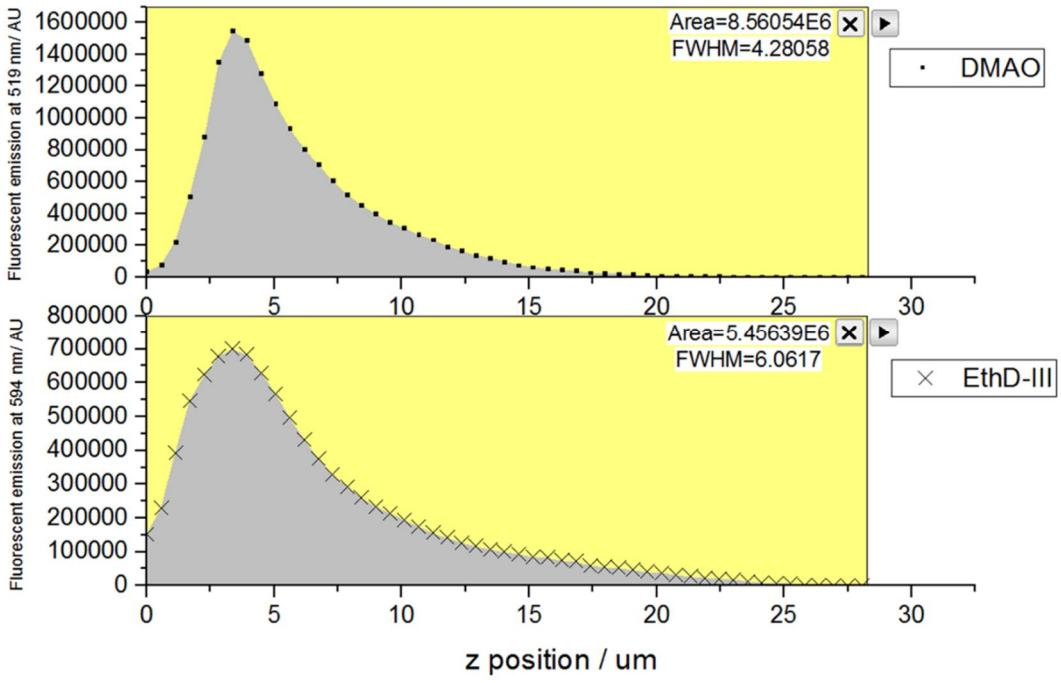

Figure 3.28. Plot of fluorescent emission vs position in the z-plane of stacks taken of an S. aureus biofilm at t = 75 mins.

Top curve represents fluorescence from DMAO (living and dead) and bottom curve fluorescence from EthD-III (dead cells). The area under the curve is calculated for each dye giving the total fluorescence of the z-stack.

Figure 3.29 shows the change in the ratio of the EthD-III emission to DMAO emission increase over the course of the experiment. This could either be attributed to an increase of cell death, photo bleaching of the DMAO dye or diffusion of the activated EthD-III dye towards the region of interest. Throughout the whole experiment the system was static in HEPES buffer (pH 7.4), therefore it is likely that some cell death would occur with no fresh nutrients being supplied to the biofilm. It could also be that the DMAO bound to DNA in living and dead cell components is the result of photo bleaching, whilst still remaining bound to its target; preventing a new molecule of DMAO from binding and regenerating the fluorescent signal. In either case the experiments suggest that when imaging cells in future experiments, the time between dye addition and acquisition of confocal images needs to be minimised.

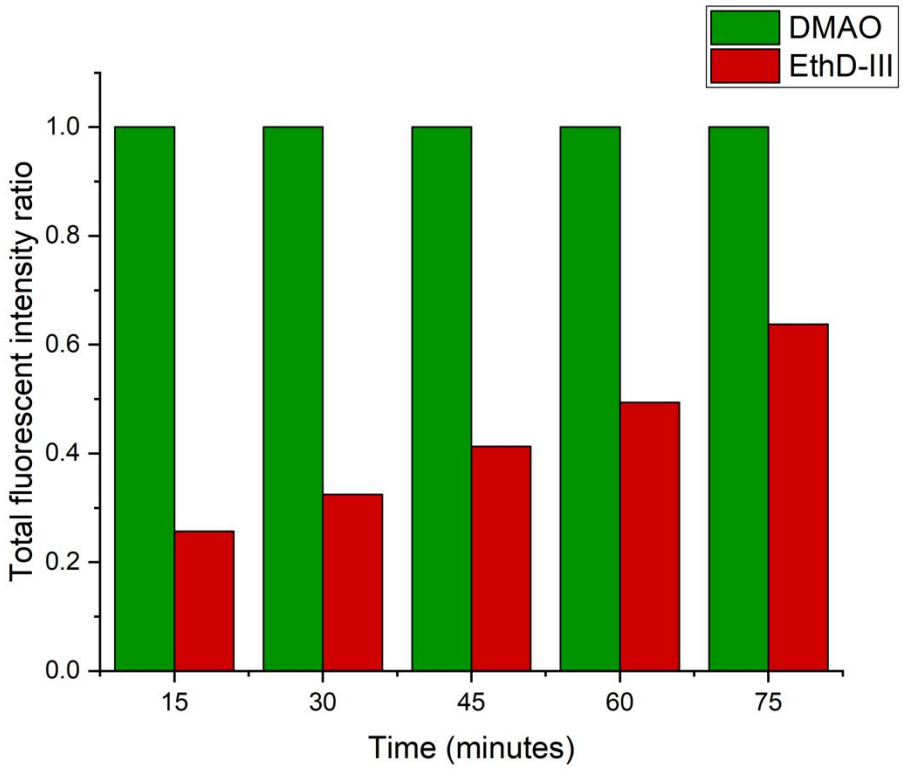

Figure 3.29. Bar chart showing the ratio of DMAO and EthD-III dye emission for the studied biofilm at 5 different time points from 0 – 75 mins.
DMAO emission is associated with the presence living and dead cell components, whereas EthD-III emission is associated with only dead cell components. As time progresses the ratio of DMAO to EthD-III emission changes.

3.2.7 Parallel flow cell microfluidic design

The results of the previous experiment proved that the three-chamber device could be used to cultivate biofilms in parallel. The three chamber device needed to be modified further so that each chamber could be subjected to a different flow of reagents. This would allow for on-chip controls for a given experiment and would form a more robust experimental model. Work by Arellano and co-workers had demonstrated the ability to use microfluidic to simultaneously test a number of experimental conditions on the same microfluidic 'array'.[180] Their system allowed for the screening of up to 48 drug combinations on 48 different cell-tissue samples. The new design needed to incorporate channels for the flow of reagents into each of the flow chambers.

Introducing the reagents from above, as described previously in section 3.2.3 (chip V 1.1, Figure 3.9), caused experimental impracticalities as the confocal microscope both excites the sample with the laser lines, and reads the incoming emission from the same plane (from underneath the sample). The bright field module of the microscope is read from below the sample with light being supplied from above the sample. At 100× magnification, it is quicker and easier to find the z position in which the biofilm is situated using the bright field microscope as a guide, before switching to the confocal imaging system. Supplying reagents using tubing fed from above biofilm chambers would obstruct the light used for bright field image acquisition. Therefore, it was proposed to introduce the reagents using a channel on the chip, with the tubing located nearer the media inlet, away from the biofilm growth chambers. Microfluidic chamber design was undertaken in collaboration with Jordan Tinkler with fabrication being solely performed by Jordan Tinkler. Figure 3.30 shows the design of the microfluidic chip (V 4.0).

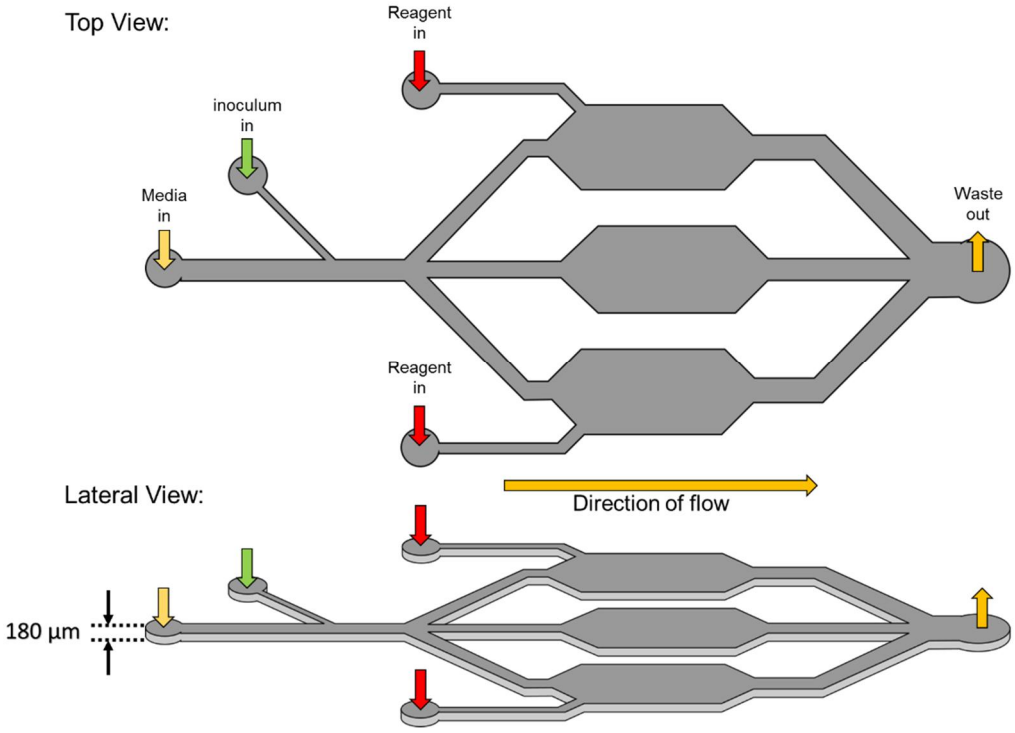

Figure 3.30. Schematic of flow cell with 3 parallel channels (V 4.0). Media in, inoculum in and waste out specified by arrows indicating direction of flow. The top and bottom flow chambers have their own reagent inlets that are fed by tubing at the points indicated by red arrows. All three channels are supplied by the same media channel and feed to the same waste outlet.

The flow of reagents was expected follow the path of least resistance and therefore only flow through one chamber - out to waste. However, preliminary flow experiments with this chip design showed that flow could not be isolated to just one chamber by flowing media into its associated reagent inlet. Figure 3.31 shows red food dye being flowed through the system (flow rates 0 – 100 µL/ min) via the reagent in 1 port. The schematic shows how the dye was expected to flow through the system, how it actually flowed and a picture of the experimental result. As all three chambers lead to the same waste outlet, dye flowing into the top chamber is moving upstream of the reagent inlet and flowing into the other two chambers, even when flow via the other reagent inlets were isolated using one way stopcocks off chip.

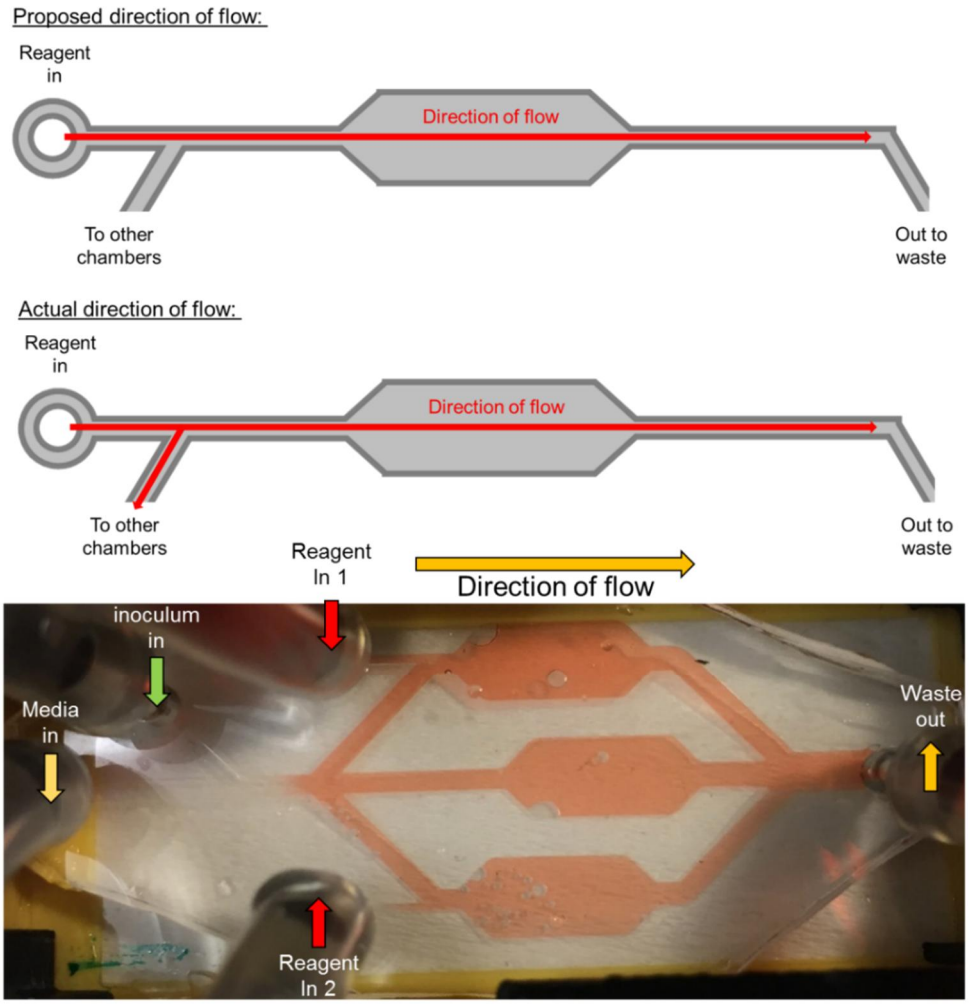

Figure 3.31. Proposed direction of flow in chip V 4.0 and photograph of experimental flow.
Top, schematic of proposed flow of media through top chamber of device. Middle, direction of flow under experimental conditions. Bottom, picture of flow cell when flow is isolated to only reagent in. Presence of red dye in all three chambers indicates an inability to isolate flow to just one chamber. Back flow via other inlets prevented by the closing of stopcocks off chip.

It was anticipated that modifying the flow cell so that each chamber had its own waste outlet channel would rectify the isolation problem. Figure 3.32 shows the amended design of the new microfluidic device (V 5.0). The flow experiment outlined previously was repeated and the device was observed to have an isolated flow of reagents through the desired chamber at flow rates ranging from 0 – 100 µL/ min. Figure 3.33 shows the flow directed through one chamber via its associated reagent in port.

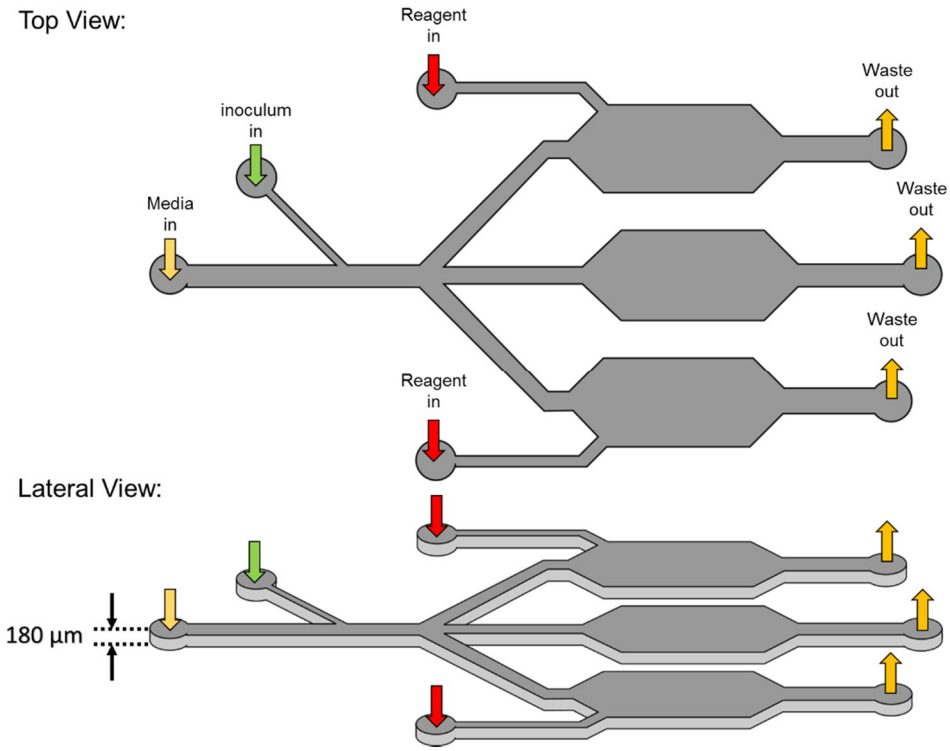

Figure 3.32. Schematic of flow cell with 3 Parallel channels each with their own waste outlet (V 5.0).

Media in, inoculum in and waste out specified by arrows indicating direction of flow. The top and bottom flow chambers have their own reagent inlets that are fed by tubing at the points indicated by red arrows.

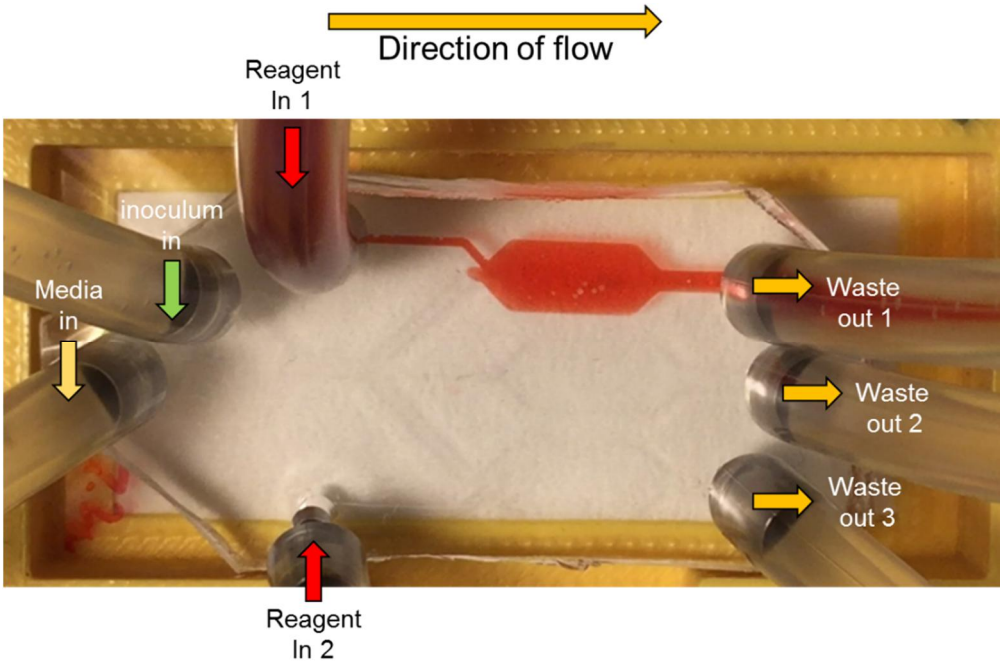

Figure 3.33. Photograph of flow cell when flow is isolated to only 'reagent in 1'.

Presence of red dye in only the top chamber indicates the flow has been isolated to one chamber. Flow to media in, inoculum in, reagent in 2, waste out 2 and waste out three preventing by closing stopcocks off chip.

The new microfluidic chip design (V 5.0) allowed for treatment of the top and bottom chamber with a unique reagent flow and allowed for on-chip controls for a given experiment. The middle chamber could be used as a untreated biofilm control if subjected to required reagents last, via the media inlet. Figure 3.34 shows a schematic of the final iteration of the microfluidic biofilm growth model.

One-way stopcocks are placed on all tubing that is connected to the microfluidic chip to allow for isolation and movement of the microfluidic device for ultrasound equipment integration.

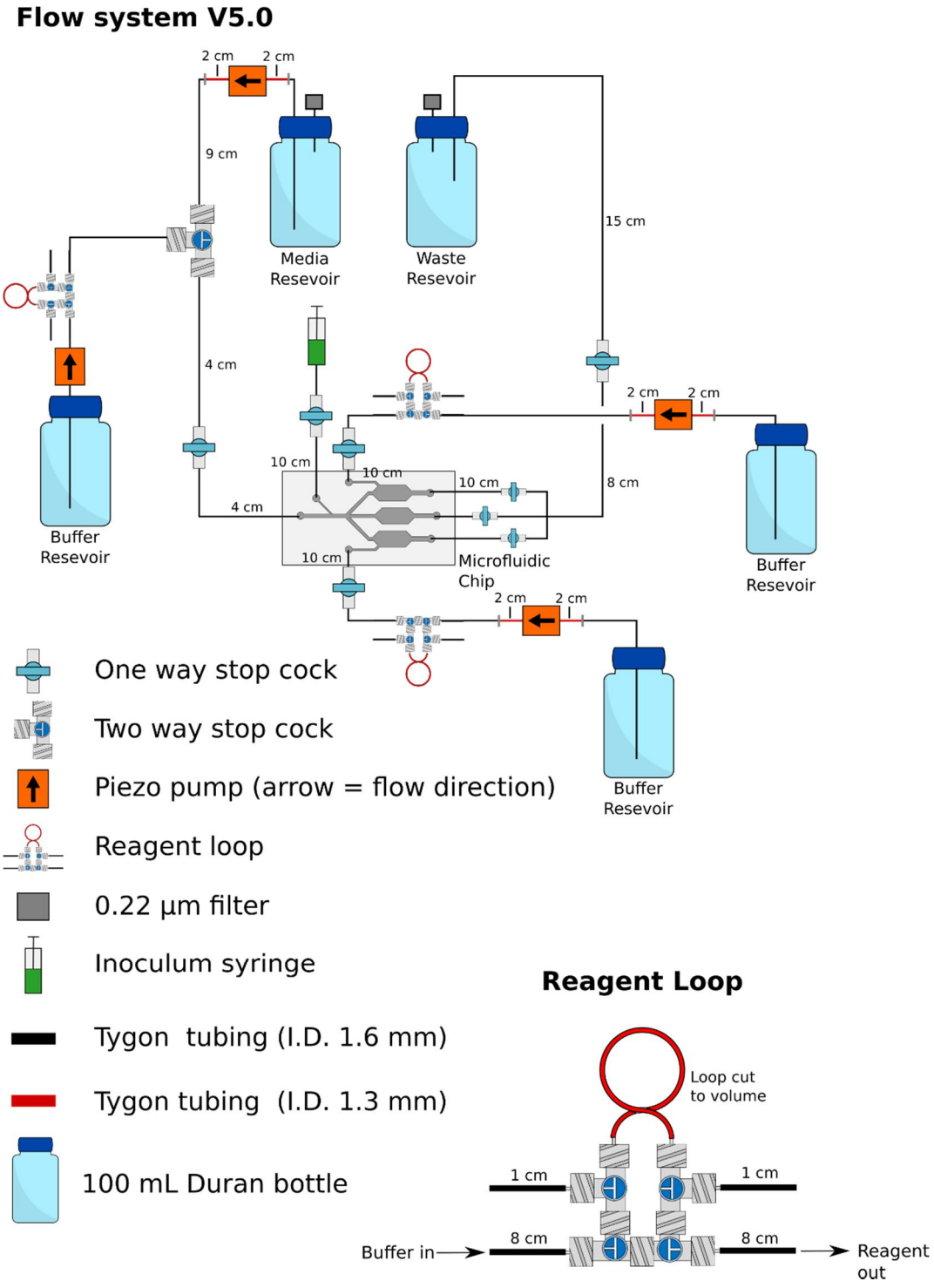

Figure 3.34. A schematic of the biofilm growth chamber V5.0.
Legend indicates what each components is and diagrams shows their relative position in the system. Direction of flow from reservoirs is downstream to waste reservoir. Every inlet has an off chip one way stopcock so that flow through the tubing can be stopped at any point.

3.3 Chapter Conclusions

The aim of this work was to develop a microfluidic flow model that could cultivate biofilms under flow and for treatment of these biofilms with numerous reagents. This model could then be used to study the interaction between microbubbles and *S. aureus* biofilms under flow.

Many issues arose over the development of this microfluidic system resulting from the blockage of channels with biofilm species. Initially, these blockages caused considerable problems as clearing obstructions required an increase in flow rate that would then cause further biofilm disruption leading to further blockages. These issues were mitigated primarily by increasing the tubing diameter and the addition of a fibrinogen-coating step. The wider bore prevented tubing blockages both upstream and downstream of the microfluidic chip. Coating the microfluidic chip with fibrinogen pre-inoculation encouraged the growth of more ‘lawn-like’ biofilms that were considerable shallower than their predecessors. These shallower biofilms prevented the formation of on-chip blockages. Furthermore, the ‘lawn-like’ biofilm allowed for a greater surface area to be observed for biofilm-reagent interaction.

The use of a LIVE/DEAD stain gave a firm foundation for observing biofilm morphology. The stain may also be used to understand the ratio of living to dead bacteria provided the dye is replenished before each image acquisition, and the time between dye introduction and image acquisition is minimal. Using this flow system biofilms could be imaged using CLSM to give cellular biofilm resolution at high magnifications (40× and 100× objectives)

The development of the triple flow chamber microfluidic device, allowed for on-chip controls in subsequent experiments. Each biofilm chamber could be subject to its own bespoke flow of reagents, with no backflow to the other two isolated channels. The introduction of on-chip controls made the experimental design more robust and would allow for multiple control experiments to take place in parallel flow cells.

Although the microfluidic biofilm study system at the end of this chapter seems relatively robust, there are some caveats to the system. The system can consistently grow an uncontaminated biofilm in all three of its chambers,

however there is little control over biofilm morphology and composition. This may cause inter-experimental variability in the structure of the biofilms cultivated. The introduction of the fibrinogen coating step minimised the likelihood of cultivating a biofilm that was so thick that there was poor dye penetration. Should such a biofilm exist within the chamber, an inability of the dye to penetrate to the biofilm centre may cause issues for quantifying cell death as a function of biofilm destruction. The stain may not be able to delineate the difference between recently killed bacteria and cells that exist in the ‘un-stained’ part of the biofilm that are already dead. This may also need to be taken in to account when using the confocal pixel data to quantify biofilm volume, as the centre mass of the biofilm may not be represented in the data set due to absent pixels.

4 Interactions with biofilms under flow

Results and discussion

Part 3

The aim of this work was to investigate the interaction between the *S. aureus* biofilm and targeting protein (Affimer), and then both targeted polystyrene beads and microbubbles, using the flow model (development described in chapter 3). With an Affimer for microbubble targeting identified, the flow model was used to ascertain if binding occurred under flow conditions for both the unbound protein receptors, the protein attached to polystyrene beads and the protein as part of targeted microbubbles.

4.1 Confirmation of Affimer binding to biofilms

In order to justify the use of an Affimer protein as targeting agent for localisation of microbubbles to the biofilm, their ability to bind biofilms in solution was first investigated.

4.1.1 ClfA1-fluorescein binding to UAMS1 biofilm

The aim of this experiment was to investigate if the Affimer proteins in solution could bind the *S. aureus* UAMS1 biofilm. Biofilms were cultivated in the flow system using the protocol described in 6.3.4. The protein was flowed over the biofilm, in a single channel of the triple flow cell microfluidic design from section 3.2.7.

Work outlined in section 2.2 identified the ClfA1 Affimer protein to be the leading candidate for targeted microbubble conjugation. ClfA1 Affimer proteins were labelled with a maleimide-fluorescein derivative, using a cysteine towards the C-terminus of the protein to make ClfA1-F (protocol described in section 6.2.22). Once a *S. aureus* UAMS1 biofilm was established, a ‘pulse’ of ClfA1 (5 µM, 500 µL) was flowed over at ~ 250 µL min^{-1}. As the emission spectra of fluorescein (λ_{em} maximum = 521 nm) and DMAO (λ_{em} maximum = 535 nm) overlap, the LIVE/DEAD stain was not used in this experiment. Figure 4.1 shows a composite of fluorescence images of the z-projection (top view of z-stack) taken at four time points during the experiment. Image at t = 6 mins was acquired mid-way through the ‘pulse’ of ClfA1-F protein; time points taken after were acquired under a constant flow of phosphate buffer. The presence of fluorescent elements at t = 38 and 98 minutes indicated that there was interaction between ClfA1-F and the biofilm.

The Affimer-biofilm interaction was confirmed by comparing the fluorescent images with their bright field image counterparts in Figure 4.2.

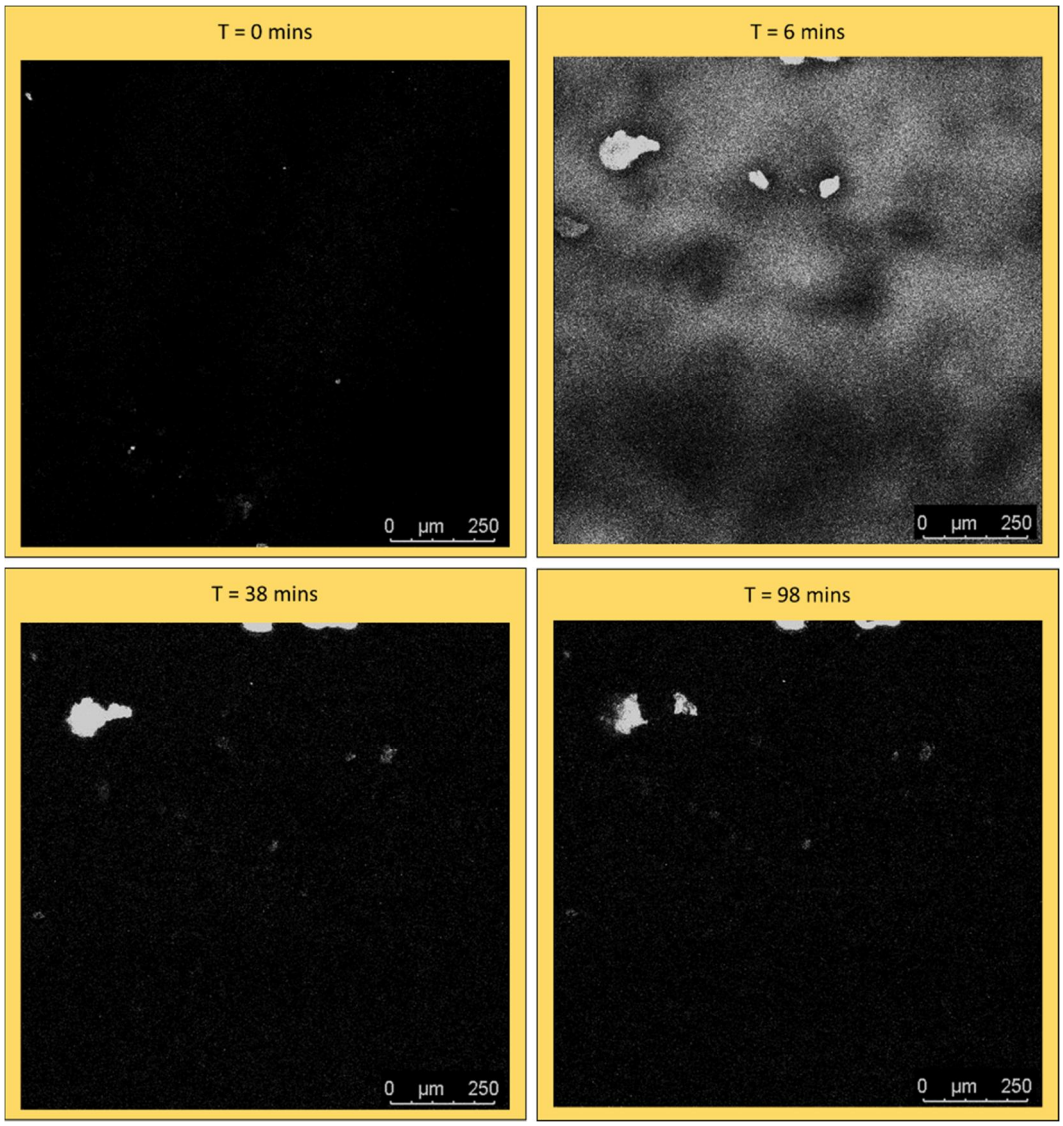

Figure 4.1. Z-projection of images of flow cell at set time points shown as a collapsed 2D image.
Images acquired viewing light emission at ~535 nm, corresponding to fluorescein emission. Images acquired at time points 0, 6, 38 and 56 minutes. Presence of fluorescent signal is associated with fluorescent Affimer.

This was confirmed by comparing the image taken at t = 6 minutes to the bright field image taken at t = 0 minutes in Figure 4.2. The overlay indicates

that localisation of Affimer to areas of the biofilm chamber is associated with features that were present before the ‘pulse’ of Affimer, presumed to be biofilm. This observation also eliminates the possibility that the observed fluorescence represents clumps of precipitated Affimer protein.

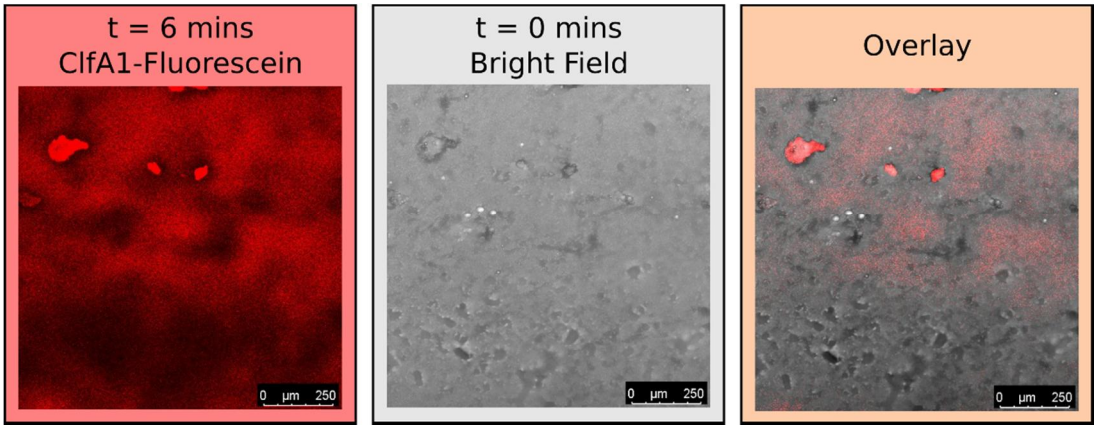

Figure 4.2. Confocal z-stack projections and overlays, taken at t = 0 and t = 6 minute time points.
From left to right. Composite z-stack images of flow cell at t= 6 for fluorescent species, Bright field image taken at t = 0 and an overlay of the two. Overlay shows that fluorescent species associated with features present before ‘pulse’ of protein.

4.1.2 ClfA1-Alexafluor647 binding to LIVE stained biofilm

The experiment was repeated as before (section 4.1.1) but the method was modified to label Affimer with Alexafluor647 NHS ester fluorescent dye so that the DMAO stain could be used to image bacteria cells alongside Affimer, to confirm that the protein was associating with the biofilm. Unlike the fluorescein-maleimide, the Alexafluor647 NHS-ester dye is covalently attached to primary amines groups associated with lysine residues and N-terminal amines, as opposed to the thiol group on a cysteine residue. This means the NHS-ester is more promiscuous and makes labelling less selective for a specific amino acid residue. Once the biofilm was established, it was stained with DMAO stain and washed with phosphate buffer. These two stain have minimal to no overlap in their emission and excitation spectra and can be viewed simultaneously using confocal microscopy.

ClfA1-A647 was then flowed over the biofilm in a 'pulse' (at ~ 250 µL min^{-1}), after which the system was washed with phosphate buffer at the same flow rate. The experiment was then repeated with Alexafluor647-labelled AAC Affimer scaffold (introduced in section 2.2.2.3) as a control.

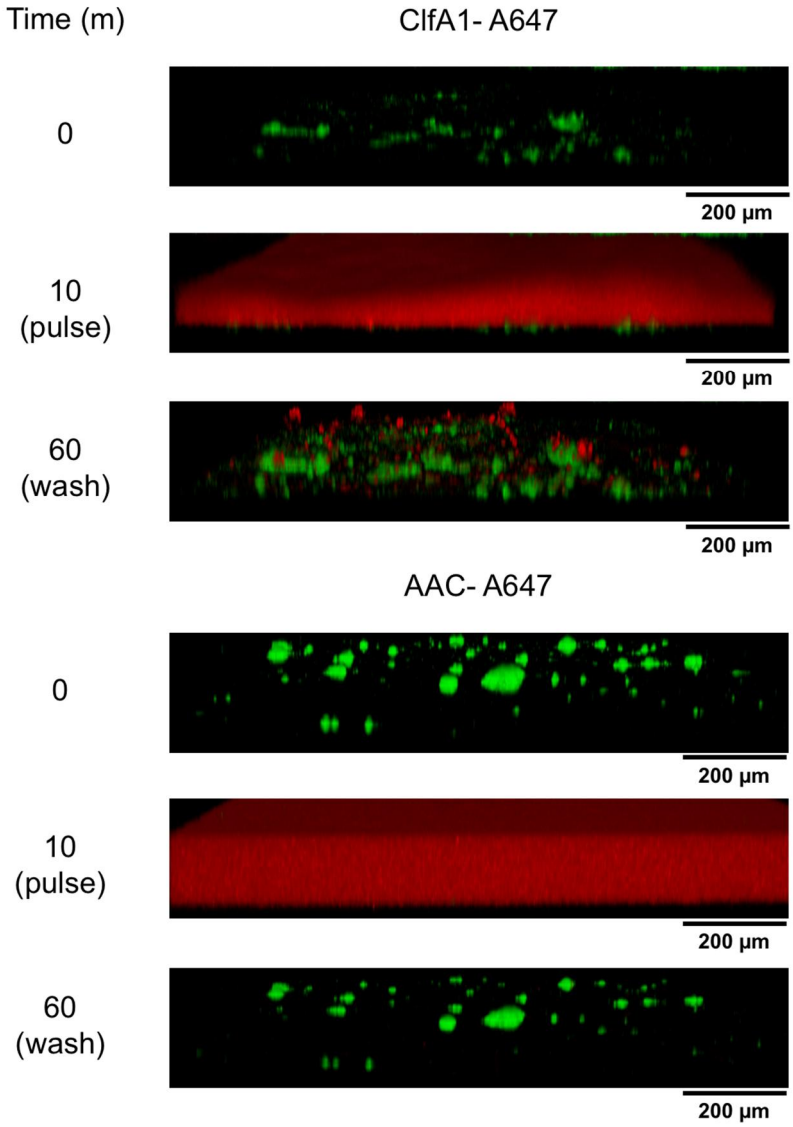

Figure 4.3. Composite 3-D rendered Z-stacks of biofilm cultivated on chip at different time points of a binding experiment with ClfA1-Alexafluor647 and AAC- Alexafluor647.

Time point t = 0 shows the biofilm before the protein pulse being washed with phosphate buffer. Time point t = 10 the protein pulse of Affimer-Alexafluor647 (5µM, 1 mL) is flowing over the biofilm. Time point = 60 minutes, the system had been washed with phosphate buffer for 40 minutes. Green represents bacterial cells in the biofilm (S. aureus UAMS1) stained with DMAO, red represents Affimer.

By the final time point of this flow experiment, ClfA1 protein was still associated with biofilm components in the flow cell, in contrast to the AAC control in which almost no AAC protein was observed. In each Affimer solution, not all of the protein had been labelled with the Alexafluor647 dye, meaning each protein solution had different levels of fluorescent protein content. Mass spectra from the reaction of each of the Affimer proteins in Appendix 7.8 shows that only around 20% of ClfA1 Affimer was labelled, compared to 100% of AAC Affimer. Therefore, the absolute fluorescence values are not directly comparable, as two protein solutions of the same concentration will give different fluorescence values. The mean grey value for the z-stacks corresponding to A647 and DMAO (live stain) were taken for images at time point t = 60 (using the method from section 3.2.6). By calculating these mean grey values normalised to the live stain, the values indicated the amount of A647 fluorescence in proportion to live stain or biomass fluorescence.

Figure 4.4 shows that after 50 minutes of washing with phosphate buffer, the proportion of Affimer to biofilm mass is higher for ClfA-A647 compared to that of AAC-A647. The results indicates that more ClfA1 Affimer has bound biofilm components than its AAC control. The qualitative results shown in Figure 4.3 and the quantitative data of Figure 4.4 indicate that the specific interaction between the ClfA1 Affimer and the *S. aureus* UAMS1 biofilm is mediated by the binding loops of the Affimer under flow conditions.

Once it had been determined that ClfA1 bound the biofilm under flow in a solution, it was then necessary to investigate whether attaching these Affimers to larger scaffold (such as microbubbles) affected their ability to bind the biofilm. The large difference in degree of labelling of each Affimer may indicate that even more ClfA1 Affimer is bound. However, for experiments described in the rest of this chapter, the labelling is only used to visualise beads and MBs and not to quantify protein binding, so the current protein stocks were continued forward.

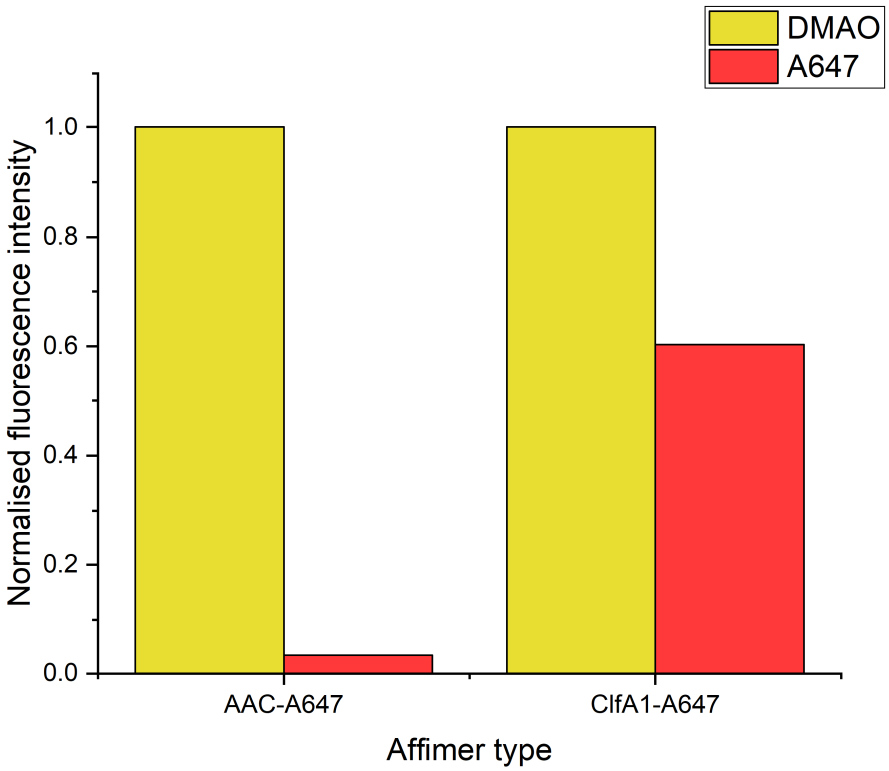

Figure 4.4. Bar chart showing the normalised mean grey values for the z-stacks of DMAO and A647 image channels at t = 60 mins for ClfA1 and AAC Affimer proteins.

Bar for DMAO represents the mean grey value of DMAO stained biofilm components, normalised to 1, and A647 showing the mean grey value of species associated with alexafluor647 labelled Affimer proteins. For AAC-A647, the value for A647 represents 3% and for ClfA1 A647 gives 60%.

4.2 Targeted polystyrene beads under flow conditions.

As described in Section 2.3, due to their similar size and shape, polystyrene beads of ~2 µm diameter provide a good approximation to the microbubbles. These beads were used as a scaffold for monitoring the effect of polyvalency of proteins bound to a solid support. The Affimer's ability to localise the beads to the biofilm's surface was used to infer the potential of the MB to do the same.

4.2.1 ClfA1-A647 beads with static pulse

Biofilms were cultivated as before, using *S. aureus* UAMS1 in the V5.0 flow cell (Section 3.2.7) as described in section 6.3.4. All biofilms were stained with DMAO, to image cellular biofilm components, and washed with phosphate buffer. The reagent loop was then loaded with protein-conjugated beads (1 mL, 10^8 particles mL^{-1}). A pulse of bead solution was flowed through the biofilm chambers at 250 µL mL^{-1}. Once the bead solution had filled the chamber, flow was stopped leaving the bead solution static in the chamber for 10 minutes. Flow was then resumed for 30 minutes in order to clear chambers of unbound beads. In each experimental chamber, 15 z-stacks were acquired at 100× magnification, each up to a height of 30 µm from the chamber bottom (glass slide surface). Figure 4.5 shows The z-projections and 3D rendered z-stacks for areas of the biofilm chamber that contained closest to the average number of beads per z-stack for the experiment.

The number of beads in each z-stack was counted and a concentration was calculated using the dimensions of the z-stack (116 × 116 × 60 µm). The experiment was repeated twice under the same conditions. Figure 4.6 shows the average concentration of beads, across all three experimental repeats, remaining in the chamber after 30 minutes of washing with phosphate buffer – post pulse.

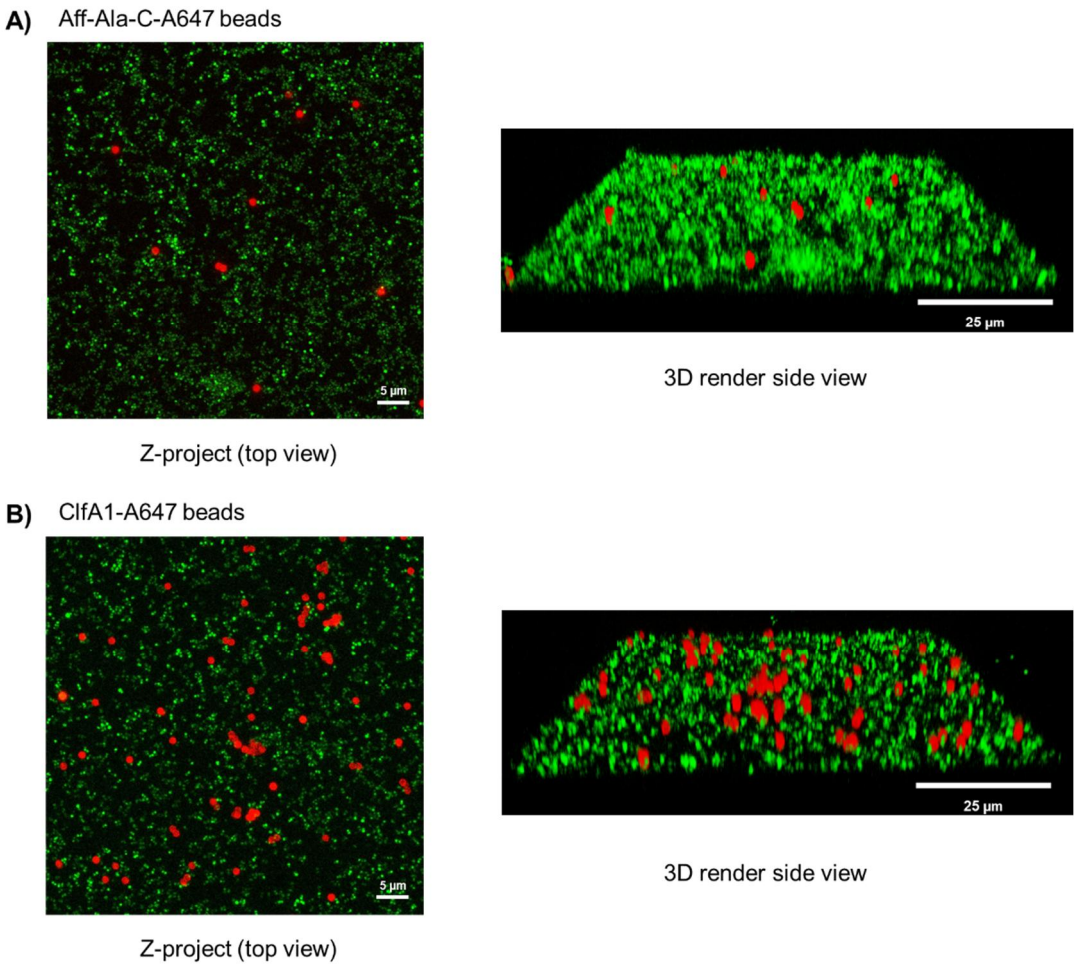

Figure 4.5. Z-stack images acquired using confocal microscopy of S. aureus UAMS1 biofilms treated with ClfA1-A647 and Aff-Ala-C-A647 conjugated beads.

Left image shows z-projection (top view) rendered in ImageJ software and right image a 3D render of the z-stack from the side created in LasX software (Leica). A pulse of beads was flowed over the biofilms and left stationary for 10 minutes, it was then washed for 30 minutes with phosphate buffer at a flow rate of 250 µL min^{-1}. A) Beads conjugated with Aff-Ala-C-A647 Affimer. B) Beads conjugated with ClfA1-A647 Affimer. Green shows cells stained with DMAO and red, beads with Alexafluor647-labelled Affimer attached to their surface.

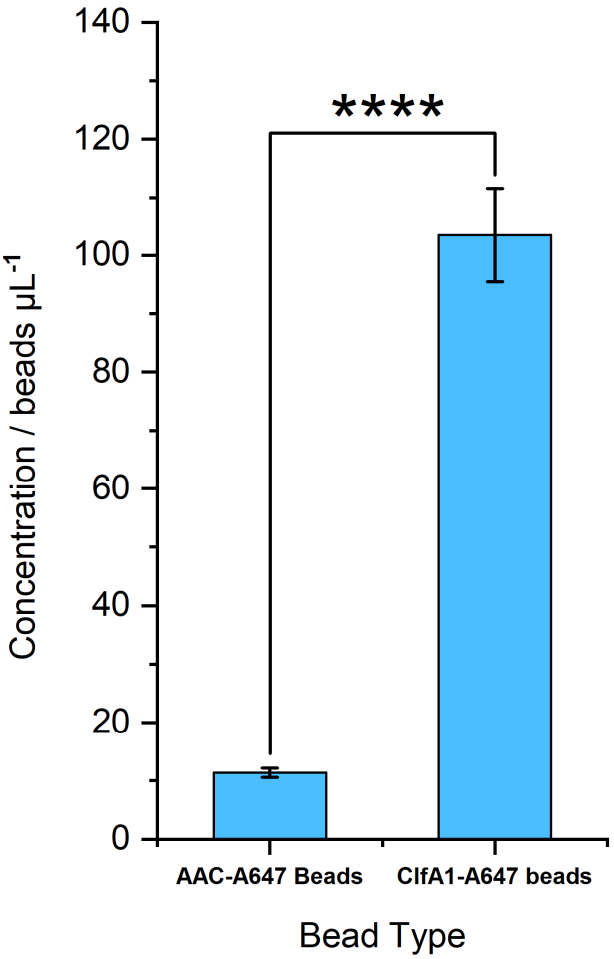

Figure 4.6. Bar graph showing the average bead concentration of ClfA1-A647 and Aff-Ala-C-A647 conjugated beads in the microfluidic chamber after 30 minutes of washing.
Biofilms cultivated in microfluidic chamber V5.0 were treated with a pulse of Affimer conjugated beads, and then washed with phosphate buffer for 30 minutes at a flow rate of 250 µL/min. Error bars show averages associated with SEM values, n = 60 (20 z-stacks acquired from three technical repeats). Paired student t-test analysis gave P <0.001 (paired student's t test).

The results from Figure 4.6 show a statistically significant increase in bead concentration when ClfA1-A647 Affimer is conjugated to the bead surface, compared to the Affimer scaffold control. Although the average bead concentration across the three experiments gave a statistically significant increase in bead concentration for ClfA1 Affimer-beads, there still existed a

large amount of variability in concentration between experiments. Figure 4.10 shows the bead concentrations for each experiment.

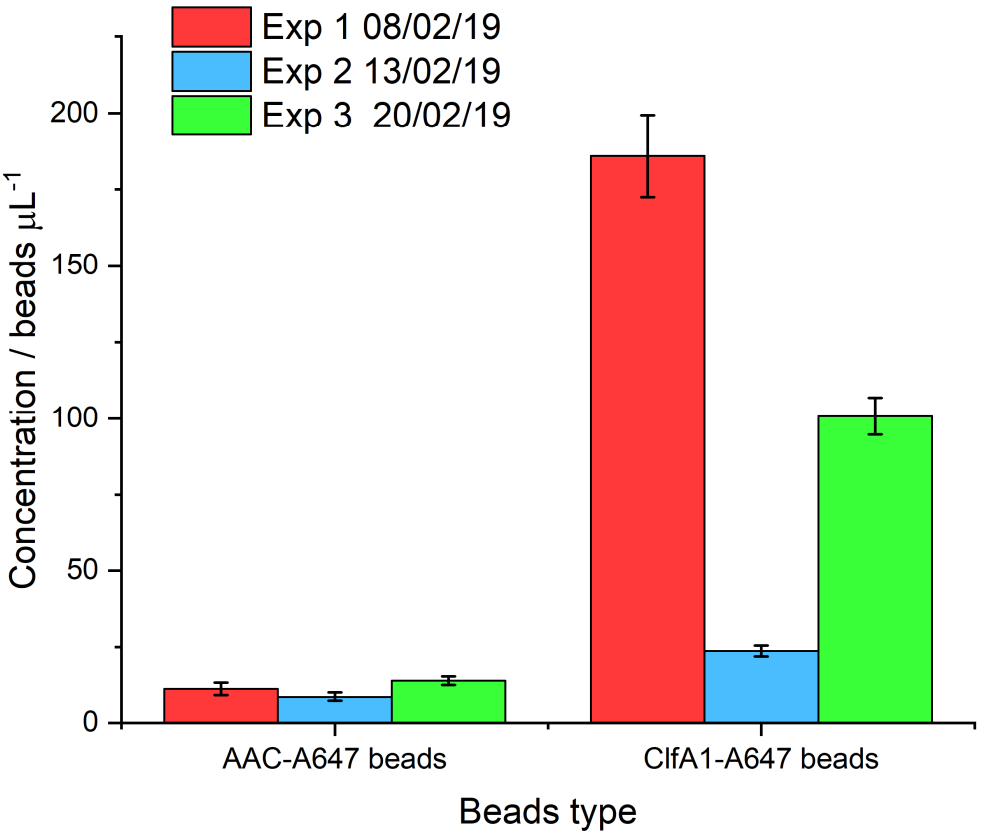

Figure 4.7. Bar graph showing the average bead concentration of ClfA1-A647 and Aff-Ala-C-A647 conjugated beads for each experimental iteration. Biofilms cultivated in microfluidic chamber V5.0 were treated with a pulse of Affimer conjugated beads, and then washed with phosphate buffer for 30 minutes at a flow rate of 250 µL/min. Error bars show averages associated with SEM values, n = 20 (20 z-stacks acquired for each experimental condition in each of the technical repeats). Legend shows experiment number and the date it was performed on.

Data collected for the Aff-Ala-C-A647 beads remained consistent across all three experiments with an average of 11.4 ± 0.8 beads μL^{-1}; conversely the average for ClfA1-A647 beads was 103.5 ± 8.0 beads μL^{-1}. The experimental variability between ClfA1-A647 bead experiments may derive from how the beads were prepared. For instance, beads used in Exp 1 and 2 were taken from the same 10× stock, which had originally been flash frozen for storage:

the stock was thawed for Exp 1. Between Exp 1 and Exp 2 the 10× was flash frozen and thawed again, which may have had some impact on the binding ability of the beads. For Exp 3 the beads were made fresh, made into their 1× stock *then* flash frozen. The freeze / thaw process may be having a detrimental effect in the protein conjugated beads. An experiment wherein the beads were produced using a erroneously high concentration of protein showed no binding at all to the biofilm. This may have been caused by a high Affimer density on the surface precluding binding. The conditions by which the beads and produced and stored are essential for preservation of the beads binding ability.

This results from Figure 4.5 and Figure 4.6 both demonstrate the specific binding of the ClfA1 Affimer to the biofilm via the binding loops, and the ability of the Affimer to localise 2µm beads to the surface of a biofilm. Considering the similarity in size between the polystyrene beads and clinically relevant microbubbles (~ 2 µm), the ability of the ClfA1 Affimer bead to bind the biofilm inferred that an ClfA1-microbubble should also be able to bind the biofilm. However, the experiment introduced the beads as a static 'pulse' in which the flow had been stopped for 10 minutes once the beads had reached the chamber. If a similar experiment were to be performed using microbubbles *in vivo*, a static pulse would not be possible under the constant flow of the vascular system. Therefore, the experiment was repeated, but flow was not stopped during bead introduction.

4.2.2 ClfA1-A647 beads under constant flow

The previous experiment showed the ClfA1 Affimer's ability to localise the polystyrene beads to the biofilm surface in the flow system, with the beads having first been left static in the flow chamber for ten minutes to promote bead adhesion. This experimental format did not mimic a more *in vivo*-like paradigm in which the beads would potentially be introduced to the bloodstream, and therefore under constant flow. The experiment was repeated as above but the beads were not allowed to stand statically in the chamber for any amount of time. The bolus of ClfA1-A647-beads (~ 10^8 beads mL^{-1}) was flowed into the chamber and then immediately washed with phosphate buffer under constant flow (~ 250 µL min^{-1}). The control chamber replicated experimental conditions from the previous section in which the beads were left static in the chamber for 10 minutes before the phosphate

buffer wash was commenced. Figure 4.8 shows the concentration of beads calculated (as in section 4.2) for each experimental chamber.

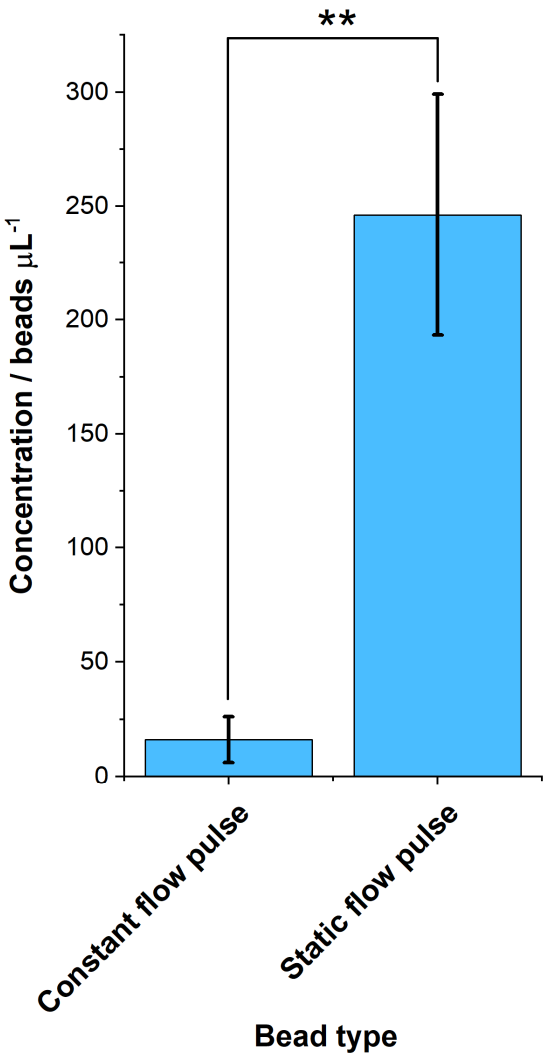

Figure 4.8. Bar graph showing the average bead concentration of ClfA1-A647 conjugated beads in the microfluidic chamber after 30 minutes of washing for both the flow pulse and static pulse conditions.

Biofilms cultivated in microfluidic chamber V5.0 were treated with a pulse of Affimer conjugated beads, and then washed with phosphate buffer for 30 minutes at a flow rate of 250 µL min^{-1}. Error bars show averages associated with SEM values, n = 10 (10 z-stacks acquired for each of the experimental conditions). Paired student t-test analysis gave P = 0.003 (paired student's t test).

From this data a significant decrease in bound beads can be seen under conditions of constant flow over the biofilm. Figure 4.9 shows composite z-stack images acquired from the experiment where the number of beads in the z-stack represents the average number of beads calculated from acquisition across the whole flow cell.

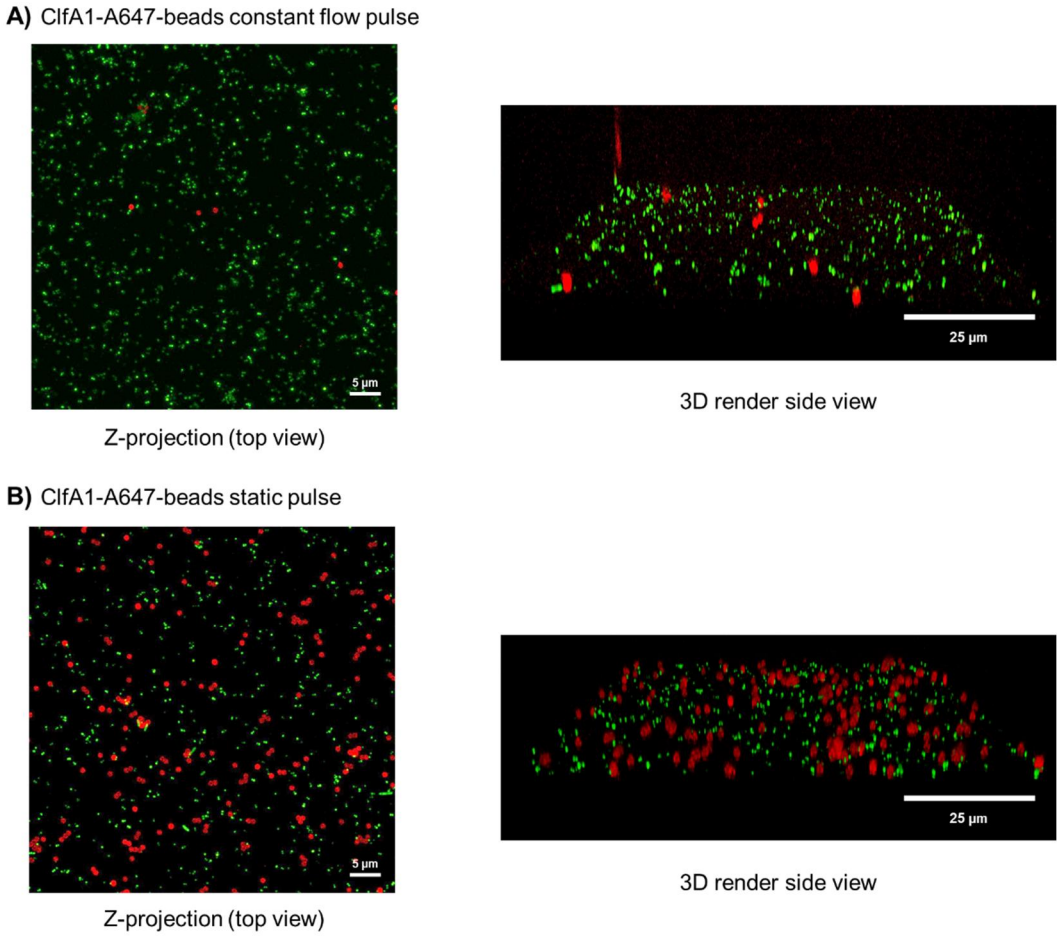

Figure 4.9. Z-stack images acquired using confocal microscopy of S. aureus UAMS1 biofilms treated with ClfA1-A647 conjugated beads under static and constant flow pulse conditions.

Left image shows z-projection (top view) rendered in ImageJ software and right image a 3D render of the z-stack from the side created in LasX software (Leica). A) beads were flown over and washed for 30 minutes with Phosphate at a flow rate of 250 µL/ min with uninterrupted flow. B) beads were flown over and washed for 30 minutes with phosphate at a flow rate of 250 µL/ min with a 10 minute static pulse. Species in green are cells stained with DMAO, and species in red are beads with Alexafluor647-labelled Affimer attached to their surface.

The data suggest that applying the beads to the biofilm under a constant flow regimen has a detrimental effect on their ability to bind the biofilm. Following 30 minutes of washing, there was a greater increase in the number of beads bound to the biofilm when they were incubated statically with the biofilm for 10 minutes, compared to being applied under a constant flow. This may have been due to the beads being slightly more dense than water (beads density = 1.03 g/ dm^3 , water density = 1.0 g/ dm^3). During the 10 minute incubation period, as the beads moved around the chamber, more beads may have come in to contact with biofilm. Conversely in the constant flow system there may be comparatively fewer beads actually making contact with the biofilm. This may mean that binding of the beads to the biofilm is dependent on the kinetics of association for ClfA1 binding to its ClfA target. If the association of the two proteins is slow, static incubation time may be essential to establish enough protein-protein interactions to secure the bead at the biofilm surface.

Whichever the reason for the decrease in binding, the experiment gives insight into how translatable the system is to a biological system, such as the human body. As the vascular system is under constant flow, it is important that future biofilm-binding candidates are explored that can capture targeting species to the biofilm under constant flow conditions. However, it was decided that for future microbubble experiments using the ClfA1-A647 protein, a 10 minute static incubation application would need to be used.

The main question that needed answering was: what was causing poor binding under flow? It may have been down to the number of beads making contact with the biofilm as opposed to the binding interaction being too weak to capture the beads onto the biofilm under constant flow conditions. The results of the ITC experiment in section 2.2.2.3 showed a tight binding with a K_D = 125 nM, but ITC does not give an idea of binding kinetics. The affinity may be high, but the protein's association (k_a) and dissociation (k_d) rate to its target may affect how quickly the beads can establish an interaction with the ClfA target on the biofilm surface, under constant flow. Surface Plasmon Resonance was used to experimentally measure the ClfA1 Affimer's k_a and k_d rate constants.

4.2.3 Surface Plasmon Resonance (SPR) analysis of ClfA1 and ClfA.

Surface plasmon resonance (SPR) is an analytical method that allows real-time monitoring of biological and chemical interactions.[181] First, one of the binding partners is immobilised to a gold chip, e.g. using the interaction between biotin and streptavidin. In this case, ClfA1 was biotinylated with biotin-maleimide, which covalently links a biotin molecule to the thiol group of the Affimer protein's cysteine residue. The biotinylated ClfA1 was passed over a gold chip with a streptavidin coated surface. Light from a light emitting diode (LED) is shone at the gold chip surface and is reflected back to a detector.[182] Electrons within the gold surface absorb energy from light of a certain wavelength, causing them to resonate (surface plasmons). The reflected light form the chip experiences a loss of intensity as a function of this resonance energy. These surface plasmons are sensitive to interactions between ClfA1 and its binding partner ClfA, which changes the resonance frequency of the electrons in the gold surface. This change in the reflected light is then converted to a response unit, and as the nature of the interaction changes over time, so does the observed response unit.

SPR can give an indication of the rate of association (k_a), the rate of dissociation (k_d) and the binding affinity (K_d). The biotinlated ClfA1 protein was used to functionalise the gold chip surface at different relative densities, (low, medium and high). The ClfA protein ligand was then flowed over the immobilised Affimer at different concentrations. As the ClfA protein bound to the ClfA1 Affimer, a change of response unit (RU) was observed. The RU increased until the protein exists in an equilibrium where on rate is equal to the off rate, at this point the RU plateaued and remained constant. Once this equilibrium has been reached, the flow of ClfA protein was replaced with a flow of buffer. During this step, the ClfA protein slowly dissociated from the immobilised Affimer and the RU then decreased, as the chip surface transitioned back to its initial unbound state. Figure 4.10 shows the output data from the Biacore SPR apparatus for association between ClfA1 and ClfA using the low density Affimer surface.

For each of the curves shown in Figure 4.10A, the maximum RU was plotted against the concentration of ClfA protein (Figure 4.10B). A curve was fitted to the data using the equation:

$$y = \frac{RU_{max} + x}{K_d + x}$$

Where,

RU_{max} is the maximum RU of the fitted curve.

K_d is the binding constant for the interaction.

The calculated K_d taken from the SPR data 97.8 ± 8 nM corresponds to a similar value calculated form the ITC studies performed in section 2.2.2.3 K_d = 125 ± 51 nM. The association rate constant for the interaction between ClfA1 and ClfA was found to be 5.84 ± 2.52 ×10^5 M^{-1} s^{-1}. Association therefore happens at a rate that is limited by diffusion i.e. < 10^5 M^{-1} s^{-1}.[183] In solution, the limiting step for the binding of ClfA1 to ClfA is the speed at which the proteins diffuse to each other. Therefore, the binding of the two proteins does not require a conformation change in order for a binding event to occur. Instead, the lower concentration of biofilm-bound beads in section 4.2.2 for beads under a constant flow pulse may be dependent on the sheer number of bead-biofilm interactions. In the static pulse, the beads have a 10 minute window in which the beads can diffuse around the whole chamber, and therefore have a greater chance of eventually making contact with the biofilm. In the constant flow chamber, the beads only have the time they are flowed through the chamber to interact with the biofilm. The amount of beads bound to biofilm under constant flow conditions could be dictated by concentration: by increasing the concentration of beads, the frequency of bead-biofilm interactions would increase. This may mean that when translated in to a therapy, the concentrations of MBs used may need to be higher to increase MB-biofilm interactions. Alternatively, the concentration of targeting molecule on the surface could be increased to make sure that when an interaction does occur, there is a higher probability of a binding event happening between the MB and the biofilm.

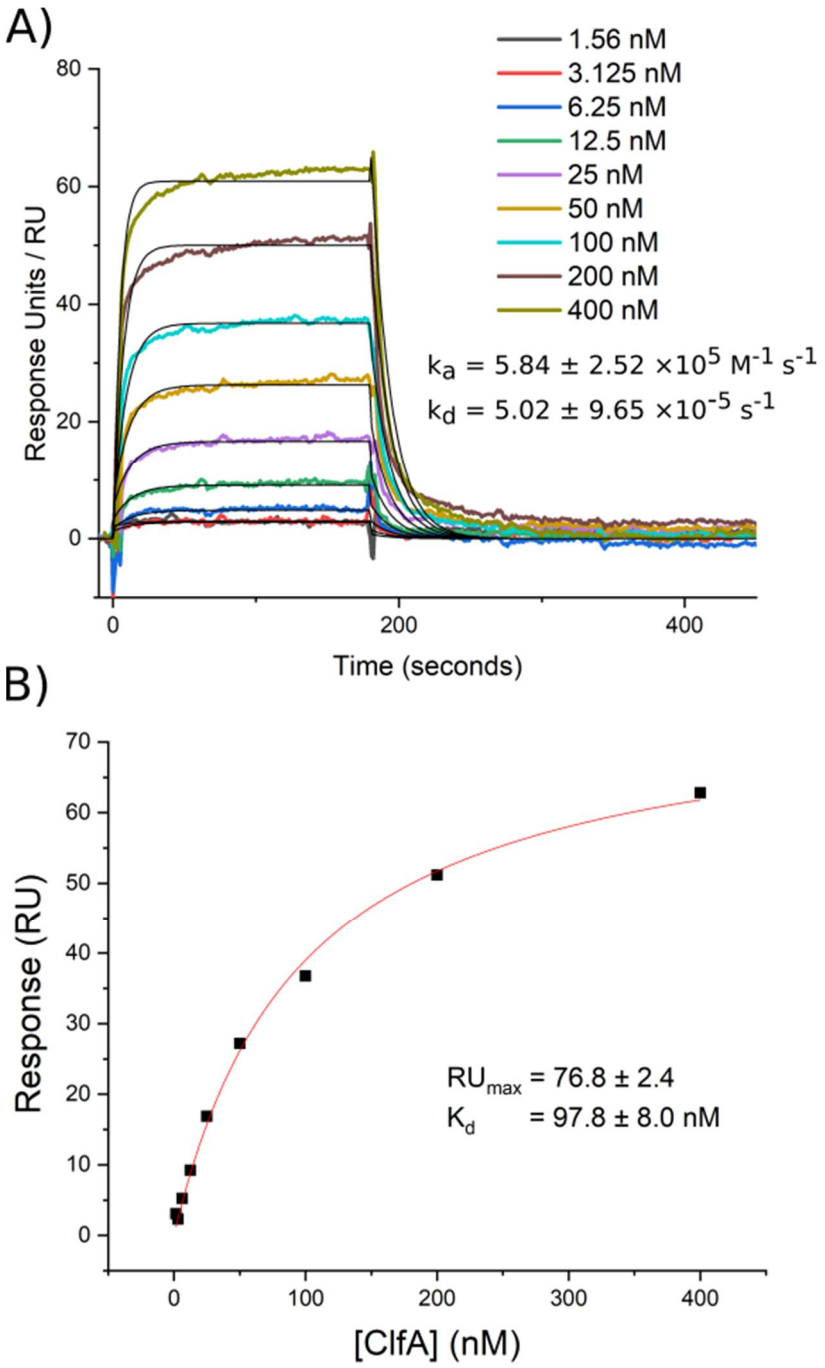

Figure 4.10. SPR sensogram and plot of RU_{max} vs [ClfA] for the interaction between ClfA1 and ClfA.

A) *Sensogram data for response unit (RU) vs time for ClfA concentrations (400, 200, 100, 50, 25, 12.5, 3.625, 1.56 nM) for the interaction between ClfA1 Affimer and ClfA protein. Black line indicates line of best fit for each curve used to calculate k_a and k_d. Rate of association k_a = 5.47 ×10^5 M^{-1} s^{-1}, rate of dissociation k_d = 5.02 ×10^{-5} s^{-1} . B) Plot of max response vs [ClfA]. A non-linear curve is fitted, from which the maximum response (R_{max}) and and binding affinity (K_d) have been calculated.*

4.2.4 ClfA1-MBP-MBL hybrid bead biofilm interaction

It been demonstrated that the ClfA1 Affimer can be used to localise the polystyrene beads to the biofilm surface. Using ClfA1 Affimer protein, a protein based on a consensus sequence from the plant protein cystatin, may invoke an immunogenic response when introduced into the bloodstream. The use of a human protein, such as MBL, could be used as a way to conjugate the MBs to the biofilm surface, and may be less likely to generate an immune response. In order to ascertain whether MBL could be used as a part of a targeted microbubble system, its ability to localise the polystyrene beads to the biofilm surface was investigated.

A biofilm was cultivated with *S. aureus* UAMS1 in the flow system (V5.0) as described in 6.3.4. Protein conjugated beads were prepared as described in 6.2.25. One set of beads were treated with ClfA1-A647 protein (10 µM in phosphate buffer), one set with MBP-MBL-A647 protein (10 µM in MBL buffer) and one set of beads with both ClfA1-A647 to MBP-MBL-A647 proteins attached to the surface (1:1, 10 µM of each protein in MBL buffer).

The biofilm was first washed with the buffer that the beads were suspended in, then the beads for a certain experimental condition were flowed into the chamber at ~250 µL min^{-1}. Once they had reached the chamber, flow was stopped and the beads incubated at for 10 minutes, static in the flow system. The biofilms were then washed for 30 minutes at ~ 250 µL min^{-1} with buffer, before 15 z-stacks were acquired for each biofilm chamber. ImageJ was used to count the number of beads per unit volume (dimensions of z-stack). Figure 4.11 shows the relative bead concentrations of each chamber after the buffer wash.

Initially it was seen (Figure 4.11) that the presence of the MBP-MBL protein on the bead surface had an inhibitory effect on binding for the ClfA1 conjugated beads, decreasing the bead concentration by almost a factor of 10. However, when the z-stacks are consulted in Figure 4.12, the MBP-MBL-A647 protein conjugated beads appear to have no fluorescent signal associated with them.

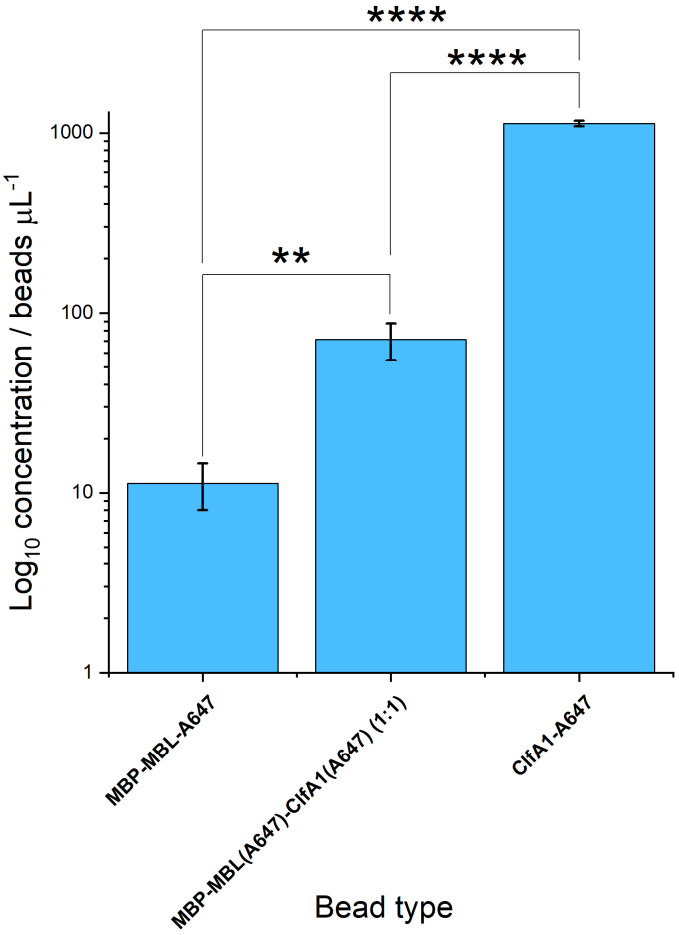

Figure 4.11. Bar graph showing the average bead concentration of ClfA1-A647, MBP-MBL-A647 and MBP-MBL-A647-ClfA1-A647 conjugated beads in the microfluidic chamber after 30 minutes of washing under static pulse conditions.

*S. aureus UAMS1 biofilms were cultivated in microfluidic chamber V5.0 and were treated with a pulse of protein conjugated beads, and then washed with buffer for 30 minutes at a flow rate of 250 µL min^{-1}. Error bars show averages associated with SEM values, n = 15 (15 z-stacks acquired for each set of experimental conditions). Paired student t-test analysis gave P< 0.002 (MBP-MBL-A647, MBP-MBL-*A647*-ClfA1-*A647*), P<0.001 (MBP-MBL-A647, ClfA1-A647), P<0.001 (MBP-MBL-*A647*-ClfA1-*A647*, ClfA1-A647).*

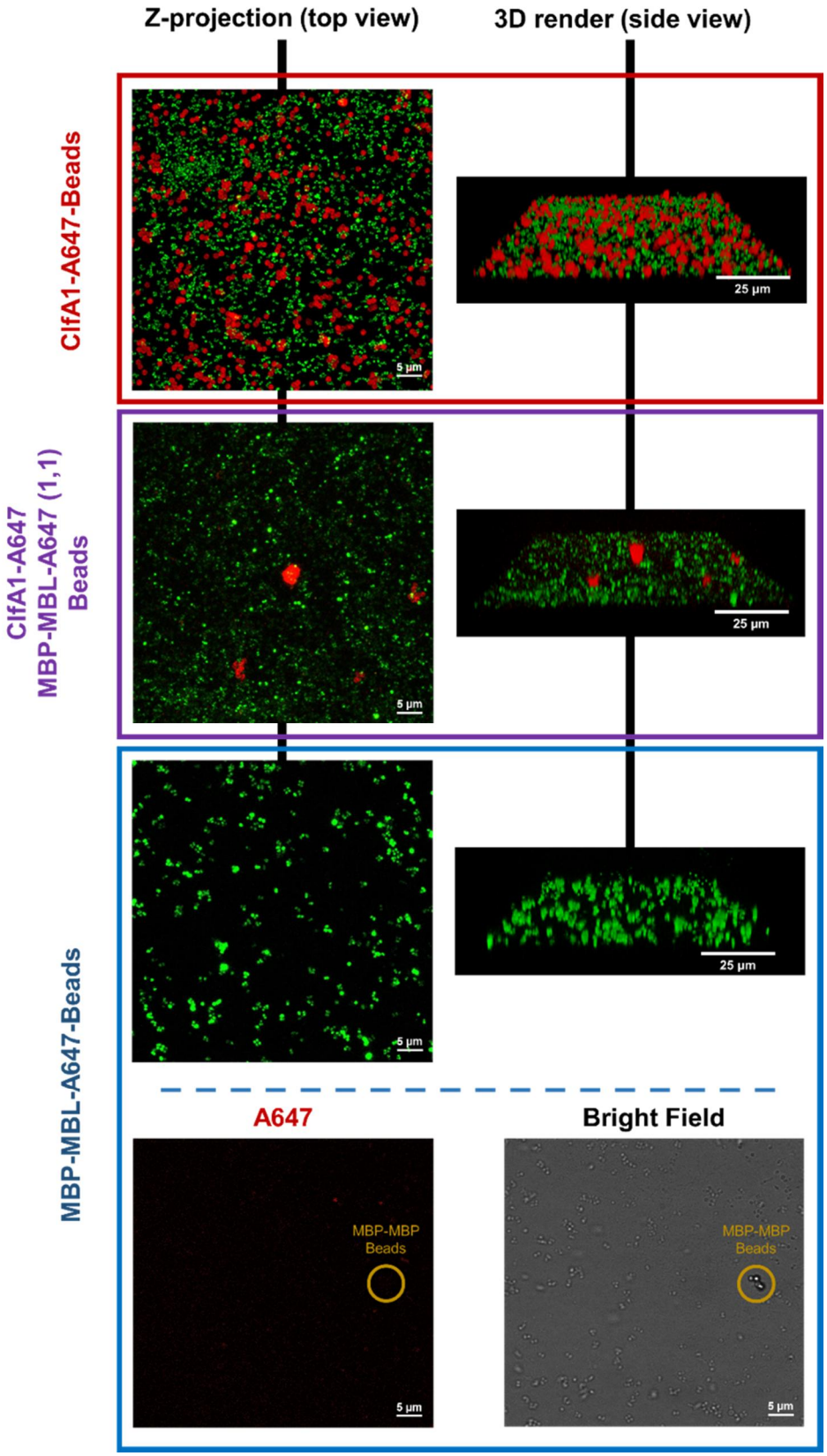

Figure 4.12. Z-stack images of ClfA1-A647, MBP-MBP-A647-ClfA1-A647 and MBP-MBL-A647 beads from a top z-projection view and a 3D rendering made in LasX (Leica) software.

*Top box, ClfA1-A647 beads associated to biofilm. Middle box, MBP-MBL-*A647-*ClfA1-*A647 *beads associated to biofilm. Bottom box, MBP-MBL-A647 bead data. Top row, Z-projection of MBP-MBL-A647 beads associated with biofilm; bottom row, z-projection of A647 associated species and its bright field components. Yellow circles show the MBP-MBP-A647 associated beads that did not display a fluorescent signal for Alexafluor 647 dye. Green species represent stained bacteria species, and red with Alexafluor647 associated species.*

The presence of the MBP-MBL protein on the surface of the beads not only had a detrimental effect on the bead-biofilm interaction, it also caused the formation of bead clusters. This occurred in both samples that had the MBP-MBL protein present, which may have contributed towards the decrease in binding of the ClfA1 beads spiked with the MBP-MBL protein. This may be due to the 'unravelling' of the coiled-coil of the MBP-MBL complex, and 're-winding' of MBP-MBL monomers on adjacent beads forming the associations in the clusters. However, work by Verde and co-workers demonstrated that triple coiled-coils, like the one associated with the MBL trimer structure [129], are resistant under high mechanical stress and coil 'opening' is unlikely to occur [184]. Alternatively, trimers of the MBP-MBL fusion complex may be cross-linking the beads via their polyhistidine purification tags. With each iteration of the MBP-MBL fusion protein binding a different Ni-NTA bead, and the trimeric coiled-coil crosslinking them together.

Although the bright field image in Figure 4.12 indicates that there was some interaction between the MBP-MBL-A647 beads and the biofilm, there was no fluorescent signal from the beads for A647-associated species, as seen in the z-stack. This initially indicated that there was no MBP-MBL-A647 conjugated to the bead surface.

However, SDS-PAGE analysis (Figure 4.13) of the beads shows the presence of fluorescent protein on the surface of the MBP-MBL-A647 beads, indicating that the protein was present on the surface of the beads during the confocal image acquisition during the flow experiment. The bead clustering may have been caused by the change in buffer (phosphate to TRIS), as MBP-

MBL conjugated beads were in a TRIS buffer. Given more time, the experiment should be repeated with all three beads suspended in TRIS buffer to see if buffer conditions affect the clustering of beads.

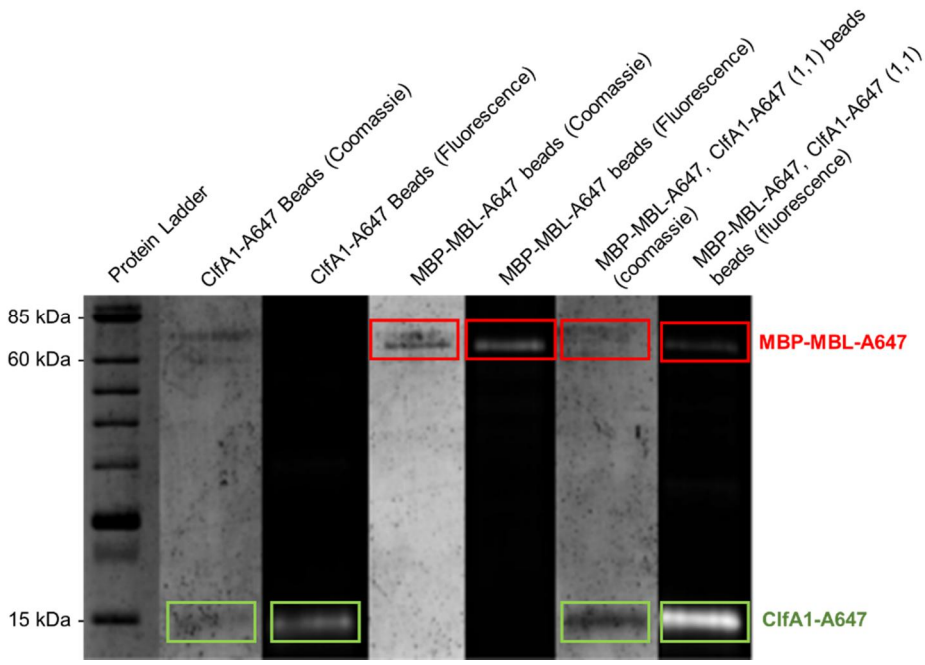

Figure 4.13. SDS-PAGE analysis of proteins on the surface of each conjugated bead sample.

MBP-MBL-A647 indicated in red and ClfA1-A647 indicated in green. For all bead types the correct proteins were shown to be present on the surface with their fluorescent ability still in-tact.

4.3 Targeted microbubble under flow conditions

Section 4.2 demonstrated the ClfA1 Affimer protein's ability to localise polystyrene beads to the biofilm surface. In order for the MBs to interact with the biofilm surface, and imaged using the 100× confocal objective, the system had to be manually inverted to allow the buoyant MBs to make contact with the glass-slide-bound biofilm. Issues regarding buoyancy of bubbles had been observed in preliminary test experiments. In practice this process had often caused detachment of tubing from the system. In order to mitigate this in subsequent experiments, tubing connected to the microfluidic chip was secured with high strength adhesive. This allowed for inversion of the system with low risk of tubing detachment.

Affimer proteins were conjugated to the MB surface using maleimide chemistry. This method for MB conjugation has been demonstrated previously by Klibanov and co-workers who attached a thiol-containing BODIPY dye to the surface of a microbubble that had a maleimide-containing lipid on its surface.[185]

4.3.1 ClfA1-MB interaction with biofilm under flow

A biofilm of *S. aureus* UAMS1 was cultivated in the flow system as described in section 6.3.4. After 24 hours of incubation the biofilm was washed with phosphate buffer at a flow rate of ~ 250 µL/ min. The biofilm was stained with DMAO so that the biofilm biomass could be imaged. Microbubbles were manufactured by Jordan Tinkler using the Horizon v3 Microspray production equipment, described in section 6.3.5. Once the microbubbles had been manufactured, Affimer solution was added (7.5 µM, 1 mL) and the bubbles incubated at RT for 1 hour. After this time, the bubbles were washed with phosphate buffer by gentle centrifugation, and decanting away of un-bound Affimer protein. Affimer-MB stocks were diluted to a concentration of 1×10^8 MB/ mL, similar to the bead concentration used in section 4.2.

The microfluidic chip was inverted, and all tubing between the reagent loop and the device was held vertically so as to reduce the risk of the buoyancy of the bubbles preventing them from reaching the microfluidic device. The microbubbles were flowed into the microfluidic chip using reagent loop, and

once the bubbles had reached the device the flow was stopped and the device remained inverted for a 10 minute incubation period. After this, the device was returned upright and mounted on the confocal microscope. The system then washed with phosphate buffer for 30 minutes at a flow rate of ~ 250 µL min^{-1}. As before, 15 z-stack scans were taken at 15 random points across each experimental chamber. The number of bubbles in each z-stack was counted using ImageJ software and a concentration per unit volume (of the z-stack) was calculated for ClfA1-A647-MBs and AAC-A647-MBs data sets. Figure 4.14 shows a z-stack images taken from each experimental chamber that reflects the average number of MBs across all z-stacks.

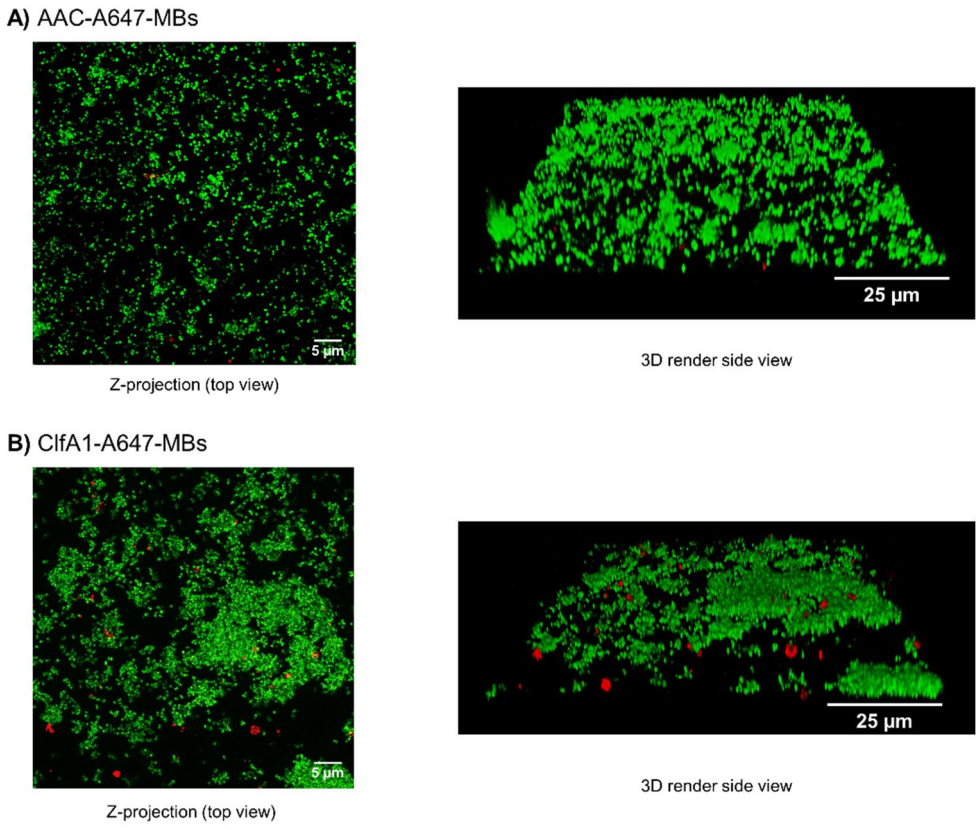

Figure 4.14. Z-stack images acquired using confocal microscopy of S aureus UAMS1 biofilms treated with ClfA1-A647 conjugated microbubbles and AAC-A647 conjugated microbubbles.

Left image shows z-projection (top view) rendered in ImageJ software and right image a 3D render of the z-stack from the side created in LasX software (Leica). A) ClfA1-A647-MBs were flowed into an inverted chamber, incubated for 10 minutes and washed for 30 minutes with phosphate buffer at a flow rate

of 250 µL/ min. B) AAC-A647-MBs treated as before. Green regions are cells stained with DMAO, and red indicates areas have Alexafluor647-labelled Affimer attached to them.

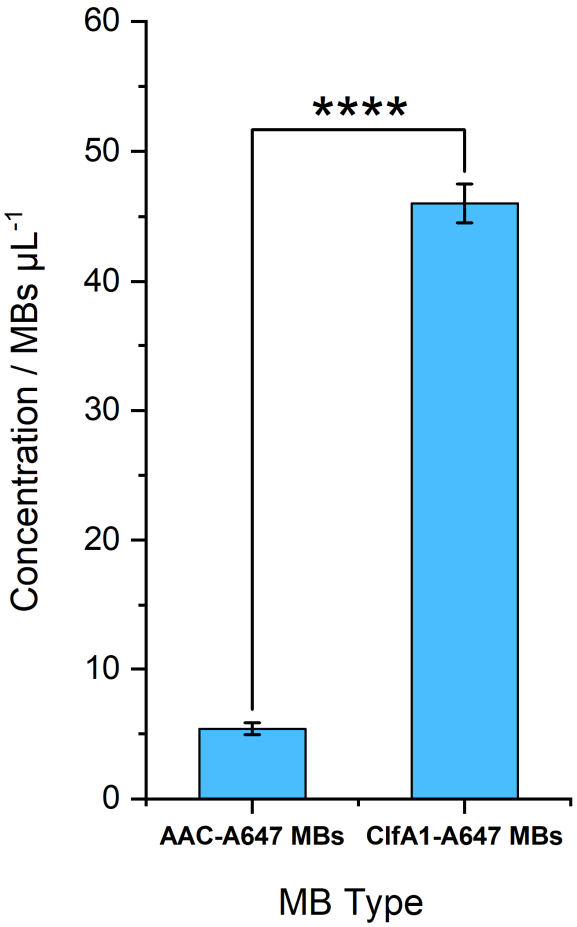

Figure 4.15. Bar graph showing the average MB concentration of ClfA1-A647 and Aff-Ala-C-A647 MBs in the microfluidic chamber after 10 minutes of static incubation in an inverted system and 30 minutes of washing with phosphate buffer.

Biofilms cultivated in microfluidic chamber V5.0 were treated with a pulse of Affimer conjugated MBs in an inverted system, and then washed with phosphate buffer for 30 minutes at a flow rate of 250 µL min^{-1}. Error bars show averages associated with SEM values, n = 44 (15 z-stacks acquired for two of the technical repeats, and 14 acquired for the final due to a data acquisition error). Paired student t-test analysis gave P = 3.9 x 10^{-14} (paired student's t test).

For the ClfA1-A647-MBs there is a statistically significant increase in MB binding compared to that of that of the AAC-A647-MB Affimer scaffold control. Not all species that have Affimer-A647 bound to them are associated with microbubbles.

When quantifying the number of MBs per image, one has to compare with the bright field in order to accurately calculate thebubble concentration. Figure 4.16 shows that A647also bound to the biofilm not in association with intact MBs. Only areas indicated with the yellow circles were assumed to be microbubbles due to the A647 fluorescent signal associated with them. Non-MB-associated fluorescent species are attributed to debris found in the MB sample, either from the MB manufacture process or from MBs that have ruptured whilst bound to the biofilm.

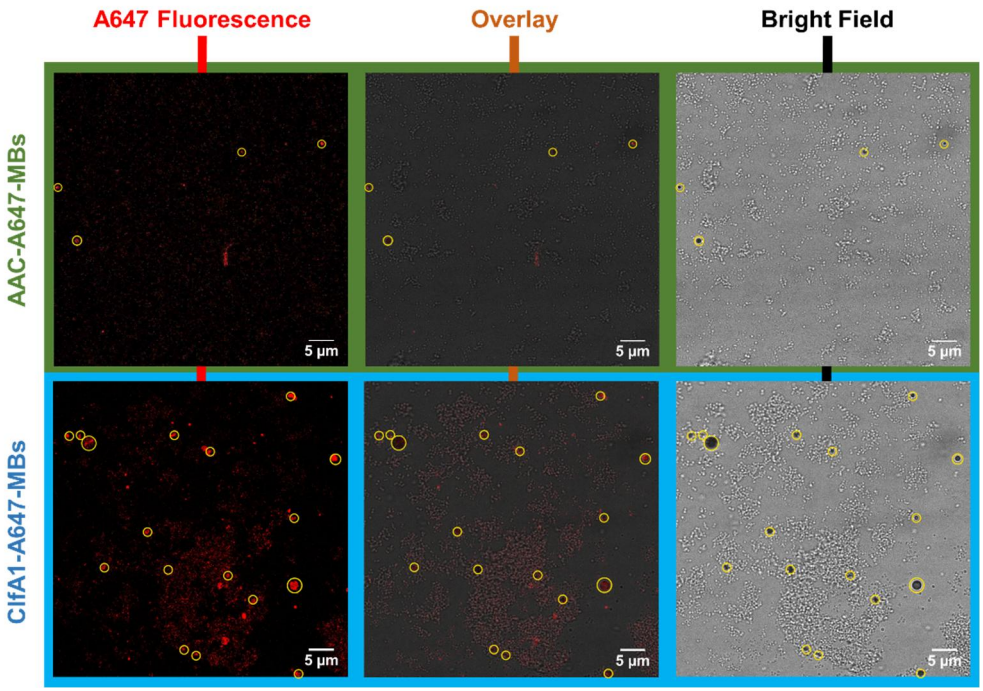

Figure 4.16. Z-projections of A647 channels taken from z-stacks from both ClfA1-A647-MB and AAC-A647-MB data sets, their bright field counterparts and an overlay of the two.

Top row shows the AAC-A647-MB z-stack, and the bottom row the ClfA-A647-MB z-stack. In all images MB are indicated by a yellow circle. There are some A647 in the z-stacks is not associated with intact MBs.

The ClfA1-A647-MBs have demonstrated the ability of the ClfA1 Affimer to successfully bind MBs to the surface of the biofilm, better than the non-specific Affimer scaffold. This shows that the ClfA1 Affimer protein can be used as an effective targeting system for microbubbles.

4.4 Chapter Conclusions

At the end of this body of work, it has been observed that the ClfA1 Affimer candidate brought forward from work in Chapter 2 has the ability to bind *S. aureus* UAMS1 biofilm in the microfluidic system.

The ability of the ClfA1 Affimer to localise larger structures to the biofilm surfaces such as 2 µm beads has been observed. When conjugated to the bead surface, the ClfA1 Affimer mediated an interaction between the bead and the biofilm surface. However, under constant flow conditions, the bead concentration at the biofilm surface was lower than when introduced as a static pulse with an incubation time of ten minutes. Further investigation of the ClfA1 and ClfA protein interaction by SPR revealed that the rate of association is probably limited by diffusion, and is therefore unlikely to limit the interaction between beads and the biofilm. It has been concluded that the difference in bead concentration at the biofilm surface is dependent on the frequency of biofilm-bead interactions, which is much higher during a static 10 minute pulse, compared to a constant flow pulse.

Polystyrene beads that had MBP-MBL conjugated to their surface showed little ability to interact with the biofilm, and caused clumping of beads. These observations may have been caused by poor buffer conditions, or interactions between the MBL-MBP proteins on adjacent beads.

When displayed on the surface of the microbubbles, the ClfA1 Affimer further proved its effectiveness at localising species to the biofilm surface. The presence of ClfA1 on the MB surface increased the MB concentration at the biofilm surface ten-fold compared to the non-binding AAC protein counterpart.

5 Conclusions and future work

5.1 Conclusions

This thesis focussed on an important human pathogen, Staphylococcus aureus, a major cause of bloodstream infection and sepsis. S. aureus bacteraemia is associated with a 30-day mortality rate ranging from 15 - 40% even when antibiotic therapy is involved.[186] Notoriously, methicillin-resistant S. aureus (MRSA) brought this strain of bacteria into the spot light in the early 21st century. The prevalence of antimicrobial resistance is being marked worldwide, prompting The World Health Organisation to declared it as one of the biggest threats to global health.[187]

More specifically, *S. aureus* causes many biofilm infections from infective endocarditis to medical device infections associated with intravascular catheters and pacemakers.[188, 189] Biofilm related infections are well known to be a challenge to treat, with a 10-100 fold decrease in antibiotic susceptibility associated with bacteria within the biofilm.[6]

Once *S. aureus* has invaded the bloodstream, it is able to seed infection in distant parts of the body, often causing severe illness which is difficult to locate and subsequently treat, causing ‘metastatic foci’ of infection, distant from the original focus.[190]

The aim of this thesis encapsulated everything from the identification of a biofilm-targeting protein that could be used to localise MBs to the *S. aureus* biofilm surface, to the development of a microfluidic flow system.

Two protein systems were investigated for their potential to mediate selective attachment of MB to *S aureus* biofilms: Affimer proteins and MBL. Ten Affimer proteins were found to bind, to varying degrees, three different clinically relevant strains of S. aureus, including a methicillin-resistant strain (USA300). Of the ten Affimer proteins investigated, ClfA1 emerged as the prime candidate to be taken forward for use on the MB surface. ITC studies on ClfA1 protein indicated a high binding affinity for its ClfA target.

Poor solubility of the MBL complex, led to further probing of overexpression and purification of the protein. The presence of a DNA impurity caused issues with purification, and different expression methods to isolate the protein from the DNA from lysed cells proved ineffective. Eventually, the production of an MBP-MBL fusion protein increased solubility, with successful purification of the fusion protein from overexpressing cells. Cleavage of the MBL from the fusion protein was investigated and shown to be successful, but purification of MBL from the cleavage mixture proved problematic. Time

constraints only permitted a full investigation into the ClfA1 protein conjugation system.

In tandem to protein development, a microfluidic flow system was developed to study biofilms under flow conditions without sacrificing cell viability. Many iterations of the flow system lead to the development of a flow cell with three parallel biofilm growth chambers, that allowed for multiple on-chip biofilm experiments as addition to controls. Issues arising from tubing blockages and flow system components were rectified by increasing the bore of the tubing used. The end result was a robust flow system in which biofilms could be observed under flow conditions via CLSM, using a LIVE/ DEAD cell viability stain. The addition of a fibrinogen coating step facilitated the cultivation of more reproducible and stable *S. aureus* biofilms that were less likely to become dislodge under the stress of flow.

Once the microfluidic system had been developed, it was used to study the interaction between the *S. aureus* UAMS1 biofilm and the targeting proteins. The ClfA1 Affimer protein was shown to bind to the biofilm under flow conditions, better than the AAC Affimer control. ClfA1 demonstrated the ability to localise polystyrene beads to the biofilm surface in the flow system. However, beads flowed into the chamber and incubated as a static pulse resulted in a higher biofilm-bound bead concentration than that of a constant flow pulse. The addition of the MBP-MBL protein to ClfA1 conjugated beads lead to a loss of binding between the beads and the biofilm. The precise nature of this inhibition was unknown, repeats were required to confirm that MBP-MBL protein's presence was hindering bead-biofilm association.

The conclusion of this project was marked by a proof-of-concept experiment in which MBs with ClfA1 conjugated to their surface were shown to bind to the biofilm in the microfluidic flow system, and remained bound to the biofilm after 30 minutes of washing.

5.1 Future Work

The interdisciplinary nature of this project meant that all branches of this body of work had to be performed in parallel, with the aim acquiring proof-of-concept data that validated further research into the use of targeted microbubbles for biofilm imaging and destruction. Given time, there are areas of this project that could be further developed in pursuit of this aim.

5.1.1 Biofilm-targeting proteins

The most underdeveloped area of work for the development of the biofilm-targeting proteins was the utilisation of the MBL protein. Although it was successfully expressed as a MBL-MBP fusion proteins, worked needs to be done in order to successfully purify the MBL protein from its MBP fusion protein. An up-scaled version of the TEV cleavage reaction may yield a soluble solution of the MBL protein with further purification by SEC. Minor success had been observed using this method, and it may result in a pure MBL protein stock.

It was concluded that the Affimer-biofilm binding assay screening experiment did not give a clear indication of relative biofilm affinity, due to the variability in biofilm biomass between each experimental well. ClfA1 was brought forward as its binding partner, ClfA, had already been identified. This infers the possibility that the other nine affimers screened may have higher affinity for the *S. aureus* biofilm. As demonstrated, the integration of these Affimer proteins into the microfluidic flow system experiments may bare fruit as potential MB-conjugates. The other ClfA binding Affimers (ClfA16, ClfA27) could be investigated using ITC and SPR to determine if their affinity is higher than that of ClfA1, and therefore could be better MB candidates.

Other proteins could be developed to target different parts of the biofilm. Proteins such as wheat germ agglutinin (WGA) and Concanavalin A (ConA) have been shown to bind *S. aureus* biofilm matrix components [191-193]. These protein could be used in conjunction with the MBs or as a biofilm matrix imaging method.

5.1.2 Microfluidic system development

A robust system for studying biofilms was developed using a microfluidic flow system that met the needs of the proof-of-concept experiment described previously. Further development of the system may allow for a greater number of flow chambers confined to one microfluidic chip, which could enable multiple MB experiments to be run at once.

Time-course experiments could be performed to understand how much time elapses during biofilm growth before the cell density reaches an equilibrium. Knowing this information may optimise the amount of time taken per experiment, allowing for multiple experiment to be ran in at the same time.

5.1.3 Interactions with biofilms under flow

Incorporation of the other Affimer proteins onto the bead and MB flow experiments may identify Affimer proteins that bind the biofilm better.

Further probing of the static vs constant flow pulse experimental findings should be investigated, as the vascular system is incapable of being ‘stopped’ to allow for MB binding. This could involve repeating the constant flow experiments with differing bead concentrations, which will test the hypothesis that the biofilm-bound bead concentration is mediated by the frequency of bead-biofilm interactions.

The next step from the proof-of-concept experiment is to investigate whether the microbubbles could be used in conjunction with ultrasound to image the biofilm and/or destroy the biofilm. The former may involve repeating the proof-of-concept experiment, and integrate US into the system to see if a signal is observed. Biofilm destruction could be quantified using the LIVE/ DEAD stain imaging method described in section **3.2.6**. Alternatively, the amount of cell death could be observed by monitoring the uptake of the EthD-III dye during bubble destruction.

Future work may include the incorporation of multiple different biofilm-targeting molecules on the surface on the each MB. Dual-targeting MB have been employed by Willmann and co-workers to target the VEGFR2 angiogenesis marker.[194] Warram and co-workers have taken this concept one step further by developing triple-targeted MBs that contained antibodies which bound a number of receptors expressed in tumour vasculature.[195] Although this previous work revolves around targeting mammalian cells, the premise of a multiple-targeting MBs is likely translatable to one that targets a biofilm.

Should these experiments prove effective, there is potential for the use of these targeted microbubbles to deliver therapeutic agents to the site of biofilm infection and use bubble destruction as a method of increasing drug uptake by the bacteria cells. Wherein lies a world of possibilities.

6 Experimental Methods

This section provides the experimental procedures performed for the laboratory work pertaining to this PhD project.

6.1 Chemical Methods

6.1.1 Solid phase peptide synthesis of biotin depsipeptide

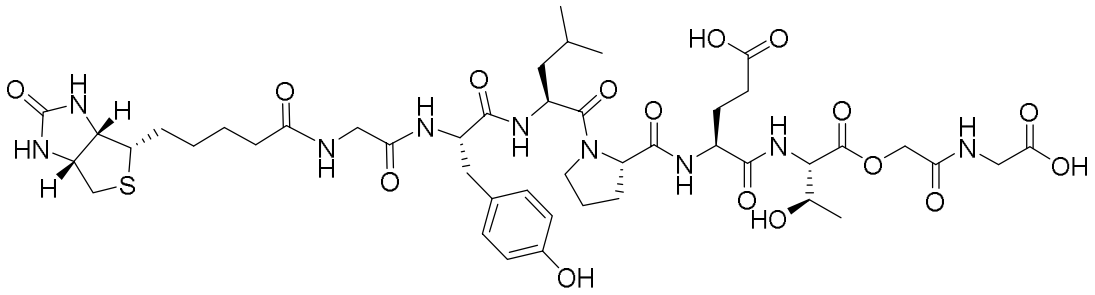

Pre-loaded 2-chlorotrityl glycine resin (50 mg) was suspended in DMF (3 mL) in a fritted 8-ml polypropylene reservoir fitted with a two-way stopcock and agitated on a rotary mixer for 3 mins. The DMF was drained by filtration under vacuum, Fmoc-Thr-Gly-(tBu)-OH (75 mg, 55 mM)[196] was dissolved in DMF (3 mL) and added along with HCTU (67 mg, 54 mM) and DIPEA (61 µL) to the syringe. The syringe was then agitated for 60 mins at RT, washed with DMF (3 x 3 mL x 1 min) and deprotected with piperidine (2 x 3 mL x 2 mins), and washed again with DMF (5 x 3 mL x 1 min). Fmoc-Glu-(tBu)-OH (102 mg, 92 mM) was dissolved in DMF (3 mL) and added along with HCTU (111 mg, 89 mM) and DIPEA (102 µL) to the syringe. The syringe was then agitated for 60 mins at RT, washed with DMF (3 x 3 mL x 1 min) and deprotected with piperidine (2 x 3 mL x 2 mins), and washed again with DMF (5 x 3 mL x 1 min). Fmoc-Pro-OH (93 mg, 91 mM) was dissolved in DMF (3 mL) and added with HCTU (111 mg, 89 mM) and DIPEA (102 µL) to the syringe. The syringe was agitated for 60 mins at RT, washed with DMF (3 x 3 mL x 1 min), deprotected with piperidine (2 x 3 mL x 2 mins) and washed with DMF (5 x 3 mL x 1 min). Fmoc-Leu-OH (97 mg, 71 mM) was dissolved in DMF (3 mL) and added with HCTU (111 mg, 89 mM) and DIPEA (102 µL) to the syringe. The syringe was agitated for 60 mins at RT, washed with DMF (3 x 3 mL), deprotected with piperidine (2 x 3 mL x 2 mins) and washed with DMF (5 x 3 mL x 1 min). Fmoc-

Tyr-OH (111 mg, 92 mM) was dissolved in DMF (3 mL) and added with HCTU (111 mg, 89 mM) and DIPEA (102 µL) to the syringe. The syringe was agitated for 60 mins at RT, washed with DMF (3 x 3 mL x 1 min), deprotected with piperidine (2 x 3 mL x 2 mins) and washed with DMF (5 x 3 mL x 1 min). Fmoc-Gly-OH (84 mg, 94 mM) was dissolved in DMF (3 mL) and added with HCTU (111 mg, 89 mM) and DIPEA (102 µL) to the syringe. The syringe was agitated for 60 mins at RT, washed with DMF (3 x 3 mL x 1 min), deprotected with piperidine (2 x 3 mL x 2 mins) and washed with DMF (5 x 3 mL x 1 min). To biotinylate the depsipeptide, Biotin-NHS ester (96 mg, 94 mM, 5 Equiv) was dissolved in DMF (3 mL) and added to the syringe along with DIPEA (95 µL). The syringed was agitated overnight at RT, washed with DMF (3 x 3 mL x 1 min), DCM (3 x 3 mL x 1 min) and MeOH (3 x 3 mL x 1 min). Resin was then dried under high vacuum for 4 h, peptide was cleaved off resin by the addition of a cleavage cocktail containing TFA:H_2O:TIS (95:2.5:2.5) (3 mL) and spun for 2 h at RT. Cleavage cocktail was removed by filtration under vacuum in to a 10 mL RB flask. Toluene (2 mL) was added and solvent was removed using a rotatory evaporator to leave a brown solid. The brown residue was re-dissolved in minimal ddH_2O, analysed by LCMS and then freeze dried to yield a fluffy white solid, Yield: 5 mg, 8.7%.

Mass Spectrum: m/z = 1020.56 [M + H^+]

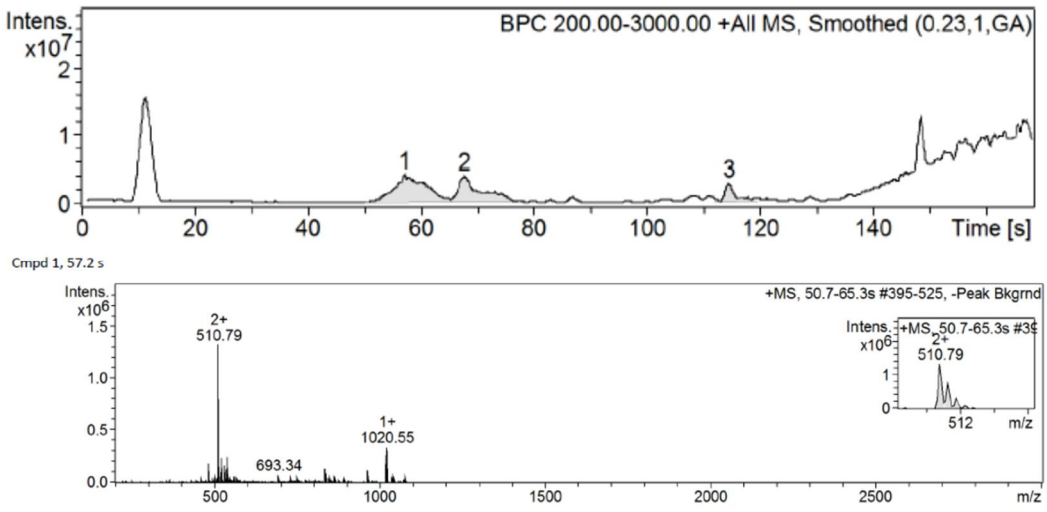

6.1.2 Production of mannose affinity resin

10 mL of Sepharose 6B resin (Sigma Aldrich) was washed with H_2O (3 × 10 mL) on a glass sinter funnel under vacuum. Resin was then suspended in 0.5 M Na_2CO_3 at pH 11 and incubated at RT with agitation (Fixed speed rotator, Stuart) for 30 minutes. To this divinyl sulphone (1 mL) was added, turning the suspension orange, it was then incubated at RT with agitation for 70 minutes until the orange colour abated.

The resin was again washed using H_2O (5 × 10 mL) on a glass sinter funnel. Resin was then suspended in 20% mannose (w/v) in 0.5 M Na_2CO_3 pH 10, and incubated overnight at RT with agitation. Resin was then washed with H_2O (5 × 10 mL) and suspended in 0.5 M Na_2CO_3 pH 8.5 with the addition of 200 µL 2-mercaptoethanol. Suspension was the incubated at RT with agitation for 2 hours. Resin was washed with H_2O (5 × 10mL), re-suspended in 20% EthOH and stored at 4 ºC.

6.2 Biological Methods

6.2.1 Buffer contents

PHOSPHATE BUFFER – 150 mM NaCl, 50 mM Sodium Phosphate (6.4 g L^{-1} Na_2HPO_4, 1.6 g L^{-1} NaH_2PO_4), 10% glycerol v/v, pH 7.4.

HEPES BUFFER – 150 mM NaCl, 50 mM HEPES, pH 7.4.

SORTASE BUFFER – HEPES buffer + 5 mM $CaCl_2$

MBL BUFFER – 1.25 M NaCl, 25 mM Tris-HCl, 5 mM $CaCl_2$, pH 7.8

PROTEIN LOADING BUFFER – 50 mM Tris HCl, 2% (w/v) sodium dodecyl sulfate, 2 mM Dithiothreitol (DTT), 10% (v/v) glycerol and bromophenol blue.

All buffers contents dissolved in H_2O purified using a PURELAB® Option-Q system (ELGA LabWater) with a resistivity of 18.2 MΩ.

6.2.2 Growth media contents

BHI BROTH – 37 g L^{-1} BHI broth freeze dried powder (Sigma Aldrich). Contains 12.5 g L^{-1} calf brains (infusion from 200g), 5 g L^{-1} beef heart (infusion from 250g), peptone 10 g L^{-1}, NaCl 5 g L^{-1}, D(+)-glucose 2 g L^{-1}, Disodium hydrogen phosphate 2.5g L^{-1}, final pH 7.4 at 25 ºC.

LB MEDIA – 25 g L^{-1} LB freeze-dried powder (Fischer) in H_2O. Contains 10 g L^{-1} Tryptone, 5 g L^{-1} Yeast extract and 10 g L^{-1} NaCl.

LB-AGAR MEDIA – 'LB media' + 15 g L^{-1} of Agar powder (Fisher) in H_2O

AUTO INDUCTION MEDIA – 10 g L^{-1} tryptone, 5 g L^{-1} yeast extract, 4% v(v/v) 25 × salts, 1000 × metals and 4.3 mM $MgCl_2$ in H_2O. Brought as hygroscopic powder (Formedium).

2YT MEDIA – 16 g L^{-1} Tryptone, 10 g L^{-1} yeast extract, 5 g L^{-1} NaCl.

All media was sterilised using an autoclaved at 120 ºC for 20 minutes.

6.2.3 DNA transformation.

Freshly thawed (having been stored at – 20 ºC in 50 µL aliquots in glycerol) competent *E. coli* strains (BL21 (DE3) Gold or XL10, Agilent) (50 µL) was held in ice for 10 minutes before the desired plasmid was added and thoroughly mixed by pipetting up and down for a few seconds. The mixture was incubated on ice for 20 minutes before being heated to 42 ºC for 20 seconds in a heating water bath (Grant Instruments) and immediately returned to ice for 2 minutes, 500 µL 2YT media was then added and the solution incubated with shaking (200 rpm, Orbital incubator, Stuart Equipment) at 37 ºC for 1 hour in air. A sample of culture (50 µL) was streaked onto an LB-agar plate containing ampicillin (50 mg mL^{-1}, Thermo Scientific) to provide single colonies after incubating statically, overnight at 37 ºC in air.

A single colony from the LB-agar plates was used to inoculate LB media (10 mL) containing ampicillin (50 mg mL^{-1}). The mini-culture was grown overnight at 37 ºC with shaking (200 rpm, Orbital incubator, Stuart Equipment) in air. Aliquots of the overnight culture (0.5 mL) were taken and thoroughly mixed with 80% (v/v) glycerol (0.5 mL) and stored at -80 ºC, until required.

6.2.4 Protein overexpression from *E. coli* (general)

A flake of frozen glycerol stock of a BL21 expression strain of *E. coli* containing the desired plasmid for protein expression was used to inoculate LB media (15 mL, 50 µg mL^{-1} ampicillin). This culture was incubated overnight at 37 ºC with shaking (200 rpm, Orbital incubator, Stuart Equipment) in air. The cells in the overnight culture were isolated by centrifugation (3000 xg, 10 min, 20 ºC, Multifuge 3 S-R centrifuge, Heraeus™), the pellet retained and the supernatant discarded. The cell pellet was re-suspended in LB media (10 mL, 50 µg mL^{-1} Ampicillin) and then used to inoculate LB Media (6 x 1 L, 50 µg mL^{-1} Ampicillin), cells were allowed to grow at 37 ºC in air, 200 rpm for 5-7 hours until OD_{550} reached ~0.8. Protein overexpression was then induced with addition of isopropyl β-D-1-thiogalactopyranoside - *IPTG* (2 mL, 10 mg mL^{-1}) and $CaCl_2$ (100 mL, 0.1 M), the cultures were incubated overnight at 24 ºC with 200 rpm shaking in air. Cells were isolated by centrifugation (6,500 rpm, 20 mins, JA-10 rotor, 4 ºC), pellet retained and supernatant discarded. Pellets were either frozen or immediately harvested for purification.

Bacterial pellets were re-suspended in 15 mL of MBL. Cells were then disrupted using a Constant Systems Cell Disrupter (20 kpsi, 40 kpsi head, 10 mL injections, 4 ºC). The lysate was then cleared by centrifugation (17,000 rpm, 45 mins, JA-30.5 rotor, 4 ºC), the pellet discarded and the supernatant retained.

6.2.5 Affimer Protein overexpression in *E. coli*

A flake of frozen glycerol stock of BL21 DE3 GOLD expression strain of *E. coli* containing the desired plasmid for protein expression was used to inoculate LB media (15 mL, 50 µg mL^{-1} ampicillin). This culture was incubated overnight at 37 ºC with shaking (200 rpm, Orbital incubator, Stuart Equipment). The cells in the overnight culture were isolated by centrifugation (3000 xg, 10 min, 20 ºC, Multifuge 3 S-R centrifuge, Heraeus™), the pellet retained and the supernatant discarded. The cell pellet was re-suspended in autoinduction LB media (400 mL, 50 µg mL^{-1} ampicillin), cells were allowed to grow overnight at 25 ºC, in air at 200 rpm shaking. Cells were isolated by centrifugation (6,500 rpm, 20 mins, JA-10 rotor, 4 ºC), pellet retained and supernatant discarded. Pellets were either frozen or immediately harvested for purification.

6.2.6 Affinity Chromatography

Desired affinity resins were packed into a Glass Econo-Column® (BioRad) of an appropriate size (where the desired amount of resin settles as a bed at least 3 cm from the column's porous polymer bed. After use, the column should be stripped of protein using the appropriate elution buffer, washed with 5 column volumes of H_2O, purified using a PURELAB® Option-Q system (ELGA LabWater) with a resistivity of 18.2 MΩ, then 2 column volumes of 20% EtOH (aq) before being stoppered and stored at 4 ºC.

6.2.6.1 Mannose Affinity Chromatography

Lysed cell supernatant was passed over a mannose affinity resin (volume dependant on amount of cell lysate) equilibrated with desired MBL buffer. The column was then washed with 2 x column volumes of lysis buffer and protein was eluted with 2 x column volumes elution buffer (MBL buffer without $CaCl_2$ + 2.5 mM EDTA, pH 7.8). Fractions collected that contained

desired protein were identified by SDS-PAGE and ESMS. Fractions combined as desired and continued to next purification step; or pooled concentrated, flash frozen in liquid nitrogen and stored at -80 ºC.

6.2.6.2 Amylose affinity chromatography

Lysed cell supernatant was passed over a Amylose affinity resin (New England Biolabs) (volume dependant on amount of cell lysate) equilibrated with desired lysis buffer. The column was then washed with 2 x column volumes of lysis buffer, and then washed with wash buffer (lysis buffer + 10 mM maltose) until the eluent no longer turned Bradford Reagent blue. Protein was eluted with elution buffer (Lysis buffer + 300 mM maltose), until the eluent no longer turned Bradford Reagent blue. Fractions collected that contained desired protein were identified by SDS-PAGE and Mass Spectrometry. Fractions combined as desired and continued to next purification step; or pooled concentrated, flash frozen in liquid nitrogen and stored at -80 ºC.

6.2.6.3 Nickel affinity chromatography

Lysed cell supernatant was passed over a Ni-NTA affinity resin (Abbkine) (volume dependant on amount of cell lysate) equilibrated with desired lysis buffer. The column was then washed with 2 x column volumes of lysis buffer, and then washed with wash buffer (lysis buffer + 30 mM imidazole) until the eluent no longer turned Bradford Reagent blue. Protein was eluted with elution buffer (Lysis buffer + 300 mM imidazole), until the eluent no longer turned Bradford Reagent blue. Fractions collected that contained desired protein were identified by SDS-PAGE and Mass Spectrometry. Fractions combined as desired and continued to next purification step; or pooled concentrated, flash frozen in liquid nitrogen and stored at -80 ºC.

6.2.7 Size exclusion chromatography

An NGC™ Chromatography system (Bio Rad) was used to purify proteins by size exclusions chromatography. Sephadex™ 75 column was used to purify proteins by their relative size. Protein was eluted from the column using 0.22 µm filtered buffer of choice. Eluent protein content was

monitored by observing the A_{280}. Fractions containing protein were analysed by SDS-PAGE or ESMS.

6.2.8 Ion exchange chromatography

An NGC™ Chromatography system (Bio Rad) was used to purify proteins by their relative net charges at a given pH. A HiTrap Q FF anion exchange chromatography column (GE Healthcare) was connected to the system and purification method from the in-house software was used. Eluent protein content was monitored by observing the A_{280}. Fractions containing protein were analysed by SDS-PAGE or ESMS.

6.2.9 Protein concentration determination

Protein concentration was determined by using a Nanodrop2000 UV/Vis spectrophotometer (Thermo Scientific) by observing the absorbance of the protein at 280 nm. Protein concentration was then calculated using the Beer-Lambert Law.

$$A = \varepsilon C L$$

A is the absorbance at 280 nm, ε is the molar extinction coefficient (ε for all proteins can be found in the appendices), C is the protein concentration and L is the path length (1 cm).

6.2.10 Sodium Dodecyl Sulphate – Polyacrylamide Gel Electrophoresis (SDS-PAGE)

SDS-PAGE was carried out in hand cast 10-15% SDS-PAGE, 15 well gels made using recipes shown below.

Resolving gel recipe

Reagent	**10%**	**12%**	**15%**
ddH_2O	10 mL	8.76 mL	7.52 mL
1.5 M TRIS pH 8.8	5 mL	5 mL	5 mL
10% APS	200 µL	200 µL	200 µL
10% SDS	200 µL	200 µL	200 µL

40% Acrylamide solution	5 mL	6.24 mL	7.52 mL
TEMED	20 µL	20 µL	20 µL

Stacking gel recipe:

Reagent	
ddH_2O	6.26 mL
1.5 M TRIS pH 8.8	2.5 mL
10% APS	100 µL
10% SDS	100 µL
40% Acrylamide solution	1.24 mL
TEMED	10 µL

Protein loading buffer (15 µL) was combined with 5 µL of protein sample and incubated at 95 ºC. Samples were ran in a miniPROTEAN® Tetra Cell gel electrophoresis tank and power source (Bio-Rad) along with 1X SDS-PAGE running buffer (125 mM TRIS, 960 mM Glycine, 0.5% w/v SDS) for 45 minutes at 180 V. 2-212 kDa Protein Marker (NEB) was used as a reference marker for molecular weight. Gels were then stained for imaging for 2 hours using Coomassie blue stain (2.5 g Coomassie blue, 100 mL water, 400 mL Methanol, 500 mL water), destained overnight by in house de-stain (1:4:5, Acetic Acid: Methanol: Water) and imaged using a GelDoc XR Molecular Imager (Bio-Rad).

6.2.11 Sortase Labelling of MBL

Labelling with biotin depsipeptide: For a total volume of 200 µL, MBL (43 µL, 30 µM), Sortase 7M enzyme (6 µL, 10 mol%) and biotin depsipeptide (2.4 µL, 120 µM) were mixed together thoroughly and incubated at RT for 1 h. Reaction was monitored by Mass Spectroscopy.

6.2.12 Site Directed Mutagenesis

First, the peptide sequence requiring alteration was identified using SnapGene software, by translating the DNA sequence information for the

plasmid encoding for protein expression. The nucleotide alteration required to make the desired mutation was identified and primers were then designed in order to generate a 1 base pair mismatch that coded for a different amino acid at a certain point in the peptide sequence. The criteria for primer design were as follows:

- 25-45 bases in length
- T_m greater than or equal to 78 °C
- 40% minimum G/C content
- One or more C or G at the end

The primer melting temperature (Tm) was calculated using the following formula:

$$Tm = 81.5 + 16.6 \times (\log 10W) + 41°C \times (\%GC) – 500/L$$

Where W corresponds to the concentration of salt in molarity in the reaction, which was typically 0.04 M, and where L is the length of the primer in nucleotides.

Under these criteria the following primers were designed for mutation of N-terminal glycine to a serine, and insertion of 2 glycines at the N-terminus. The mutated genes were named MBL G1S and MBL G1GGins, respectively.

Primer Name	**Sequence**	**Additional information**
MBL_G1S_fwd	5'-CAGGCTACTATCACTGGCCTGCGCTACGG -3'	For site direct mutagenesis of N-terminal glycine to serine in MBL. MBL gene is pINIIIompA2 plasmid provided by Kurt Drickamer (Imperial College London)
MBL_G1S_fwd	5'-CCGTAGCGCAGGCCAGTGATAGTAGCCTC -3'	
MBLGGins1G fwd	5'-GGCGGCGGTGATAGTAGCCTGGCTGC -3'	For site direct mutagenesis of MBL, to insert 2 more glycine residues at N-terminus. MBL gene is pINIIIompA2 plasmid provided by Kurt Drickamer (Imperial College London).
MBLGGins1G rev	5'-GGCCTGCGCTACGGTAGC -3'	

6.2.13 Polymerase Chain Reaction

Polymerase chain reaction (PCR) was used to amplify DNA for gel extraction, or for product analysis, to ensure that all primers resulted in a single, specific DNA fragment being produced. In all cases, NEB enzymes and buffers were used, and all products were analysed by nucleic acid electrophoresis. Standard PCRs were set up in 50 µl tubes, and contained the following:

5 µl 10x KOD hot start polymerase buffer
0.7 µl 10 µM Forward primer
0.7 µl 10 µM Reverse primer
5 µl 2 mM dNTP
3 µl 25 mM $MgSO_4$
1 unit KOD hot start DNA polymerase
50 ng DNA template
The solution made up to 50 µl with sterile H_2O, and the following cycling conditions were used:

95 °C 2 minutes
95 °C 20 seconds
55 °C 30 seconds
70 °C 2 minutes 30 seconds
} 20 cycles
72 °C 10 minutes

1 µl of Dpn1 enzyme was added to 5 µl of PCR product and the sample incubated at 37 ºC for 1-2 hours. 5 µl samples of PCR product and PCR product post Dpn1 digestion were run on a 1 % agarose gel. Gels were made by dissolving 400 mg Agarose in 40 mL hot TAE Buffer (400 mM TRIS-acetate, 10 mM EDTA, pH 8.4) and 2 µl of SYBR® Safe DNA gel stain, set in a DNA gel bracket and comb. If a band did not disappear post Dpn1 digestion, the DNA was successfully amplified

6.2.14 DNA Extraction and Quantification

A single colony of *E. coli* XL10 was selected from an agar plate to inoculate 5 mL of LB media containing the necessary antibiotic. This overnight culture was incubated overnight at 37 ºC with 200 rpm shaking prior to use for large scale protein overexpression (BL21 Gold) or used to extract it's DNA (XL10). DNA Extraction was performed using QIAprep® Spin miniprep kit following its accompanying manufacturer's protocol.

6.2.15 Periplasmic Extraction of MBL

E. coli BL21 Gold cells were cultured as in general protein overexpression (section 6.2.4). Pelleted cells were re-suspended in 8 mL of sucrose solution (20% sucrose, 30 mM TRIS-HCl, 1 mM EDTA, pH 8) at 24 ºC, shaken for 15 mins at 180 rpm. Cells were then pelleted by centrifugation (13, 000 xg, 10 mins, JA-10 rotor). Supernatant was decanted and the cells were re-suspended in cold 15 MΩ purified H_2O, the cells were then shaken on ice for 20 mins at 180 rpm. Cells were pelleted by centrifugation (13,000xg, 10 mins, JA-10 rotor), and the supernatant was concentrated by ultrafiltration.

6.2.16 Expression Study

pINIIIompA2 plasmid DNA expressing MBL (provided by Kurt Drickamer, Imperial College London) was transfected into Rosetta cells, which were then plated out onto LB-Agar containing ampicillin (50mg L^{-1}) and chloramphenicol (34 mg L^{-1}), and incubated overnight at 37 ºC. A single or three colonies from the plate were picked to inoculate 5 mL LB media containing ampicillin (50mg L^{-1}) and chloramphenicol (34 mg L^{-1}). At the same time glycerol stocks of hMBP33 *E. coli* BL21 Gold DE3 cells were used to inoculate 5 mL LB media with ampicillin (50 mg L^{-1}). These overnight cultures were used to inoculate 100 mL LB media with the relevant antibiotic concentrations. as the mentioned above. The cultures were incubated at 37 ºC in air at 200 rpm shaking. Once both cultures had reached an OD_{550} = 0.8, 2 mL IPTG (5 mg mL^{-1}) was added along with 10 mL $CaCl_2$ (1M) and the cells were left to express the target protein for 2 hours. 1 mL of cells from each flask was flash frozen, and the rest of the cells were incubated overnight as before. 1 mL of cells from each flask were taken and flash frozen. Cells were pelleted

(4,500 xg, 10 mins). The supernatant was decanted and 10 mL ethanol added to precipitate out any proteins in the media, then the insoluble proteins were pelleted by centrifugation (4,500 xg, 10 mins). Cell pellet was then re-suspended in BugBuster® (Novagen) and allowed to react at RT for 20 mins. This was then repeated for all flash frozen cell stocks. Samples analysed by SDS-PAGE.

6.2.17 TEV-H6 protease overexpression

A flake of frozen glycerol stock of expression strain of *E. coli* BL21 Gold containing plasmid pET-28A containing genetic information for the expression of a his-tagged TEV protease (Appendix B) was used to inoculate LB media (5 mL, 80 mg L^{-1} kanamycin). This culture was incubated overnight at 37 ºC in air, with shaking (200 rpm, Orbital incubator, Stuart Equipment). The cells in the overnight culture were isolated by centrifugation (3000 xg, 10 min, 20 ºC, Multifuge 3 S-R centrifuge, Heraeus™), the pellet retained and the supernatant discarded. The cell pellet was re-suspended in LB media (10 mL, 80 mg L^{-1} kanamycin) and then used to inoculate LB Media (6 x 1 L, 80 mg L^{-1} kanamycin), cells were allowed to grow at 37 ºC in air, 200 rpm for 4 hours until OD_{600} reached ~0.5. Protein overexpression was then induced with addition of IPTG (final concentration 0.5 mM), the cultures were incubated overnight at 20 ºC. Cells were isolated by centrifugation (10,000 rpm, 20 mins, JA-10 rotor, 4 ºC), pellet retained and supernatant discarded. Pellets were either frozen or immediately harvested for purification.

6.2.18 TEV-H6 Protease purification

Bacteria pellets were re-suspended in 15 mL of lysis buffer (20 mM TRIS, 200 mM NaCl, 10 mM imidazole, 2 mM mercaptoethanol, 0.2% Triton X-100, pH 8). Cells were then sonicated on ice (3 x 3 mins, 50 W, 50% pulse cycle). The lysate was then cleared by centrifugation (20,000 rpm, 30 mins, JA-30.5 rotor, 4 ºC), the pellet discarded and the supernatant retained. Supernatant was then passed over a nickel affinity resin (10 mL) equilibrated with lysis buffer. The column was then washed with 3 x CV of low salt buffer (20 mM TRIS, 200 mM NaCl, 10 mM imidazole, 2 mM mercaptoethanol, pH 8), then 3 x CV of high salt buffer (20 mM TRIS, 1 M NaCl, 10 mM imidazole, 2 mM mercaptoethanol, pH 8), then a further 3 x CV of low salt buffer. Protein

was then eluted from the column using elution buffer (20 mM TRIS, 200 mM NaCl, 300 mM imidazole, 2 mM mercaptoethanol, pH 8). Fractions were analysed by SDS-PAGE (appendix B). Fraction showed to contain TEV-protease were pooled and loaded onto a Superdex 75 16/ 60 size exclusion column. Fraction corresponding to peaks on the UV Chromatogram were analysed by SDS-PAGE. Bands showing the presence of only TEV-Protease were pooled and concentrated by ultracentrifugation to 83 µM (1.5 mL). Aliquots were flash frozen in liquid nitrogen and stored in a -80 ºC freezer until required.

6.2.19 MBP-MBL overexpression and purification.

DNA coding for MBP-MBL expression was order contained in a pMalp5X vector, named '*MBP-His-TEV-hMBL_PMAl-p5x*'. This plasmid was transfected into *E. coli* BL21 Gold cells, plated out onto LB-Agar/ ampicillin (50 mg L^{-1}) and incubated overnight at 37 ºC. Colonies from the plate were picked to inoculate 5 mL of LB-Agar/ ampicillin (50 mg L^{-1}), which was incubated overnight at 37 ºC with 200 rpm shaking (200 rpm, Orbital incubator, Stuart Equipment). The same overexpression procedure as for MBL was followed.

The cell lysate was flowed over an amylose affinity resin (10 mL) equilibrated with MBL lysis buffer. Resin was washed with 3 x CV of lysis buffer. Protein was eluted from the column with elution buffer (MBL lysis buffer + 10 µM Maltose). Fraction monitored by SDS-PAGE, fractions shown to contain MBP-MBL were pooled and dialysed into sortase buffer (150 mM NaCl, 50 mM HEPES, 5 mM $CaCl_2$, pH 7.5) in 10,000 MWCO dialysis tubing. The contents on the dialysis bag was then concentrated by immersing the bag in PEG (as in MBL concentration). Final concentration 321 µM (7 x 1 mL). Aliquots were flash frozen in liquid nitrogen and stored in a -80 ºC freezer. Stocks analysed by LCMS, mass = 58918 Da.

6.2.20 MBP-MBL TEV cleavage test reactions.

MBP-MBL (100 µM) was combined with TEV-protease (25 mol%) in sortase buffer (200 mM NaCl, 50 mM HEPES, 5 mM $CaCl_2$, pH 7.5) to a final volume of 200 µL. The reaction was then incubated overnight at 4 ºC. Then loaded onto 3 mL Nickel affinity resin equilibrated with sortase buffer. Column

was then washed with 3 x CV sortase buffer. Protein on column eluted when required with elution buffer (sortase buffer + 300 mM imidazole). All fractions were analysed by SDS-PAGE or ESMS.

6.2.21 MBP-MBL cleavage reaction and purification.

MBP-MBL (100 µM) was combined with TEV-Protease (25 mol%) in sortase buffer to a final volume of 500 µL. The reaction was then incubated overnight at 4 ºC. Reaction mixture was then loaded onto a Superdex 75 16/ 60 size exclusion column. Protein species eluting from column were monitored by A_{280}. Fractions corresponding to peaks at A_{280} were analysed by SDS-PAGE.

6.2.22 Protein labelling with fluorescein-5-maleimide

Protein of a known concentration was combined with Fluorescein-5-malimide (Thermo Scientific) at a 10-fold molar excess to a final volume of 500 µL in a 1.5 mL lidded tube (Eppendorf). The reaction is then incubated at 4 ºC, overnight.

The formation of products is monitored by ESMS, and the reaction is considered complete when no peak for unlabelled protein is seen in the spectra. Peak at +425 Da above protein molecular weight associated with labelled protein. For all Affimer, 100% labelling was achieved.

Unreacted fluorescein-5-maleimide is the removed from protein solution using a Sephadex G-25 medium desalting column (GE Life Sciences). Column equilibrated in desired buffer and product protocol followed.

6.2.23 Affimer-Biofilm Binding Assay (ABBA)

A flake from each *S. aureus* strain glycerol stock was used to inoculate a separate 1 x 5 mL autoclaved BHI Broth in a 25 mL Falcon tube. In these experiments strains of *S. aureus* used were SH1000 (donated by Chris Randall, University of Leeds), USA300 (CCOS666, Culture Collection of Switzerland) and UAMS1 (CCOS667, Culture Collection of Switzerland. These tubes were then incubated overnight at 37 ºC in air, 200 rpm shaking. The following day these stocks were used to make up a 1 in 100 stock by the

addition of 100 µL the BHI broth cultures to 10 mL of fresh, autoclaved BHI broth.

200 µL of the suspension above was added to the relevant wells in a white, opaque, polystyrene 96 well plate (Greiner Biotech). Figure 6.1 shows the general layout of the plate for all experiments. Cells were added to highlighted wells in columns labelled ‘protein concentration’ and ‘Plate Purity’. To the wells highlighted in columns labelled ‘BHI Broth’, 100 µL of sterile, inoculated BHI broth was added as a biofilm negative control. The plate was then covered with its accompanying transparent plastic cover and placed in a 37 ºC in air, incubator for 48 hours at 40 rpm shaking.

General format of the two 96 well plates used in biofilm protein binding assays is shown in Figure 6.1. Each row corresponds to a certain strain of *S. aureus*, three strains were screened over two 96 well plates. ‘BHI Broth’ columns correspond to wells that have been incubated with sterile BHI Broth. The wells highlighted with crystal violet controls have an established biofilm in them that was then stained with 0.1% Crystal violet solution.

The liquid in wells of the column labelled ‘BHI Broth’ and wells highlighted in the ‘Plate Purity’ column were used to inoculate a Blood agar plate. ‘Plate Purity’ wells were streaked out on these plates whereas all ‘BHI Broth’ wells were used to inoculate the same plate split into 3 sections for each strain. The purpose of these plates is to ensure each cell strain grows a homogenous biofilm and that the BHI broth and the well contents remained sterile. The cells and broth were aspirated from the wells using a 200 µL, 12 channel pipette. Wells were then washed with 3 x 200 µL of phosphate buffer by gently pipetting the buffer in and slowly aspirating it back out again. To wells highlighted in columns ‘Protein concentration’, 50 µL of fluorescently labelled protein was added at each specified concentration (1 in 3 dilution series). The plate was then covered, wrapped in tin foil to prevent photo bleaching and incubated at RT for 1 hour. After this the wells were then washed as described above with 3 x 200 µL of wash buffer.

The plate was then loaded into an envision plate reader and the fluorescence of each wells was measured by emission of the wells at the desired wavelength (Fluorescein = 535 nm).

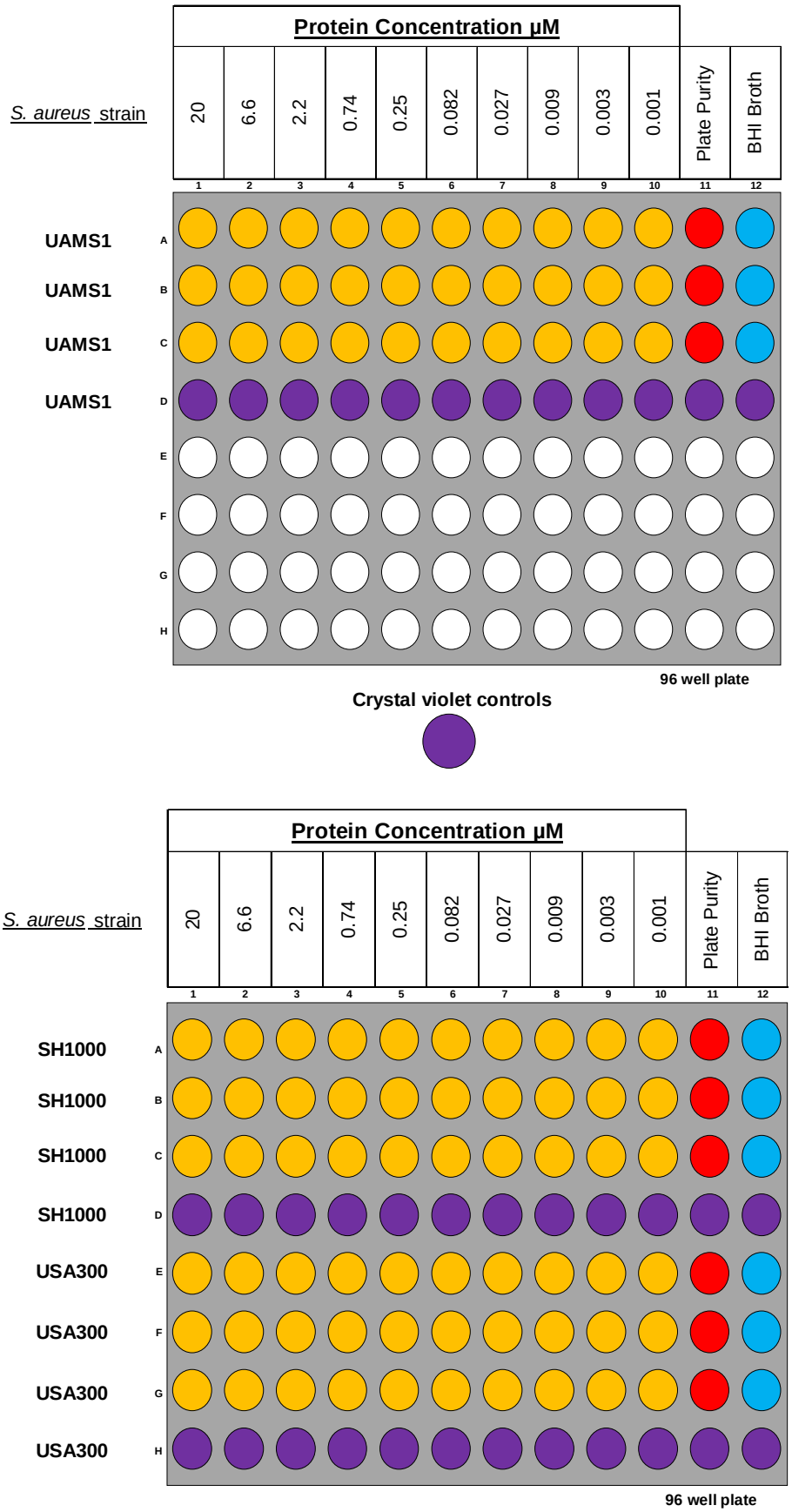

Figure 6.1. Experimental layout of two 96 well plates used in the ABBA experiments.

6.2.24 Protein labelling with NHS-ester

Protein of a known concentration is combined with an NHS-ester derivative (listed below) at a 10-fold molar excess in buffer containing 0.1M sodium bicarbonate (pH 8.3-9), to a final volume of 500 µL in a 1.5 mL Eppendorf tube. Reaction is incubated overnight at 4 ºC.

Degree of labelling is monitored by ESMS, if not all of the protein was labelled after an overnight incubation the labelled protein solution was purified regardless of amount converted. Degree of conversion ascertained by intensities of labelled and unlabelled protein peaks in the mass spectra (Appendix 7.9).

Unreacted NHS ester is the removed from protein solution using a Sephadex G-25 medium desalting column (GE Life Sciences). Column equilibrated in desired buffer and product protocol followed.

NHS ester derivatives used in this thesis:

Alexafluor488 NHS ester

Alexafluor647 NHS ester

Biotin-PEG-NHS ester

6.2.25 Protein-bead conjugation.

A known volume of 2 mL Ni-NTA polystyrene beads (10^9 beads mL^{-1}, micromod Partikeltechnologie GmbH, product code: 01-48-203) were pelleted using ultracentrifugation (13.3 xg, 2 mins) in a 1.5 mL Eppendorf tube. Water storage solution was decanted away and the beads re-suspended with an equal volume of the desired buffer. The beads were then pelleted as before by ultracentrifugation.

Pelleted beads were then re-suspended in 10 µM of protein in the desired buffer, at the same volume used to wash the beads. The presence of a His-tag on the protein was essential for conjugation. If protein had fluorophore attached, the tube was wrapped in foil and incubated at RT for 3-4 hours with slight shaking.

The beads were then pelleted, protein solution decanted, and the beads suspended in buffer. Decanting and resuspension steps were repeated

twice to wash beads of unconjugated protein. Final beads solution is assumed to be ~10^9 beads/ mL and diluted to ~10^8 beads mL^{-1} for biofilm experiments.

6.2.26 Non-specific bead binding using light microscopy

Biofilms of *S. aureus* UAMS1 were cultivated as in Section 6.2.23, using the same volume of inoculum for biofilm growth and buffer for washing. To each experimental well 50 µL of either buffer, non-conjugated beads or Affimer bound beads was added and incubated at RT for one hour. After this wells were washed with 3 x 200 µL of phosphate buffer, by gently aspirating the buffer in and out with a 200 µL Gilson pipette.

Once washed, the well were treated with paraformaldehyde (4% w/v, 50 µL). During treatment with paraformaldehyde the biofilms were mechanically disrupted by the end of the pipette tip and the solution aspirated vigorously to disrupt the biofilm and homogenise the biofilm solution.

A microscope sample was prepared using a 0.8-1 mm microscope sample slide, upon which 2 × 50 µm spacers are placed roughly 2 cm apart. On top of these spacers a 22 × 22 mm cover slip was placed. 30 µL of the biofilm sample taken from the wells was pipetted carefully between the cover slip and the slide in the opening created by the 50 µm spacers. The sample fills the space by capillary action. The slides were then mounted on a Nikon Eclipse 80i Microscope fitted with a Hamamatsu digital camera (Model C4742-95) and for each well sample, 20 images were acquired at various positions across the sample slide.

These images were then imported into MATLAB software and MATAB code developed by Damien Batchelor (University of Leeds) was used to count spherical species in the sample images. By imputing the physical dimension of a pixel in the image and the size of the spacers (50 µm) the volume and concentration was calculated by the software. The MATLAB code then exports the results as a .csv Excel file and a .tiff image of a histogram showing the distribution of sizes in each sample.

6.2.27 Isothermal titration calorimetry

Both ClfA, ClfA1 and AAC proteins were purified for ITC using nickel affinity chromatography and dialysed into phosphate buffer (50 mM Na_2HPO_4/ NaH_2PO_4, 150 mM NaCl, pH 7.4). Proteins were concentrated by centrifugal concentration (Amicon 10 kDa MWCO). ITC binding assays were performed using a Microcal ITC200 (GE Healthcare) thermostated at 25 °C. The ClfA sample was loaded into the sample cell (200 µL, 16-20 µM), and the Affimer titrant was loaded into the sample syringe (70 µL, 200 µM). Each titration experiment consisted of a sacrificial injection of 0.4 µL followed by 19 injections of 2 µL. Titration data were analysed using a one site binding model in the GE Healthcare Origin 7 ITC software.

6.2.28 Surface plasmon resonance

SPR experiments were performed on a Biacore 3000 instrument using streptavidin-coated chips (Sensor Chip SA, GE Healthcare). System was equilibrated with degassed phosphate buffer. The four flow cells of the sensor chip were conditions with 3 x 40 µL injections of conditioning solution (1 M NaCl, 50 mM NaOH) at 40 µL min^{-1}. ClfA1-biotin was diluted to 20 µM and injected over three of the flow cells to derivitise the chip with Affimer. The sensorgram was observed so that three differing density of Affimer were observed in each chamber; low, medium and high density. The density of the surface is defined by the response unit maximum, R_{max}, achieved by flowing the analyte over the surface. For the low density surface the following equation is used to get the R_{max} when flowing over the ClfA1-biotin Affimer:

$$R_L = \frac{MW_L}{MW_A} \times \frac{R_{max}}{s}$$

Where, $R_{L=}$ response level of immobilised ligand (RU), MW_L = molecular weight of ligand (for ClfA1 = 12630 Da), MW_A = molecular weight of analyte (for ClfA = 36979 Da), R_{max} is the maximum binding capacity (set as 100 RU) and s = number of sites per ligand (1 for ClfA1)

For the low density surface, the gold surface was functionalised with ClfA1- biotin until the RU got as close to 30 (calculated using above

equation) as possible. The high density surface was set as the maximum amount of ClfA1 that could coat the surface (ClfA1 being flowed through chamber until RU reached a plateaux), 2300 RU. The medium density surface was set as a value that lay between the maximum density surface and low density surface, 500 RU.

The fourth lane was left un-derivitized for a control. Experiments were then carried out using 1 in 2 serial dilution of ClfA starting at 400 nM ending at 1.56 nM. Flow rate of the experiment was 30 µL min^{-1}. Analyte was flowed into the flow chambers for three minutes, then the chamber were washed for a further seven minutes. Flow chambers were then washed of analyte until the RU returned to the baseline (RU before introduction of analyte) ~ 20 minutes. If the RU did not return to baseline, the chambers would need to be functionalised with the ClfA1 Affimer, again. However, this was not the case with these experiments as RU returned to baseline. BIAevaluation (Biacore) software was used to analyse data and perform curve fittings used to calculate binding kinetics values.

6.3 Microfluidic Methods

6.3.1 Microfluidic device manufacture.

Microfluidic devices were fabricated by Jordan Tinkler (University of Leeds) and Peng Bao (University of Leeds) using photo and soft lithographic techniques. A 3-inch diameter silicon wafer (Pi-Kem Ltd, UK) was initially cleaned by immersing in acetone, isopropanol, distilled water, and then drying under a stream of compressed air. A layer of SU-8 2075 (Microchem, Warwickshire, UK) was spin coated on a Photo resist spinner (EMS 6000, Electronic Microsystems) onto the wafer to a height of 180 µm using the following speeds: 10 seconds at 200 RPM, 10 seconds at 400 RPM, 10 seconds at 600 RPM, then 40 seconds at 1350 RPM. Microfluidic chip was designed using AutoCAD (Autodesk) software. Designs are further edited using CleWin (WieWeb) software before being transferred to the wafer using a 375 nm laser (MicroWriter ML, Durham Magneto-Optics, Durham, UK). Laser contact with the SU-8 photoresist causes polymerisation by cross-linking, creating a silicon master with the ‘negative’ imprint of the microfluidic

chip design, caused by the now insoluble SU-8 photoresist. Devices were cast from the silicon master in polydimethylsiloxane (PDMS) using a 1:10 ratio of cross linker to polymer base (Sylgard 184). The PDMS was left under vacuum for ~30 minutes to remove air bubbles, and then allowed to set for ~1 hour in an oven at 75°C. Individual devices were then cut away, hole punched, and bound to #1 22 x 50 mm glass cover slips using oxygen plasma treatment.[197] Flow rate modelling, performed by Jordan Tinkler (University of Leeds) of the devices during the design phase confirmed that the flow rates within the growth chambers is comparable to that found in vasculature.

6.3.2 Microfluidic biofilm study system manufacture.

The microfluidic biofilm study system (MBSS) was designed and manufactured by Dr Ben Johnson in the Department of Physics and Astronomy.

6.3.3 Piezo pump calibration.

The piezo pump in the MBSS was connected to an Extended micropump control unit (Bartels microtechnik). Two calibration experiments were set up at constant frequencies of 50 Hz and 100 Hz. Calibration was performed with H_2O in the media inlet. Microfluidic chip was attached to the system. The H_2O was flowed through at frequency 50 Hz and amplitude 250 Vpp for 5 minutes to fill system with water and check for any leaks in the system.

10 x 1.5 mL Eppendorf tubes labelled with numbers 1 – 10 and pre-weighed. For each numbered tube, an amplitude was assigned from 25 to 250 Vpp. Frequency was set to the relevant value for the experiment, and amplitude set to the right value for that tube number. The pump was then turned on at the same time as starting a stop watch and water was allowed to flow into the Eppendorf tube. When the water meniscus reached to the 1 mL mark by eye, the pump is turned off and the stop watch paused. The tube sealed and the tube weighed and time taken to fill noted. This process is repeated for all tubes. Pre-weighed value (in g) is taken away from end weight value to yield the weight of water in the tube. The resultant weight (in grams) was divided by density of water (1 g mL^{-1}) to give a volume of water in (mL). This volume was then converted to microliters and divided by the time taken

for tube to reach ~ 1 mL in minutes. The final value was reported as a flow rate in microliters per minute for a given frequency and amplitude.

Frequency 100 Hz

Table 6.1*. values for calibration of pump at 100 Hz frequency.*

Tube	Amp Vdd	Flow µl/min	Volume µl	time s	time min
1	30	97.96026	926.1	567.23	9.453833
2	60	222.2674	964.9	260.47	4.341167
4	90	374.5152	975.3	156.25	2.604167
5	120	521.2667	973.9	112.1	1.868333
6	150	656.7442	917.8	83.85	1.3975
7	180	843.3778	863.9	61.46	1.024333
8	210	1012.841	854.5	50.62	0.843667
9	240	1232.356	917.9	44.69	0.744833

Table 6.2*. values for calibration of pump at 50 Hz frequency.*

Tube	Amp Vdd	Flow µl/min	Volume µl	time s	time min
1	25	67.46686	1076.4	957.27	15.9545
2	50	162.2279	973.8	360.16	6.002667
3	75	273.4438	945.4	207.443	3.457383
4	100	391.609	1000.3	153.26	2.554333
5	125	483.9858	910.7	112.9	1.881667
6	150	632.4762	1053.6	99.95	1.665833
7	175	736.4839	974	79.35	1.3225
8	200	876.8852	891.5	61	1.016667
9	225	995.1749	962.5	58.03	0.967167
10	250	1110.376	989.9	53.49	0.8915

Flow rates were plotted against amplitude for a given frequency in ‘Origin 2016’ graphical software. For each plot the values are assigned a linear line of best fit.

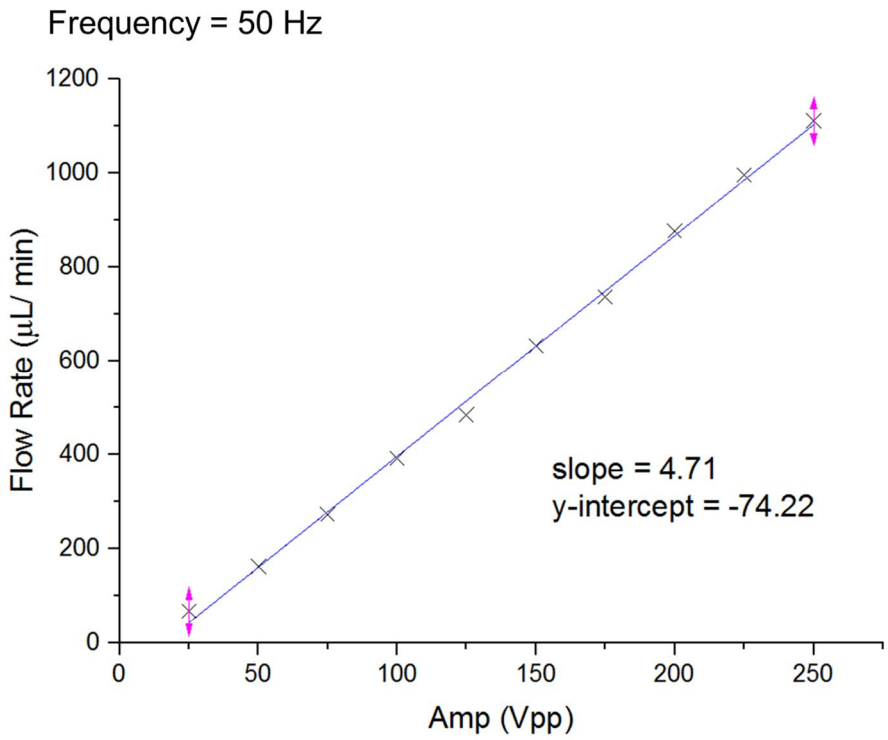

Figure 6.2. Graphical plot of flow rate (µL/ min) against amplitude (Vpp) for frequency 50 Hz.

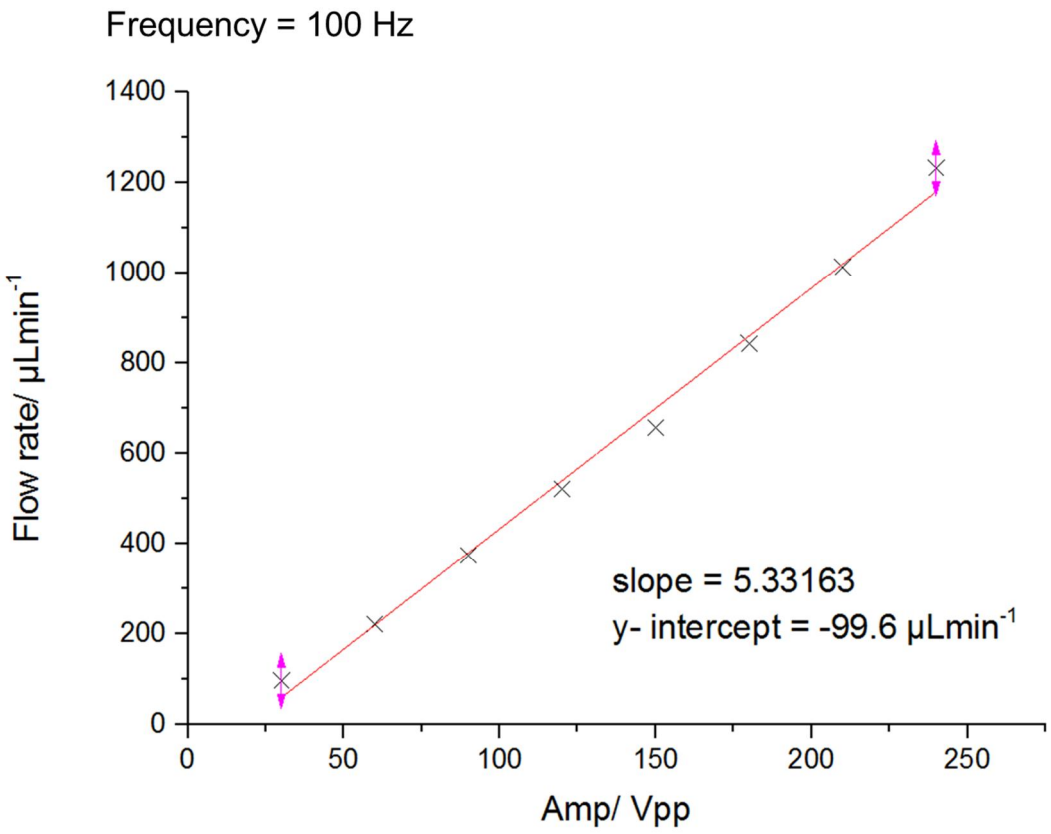

Figure 6.3. graphical plot of flow rate (µL/ min) against amplitude (Vpp) for frequency 50 Hz.

Using the equation for a linear line of best fit (y = mx + c), for a given flow rate, the amplitude could be calculated (See section 2.7.2.1.).

6.3.4 Standard Operating Procedure for biofilm cultivation

1.1. Preparation of stock cultures

- 1L BHI broth was autoclaved and allowed to cool to room temperature.
- Glycerol stocks were streaked out onto a primary culture plate of Horse-blood agar (ordered premade from Thermo-Fischer Scientific UK, LOT 12972568)
- The growth of bacteria was checked on the primary plate culture for purity, based on colony morphology.
- If there was no suggestion of contamination on the primary culture plate, three separate colonies of test bacteria were touched using a flame sterilized or sterile disposable loop and used to inoculate 100 mL of BHI broth. This culture was incubated at 37 ºC in air, overnight;

at the same time the culture was used to inoculate an LB-Agar plate to check sterility of broth culture.

- Bacterial broth was then used to make 100 x 1mL aliquots, flash froze and stored in a -80 ºC freezer for future cultures.

1.2 Leak Check & Sterilisation

- All apparatus that can be autoclaved was wrapped loosely in aluminium foil (to prevent contamination during transfer to category 2 safety cabinet), and autoclaved (see below). Parts which are not were soaked in 70% ethanol.

	Sterilisation technique		
Component	Rinse with 70% EtOH (aq)	UV Light (30 mins)	Autoclave
Microfludic chip	✓	✗	✓
Piezo pump	✓	✗	✓
one-way stop cocks	✓	✓	✗
Three-way splitter	✓	✓	✗
Male/Female luer lock adapters	✓	✗	✓
Needle-free luer check valve	✓	✓	✗
Tygon tubing	✓	✗	✓

- All apparatus was then transported to a category 2 safety cabinet, removed from foil and irradiated with UV light for 30 minutes.
- Within the safety cabinet, the whole system was assembled. Stopcocks were all opened and 70% ethanol was flushed throughout the whole system. This was either be done by drawing liquid through with a syringe or by loading 70% ethanol into reservoirs and using piezo pumps to push liquid through. The same was then done with air, pulled through a 0.2 µm filter, to dry the system.
- The system was then primed using sterilised BHI broth. For priming reagent loop see below. System was primed by attaching syringes to luer lock adapters and drawing/ pushing liquid through the system.
- Stopcocks connecting to inoculum and both reagent in ports were closed, stopcocks connecting media to chip and chip to waste were

opened. Three way stopcock positioned so only media inlet is feeding onto the microfluidic chip. Reagent loops were connected post biofilm cultivation.

- Make sure media reservoir was filled with autoclaved BHI broth.
- System was transported to safety cabinet and checked for leaks. Media in the waste reservoir was used to inoculate a horse-blood agar (Thermo Fisher Scientific) and Sabouraud dextrose 4% agar plate (VWR Chemicals, LOT 1292) using a sterile plastic loop. Lid of waste reservoir was removed carefully during this step and immediately placed back on after inoculation.

1.3. Fibrinogen coating of chip[1].

- 10 mg mL^{-1} of human fibrinogen (Sigma-Aldrich) in PBS was made up to a volume of 2 mL. The solution was then filter-sterilised with a 0.22 µm syringe filter, in a Category 2 safety cabinet.
- All stop cocks were closed, excluding the ones attached to the inoculum in and waste out ports. In a fresh sterile syringe, the fibrinogen solution was introduced into the microfluidic chamber by the inoculum in port.
- All stop cocks were closed and the system in placed in the incubator, without heat, overnight in air.

1.4 Sterility check of the system

- System was transported to safety cabinet and checked for leaks. Media in the waste reservoir was used to inoculate a horse-blood agar and sabouraud agar plate using a sterile plastic loop, incubated at 37 ºC in air, statically, overnight. The lid of the waste reservoir was removed carefully during this step and immediately placed back on after inoculation.

1.5 Inoculation of system

[1] Fibrinogen coating step only applicable for experiments proceeding section 3.2.5 of this body of work.

- 5 mL of overnight *S. aureus* cell culture was drawn into a 5 mL syringe. The syringe was then connected to the system upstream of stopcock 1 by female Luer fitting.
- The one way stopcock was turned to isolate the media reservoir from the chip.
- Stopcock connecting inoculum syringe to the chip was opened. Syringe plunger carefully pushed down to allow bacteria to flow through the flow cell into waste reservoir. Once bacteria had been added the SYRINGE WAS NOT REMOVED AT ANY POINT!
- System was transferred to incubator and left to incubate statically at 37 ºC for 1 hour.

Begin the flow system

- The three way stopcock was turned so that media can flow through to chip but the reagent loops are isolated. The one way stopcocks were closed between inoculum syringe and the chip. The piezo pump was set to the desired flow rate and media was allowed to flow through chip - out to waste. Biofilms were cultivated for the desired amount of time.

Staining of Biofilm & Reagent Loop Priming.

- Make 1× solution of desired LIVE/DEAD stain (Viability/ Cytotoxicity Assay kit, Biotium, LOT 30027) .
- Reagent loop can be primed with buffer using the conformation shown in figure 6a. Conformation of stopcocks in the Figure 6.4b can be used to eliminate introduction of bubbles in reagent inlet and outlet. Loop is primed with LIVE/DEAD stain using conformation shown in Figure 6.4c.
- Once loop is primed with LIVE/DEAD stain, introduce stain by using conformation in Figure 6.4d, which will flow the reagent into the system using a piezo pump 2 set at desired flow rate. The three way stopcock on the system is turned to isolate media inlet from the chip but allow flow of stain into system.
- Once stain protocol has been performed stop piezo pump 2.

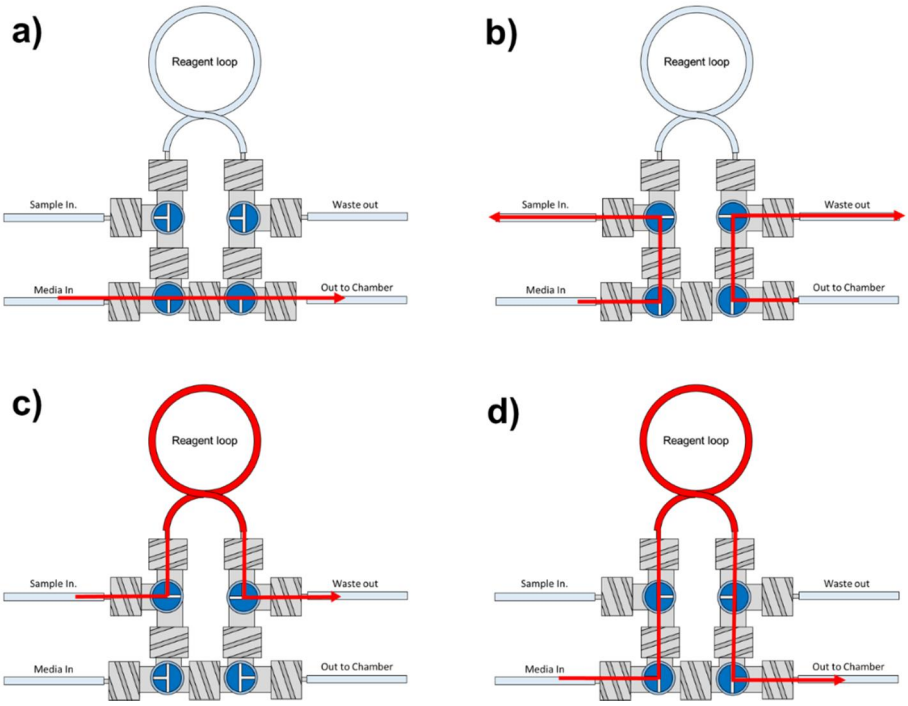

Figure 6.4. Conformational arrangement of reagent loop 3 way stopcocks for flow isolation to certain channels.
a) Conformation for 'media in' to microfluidic 'chamber' omitting the reagent loop. b) Conformation for media in to 'sample in', and 'waste out' to chamber out omitting the reagent loop. c) Conformation for 'sample in' to 'waste out' via reagent loop. d) Conformation for 'media in' to 'chamber out' via reagent loop.

<u>Confocal Imaging</u>

- Transport to imaging facility in sealed box.
- Place box down in confocal microscope room, open box and remove whole system. Place chip mount on confocal microscope along with system in the 3-D printed brackets and follow imaging instructions accompanying the instrument.
- Once finished carefully return system to the sealed box and transport back to the incubator

<u>Introducing reagents</u>

- Reagent loops can be introduced using Luer fitting at one way stopcocks connecting to tubing at reagent in ports on the chip. When attaching tubing make sure no air is introduced into the system.

- When flowing reagent into a chamber, make sure the necessary stopcocks are closed in order to isolate the flow to the desired chamber.

Cleaning

- All parts that can be are autoclaved.
- All tubing is thrown into hazardous waste bins, along with chip.
- Duran bottles are sterilised overnight in Virkon before autoclaving.
- Stopcocks are soaked overnight in 70% ethanol.

6.3.5 Microspray microbubble manufacture.

Microbubbles were produced using a multiplexed microfluidic microspray device, performed by Jordan Tinkler (University of Leeds).[198] The lipid solution was introduced at a flow rate of 80 µL min^{-1} and combined perfluorobutane gas stream using a pressure of 1100 mbar. Following production, samples were removed and diluted 5× in phosphate buffer for optical microscopy (Eclipse E600, Nikon, Japan) performed using a 50 µm deep observation chamber. Matlab was used to analyse the MB samples and obtain sizing and concentration data.

6.3.6 MB-Affimer Attachment and Washing.

AlexaFluor647 tagged ClfA1 and AAC Affimer protein were added to separate MB samples, mixed gently, and incubated in a fridge at 4°C for 30 minutes to allow binding. The volume of 7.5 µM Affimer protein required for each sample was calculated based on the number of MBs in each sample and the maximum packing efficiency of the Affimer. A two-step centrifugation wash process, applying a RCF of 300g for 10 minutes, to separate buoyant MBs and unbound Affimer contained in solution. Preliminary work showed this method to significantly reduce the background fluorescence level whilst preserving the MB population for use, as unbound Affimer could be decanted away. MBs were diluted to a concentration of 1×10^8 MBs mL^{-1} for on-chip use.

6.3.7 Confocal Imaging

Confocal images were acquired on a Leica DMi8 inverted confocal microscope. The biofilm images were obtained using a 10× dry objective and a 100× oil immersion objective (HC PL APO CS2 FWD 0.13 mm NA 1.4). Due to the spectral overlap between EthDIII and Alexafluor647, biofilms in subsequent experiments that used Alexafluor647-tagged molecules were only stained with the LIVE DMAO dye. DMAO identifies both living and dead cell components, so allowed for imaging of the biofilm's biomass, and does not give any indication as the viability of cells imaged. Confocal z-stacks were exported at .JPEG files and analysed in ImageJ (FIJI) software. 3-D z-stack rendering was performed in LasX (Leica) software on the console that controlled the confocal microscope.

6.3.8 Biofilm- reagent interaction under flow.

6.3.8.1 Biofilm-bead interaction

Once a biofilm has been cultivated using methods outlined in 6.3.4, it was stained and mounted on the confocal microscope for imaging. The piezo pump control box was connected to the reagent in pump and reagent was introduced at ~ 250 µL min^{-1} via the reagent loop. In static pulse experiments, the bright field optical lens on the microscope was used to observe the chamber until the pulse of beads was seen filling the chamber. At this point the piezo pump was stopped, stop-cocks up and downstream of the chamber were closed, and the chip left mounted on the confocal for 10 minutes. After this time, the stop cocks were opened and flow was resumed for a further 30 minutes at ~ 250 µL min^{-1}. Z-stack images were then acquired of 15 random positions across the chamber, acquired at a height of 30 µm.

In constant flow experiments there was no pause between introduction of the beads into the chamber and the 30 minutes buffer wash. The 30 minute buffer wash was presumed to start once no stream of bead was observed moving through the chamber.

6.3.8.2 Biofilm-MB interaction

Protocol identical to section 6.3.8.1 up until reagent introduction. At the time of MB introduction, the system was removed from the confocal mount,

inverted so that all tubing between the reagent loop and the microfluidic chip was orientated vertically. This meant the buoyant MB could move with the prevailing buoyant force towards the microfluidic device. Once the MB had reached the chamber, the system was held vertically with the microfluidic chip inverted for 10 minutes. After this time the chip was returned to the confocal microscope mount and washed for 30 minutes with buffer at ~ 250 µL min^{-1}. Z-stacks from 15 random points were acquired as above for concentration analysis.

7 Appendices

7.1 Mannose binding lectin structural information.

Amino acid Sequence:

```
        10         20         30         40         50         60
GDSSLAASER KALQTEMARI KKWLTFSLGK QVGNKFFLTN GEIMTFEKVK ALCVKFQASV
        70         80         90        100        110        120
ATPRNAAENG AIQNLIKEEA FLGITDEKTE GQFVDLTGNR LTYTNWNEGE PNNAGSDEDC
       130        140
VLLLKNGQWN DVPCSTSHLA VCEFPI
```

Number of amino acids: 146

Molecular weight: 16076.15

Theoretical pI: 5.06

Formula: $C_{708}H_{1114}N_{192}O_{223}S_6$

Total number of atoms: 2243

Ext. coefficient 18240

7.2 MBP-MBL structural information

Amino acid Sequence:

```
        10         20         30         40         50         60
KIEEGKLVIW INGDKGYNGL AEVGKKFEKD TGIKVTVEHP DKLEEKFPQV AATGDGPDII
        70         80         90        100        110        120
FWAHDRFGGY AQSGLLAEIT PDKAFQDKLY PFTWDAVRYN GKLIAYPIAV EALSLIYNKD
       130        140        150        160        170        180
LLPNPPKTWE EIPALDKELK AKGKSALMFN LQEPYFTWPL IAADGGYAFK YENGKYDIKD
       190        200        210        220        230        240
VGVDNAGAKA GLTFLVDLIK NKHMNADTDY SIAEAAFNKG ETAMTINGPW AWSNIDTSKV
       250        260        270        280        290        300
NYGVTVLPTF KGQPSKPFVG VLSAGINAAS PNKELAKEFL ENYLLTDEGL EAVNKDKPLG
       310        320        330        340        350        360
AVALKSYEEE LVKDPRIAAT MENAQKGEIM PNIPQMSAFW YAVRTAVINA ASGRQTVDEA
       370        380        390        400        410        420
LKDAQTNSSS SSNNHHHHHH NNENLYFQGD SSLAASERKA LQTEMARIKK WLTFSLGKQV
       430        440        450        460        470        480
GNKFFLTNGE IMTFEKVKAL CVKFQASVAT PRNAAENGAI QNLIKEEAFL GITDEKTEGQ
       490        500        510        520        530
FVDLTGNRLT YTNWNEGEPN NAGSDEDCVL LLKNGQWNDV PCSTSHLAVC EFPI
```

Number of amino acids: 534

Molecular weight: 58918.50

Theoretical pI: 5.30

Formula: $C_{2650}H_{4088}N_{694}O_{804}S_{12}$

Total number of atoms: 8248

Ext. coefficient 86080

7.3 Affimer proteins structural information

Amino acid sequence:

```
        10         20         30         40         50         60
ASGNENSLEI EELARFAVDE HNKKENALLE FVRVVKAKEQ XXXXXXXXXT MYYLTLEAKD
        70         80         90        100
GGKKKLYEAK VWVKXXXXXX XXXNFKELQE FKPVGDACAA AHHHHHHHH
```

XXXXXXXXX = Variable loop 1

XXXXXXXXX = Variable Loop 2

Affimer	Amino acid sequence for Variable loop 1	Amino Acid sequence at Variable loop 2	Molecular weight (Da)	Extinction coefficient, ε (M^{-1} cm^{-1})
ClfA1	MLTTQVNTR	FPSTPLFLY	12630.97	11460
AAC	AAAA	AA	10774.20	9970
SH6	TQMLSPSQH	WIKFWPEYG	12436.14	22460
USA50	PNFKSRWGP	NEPWQTNYS	12408.97	22460
SH30	YSYGMIKES	APSVWPFLA	12246.96	18450
USA49	GATNGRQHH	YDDIWFQSY	12395.89	18450
SH31	LEMLMPSSH	LTKFFNTFS	12331.10	9970
ClfA27	VYWQDVVER	DHFVYLRLI	12851.57	18450
ClfA16	GATNGRQHH	YDDIWFQSY	12696.16	9970
UAMS11	PQDSSEYHT	RFGYPYDGH	12356.81	14440
UAMS1A	NPETKEHHV	GYWFQAHRM	12468.10	16960

7.4 MBP-ClfA

Amino acid sequence:

```
        10         20         30         40         50         60
MKIEEGKLVI WINGDKGYNG LAEVGKKFEK DTGIKVTVEH PDKLEEKFPQ VAATGDGPDI

        70         80         90        100        110        120
IFWAHDRFGG YAQSGLLAEI TPDKAFQDKL YPFTWDAVRY NGKLIAYPIA VEALSLIYNK

       130        140        150        160        170        180
DLLPNPPKTW EEIPALDKEL KAKGKSALMF NLQEPYFTWP LIAADGGYAF KYENGKYDIK

       190        200        210        220        230        240
DVGVDNAGAK AGLTFLVDLI KNKHMNADTD YSIAEAAFNK GETAMTINGP WAWSNIDTSK

       250        260        270        280        290        300
VNYGVTVLPT FKGQPSKPFV GVLSAGINAA SPNKELAKEF LENYLLTDEG LEAVNKDKPL

       310        320        330        340        350        360
GAVALKSYEE ELVKDPRIAA TMENAQKGEI MPNIPQMSAF WYAVRTAVIN AASGRQTVDE

       370        380        390        400        410        420
ALKDAQTNSS SENLYFQSVH HHHHHGTDIT NQLTNVTVGI DSGTTVYPHQ AGYVKLNYGF

       430        440        450        460        470        480
SVPNSAVKGD TFKITVPKEL NLNGVTSTAK VPPIMAGDQV LANGVIDSDG NVIYTFTDYV

       490        500        510        520        530        540
NTKDDVKATL TMPAYIDPEN VKKTGNVTLA TGIGSTTANK TVLVDYEKYG KFYNLSIKGT

       550        560        570        580        590        600
IDQIDKTNNT YRQTIYVNPS GDNVIAPVLT GNLKPNTDSN ALIDQQNTSI KVYKVDNAAD

       610        620        630        640        650        660
LSESYFVNPE NFEDVTNSVN ITFPNPNQYK VEFNTPDDQI TTPYIVVVNG HIDPNSKGDL

       670        680        690        700        710
ALRSTLYGYN SNIIWRSMSW DNEVAFNNGS GSGDGIDKPV VPEQPDEPGE IEPIPE
```

Number of amino acids: 716

Molecular weight: 78498.98

Theoretical pI: 4.88

Formula: C3527H5437N907O1102S10

Total number of atoms: 10983

Ext. coefficient: 104170

7.5 ClfA structural information

Amino acid sequence:

```
        10         20         30         40         50         60
SVHHHHHHGT DITNQLTNVT VGIDSGTTVY PHQAGYVKLN YGFSVPNSAV KGDTFKITVP

        70         80         90        100        110        120
KELNLNGVTS TAKVPPIMAG DQVLANGVID SDGNVIYTFT DYVNTKDDVK ATLTMPAYID

       130        140        150        160        170        180
PENVKKTGNV TLATGIGSTT ANKTVLVDYE KYGKFYNLSI KGTIDQIDKT NNTYRQTIYV

       190        200        210        220        230        240
NPSGDNVIAP VLTGNLKPNT DSNALIDQQN TSIKVYKVDN AADLSESYFV NPENFEDVTN

       250        260        270        280        290        300
SVNITFPNPN QYKVEFNTPD DQITTPYIVV VNGHIDPNSK GDLALRSTLY GYNSNIIWRS

       310        320        330
MSWDNEVAFN NGSGSGDGID KPVVPEQPDE PGEIEPIPE
```

Number of amino acids: 339

Molecular weight: 36978.86

Theoretical pI: 4.72

Formula: $C_{1638}H_{2530}N_{432}O_{538}S_3$

Total number of atoms: 5141

Ext. coefficient 36330

7.6 Plasmids

Plasmid	Protein	Cell lines used	Origin
pET11a	Affimer Proteins	BL21 (DE3) GOLD XL10	Fayez Alsulaimani, University of Leeds
pINIIIompA2	hMBL MBL G1S	BL21 GOLD XL10	Kurt Drickamer, Imperial College London
pMAL-p5x	MBP-MBL (labelled: '*MBP-His-TEV-hMBL_PMAl-p5x'*)	BL21 GOLD XL10	GenScript®
pMAL-c5x	MBP-ClfA (labelled: '*ClfA_pMAL-c5x'*)	BL21 GOLD	GenScript®
pET28a	TEV protease	BL21 GOLD	Gemma Wildsmith, University of Leeds

7.7 Affimer-Biofilm Binding Assay single strain data.

ABBA results for individual Affimer proteins against SH1000, USA300 and UAMS1 S. aureus biofilms. All show correlation between relative fluorescent emission and Affimer concentration.

7.7.1 ClfA1

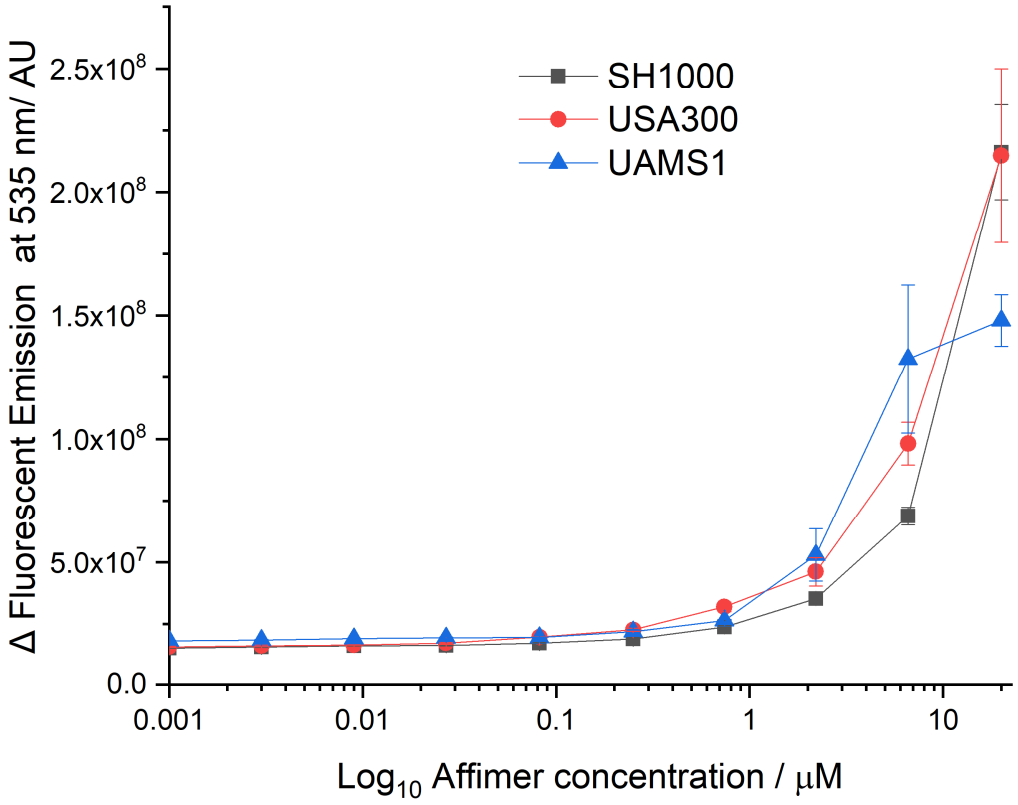

7.7.2 SH6

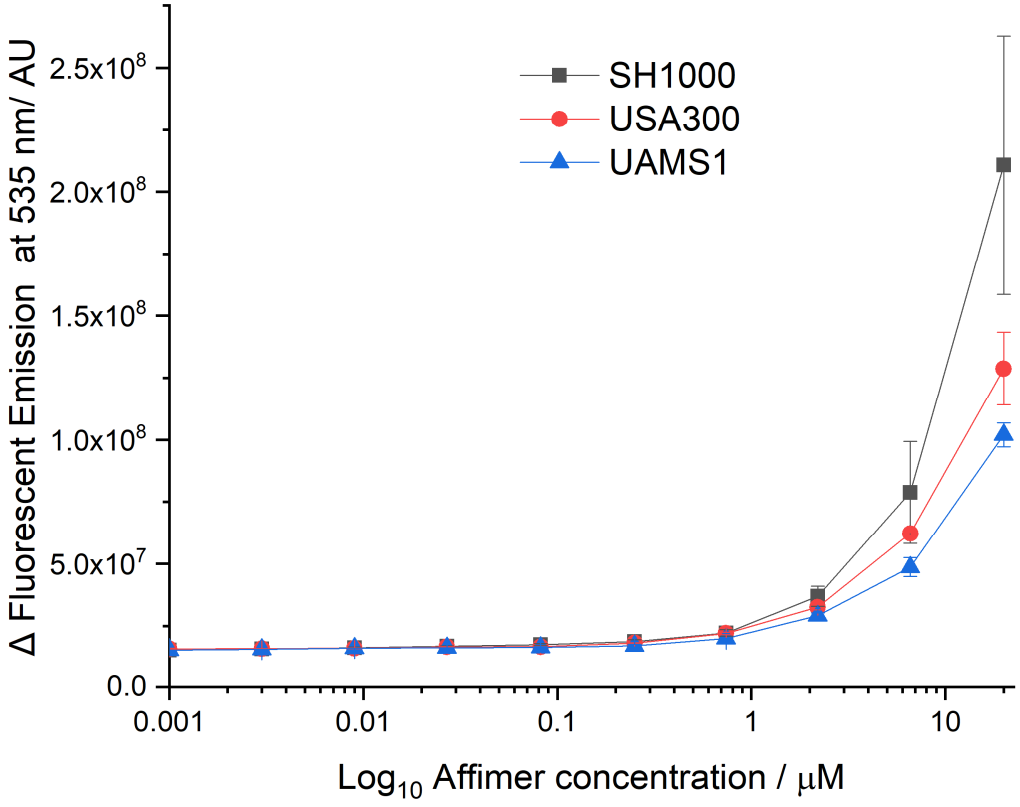
SH1000
USA300
UAMS1
Δ Fluorescent Emission at 535 nm/ AU
2.5x10^8
2.0x10^8
1.5x10^8
1.0x10^8
5.0x10^7
0.0
0.001
0.01
0.1
1
10
Log10 Affimer concentration / μM

7.7.3 USA50

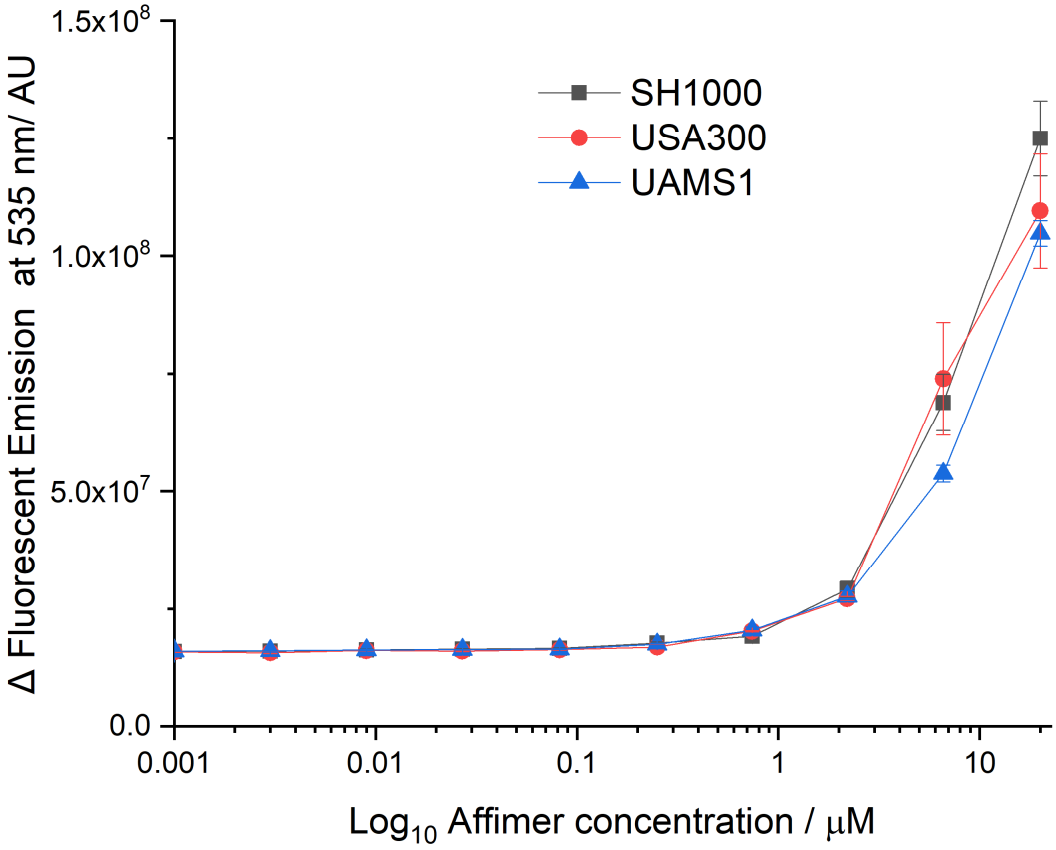

7.7.4 SH30

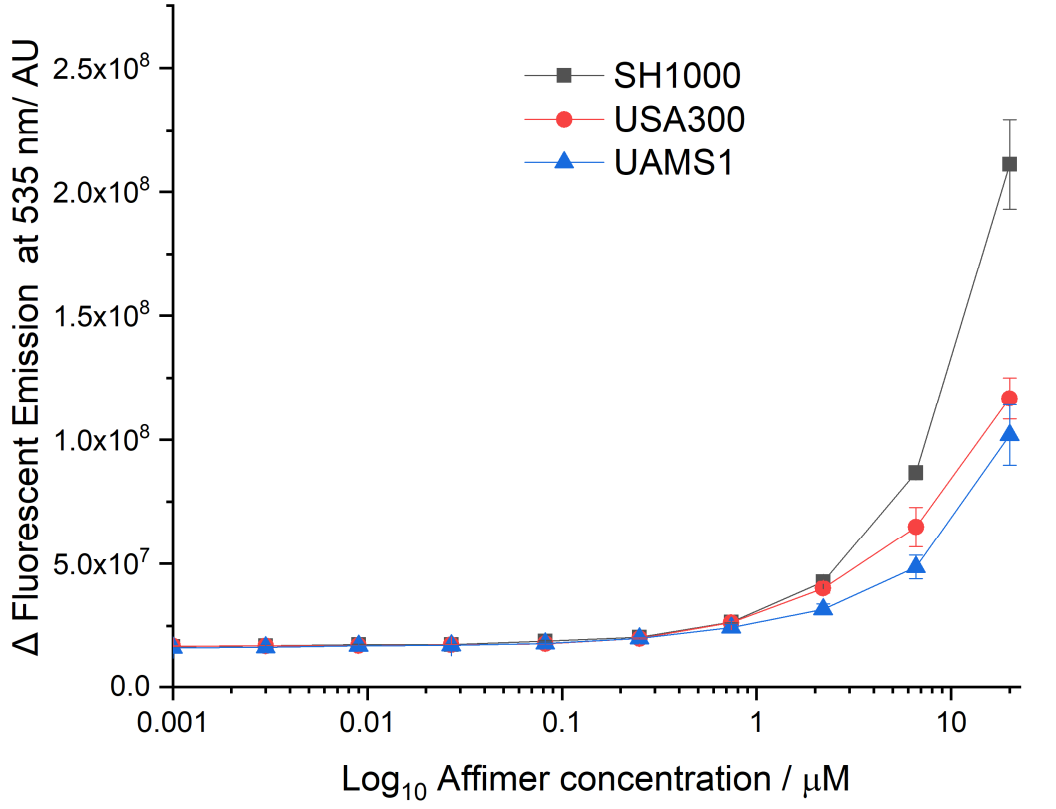

7.7.5 USA49

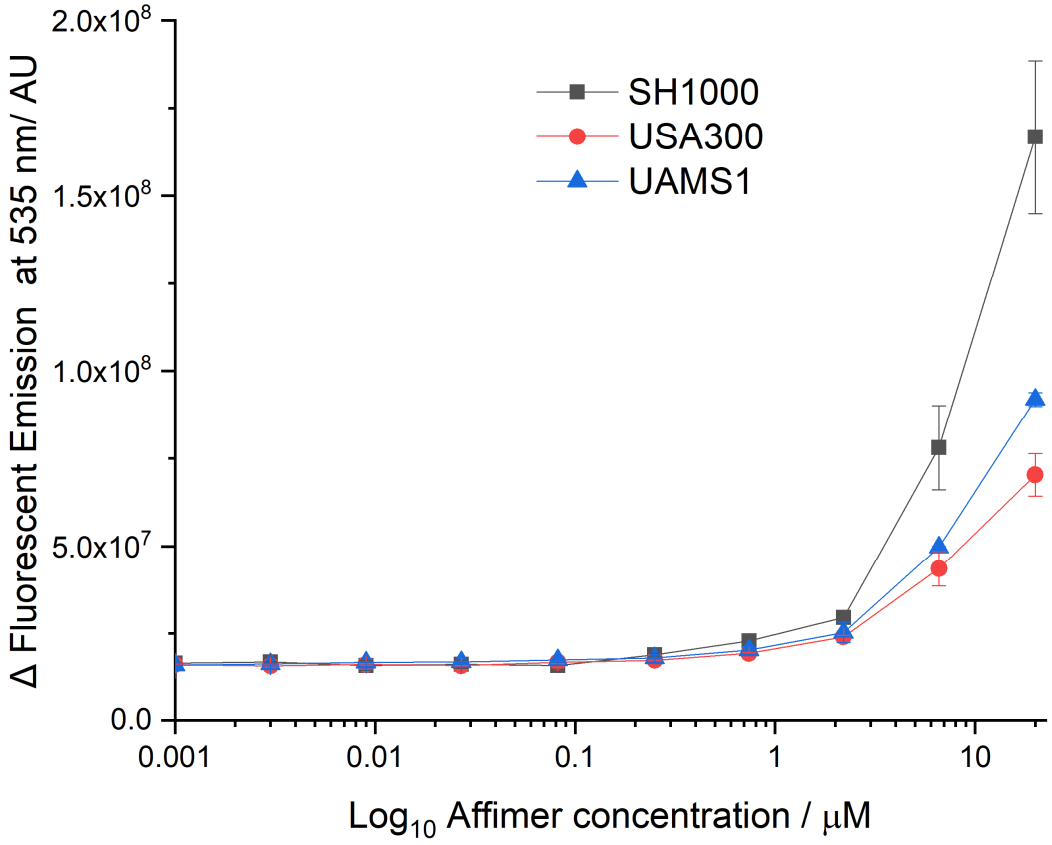

7.7.6 SH31

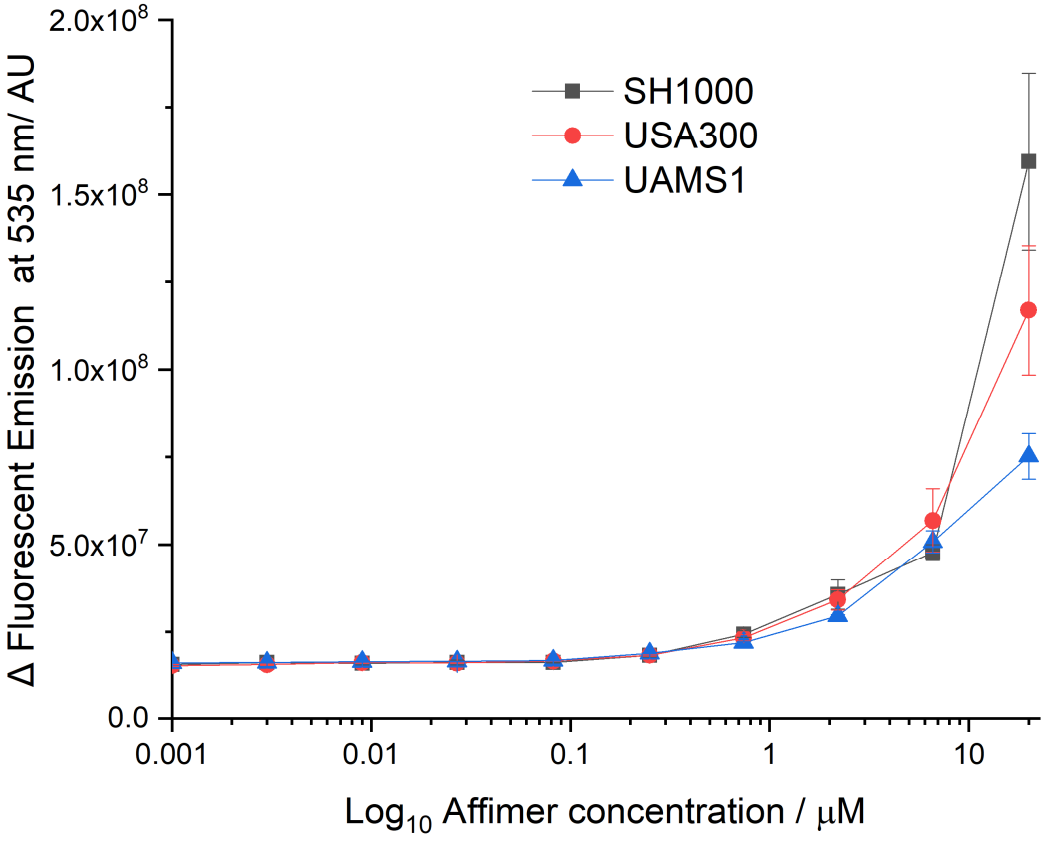

7.7.7 ClfA27

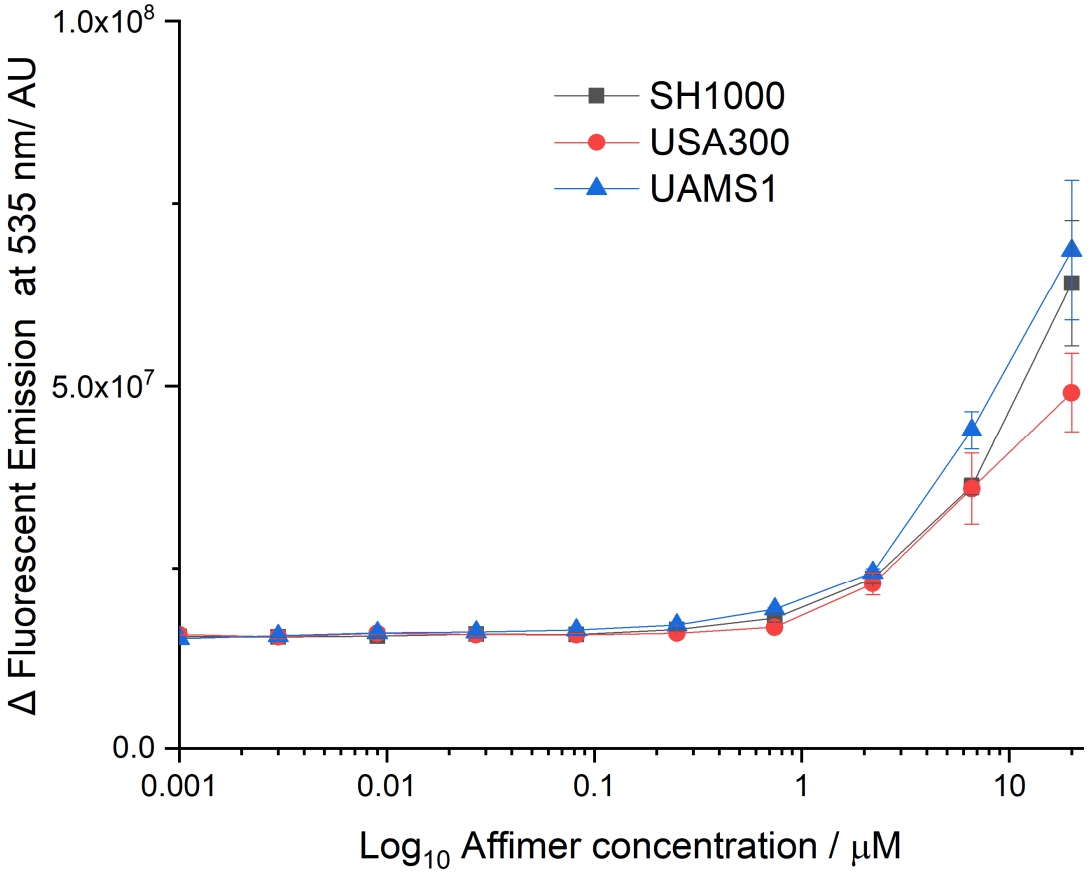

7.7.8 ClfA16

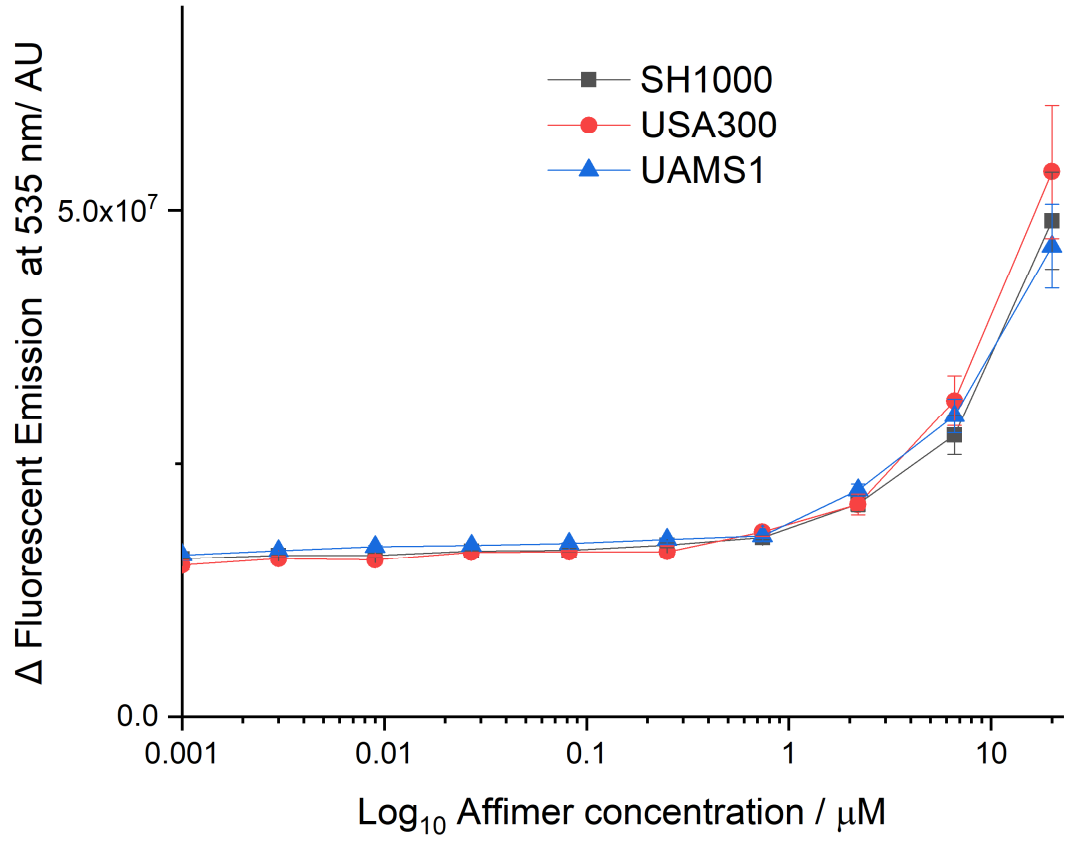

7.7.9 UAMS11

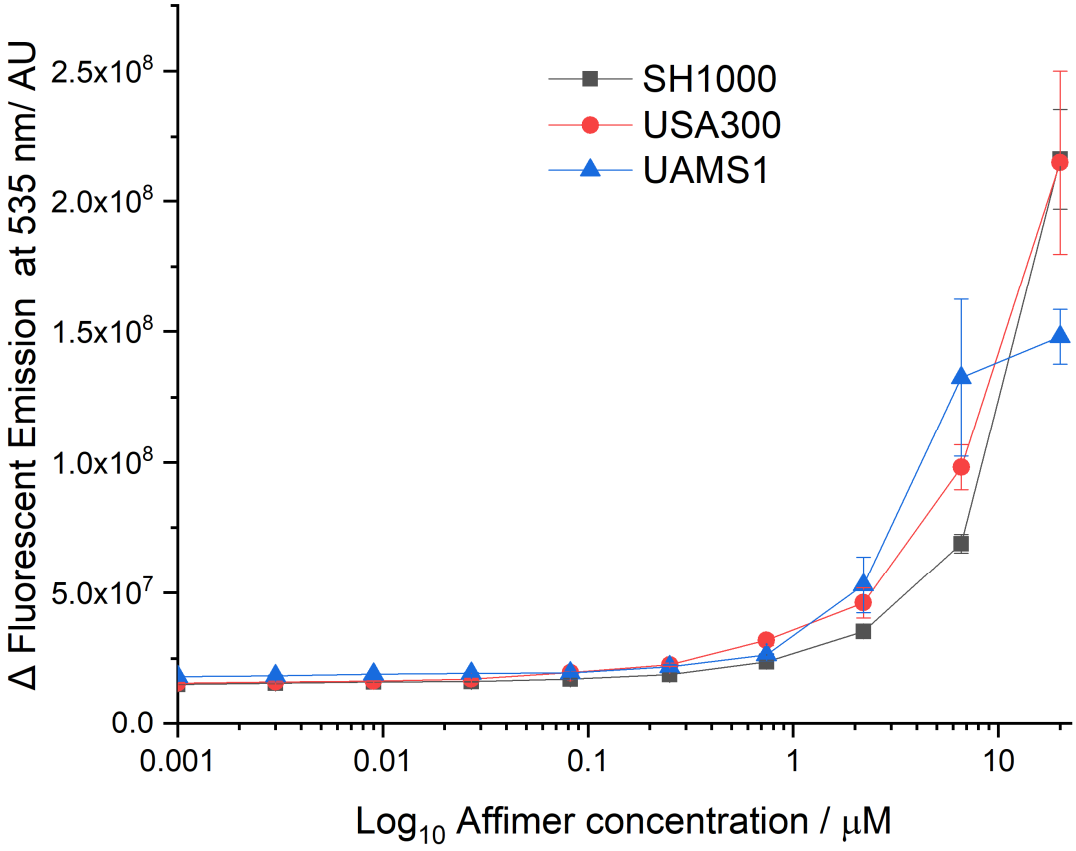

7.7.10 UAMS1A

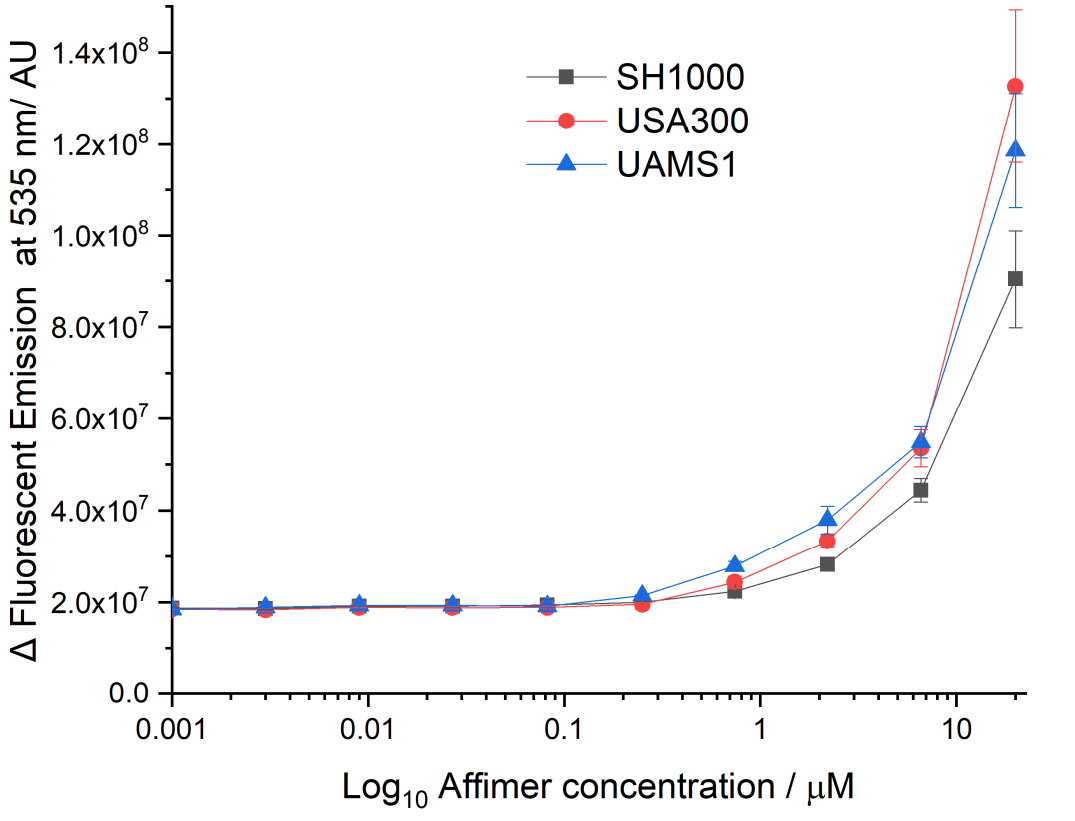

7.8 Extension of ClfA1 ABBA binding curve.

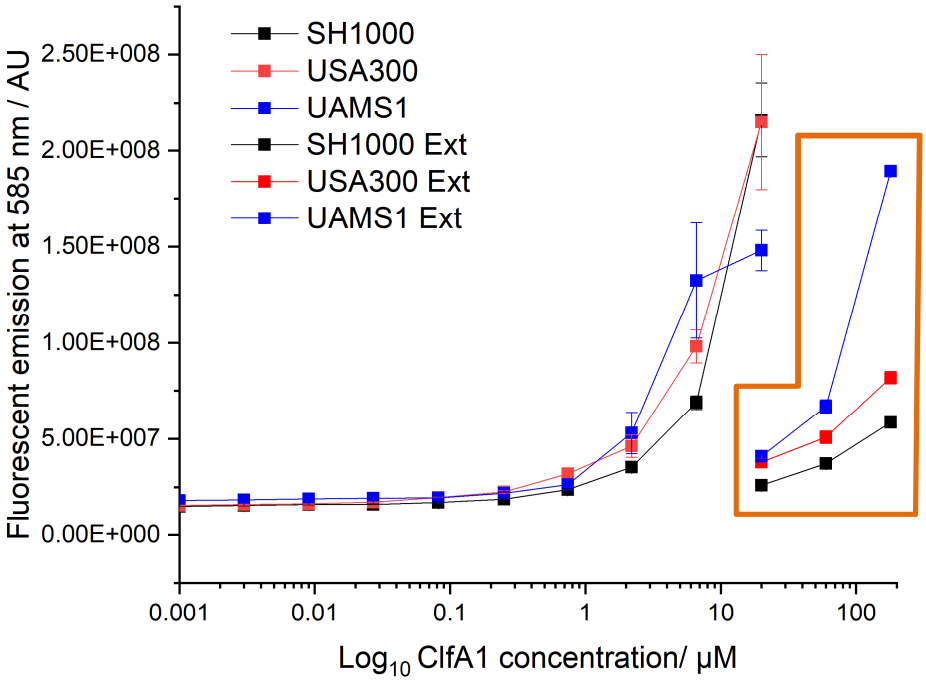

Plot of fluorescent emission of ClfA1-fluorescein at a given concentration screened against SH1000, USA300 and UAMS1 strains of biofilm individually. Biofilms were cultivated then washed with phosphate buffer, 50 µL of Affimer-fluorescein was added at various concentrations and incubated at RT for 1 hour. After this the wells were washed again with phosphate buffer and the fluorescent emission of fluorescein at 535 nm measured using an Envision plate reader. Fluorescent emission at 535 nm is associated with the presence of ClfA1-fluorescein and is attributed to the binding of the protein to the S. aureus biofilm and their associated SEM values shown as error bars. The data points in the orange box correspond to a separate experiment in which the concentrations were increased. Affimer was screened against three strains of biofilm; SH1000, USA300 and UAMS1.

7.9 Alexafluor647 labelling of ClfA1 and AAC

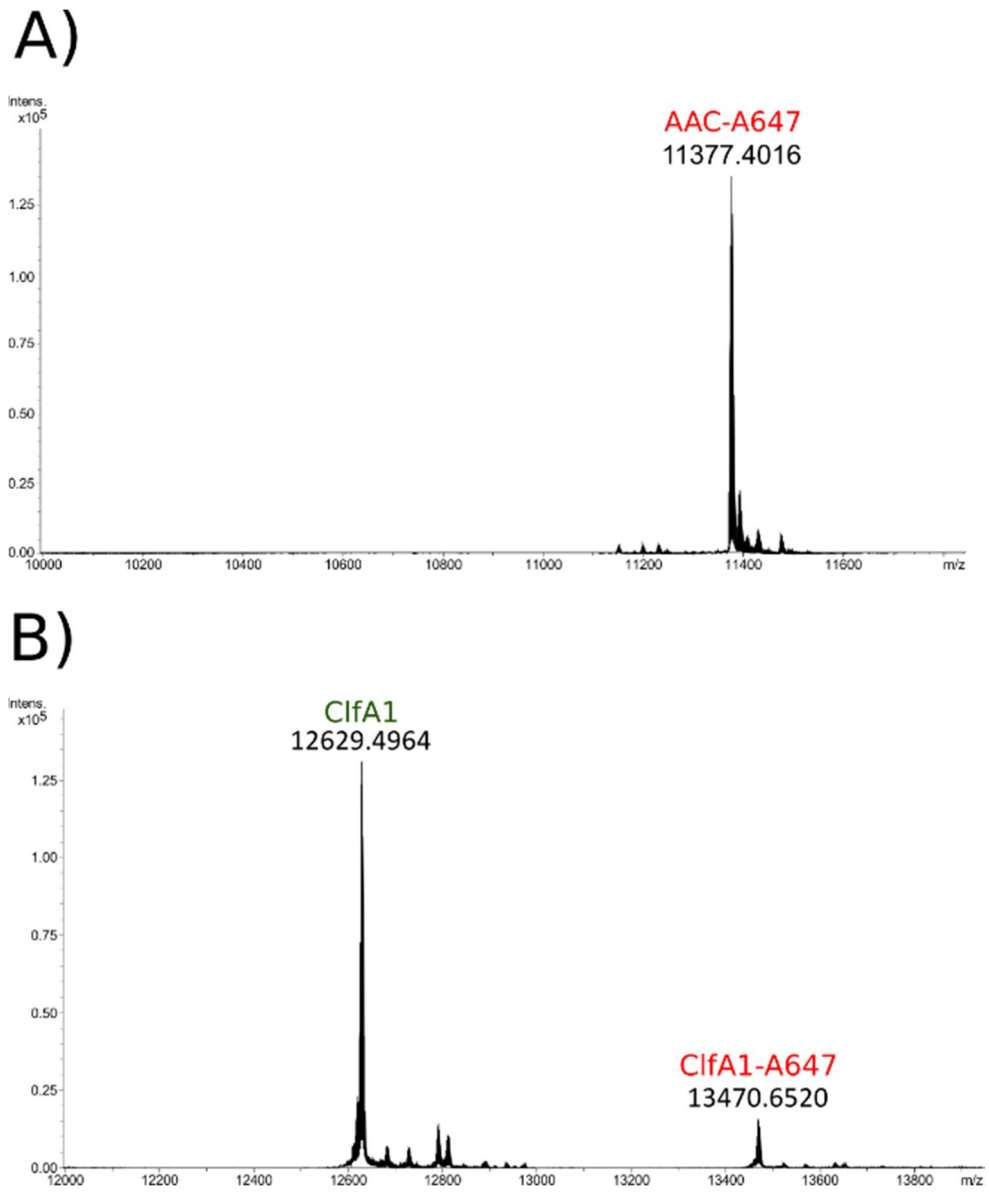

ESMS mass spectra of AAC and ClfA1 labelling reactions used for experiments in chapter 4. A) shows the AAC Alexafluor647 NHA ester reaction after overnight incubation at 4 ºC. B) shows the ClfA1 Alexafluor647 NHS ester reaction after overnight incubation at 4 ºC.

8 Bibliography

1. M. Otto, Staphylococcus epidermidis — the 'accidental' pathogen, *Nature Reviews Microbiology*, 2009, **7**, 555-567.
2. R. O. Darouiche, Treatment of Infections Associated with Surgical Implants, *New England Journal of Medicine*, 2004, **350**, 1422-1429.
3. U. Römling and C. Balsalobre, Biofilm infections, their resilience to therapy and innovative treatment strategies, *Journal of Internal Medicine*, 2012, **272**, 541-561.
4. H.-C. Flemming and J. Wingender, The biofilm matrix, *Nature Reviews Microbiology*, 2010, **8**, 623.
5. R. M. Donlan, J. W. Costerton, R. M. Donlan and J. W. Costerton, Biofilms : Survival Mechanisms of Clinically Relevant Microorganisms, *Clinical Microbiology*, 2002, **15**, 167-193.
6. S. T. Aka and S. H. Haji, Sub-MIC of antibiotics induced biofilm formation of Pseudomonas aeruginosa in the presence of chlorhexidine, *Braz J Microbiol*, 2015, **46**, 149-154.
7. D. E. Moormeier and K. W. Bayles, Staphylococcus aureus biofilm: a complex developmental organism, *Molecular Microbiology*, 2017, **104**, 365-376.
8. L. Hall-Stoodley and P. Stoodley, Evolving concepts in biofilm infections, *Cellular Microbiology*, 2009, **11**, 1034-1043.
9. V. J. Ribas, J. C. López, A. Ruiz-Sanmartín, J. C. Ruiz-Rodríguez, J. Rello, A. Wojdel and A. Vellido, presented in part at the 2011 Annual International Conference of the IEEE Engineering in Medicine and Biology Society, 30 Aug.-3 Sept. 2011, 2011.
10. T. H. C. de Oliveira, A. T. Amorin, I. S. Rezende, M. Santos Barbosa, H. B. Martins, A. K. P. Brito, E. F. Andrade, G. K. N. Gonçalves, G. B. Campos, R. A. A. Silva, J. Timenetsky and L. M. Marques, Sepsis induced by Staphylococcus aureus: participation of biomarkers in a murine model, *Medical science monitor : international medical journal of experimental and clinical research*, 2015, **21**, 345-355.
11. J. Paulsen, A. Mehl, Å. Askim, E. Solligård, B. O. Åsvold and J. K. Damås, Epidemiology and outcome of Staphylococcus aureus bloodstream infection and sepsis in a Norwegian county 1996-2011: an observational study, *BMC infectious diseases*, 2015, **15**, 116-116.
12. A. E. Paharik and A. R. Horswill, The Staphylococcal Biofilm: Adhesins, regulation, and host response, 2016, **4**, 1-48.
13. M. R. Kiedrowski and A. R. Horswill, New approaches for treating staphylococcal biofilm infections, *Annals of the New York Academy of Sciences*, 2011, **1241**, 104-121.
14. D. E. Moormeier, J. L. Bose, A. R. Horswill and K. W. Bayles, Temporal and stochastic control of staphylococcus aureus biofilm development, *mBio*, 2014, **5**, 1-12.
15. P. S. Stewart, Mechanisms of antibiotic resistance in bacterial biofilms., *International journal of medical microbiology : IJMM*, 2002, **292**, 107-113.
16. P. Gilbert, T. Maira-Litran, A. J. McBain, A. H. Rickard and F. W. Whyte, in *Advances in Microbial Physiology*, Academic Press, 2002, vol. 46, pp. 203-256.

17. E. J. Wentland, P. S. Stewart, C.-T. Huang and G. A. McFeters, Spatial Variations in Growth Rate within Klebsiellapneumoniae Colonies and Biofilm, *Biotechnology Progress*, 1996, **12**, 316-321.
18. D. T. King, S. Sobhanifar and N. C. J. Strynadka, in *Handbook of Antimicrobial Resistance*, eds. A. Berghuis, G. Matlashewski, M. A. Wainberg and D. Sheppard, Springer New York, New York, NY, 2017, DOI: 10.1007/978-1-4939-0694-9_10, pp. 177-201.
19. B. R. Boles and A. R. Horswill, agr-mediated dispersal of Staphylococcus aureus biofilms, *PLoS Pathogens*, 2008, **4**.
20. B. R. Boles and A. R. Horswill, Staphylococcal biofilm disassembly, *Trends in Microbiology*, 2011, **19**, 449-455.
21. C. C. S. Deivanayagam, E. R. Wann, W. Chen, M. Carson, K. R. Rajashankar, M. Höök and S. V. L. Narayana, A novel variant of the immunoglobulin fold in surface adhesins of Staphylococcus aureus: crystal structure of the fibrinogen-binding MSCRAMM, clumping factor A, *The EMBO journal*, 2002, **21**, 6660-6672.
22. D. McDevitt, P. Francois, P. Vaudaux and T. J. Foster, Molecular characterization of the clumping factor (fibrinogen receptor) of Staphylococcus aureus, *Molecular Microbiology*, 1994, **11**, 237-248.
23. E. J. Walsh, H. Miajlovic, O. V. Gorkun and T. J. Foster, Identification of the Staphylococcus aureus MSCRAMM clumping factor B (ClfB) binding site in the alphaC-domain of human fibrinogen, *Microbiology (Reading, England)*, 2008, **154**, 550-558.
24. E. R. Wann, S. Gurusiddappa and M. Höök, The Fibronectin-binding MSCRAMM FnbpA ofStaphylococcus aureus Is a Bifunctional Protein That Also Binds to Fibrinogen, *Journal of Biological Chemistry*, 2000, **275**, 13863-13871.
25. T. J. Foster, J. A. Geoghegan, V. K. Ganesh and M. Höök, Adhesion, invasion and evasion: the many functions of the surface proteins of Staphylococcus aureus, *Nature Reviews Microbiology*, 2013, **12**, 49.
26. T. J. Foster, Immune evasion by staphylococci, *Nature Reviews Microbiology*, 2005, **3**, 948-958.
27. K. A. Lacey, J. A. Geoghegan and R. M. McLoughlin, The Role of Staphylococcus aureus Virulence Factors in Skin Infection and Their Potential as Vaccine Antigens, *Pathogens (Basel, Switzerland)*, 2016, **5**, 22.
28. A. P. A. Hendrickx, J. M. Budzik, S.-Y. Oh and O. Schneewind, Architects at the bacterial surface — sortases and the assembly of pili with isopeptide bonds, *Nature Reviews Microbiology*, 2011, **9**, 166.
29. S. K. Mazmanian, G. Liu, H. Ton-That and O. Schneewind, Staphylococcus aureus Sortase, an Enzyme that Anchors Surface Proteins to the Cell Wall, *Science*, 1999, **285**, 760.
30. H. Ton-That, G. Liu, S. K. Mazmanian, K. F. Faull and O. Schneewind, Purification and characterization of sortase, the transpeptidase that cleaves surface proteins of Staphylococcus aureus at the LPXTG motif, *Proceedings of the National Academy of Sciences*, 1999, **96**, 12424.
31. K. W. Clancy, J. A. Melvin and D. G. McCafferty, Sortase transpeptidases: Insights into mechanism, substrate specificity, and inhibition, *Peptide Science*, 2010, **94**, 385-396.

32. S. Wanner, J. Schade, D. Keinhörster, N. Weller, S. E. George, L. Kull, J. Bauer, T. Grau, V. Winstel, H. Stoy, D. Kretschmer, J. Kolata, C. Wolz, B. M. Bröker and C. Weidenmaier, Wall teichoic acids mediate increased virulence in Staphylococcus aureus, *Nature Microbiology*, 2017, **2**, 16257.
33. S. Brown, J. P. Santa Maria, Jr. and S. Walker, Wall teichoic acids of gram-positive bacteria, *Annual review of microbiology*, 2013, **67**, 313-336.
34. C. Weidenmaier and A. Peschel, Teichoic acids and related cell-wall glycopolymers in Gram-positive physiology and host interactions, *Nature Reviews Microbiology*, 2008, **6**, 276.
35. J. P. O'Gara, ica and beyond: biofilm mechanisms and regulation in Staphylococcus epidermidis and Staphylococcus aureus, *FEMS Microbiology Letters*, 2007, **270**, 179-188.
36. C. Vuong, J. M. Voyich, E. R. Fischer, K. R. Braughton, A. R. Whitney, F. R. DeLeo and M. Otto, Polysaccharide intercellular adhesin (PIA) protects Staphylococcus epidermidis against major components of the human innate immune system., *Cellular Microbiology*, 2004, **6**, 269-275.
37. P. Speziale, G. Pietrocola, T. J. Foster and J. A. Geoghegan, Protein-based biofilm matrices in Staphylococci, *Front Cell Infect.Microbiol.*, 2014, **4:171**, 1-10.
38. T. Chavakis, K. Wiechmann, K. T. Preissner and M. Herrmann, Staphylococcus aureus interactions with the endothelium The role of bacterial “Secretable Expanded Repertoire Adhesive Molecules“ (SERAM) in disturbing host defense systems, *Thrombosis and Haemostasis*, 2005, **94**, 278-285.
39. M. Kloczewiak, S. Timmons and J. Hawiger, Reactivity of Chemically Cross-Linked Fibrinogen and Its Fragments D Toward the Staphylococcal Clumping Receptor, *Biochemistry*, 1987, **26**, 6152.
40. B. Sinha, P. P. François, O. Nüße, M. Foti, O. M. Hartford, P. Vaudaux, T. J. Foster, D. P. Lew, M. Herrmann and K.-H. Krause, Fibronectin-binding protein acts as Staphylococcus aureus invasin via fibronectin bridging to integrin α5β1, *Cellular Microbiology*, 1999, **1**, 101-117.
41. R. P. Novick, S. J. Projan, J. Kornblum, H. F. Ross, G. Ji, B. Kreiswirth, F. Vandenesch, S. Moghazeh and R. P. Novick, Theagr P2 operon: An autocatalytic sensory transduction system inStaphylococcus aureus, *Molecular and General Genetics MGG*, 1995, **248**, 446-458.
42. B. Wang and T. W. Muir, Regulation of Virulence in Staphylococcus aureus: Molecular Mechanisms and Remaining Puzzles, *Cell chemical biology*, 2016, **23**, 214-224.
43. S. Schlafer and R. L. Meyer, Confocal microscopy imaging of the biofilm matrix, *Journal of Microbiological Methods*, 2015, DOI: 10.1016/j.mimet.2016.03.002.
44. T. R. Neu and J. R. Lawrence, Innovative techniques, sensors, and approaches for imaging biofilms at different scales, *Trends in Microbiology*, 2015, **23**, 233-242.
45. P. Stiefel, U. Rosenberg, J. Schneider, S. Mauerhofer, K. Maniura-Weber and Q. Ren, Is biofilm removal properly assessed?

Comparison of different quantification methods in a 96-well plate system, *Applied microbiology and biotechnology*, 2016, **100**, 4135-4145.
46. L. L.-Y. Chan, K. J. McCulley and S. L. Kessel, in *Cell Viability Assays: Methods and Protocols*, eds. D. F. Gilbert and O. Friedrich, Springer New York, New York, NY, 2017, DOI: 10.1007/978-1-4939-6960-9_3, pp. 27-41.
47. D. Bratosin, L. Mitrofan, C. Palii, J. Estaquier and J. Montreuil, Novel fluorescence assay using calcein-AM for the determination of human erythrocyte viability and aging, *Cytometry A*, 2005, **66**, 78-84.
48. S. Aldrich, Live/Dead Cell Double Staining Kit.
49. T. R. Neu, G. D. W. Swerhone and J. R. Lawrence, Assessment of lectin-binding analysis for in situ detection of glycoconjugates in biofilm systems, 2001, **147**, 299-313.
50. J. R. Lawrence, G. D. W. Swerhone, G. G. Leppard, T. Araki, X. Zhang, M. M. West and A. P. Hitchcock, Scanning transmission X-ray, laser scanning, and transmission electron microscopy mapping of the exopolymeric matrix of microbial biofilms, *Applied and environmental microbiology*, 2003, **69**, 5543-5554.
51. R. M. Zucker, P. Rigby, I. Clements, W. Salmon and M. Chua, Reliability of confocal microscopy spectral imaging systems: Use of multispectral beads, *Cytometry Part A*, 2007, **71A**, 174-189.
52. M. G. L. Gustafsson, L. Shao, P. M. Carlton, C. J. R. Wang, I. N. Golubovskaya, W. Z. Cande, D. A. Agard and J. W. Sedat, Three-Dimensional Resolution Doubling in Wide-Field Fluorescence Microscopy by Structured Illumination, *Biophysical journal*, 2008, **94**, 4957-4970.
53. L. Schermelleh, R. Heintzmann and H. Leonhardt, A guide to super-resolution fluorescence microscopy, *The Journal of Cell Biology*, 2010, **190**, 165.
54. G. M. Whitesides, The origins and the future of microfluidics., *Nature*, 2006, **442**, 368-373.
55. M. T. Meyer, V. Roy, W. E. Bentley and R. Ghodssi, Development and validation of a microfluidic reactor for biofilm monitoring via optical methods, *Journal of Micromechanics and Microengineering*, 2011, **21**, 054023.
56. F. Paquet-Mercier, M. Parvinzadeh Gashti, J. Bellavance, S. M. Taghavi and J. Greener, Through thick and thin: a microfluidic approach for continuous measurements of biofilm viscosity and the effect of ionic strength, *Lab Chip*, 2016, DOI: 10.1039/C6LC01101B, 1-14.
57. M. R. Benoit, C. G. Conant, C. Ionescu-Zanetti, M. Schwartz and A. Matin, New device for high-throughput viability screening of flow biofilms, *Applied and environmental microbiology*, 2010, **76**, 4136-4142.
58. B. Li, Y. Qiu, J. Zhang, X. Huang, H. Shi and H. Yin, Real-Time Study of Rapid Spread of Antibiotic Resistance Plasmid in Biofilm Using Microfluidics, *Environmental Science & Technology*, 2018, **52**, 11132-11141.
59. M. Mukherjee, N. V. Menon, X. Liu, Y. Kang and B. Cao, Confocal Laser Scanning Microscopy-Compatible Microfluidic Membrane Flow

Cell as a Nondestructive Tool for Studying Biofouling Dynamics on Forward Osmosis Membranes, *Environmental Science & Technology Letters*, 2016, DOI: 10.1021/acs.estlett.6b00218, acs.estlett.6b00218.

60. C. A. Grant, J. E. McKendry and S. D. Evans, Temperature dependent stiffness and visco-elastic behaviour of lipid coated microbubbles using atomic force microscopy, *Soft Matter*, 2012, **8**, 1321-1326.
61. F. Calliada, R. Campani, O. Bottinelli, A. Bozzini and M. G. Sommaruga, Ultrasound contrast agents: Basic principles, *European Journal of Radiology*, 1998, **27**, S157-S160.
62. N. De Jong, A. Bouakaz and P. Frinking, Basic Acoustic Properties of Microbubbles, *Echocardiography*, 2002, **19**, 229-240.
63. P. Hauff, M. Reinhardt and S. Foster, in *Molecular Imaging I*, eds. W. Semmler and M. Schwaiger, Springer Berlin Heidelberg, Berlin, Heidelberg, 2008, DOI: 10.1007/978-3-540-72718-7_11, pp. 223-245.
64. T. Faez, D. Goertz and N. De Jong, Characterization of Definity™ Ultrasound Contrast Agent at Frequency Range of 5–15 MHz, *Ultrasound in Medicine & Biology*, 2011, **37**, 338-342.
65. E. Kanbar, D. Fouan, C. A. Sennoga, A. A. Doinikov and A. Bouakaz, Impact of Filling Gas on Subharmonic Emissions of Phospholipid Ultrasound Contrast Agents, *Ultrasound in Medicine & Biology*, 2017, **43**, 1004-1015.
66. N. Kudo, T. Miyaoka, K. Okada, K. Yamamoto and K. Niwa, 2002.
67. R. V. Shohet and P. A. Grayburn, Potential Bioeffects of Ultrasonic Destruction of Microbubble Contrast Agents, *Journal of the American College of Cardiology*, 2006, **47**, 1469-1470.
68. N. Kudo, K. Okada and K. Yamamoto, Sonoporation by single-shot pulsed ultrasound with microbubbles adjacent to cells, *Biophysical journal*, 2009, **96**, 4866-4876.
69. F. Hussein, C. Antonescu and R. Karshafian, Ultrasound and microbubble induced release from intracellular compartments, *BMC biotechnology*, 2017, **17**, 45-45.
70. K. R. Lattwein, H. Shekhar, W. J. B. van Wamel, T. Gonzalez, A. B. Herr, C. K. Holland and K. Kooiman, An in vitro proof-of-principle study of sonobactericide, *Scientific Reports*, 2018, **8**, 3411.
71. K. R. Lattwein, H. Shekhar, W. J. van Wamel, A. B. Herr, C. K. Holland and K. Kooiman, Sonobactericide: An ultrasound-mediated adjunct treatment for bacterial infective endocarditis—In vitro proof-of-principle, *The Journal of the Acoustical Society of America*, 2017, **141**, 4012-4012.
72. Y. Dong, S. Chen, Z. Wang, N. Peng and J. Yu, Synergy of ultrasound microbubbles and vancomycin against Staphylococcus epidermidis biofilm, *Journal of Antimicrobial Chemotherapy*, 2013, **68**, 816-826.
73. M. Tomizawa, F. Shinozaki, Y. Motoyoshi, T. Sugiyama, S. Yamamoto and M. Sueishi, Sonoporation: Gene transfer using ultrasound, *World journal of methodology*, 2013, **3**, 39-44.
74. N. He, J. Hu, H. Liu, T. Zhu, B. Huang, X. Wang, Y. Wu, W. Wang and D. Qu, Enhancement of vancomycin activity against biofilms by using ultrasound-targeted microbubble destruction, *Antimicrobial agents and chemotherapy*, 2011, **55**, 5331-5337.

75. P. Anastasiadis, K. D. a. Mojica, J. S. Allen and M. L. Matter, Detection and quantification of bacterial biofilms combining high-frequency acoustic microscopy and targeted lipid microparticles., *Journal of nanobiotechnology*, 2014, **12**, 24.
76. G. Gerold, A. Zychlinsky and J. L. de Diego, What is the role of Toll-like receptors in bacterial infections?, *Seminars in Immunology*, 2007, **19**, 41-47.
77. T. Ramani, C. S. Auletta, D. Weinstock, B. Mounho-Zamora, P. C. Ryan, T. W. Salcedo and G. Bannish, Cytokines: The Good, the Bad, and the Deadly, *International Journal of Toxicology*, 2015, **34**, 355-365.
78. I. M. Velsko, Y. Cruz-Almeida, H. Huang, S. M. Wallet and L. M. Shaddox, Cytokine response patterns to complex biofilms by mononuclear cells discriminate patient disease status and biofilm dysbiosis, *Journal of oral microbiology*, 2017, **9**, 1330645-1330645.
79. P. Speziale, S. Rindi and G. Pietrocola, Antibody-Based Agents in the Management of Antibiotic-Resistant Staphylococcus aureus Diseases, *Microorganisms*, 2018, **6**, 25.
80. T. Rukkawattanakul, N. Sookrung, W. Seesuay, N. Onlamoon, P. Diraphat, W. Chaicumpa and N. Indrawattana, Human scFvs That Counteract Bioactivities of Staphylococcus aureus TSST-1, *Toxins*, 2017, **9**, 50.
81. J. L. Aguilar, A. K. Varshney, X. Pechuan, K. Dutta, J. D. Nosanchuk and B. C. Fries, Monoclonal antibodies protect from Staphylococcal Enterotoxin K (SEK) induced toxic shock and sepsis by USA300 Staphylococcus aureus, *Virulence*, 2017, **8**, 741-750.
82. E. Diago-Navarro, M. P. Motley, G. Ruiz-Peréz, W. Yu, J. Austin, B. M. S. Seco, G. Xiao, A. Chikhalya, P. H. Seeberger and B. C. Fries, Novel, Broadly Reactive Anticapsular Antibodies against Carbapenem-Resistant Klebsiella pneumoniae Protect from Infection, *mBio*, 2018, **9**, e00091-00018.
83. S. D. Kobayashi, A. R. Porter, B. Freedman, R. Pandey, L. Chen, B. N. Kreiswirth and F. R. DeLeo, Antibody-Mediated Killing of Carbapenem-Resistant ST258 Klebsiella pneumoniae by Human Neutrophils, *mBio*, 2018, **9**, e00297-00218.
84. C. R. Doyle, J.-Y. Moon, J. P. Daily, T. Wang and L.-A. Pirofski, A Capsular Polysaccharide-Specific Antibody Alters Streptococcus pneumoniae Gene Expression during Nasopharyngeal Colonization of Mice, *Infection and immunity*, 2018, **86**, e00300-00318.
85. R. Jain, V. V. Beckett, M. W. Konstan, F. J. Accurso, J. L. Burns, N. Mayer-Hamblett, C. Milla, D. R. VanDevanter and J. F. Chmiel, KB001-A, a novel anti-inflammatory, found to be safe and well-tolerated in cystic fibrosis patients infected with Pseudomonas aeruginosa, *Journal of Cystic Fibrosis*, 2018, **17**, 484-491.
86. S. O. Ali, X. Q. Yu, G. J. Robbie, Y. Wu, K. Shoemaker, L. Yu, A. DiGiandomenico, A. E. Keller, C. Anude, M. Hernandez-Illas, T. Bellamy, J. Falloon, F. Dubovsky and H. S. Jafri, Phase 1 study of MEDI3902, an investigational anti–Pseudomonas aeruginosa PcrV

and Psl bispecific human monoclonal antibody, in healthy adults, *Clinical Microbiology and Infection*, 2019, **25**, 629.e621-629.e626.

87. L. Visan, N. Rouleau, E. Proust, L. Peyrot, A. Donadieu and M. Ochs, Antibodies to PcpA and PhtD protect mice against Streptococcus pneumoniae by a macrophage- and complement-dependent mechanism, *Human vaccines & immunotherapeutics*, 2018, **14**, 489-494.
88. J. Cao, F. Yi, Q. Tian, G. Dang, W. Si, S. Liu and S. Yu, Targeting the gram-negative bacteria peptidoglycan synthase MraY as a new approach for monoclonal antibody anti-bacterial activity, *Human vaccines & immunotherapeutics*, 2017, **13**, 2086-2091.
89. Y. Wang, L. I. Cheng, D. R. Helfer, A. G. Ashbaugh, R. J. Miller, A. J. Tzomides, J. M. Thompson, R. V. Ortines, A. S. Tsai, H. Liu, C. A. Dillen, N. K. Archer, T. S. Cohen, C. Tkaczyk, C. K. Stover, B. R. Sellman and L. S. Miller, Mouse model of hematogenous implant-related Staphylococcus aureus biofilm infection reveals therapeutic targets, *Proceedings of the National Academy of Sciences of the United States of America*, 2017, **114**, E5094-E5102.
90. E. O'Neill, C. Pozzi, P. Houston, H. Humphreys, D. A. Robinson, A. Loughman, T. J. Foster and J. P. O'Gara, A Novel Staphylococcus aureus Biofilm Phenotype Mediated by the Fibronectin-Binding Proteins, FnBPA and FnBPB, 2008, **190**, 3835-3850.
91. A. Rennermalm, Y.-H. Li, L. Bohaufs, C. Jarstrand, A. Brauner, F. R. Brennan and J.-I. Flock, Antibodies against a truncated Staphylococcus aureus fibronectin-binding protein protect against dissemination of infection in the rat, *Vaccine*, 2001, **19**, 3376-3383.
92. C. Kelly-Quintos, L. A. Cavacini, M. R. Posner, D. Goldmann and G. B. Pier, Characterization of the opsonic and protective activity against Staphylococcus aureus of fully human monoclonal antibodies specific for the bacterial surface polysaccharide poly-N-acetylglucosamine, *Infection and immunity*, 2006, **74**, 2742-2750.
93. C. Tkaczyk, M. M. Hamilton, A. Sadowska, Y. Shi, C. S. Chang, P. Chowdhury, R. Buonapane, X. Xiao, P. Warrener, J. Mediavilla, B. Kreiswirth, J. Suzich, C. K. Stover and B. R. Sellman, Targeting Alpha Toxin and ClfA with a Multimechanistic Monoclonal-Antibody-Based Approach for Prophylaxis of Serious Staphylococcus aureus Disease, *mBio*, 2016, **7**, e00528-00516.
94. P. J. Domanski, P. R. Patel, A. S. Bayer, L. Zhang, A. E. Hall, P. J. Syribeys, E. L. Gorovits, D. Bryant, J. H. Vernachio, J. T. Hutchins and J. M. Patti, Characterization of a humanized monoclonal antibody recognizing clumping factor A expressed by Staphylococcus aureus, *Infection and immunity*, 2005, **73**, 5229-5232.
95. A. E. Hall, P. J. Domanski, P. R. Patel, J. H. Vernachio, P. J. Syribeys, E. L. Gorovits, M. A. Johnson, J. M. Ross, J. T. Hutchins and J. M. Patti, Characterization of a protective monoclonal antibody recognizing Staphylococcus aureus MSCRAMM protein clumping factor A, *Infection and immunity*, 2003, **71**, 6864-6870.

96. N. Cerca, T. Maira-Litrán, K. K. Jefferson, M. Grout, D. A. Goldmann and G. B. Pier, Protection against Escherichia coli infection by antibody to the Staphylococcus aureus poly-N-acetylglucosamine surface polysaccharide, *Proceedings of the National Academy of Sciences of the United States of America*, 2007, **104**, 7528-7533.
97. T. Maira-Litrán, A. Kropec, D. A. Goldmann and G. B. Pier, Comparative opsonic and protective activities of Staphylococcus aureus conjugate vaccines containing native or deacetylated Staphylococcal Poly-N-acetyl-beta-(1-6)-glucosamine, *Infection and immunity*, 2005, **73**, 6752-6762.
98. C. Cywes-Bentley, D. Skurnik, T. Zaidi, D. Roux, R. B. Deoliveira, W. S. Garrett, X. Lu, J. O'Malley, K. Kinzel, T. Zaidi, A. Rey, C. Perrin, R. N. Fichorova, A. K. K. Kayatani, T. Maira-Litràn, M. L. Gening, Y. E. Tsvetkov, N. E. Nifantiev, L. O. Bakaletz, S. I. Pelton, D. T. Golenbock and G. B. Pier, Antibody to a conserved antigenic target is protective against diverse prokaryotic and eukaryotic pathogens, *Proceedings of the National Academy of Sciences of the United States of America*, 2013, **110**, E2209-E2218.
99. A. Estellés, A.-K. Woischnig, K. Liu, R. Stephenson, E. Lomongsod, D. Nguyen, J. Zhang, M. Heidecker, Y. Yang, R. J. Simon, E. Tenorio, S. Ellsworth, A. Leighton, S. Ryser, N. K. Gremmelmaier and L. M. Kauvar, A High-Affinity Native Human Antibody Disrupts Biofilm from Staphylococcus aureus Bacteria and Potentiates Antibiotic Efficacy in a Mouse Implant Infection Model, *Antimicrobial agents and chemotherapy*, 2016, **60**, 2292-2301.
100. Y. Q. Xiong, A. Estellés, L. Li, W. Abdelhady, R. Gonzales, A. S. Bayer, E. Tenorio, A. Leighton, S. Ryser and L. M. Kauvar, A Human Biofilm-Disrupting Monoclonal Antibody Potentiates Antibiotic Efficacy in Rodent Models of both Staphylococcus aureus and Acinetobacter baumannii Infections, *Antimicrobial agents and chemotherapy*, 2017, **61**, e00904-00917.
101. V. Oganesyan, L. Peng, M. M. Damschroder, L. Cheng, A. Sadowska, C. Tkaczyk, B. R. Sellman, H. Wu and W. F. Dall'Acqua, Mechanisms of neutralization of a human anti-α-toxin antibody, *The Journal of biological chemistry*, 2014, **289**, 29874-29880.
102. R. V. Ortines, H. Liu, L. I. Cheng, T. S. Cohen, H. Lawlor, A. Gami, Y. Wang, C. A. Dillen, N. K. Archer, R. J. Miller, A. G. Ashbaugh, B. L. Pinsker, M. C. Marchitto, C. Tkaczyk, C. K. Stover, B. R. Sellman and L. S. Miller, Neutralizing Alpha-Toxin Accelerates Healing of Staphylococcus aureus-Infected Wounds in Nondiabetic and Diabetic Mice, *Antimicrobial agents and chemotherapy*, 2018, **62**, e02288-02217.
103. A. Badarau, H. Rouha, S. Malafa, M. B. Battles, L. Walker, N. Nielson, I. Dolezilkova, A. Teubenbacher, S. Banerjee, B. Maierhofer, S. Weber, L. Stulik, D. T. Logan, M. Welin, I. Mirkina, C. Pleban, G. Zauner, K. Gross, M. Jägerhofer, Z. Magyarics and E. Nagy, Context matters: The importance of dimerization-induced conformation of the LukGH leukocidin of Staphylococcus aureus for the generation of neutralizing antibodies, *mAbs*, 2016, **8**, 1347-1360.

104. A. C. DeDent, M. McAdow and O. Schneewind, Distribution of protein A on the surface of Staphylococcus aureus, *Journal of Bacteriology*, 2007, **189**, 4473-4484.
105. U. J. E. Seidel, P. Schlegel and P. Lang, Natural killer cell mediated antibody-dependent cellular cytotoxicity in tumor immunotherapy with therapeutic antibodies, *Frontiers in immunology*, 2013, **4**, 76-76.
106. P. Chames, M. Van Regenmortel, E. Weiss and D. Baty, Therapeutic antibodies: Successes, limitations and hopes for the future, *British journal of pharmacology*, 2009, **157**, 220-233.
107. A. Giritch, S. Marillonnet, C. Engler, G. van Eldik, J. Botterman, V. Klimyuk and Y. Gleba, Rapid high-yield expression of full-size IgG antibodies in plants coinfected with noncompeting viral vectors, *Proceedings of the National Academy of Sciences of the United States of America*, 2006, **103**, 14701-14706.
108. K. Škrlec, B. Štrukelj and A. Berlec, Non-immunoglobulin scaffolds: a focus on their targets, *Trends in Biotechnology*, 2015, **33**, 408-418.
109. C. Tiede, R. Bedford, S. J. Heseltine, G. Smith, I. Wijetunga, R. Ross, D. AlQallaf, A. P. Roberts, A. Balls, A. Curd, R. E. Hughes, H. Martin, S. R. Needham, L. C. Zanetti-Domingues, Y. Sadigh, T. P. Peacock, A. A. Tang, N. Gibson, H. Kyle, G. W. Platt, N. Ingram, T. Taylor, L. P. Coletta, I. Manfield, M. Knowles, S. Bell, F. Esteves, A. Maqbool, R. K. Prasad, M. Drinkhill, R. S. Bon, V. Patel, S. A. Goodchild, M. Martin-Fernandez, R. J. Owens, J. E. Nettleship, M. E. Webb, M. Harrison, J. D. Lippiat, S. Ponnambalam, M. Peckham, A. Smith, P. K. Ferrigno, M. Johnson, M. J. McPherson and D. C. Tomlinson, Affimer proteins are versatile and renewable affinity reagents, *eLife*, 2017, **6**, e24903.
110. C. Tiede, A. A. S. Tang, S. E. Deacon, U. Mandal, J. E. Nettleship, R. L. Owen, S. E. George, D. J. Harrison, R. J. Owens, D. C. Tomlinson and M. J. McPherson, Adhiron: a stable and versatile peptide display scaffold for molecular recognition applications, *Protein engineering, design & selection : PEDS*, 2014, **27**, 145-155.
111. J. Löfblom, J. Feldwisch, V. Tolmachev, J. Carlsson, S. Ståhl and F. Y. Frejd, Affibody molecules: Engineered proteins for therapeutic, diagnostic and biotechnological applications, *FEBS Letters*, 2010, **584**, 2670-2680.
112. A. Plückthun, Designed Ankyrin Repeat Proteins (DARPins): Binding Proteins for Research, Diagnostics, and Therapy, *Annual Review of Pharmacology and Toxicology*, 2015, **55**, 489-511.
113. L. Ledsgaard, M. Kilstrup, A. Karatt-Vellatt, J. McCafferty and A. H. Laustsen, Basics of Antibody Phage Display Technology, *Toxins*, 2018, **10**.
114. R. Kushwaha, K. R. Schäfermeyer and A. B. Downie, A protocol for phage display and affinity selection using recombinant protein baits, *Journal of visualized experiments : JoVE*, 2014, DOI: 10.3791/50685, e50685-e50685.
115. G. Smith, Filamentous fusion phage: novel expression vectors that display cloned antigens on the virion surface, *Science*, 1985, **228**, 1315-1317.

116. R. Barderas and E. Benito-Peña, The 2018 Nobel Prize in Chemistry: phage display of peptides and antibodies, *Analytical and Bioanalytical Chemistry*, 2019, **411**, 2475-2479.
117. L.-W. Deng, P. Malik and R. N. Perham, Interaction of the Globular Domains of pIII Protein of Filamentous Bacteriophage fd with the F-Pilus ofEscherichia coli, *Virology*, 1999, **253**, 271-277.
118. E. Dias-Neto, D. N. Nunes, R. J. Giordano, J. Sun, G. H. Botz, K. Yang, J. C. Setubal, R. Pasqualini and W. Arap, Next-Generation Phage Display: Integrating and Comparing Available Molecular Tools to Enable Cost-Effective High-Throughput Analysis, *PLOS ONE*, 2009, **4**, e8338.
119. K. Wilson, & Walker, J., *Principles and Techniques of Biochemistry and Molecular Biology*, Cambridge University Press, Cambridge, 7 edn., 2010.
120. S. Yamaguchi, E. Yamamoto, T. Mannen, T. Nagamune and T. Nagamune, Protein refolding using chemical refolding additives, *Biotechnol J*, 2013, **8**, 17-31.
121. M. Lindborg, A. Dubnovitsky, K. Olesen, T. Bjorkman, L. Abrahmsen, J. Feldwisch and T. Hard, High-affinity binding to staphylococcal protein A by an engineered dimeric Affibody molecule, *Protein Eng Des Sel*, 2013, **26**, 635-644.
122. X. Yu, Y.-P. Yang, E. Dikici, S. K. Deo and S. Daunert, Beyond Antibodies as Binding Partners: The Role of Antibody Mimetics in Bioanalysis, *Annual review of analytical chemistry (Palo Alto, Calif.)*, 2017, **10**, 293-320.
123. P. Garred, F. Larsen, H. O. Madsen and C. Koch, Mannose-binding lectin deficiency—revisited, *Molecular Immunology*, 2003, **40**, 73-84.
124. M. W. Turner, Mannose-binding lectin: The pluripotent molecule of the innate immune system, *Immunology Today*, 1996, **17**, 532-540.
125. D. P. Eisen and R. M. Minchinton, Impact of Mannose-Binding Lectin on Susceptibility to Infectious Diseases, *Clinical Infectious Diseases*, 2003, **37**, 1496-1505.
126. J. Nadesalingam, A. W. Dodds, K. B. M. Reid and N. Palaniyar, Mannose-binding lectin recognizes peptidoglycan via the N-acetyl glucosamine moiety, and inhibits ligand-induced proinflammatory effect and promotes chemokine production by macrophages., *Journal of Immunology*, 2005, **175**, 1785-1794.
127. M. W. Turner, The role of mannose-binding lectin in health and disease, *Netherlands Journal of Medicine*, 2004, **62**, 4-9.
128. S. T. Iobst, M. R. Wormald, W. I. Weis, R. A. Dwek and K. Drickamer, Binding of sugar ligands to Ca(2+)-dependent animal lectins. I. Analysis of mannose binding by site-directed mutagenesis and NMR, 1994, **269**, 15505-15511.
129. R. Wallis and J. Y. T. Cheng, Molecular Defects in Variant Forms of Mannose-Binding Protein Associated with Immunodeficiency, 1999, **163**, 4953-4959.
130. D. L. Jack, N. J. Klein and M. W. Turner, Mannose-binding lectin: targeting the microbial world for complement attack and opsonophagocytosis., *Immunological reviews*, 2001, **180**, 86-99.
131. O. Neth, D. L. Jack, A. W. Dodds, H. Holzel, N. J. Klein and M. W. Turner, Mannose-Binding Lectin Binds to a Range of Clinically

Relevant Microorganisms and PromotesComplement Deposition, *Infection and Immunity*, 2000, **68**, 688-693.
132. J.-C. Yu, C.-C. Hu, W.-H. Chang, P.-C. Chen, M. S. Lee, K.-T. Peng and G.-B. Lee, An integrated microfluidic system using mannose-binding lectin for bacteria isolation and biofilm-related gene detection, *Microfluidics and Nanofluidics*, 2018, **22**, 13.
133. K. Drickamer, Engineering galactose-binding activity into a C-type mannose-binding protein, *Nature*, 1992, **360**, 183-186.
134. G. S. Butler, D. Sim, E. Tam, D. Devine and C. M. Overall, Mannose-binding Lectin (MBL) Mutants Are Susceptible to Matrix Metalloproteinase Proteolysis: POTENTIAL ROLE IN HUMAN MBL DEFICIENCY, 2002, **277**, 17511-17519.
135. B. J. Smith, in *Proteins*, ed. J. M. Walker, Humana Press, Totowa, NJ, 1984, DOI: 10.1385/0-89603-062-8:41, pp. 41-55.
136. T. Spirig, E. M. Weiner and R. T. Clubb, Sortase enzymes in Gram-positive bacteria, *Mol Microbiol*, 2011, **82**, 1044-1059.
137. M. W.-L. Popp and H. L. Ploegh, Making and Breaking Peptide Bonds: Protein Engineering Using Sortase, *Angewandte Chemie International Edition*, 2011, **50**, 5024-5032.
138. D. J. Williamson, M. A. Fascione, M. E. Webb and W. B. Turnbull, Efficient N-Terminal Labeling of Proteins by Use of Sortase, *Angewandte Chemie International Edition*, 2012, **51**, 9377-9380.
139. A. Holmberg, A. Blomstergren, O. Nord, M. Lukacs, J. Lundeberg and M. Uhlen, The biotin-streptavidin interaction can be reversibly broken using water at elevated temperatures, *Electrophoresis*, 2005, **26**, 501-510.
140. S. Unnikrishnan and A. L. Klibanov, Microbubbles as Ultrasound Contrast Agents for Molecular Imaging: Preparation and Application, *American Journal of Roentgenology*, 2012, **199**, 292-299.
141. A. Lyshchik, A. C. Fleischer, J. Huamani, D. E. Hallahan, M. Brissova and J. C. Gore, Molecular imaging of vascular endothelial growth factor receptor 2 expression using targeted contrast-enhanced high-frequency ultrasonography, *Journal of ultrasound in medicine : official journal of the American Institute of Ultrasound in Medicine*, 2007, **26**, 1575-1586.
142. A. Dirksen, T. M. Hackeng and P. E. Dawson, Nucleophilic catalysis of oxime ligation, *Angew Chem Int Ed Engl*, 2006, **45**, 7581-7584.
143. C. M. Stoscheck, in *Methods in Enzymology*, ed. M. P. Deutscher, Academic Press, 1990, vol. 182, pp. 50-68.
144. A. Karyolaimos, H. Ampah-Korsah, T. Hillenaar, A. Mestre Borras, K. M. Dolata, S. Sievers, K. Riedel, R. Daniels and J.-W. de Gier, Enhancing Recombinant Protein Yields in the E. coli Periplasm by Combining Signal Peptide and Production Rate Screening, 2019, **10**.
145. M. Jeiranikhameneh, F. Moshiri, S. K. Falasafi and A. Zomorodipour, Designing Signal Peptides for Efficient Periplasmic Expression of Human Growth Hormone in Escherichia coli, *Journal of Microbiology and Biotechnology*, 2017, **27**, 1999-2009.
146. H. C. Neu and L. A. Heppel, The Release of Enzymes from Escherichia coli by Osmotic Shock and during the Formation of Spheroplasts, *Journal of Biological Chemistry*, 1965, **240**, 3685-3692.

147. J. F. Kane, Effects of rare codon clusters on high-level expression of heterologous proteins in Escherichia coli, *Current Opinion in Biotechnology*, 1995, **6**, 494-500.
148. D. Esposito and D. K. Chatterjee, Enhancement of soluble protein expression through the use of fusion tags, *Curr Opin Biotechnol*, 2006, **17**, 353-358.
149. P. Sun, J. E. Tropea and D. S. Waugh, in *Heterologous Gene Expression in E.coli: Methods and Protocols*, eds. J. T. C. Evans and M.-Q. Xu, Humana Press, Totowa, NJ, 2011, DOI: 10.1007/978-1-61737-967-3_16, pp. 259-274.
150. S. Nallamsetty, B. P. Austin, K. J. Penrose and D. S. Waugh, Gateway vectors for the production of combinatorially-tagged His6-MBP fusion proteins in the cytoplasm and periplasm of Escherichia coli, *Protein Sci*, 2005, **14**, 2964-2971.
151. I. H. Walker, P. C. Hsieh and P. D. Riggs, Mutations in maltose-binding protein that alter affinity and solubility properties, *Appl Microbiol Biotechnol*, 2010, **88**, 187-197.
152. K. Terpe, Overview of tag protein fusions: from molecular and biochemical fundamentals to commercial systems, *Appl Microbiol Biotechnol*, 2003, **60**, 523-533.
153. B. D. Hames and N. M. Hooper, *Biochemistry*, Garland Science, 2011.
154. F. Alsulaimani, University of Leeds.
155. R. Kunin and F. X. McGarvey, Ion Exchange Chromatography, *Analytical Chemistry*, 1962, **34**, 48R-50r.
156. E. Freire, O. L. Mayorga and M. Straume, Isothermal titration calorimetry, *Analytical Chemistry*, 1990, **62**, 950A-959A.
157. W. Lu and R. J. Pieters, Carbohydrate–protein interactions and multivalency: implications for the inhibition of influenza A virus infections, *Expert Opinion on Drug Discovery*, 2019, **14**, 387-395.
158. L. L. Kiessling, T. Young, T. D. Gruber and K. H. Mortell, in *Glycoscience: Chemistry and Chemical Biology*, eds. B. O. Fraser-Reid, K. Tatsuta and J. Thiem, Springer Berlin Heidelberg, Berlin, Heidelberg, 2008, DOI: 10.1007/978-3-540-30429-6_64, pp. 2483-2523.
159. Y.-R. Liou, Y.-H. Wang, C.-Y. Lee and P.-C. Li, Buoyancy-Activated Cell Sorting Using Targeted Biotinylated Albumin Microbubbles, *PLOS ONE*, 2015, **10**, e0125036.
160. R. Lukáč, Z. Kauerová, J. Mašek, E. Bartheldyová, P. Kulich, Š. Koudelka, Z. Korvasová, J. Plocková, F. Papoušek, F. Kolář, R. Schmidt and J. Turánek, Preparation of Metallochelating Microbubbles and Study on Their Site-Specific Interaction with rGFP-HisTag as a Model Protein, *Langmuir*, 2011, **27**, 4829-4837.
161. J. R. Lakowicz, J. Malicka, S. D'Auria and I. Gryczynski, Release of the self-quenching of fluorescence near silver metallic surfaces, *Analytical Biochemistry*, 2003, **320**, 13-20.
162. K. E. Al Ani and A. M. Suleiman, Substituent effect on the fluorescence quenching of polystyrene derivatives by polymeric plasticizers, *Journal of Photochemistry and Photobiology A: Chemistry*, 2007, **188**, 177-184.

163. J.-M. Entenza, P. Moreillon, M. M. Senn, J. Kormanec, P. M. Dunman, B. Berger-Bächi, S. Projan and M. Bischoff, Role of sigmaB in the expression of Staphylococcus aureus cell wall adhesins ClfA and FnbA and contribution to infectivity in a rat model of experimental endocarditis, *Infection and immunity*, 2005, **73**, 990-998.
164. R. Saini, S. Saini and S. Sharma, Biofilm: A dental microbial infection, *Journal of natural science, biology, and medicine*, 2011, **2**, 71-75.
165. S. Torino, B. Corrado, M. Iodice and G. Coppola, PDMS-Based Microfluidic Devices for Cell Culture, *Inventions*, 2018, **3**.
166. T. C. Merkel, V. I. Bondar, K. Nagai, B. D. Freeman and I. Pinnau, Gas sorption, diffusion, and permeation in poly(dimethylsiloxane), 2000, **38**, 415-434.
167. A. Bernard, E. Delamarche, H. Schmid, B. Michel, H. R. Bosshard and H. Biebuyck, Printing Patterns of Proteins, *Langmuir*, 1998, **14**, 2225-2229.
168. A. Piruska, I. Nikcevic, S. H. Lee, C. Ahn, W. R. Heineman, P. A. Limbach and C. J. Seliskar, The autofluorescence of plastic materials and chips measured under laser irradiation, *Lab on a Chip*, 2005, **5**, 1348-1354.
169. H. Ma, B. R. Hou, H. Y. Wu, C. Y. Lin, J. J. Gao and M. C. Kou, Development and Application of a Diaphragm Micro-Pump with Piezoelectric Device, *Microsystem Technologies*, 2008, **14**, 1001-1007.
170. L. W. McKeen, in *The Effect of Creep and Other Time Related Factors on Plastics and Elastomers (Second Edition)*, ed. L. W. McKeen, William Andrew Publishing, Boston, 2009, DOI: https://doi.org/10.1016/B978-0-8155-1585-2.50004-2, pp. 33-81.
171. J. K. Tung, K. Berglund, C.-A. Gutekunst, U. Hochgeschwender and R. E. Gross, Bioluminescence imaging in live cells and animals, *Neurophotonics*, 2016, **3**, 025001-025001.
172. B. Gantenbein, C. Sprecher, S. Chan, S. Illien-Junger and S. Grad, *Confocal Imaging Protocols for Live/Dead Staining in Three-Dimensional Carriers*, 2011.
173. Biotium, https://biotium.com/product/dmao-2mm-in-dmso/, (accessed 01/08/2019, 2019).
174. H. H. Cui, J. G. Valdez, J. A. Steinkamp and H. A. Crissman, Fluorescence lifetime-based discrimination and quantification of cellular DNA and RNA with phase-sensitive flow cytometry, 2003, **52A**, 46-55.
175. E. Paramonova, E. D. de Jong, B. P. Krom, H. C. van der Mei, H. J. Busscher and P. K. Sharma, Low-load compression testing: a novel way of measuring biofilm thickness, *Applied and environmental microbiology*, 2007, **73**, 7023-7028.
176. I. W. Sutherland, The biofilm matrix – an immobilized but dynamic microbial environment, *Trends in Microbiology*, 2001, **9**, 222-227.
177. L. Bonifait, L. Grignon and D. Grenier, Fibrinogen induces biofilm formation by Streptococcus suis and enhances its antibiotic resistance, *Applied and environmental microbiology*, 2008, **74**, 4969-4972.

178. R. C. Becker, P. M. DiBello and F. V. Lucas, Bacterial tissue tropism: an in vitro model for infective endocarditis, *Cardiovascular Research*, 1987, **21**, 813-820.
179. Biotium, https://biotium.com/technology/cell-viability-apoptosis/, (accessed 06/09/2019, 2019).
180. J. A. Arellano, T. A. Howell, J. Gammon, S. Cho, M. M. Janát-Amsbury and B. Gale, Use of a highly parallel microfluidic flow cell array to determine therapeutic drug dose response curves, *Biomedical Microdevices*, 2017, **19**, 25.
181. S. Zeng, D. Baillargeat, H.-P. Ho and K.-T. Yong, Nanomaterials enhanced surface plasmon resonance for biological and chemical sensing applications, *Chemical Society Reviews*, 2014, **43**, 3426-3452.
182. J. Homola, S. S. Yee and G. Gauglitz, Surface plasmon resonance sensors: review, *Sensors and Actuators B: Chemical*, 1999, **54**, 3-15.
183. G. Schreiber, G. Haran and H. X. Zhou, Fundamental aspects of protein-protein association kinetics, *Chemical reviews*, 2009, **109**, 839-860.
184. A. E. Bergues-Pupo, K. G. Blank, R. Lipowsky and A. Vila Verde, Trimeric coiled coils expand the range of strength, toughness and dynamics of coiled coil motifs under shear, *Physical Chemistry Chemical Physics*, 2018, **20**, 29105-29115.
185. A. L. Klibanov, Preparation of targeted microbubbles: ultrasound contrast agents for molecular imaging, *Medical & Biological Engineering & Computing*, 2009, **47**, 875-882.
186. E. D. Austin, S. S. Sullivan, N. Macesic, M. Mehta, B. A. Miko, S. Nematollahi, Q. Shi, F. D. Lowy and A.-C. Uhlemann, Reduced Mortality of Staphylococcus aureus Bacteremia in a Retrospective Cohort Study of 2139 Patients: 2007–2015, *Clinical Infectious Diseases*, 2019, DOI: 10.1093/cid/ciz498.
187. W. H. Organisation, Antibiotic resistance, https://www.who.int/en/news-room/fact-sheets/detail/antibiotic-resistance, (accessed 17/09/19).
188. S. Hogan, E. Kasotakis, S. Maher, B. Cavanagh, J. P. O'Gara, A. Pandit, T. E. Keyes, M. Devocelle and E. O'Neill, A novel medical device coating prevents Staphylococcus aureus biofilm formation on medical device surfaces, *FEMS Microbiology Letters*, 2019, **366**.
189. J. L. Lister and A. R. Horswill, Staphylococcus aureus biofilms: recent developments in biofilm dispersal, 2014, **4**.
190. F. J. Vos, B. J. Kullberg, P. D. Sturm, P. F. M. Krabbe, A. P. J. van Dijk, G. J. A. Wanten, W. J. G. Oyen and C. P. Bleeker-Rovers, Metastatic Infectious Disease and Clinical Outcome in Staphylococcus aureus and Streptococcus species Bacteremia, 2012, **91**, 86-94.
191. M. E. Skogman, P. M. Vuorela and A. Fallarero, A Platform of Anti-biofilm Assays Suited to the Exploration of Natural Compound Libraries, *Journal of visualized experiments : JoVE*, 2016, DOI: 10.3791/54829, 54829.
192. M. E. Skogman, P. M. Vuorela and A. Fallarero, Combining biofilm matrix measurements with biomass and viability assays in

susceptibility assessments of antimicrobials against Staphylococcus aureus biofilms, *The Journal Of Antibiotics*, 2012, **65**, 453.

193. D. Rodríguez-Lázaro, C. Alonso-Calleja, E. A. Oniciuc, R. Capita, D. Gallego, C. González-Machado, M. Wagner, V. Barbu, J. M. Eiros-Bouza, A. I. Nicolau and M. Hernández, Characterization of Biofilms Formed by Foodborne Methicillin-Resistant Staphylococcus aureus, *Frontiers in microbiology*, 2018, **9**, 3004-3004.
194. J. K. Willmann, A. M. Lutz, R. Paulmurugan, M. R. Patel, P. Chu, J. Rosenberg and S. S. Gambhir, Dual-targeted contrast agent for US assessment of tumor angiogenesis in vivo, *Radiology*, 2008, **248**, 936-944.
195. J. M. Warram, A. G. Sorace, R. Saini, H. R. Umphrey, K. R. Zinn and K. Hoyt, A triple-targeted ultrasound contrast agent provides improved localization to tumor vasculature, *Journal of ultrasound in medicine : official journal of the American Institute of Ultrasound in Medicine*, 2011, **30**, 921-931.
196. D. J. Williamson, M. E. Webb and W. B. Turnbull, Depsipeptide substrates for sortase-mediated N-terminal protein ligation, *Nat Protoc*, 2014, **9**, 253-262.
197. S. H. Tan, N.-T. Nguyen, Y. C. Chua and T. G. Kang, Oxygen plasma treatment for reducing hydrophobicity of a sealed polydimethylsiloxane microchannel, *Biomicrofluidics*, 2010, **4**, 32204-32204.
198. S. A. Peyman, R. H. Abou-Saleh, J. R. McLaughlan, N. Ingram, B. R. G. Johnson, K. Critchley, S. Freear, J. A. Evans, A. F. Markham, P. L. Coletta and S. D. Evans, Expanding 3D geometry for enhanced on-chip microbubble production and single step formation of liposome modified microbubbles, *Lab on a Chip*, 2012, **12**, 4544-4552.